SoftCOM '18

tutorials

On the Computational Methods in Electromagnetics: Applications in Electromagnetic Compatibility, Ground Penetrating Radar, Bioelectromagnetics and Magnetohydrodynamics

by

Dragan Poljak

University of Split, Croatia

September 13 - 15, 2018.

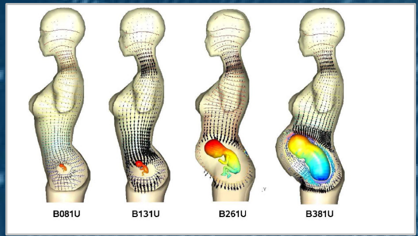

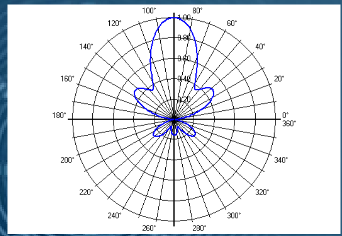

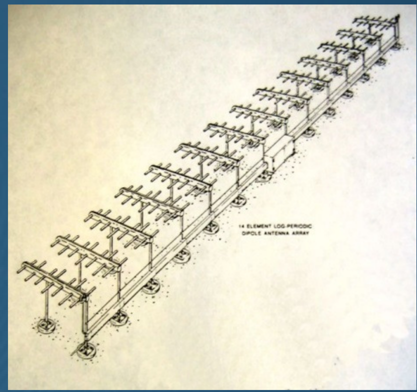

Department of Electronics
University of Split,
Split, Croatia

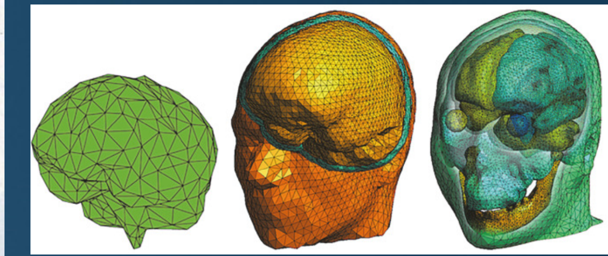

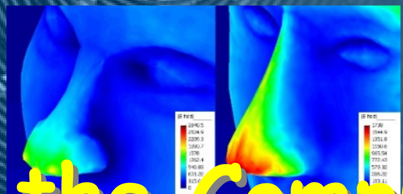

On the Computational Methods in Electromagnetic Compatibility:

Applications in antennas, ground penetrating radar, bioelectromagnetics, grounding systems, transmission lines, lightning and plasma physics

$$\nabla \times \vec{E} = -\frac{\partial \vec{B}}{\partial t}$$

$$\nabla \times \vec{H} = \vec{J} + \frac{\partial \vec{D}}{\partial t}$$

$$\nabla \cdot \vec{D} = \rho$$

$$\nabla \cdot \vec{B} = 0$$

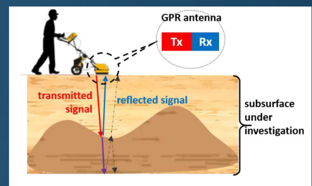

Fig. 1. Principles of GPR use

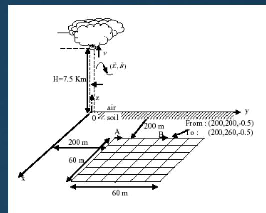

Figure 6. Grounding grid illuminated by lightning channel.

Dragan Poljak
University of Split, Croatia

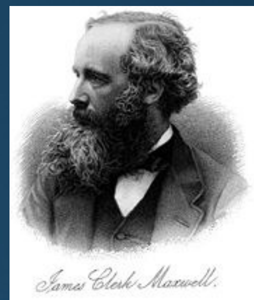

Clermont-Ferrand, 03 April 2018

UNIVERSITÉ Clermont Auvergne

Department of Electronics
University of Split,
Split, Croatia

CONTENTS

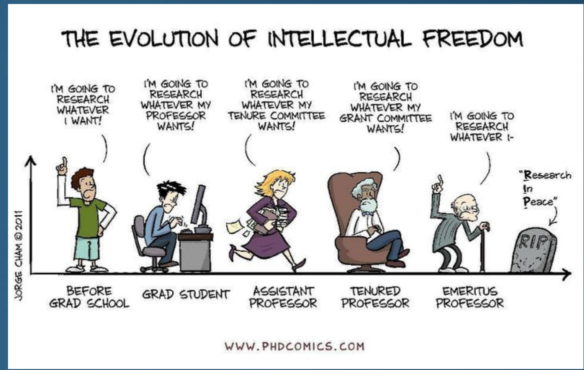

- Introduction to Computational Electromagnetics (CEM)
- Wire Antennas
- Transmission Lines (Overhead and buried wires)
- Lightning Electromagnetics
- Human Exposure to Electromagnetic Fields
- Numerical Modeling of Magnetohydrodynamics phenomena
- On-going work in deterministic and stochastic modeling
- Concluding remarks

Clermont-Ferrand, 03 April 2018

Department of Electronics
University of Split,
Split, Croatia

ON-GOING PROJECTS

- ICES SC6 The IEEE International Committee on Electromagnetic Safety (ICES, Tecnical Committee 95), Subcommittee SC6 on Electromagnetic Field Dosimetry
- COST Action BM1309: European network for innovative uses of EMFs in biomedical applications
- COST Action TU1208: Civil Engineering Applications of Ground Penetrating Radar

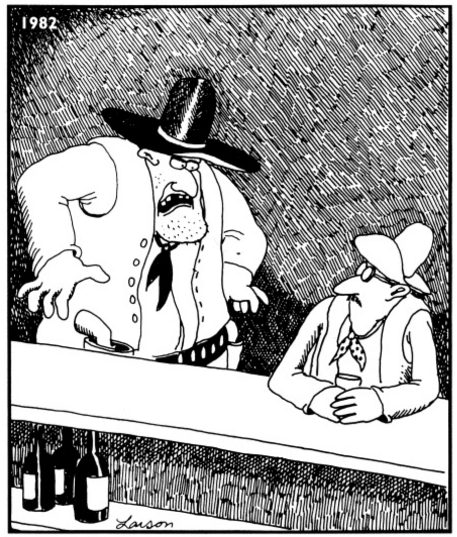

"I asked you a question, buddy. … What's the square root of 5,248?"

- COST ACTION IC 1407: Advanced characterisation and classification of radiated emissions in densely integrated technologies (ACCREDIT)
- ITER Physics, EUROFusion, WPCD (Code development for Integrated Modeling)
- Centre of Research Excellence for Data Science and Cooperative Systems: Research Unit for Cooperative Systems

Department of Electronics
University of Split,
Split, Croatia

Introduction to Computational Electromagnetics (CEM) and Electromagnetic Compatibility (EMC)

Historical note on modeling in electromagnetics

- Electromagnetics as a rigorous theory started when *James Clerk Maxwell* derived his celebrated four equations and published this work in the famous treatise in 1865.
- In addition to *Maxwell's equations* themselves, relating the behaviour of EM fields and sources we need:

  ✓ the constitutive relations of the medium

  ✓ the imposed boundary conditions of the physical problem of interest.

UNIVERSITÉ Clermont Auvergne

Department of Electronics
University of Split,
Split, Croatia

Introduction to Computational Electromagnetics (CEM) and Electromagnetic Compatibility (EMC)

Historical note on modeling in electromagnetics

- One of the first digital computer solution of the *Pocklington's equation* was reported in 1965.
- This was followed by the one of the first implementations of the **Finite Difference Method (FDM)** to the solution of partial differential equations in 1966 and time domain integral equation formulations in 1968 and 1973.
- Through 1970s the **Finite Element Method (FEM)** became widely used in almost all areas of applied EM applications.
- The **Boundary Element Method (BEM)** developed in the late seventies for the purposes of civil and mechanical engineering started to be used in electromagnetics in 1980s.

Department of Electronics
University of Split,
Split, Croatia

Introduction to Computational Electromagnetics (CEM) and Electromagnetic Compatibility (EMC)

EMC computational models and solution methods

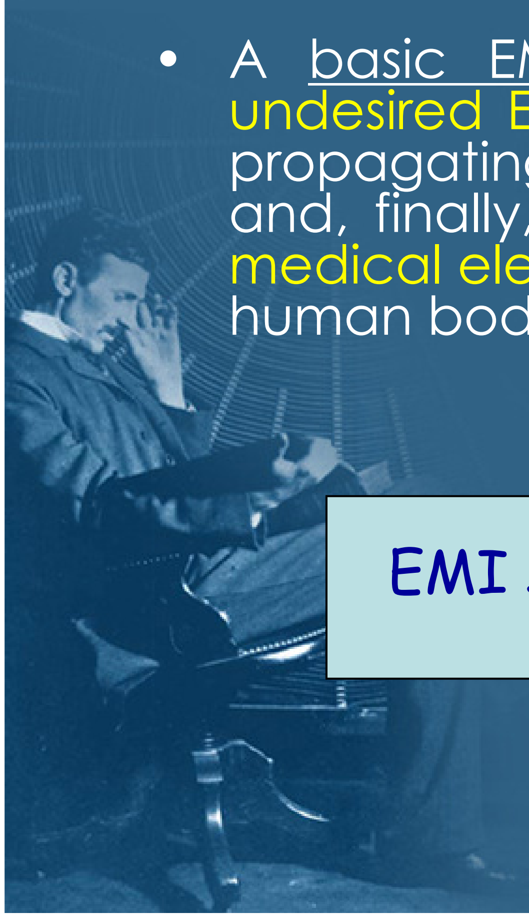

- A basic EMC model, includes *EMI source* (any kind of undesired EMP), *coupling path* which is related to EM fields propagating in free space, material medium or conductors, and, finally, *EMI victim* - any kind of electrical equipment, medical electronic equipment (e.g. pacemaker), or even the human body itself.

EMI source ⟷ Coupling path ⟷ EMI victim

A basic EMC model

Université Clermont Auvergne

Department of Electronics
University of Split,
Split, Croatia

Introduction to Computational Electromagnetics (CEM) and Electromagnetic Compatibility (EMC)

EMC computational models and solution methods

- In principle, all EMC models arise from the rigorous EM theory concepts and foundations based on *Maxwell equations*.
- EMC models are analysed using either *analytical* or *numerical methods.*
- *Analytical models* are not useful for accurate simulation of electric systems, or their use is restricted to the solution of rather simplified geometries.
- More accurate simulation of various practical engineering problems is possible by the use of *numerical methods.*

Introduction to Computational Electromagnetics (CEM) and Electromagnetic Compatibility (EMC)

Classification of EMC models

- Regarding underlying *theoretical background* EMC models can be classified as:

  ✓ circuit theory models featuring the concentrated electrical parameters
  ✓ transmission line models using distributed parameters in which low frequency electromagnetic field coupling are taken into account
  ✓ models based on the full-wave approach taking into account radiation effects for the treatment of electromagnetic wave propagation problems

Department of Electronics
University of Split,
Split, Croatia

Introduction to Computational Electromagnetics (CEM) and Electromagnetic Compatibility (EMC)

Summary remarks on EMC modeling

- The *main limits* to EMC modeling arise from the ***physical complexity*** of the considered electric system.

- Sometimes even the *electrical properties of the system* are too difficult to determine, or the number of independent parameters necessary for building a valid EMC model is too large for a practical computer code to handle.

Department of Electronics
University of Split,
Split, Croatia

Introduction to Computational Electromagnetics (CEM) and Electromagnetic Compatibility (EMC)

Summary remarks on EMC modeling

- The advanced EMC modeling approach is based on ***integral equation formulations*** in the FD and TD and related *BEM* solution featuring the direct and indirect approach, respectively.
- This approach is preferred over a partial differential equation formulations and related numerical methods of solution, as the integral equation approach is based on the corresponding *fundamental solution of the linear operator* and, therefore, provides more accurate results.
- This *higher accuracy level* is paid with more complex formulation, than it is required within the framework of the partial differential equation approach, and related computational cost.

Department of Electronics
University of Split,
Split, Croatia

WIRE ANTENNAS

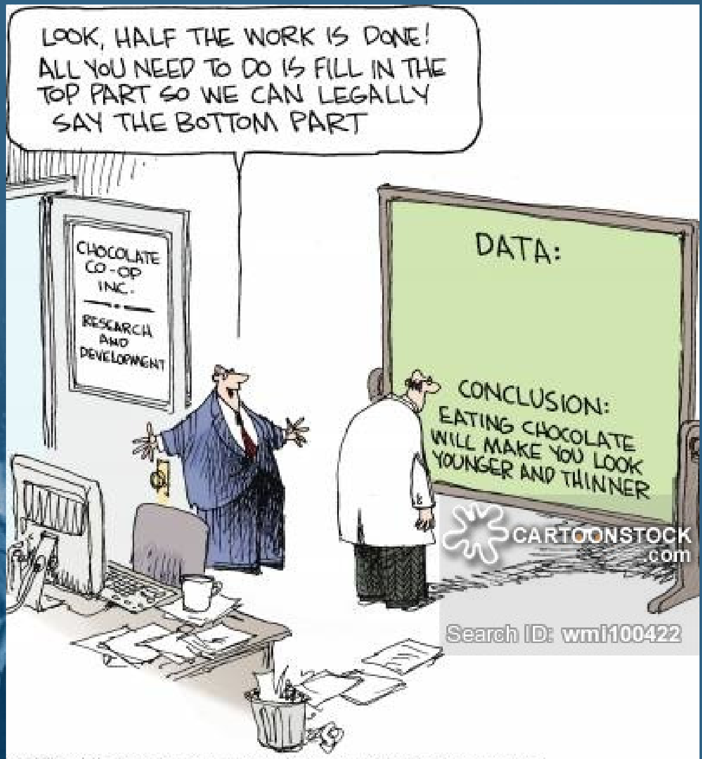

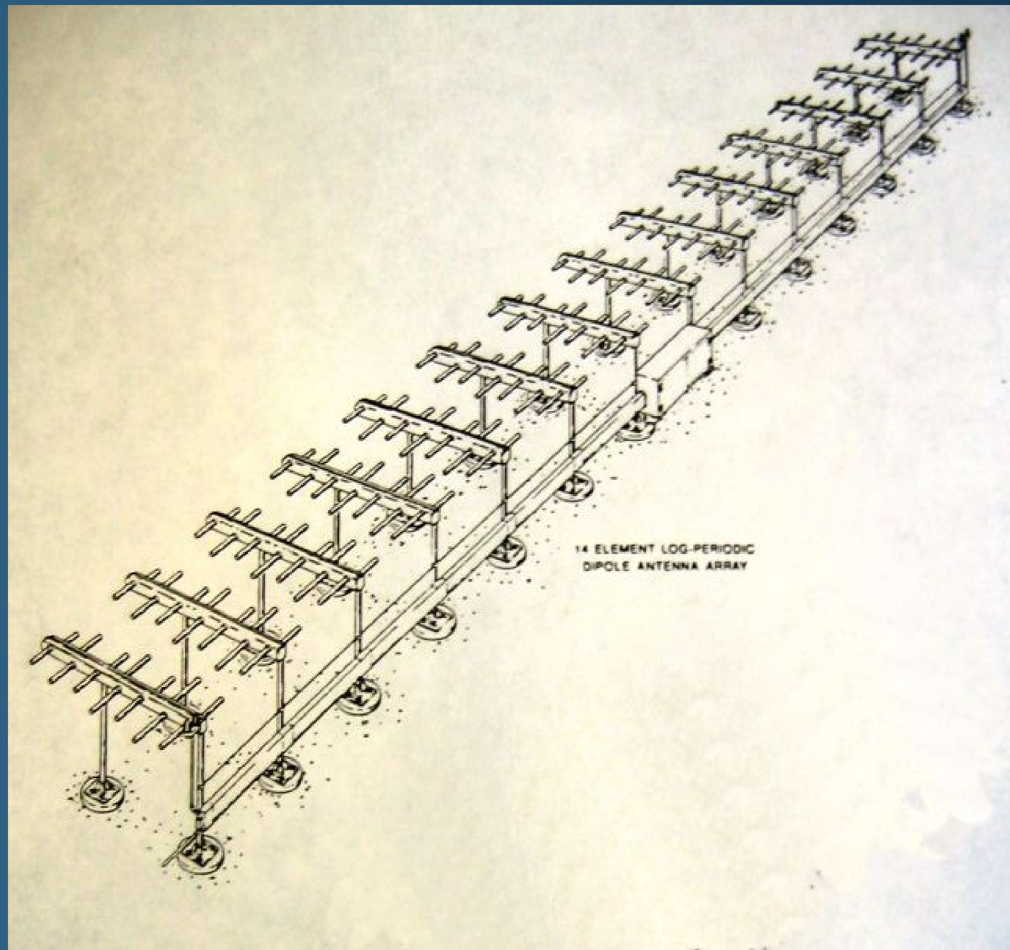

Department of Electronics
University of Split,
Split, Croatia

Frequency domain analysis of wire antennas

- In addition to antenna design the model of horizontal wires above lossy half-space has numerous applications in (EMC) in the analysis of aboveground lines and cables.
- The current distribution along the multiple wire structure is governed by the set of Pocklington equation for half-space problems.
- The influence of lossy half-space can be taken into account via the reflection coefficient (RC) approximation.

Université Clermont Auvergne

FD analysis of wire antennas

Department of Electronics
University of Split,
Split, Croatia

- The geometry of interest consists of *M* parallel straight wires horizontally placed above a lossy ground at height *h*.

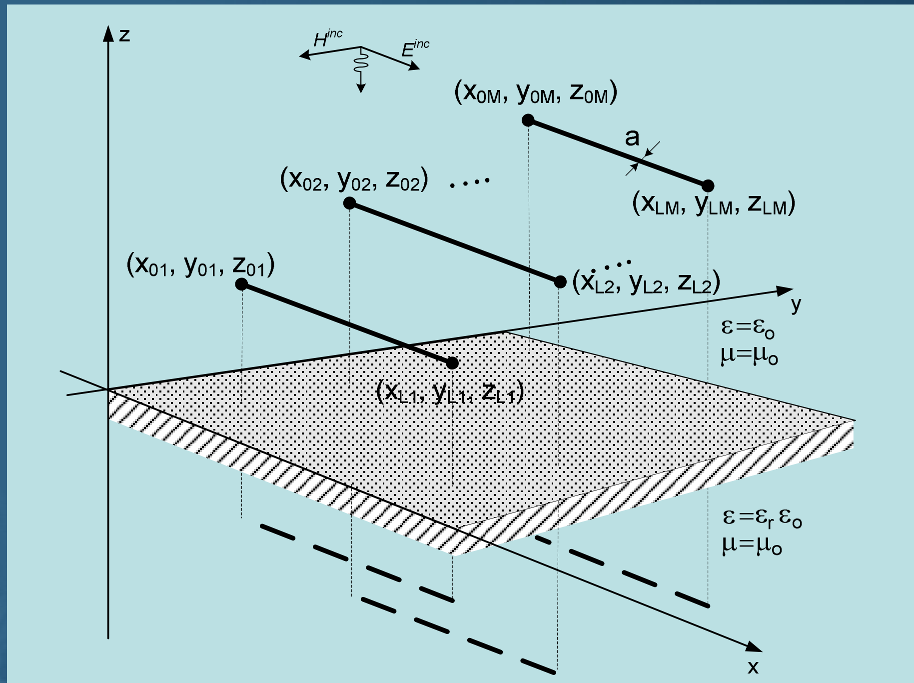

The geometry of the problem

- All wires are assumed to have same radius *a* and the length of the m-th wire is equal L_m.

FD analysis of wire antennas

Department of Electronics
University of Split,
Split, Croatia

The analysis starts by considering a single straight wire above a dissipative half-space.

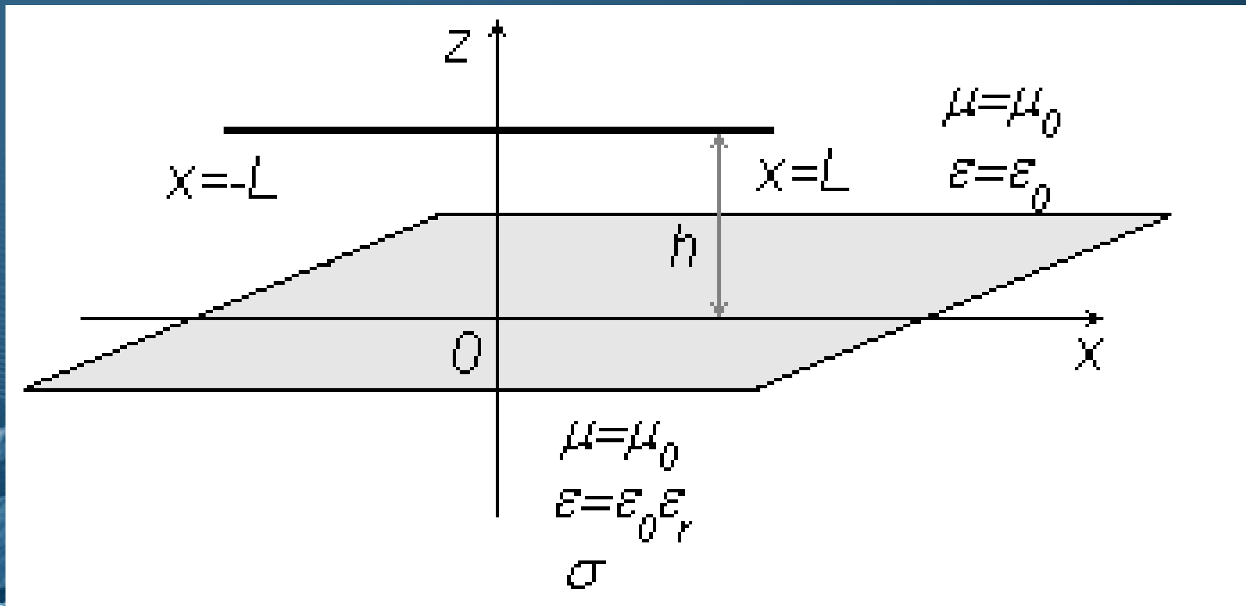

Horizontal antenna over imperfect ground

UNIVERSITÉ Clermont Auvergne

Department of Electronics
University of Split,
Split, Croatia

FD analysis of wire antennas

- The integral equation can be derived by enforcing the interface conditions for the *E*-field at the wire surface:

$$\vec{e}_x \cdot \left(\vec{E}^{exc} + \vec{E}^{sct} \right) = 0$$

- The excitation represents the sum of the incident field and field reflected from the lossy ground:

$$\vec{E}^{exc} = \vec{E}^{inc} + \vec{E}^{ref}$$

- The scattered field can be written as:

$$\vec{E}^{sct} = -j\omega\vec{A} - \nabla\varphi$$

where **A** is the magnetic vector potential and ϕ is the scalar potential.

According to the thin wire approximation (TWA) only the axial component of the magnetic potential differs from zero:

$$E_x^{sct} = -j\omega A_x - \frac{\partial\varphi}{\partial x}$$

$$A_x = \frac{\mu}{4\pi}\int_0^L I(x')g(x,x')dx' \qquad \varphi(x) = \frac{1}{4\pi\varepsilon}\int_0^L q(x')g(x,x')dx'$$

while *q*(*x*) is the charge distribution and *I*(*x'*) is the induced current along the wire.

Department of Electronics
University of Split,
Split, Croatia

FD analysis of wire antennas

- Green function $g(x,x')$ is given by:

$$g(x,x') = g_0(x,x') - R_{TM}\, g_i(x,x')$$

where $g_0(x, x')$ is the free space-Green function and $g_i(x, x')$ arises from the image theory:

$$g_o(x,x') = \frac{e^{-jk_o R_o}}{R_o} \qquad g_i(x,x') = \frac{e^{-jk_o R_i}}{R_i}$$

R_o and Ri, respectively, is the distance from the source to the observation point, and the reflection coefficient is

$$R_{TM} = \frac{n\cos\Theta - \sqrt{n - \sin^2\Theta}}{n\cos\Theta + \sqrt{n - \sin^2\Theta}} \qquad n = \varepsilon_r - j\frac{\sigma}{\omega\varepsilon_0} \qquad \Theta = \operatorname{arctg}\frac{|x - x'|}{2h}$$

Department of Electronics
University of Split,
Split, Croatia

FD analysis of wire antennas

- The linear charge density and the current distribution along the line are related through the equation of continuity:

$$q = -\frac{1}{j\omega}\frac{dI}{dx}$$

- After mathematical manipulation it follows:

$$\varphi(x) = -\frac{1}{j4\pi\omega\varepsilon}\int_0^L \frac{\partial I(x')}{\partial x'} g(x,x')dx'$$

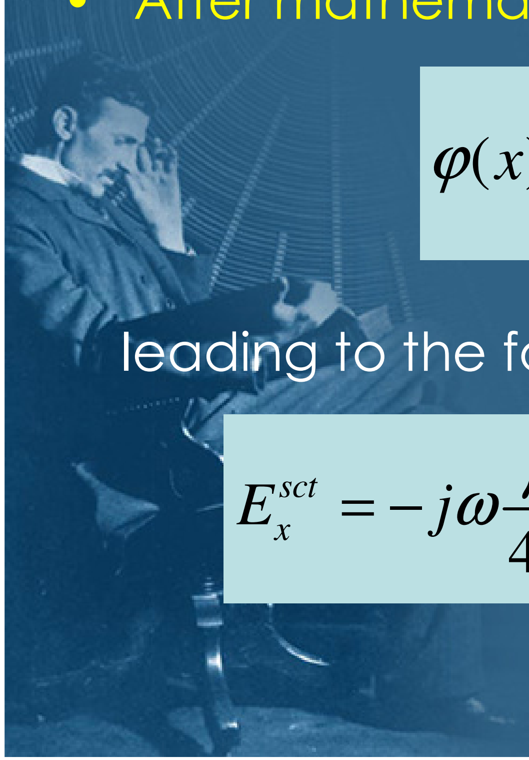

leading to the following integral relationship for the scattered field:

$$E_x^{sct} = -j\omega\frac{\mu}{4\pi}\int_0^L I(x')g(x,x')dx' + \frac{1}{j4\pi\omega\varepsilon}\frac{\partial}{\partial x}\int_0^L \frac{\partial I(x')}{\partial x'} g(x,x')dx'$$

FD analysis of wire antennas

Department of Electronics
University of Split,
Split, Croatia

- Combining previous equations results in the following integral equation for the current distribution induced along the wire:

$$\boxed{E_x^{exc} = j\omega \frac{\mu}{4\pi} \int_0^L I\left(x'\right) g\left(x, x'\right) dx' - \frac{1}{j4\pi\omega\varepsilon} \frac{\partial}{\partial x} \int_0^L \frac{\partial I\left(x'\right)}{\partial x'} g\left(x, x'\right) dx'}$$

- This equation is well-known in antenna theory representing one of the most commonly used variants of the Pocklington's integro-differential equation for half space problems.

- This integro-differential equation is particularly attractive for numerical modeling, as there is no second-order differential operator under the integral sign.

The electric field components are:

$$E_x = \frac{1}{j4\pi\omega\varepsilon_0} \left[-\int_{-L}^{L} \frac{\partial I(x')}{\partial x'} \frac{\partial g(x, x')}{\partial x'} dx' + k^2 \int_{-L}^{L} g(x, x') I(x') dx' \right]$$

$$E_z = \frac{1}{j4\pi\omega\varepsilon_0} \int_{-L}^{L} \frac{\partial I(x')}{\partial x'} \frac{\partial g(x', z)}{\partial z} dx' \qquad E_y = \frac{1}{j4\pi\omega\varepsilon_0} \int_{-L}^{L} \frac{\partial I(x')}{\partial x'} \frac{\partial g(x', y)}{\partial y} dx'$$

Department of Electronics
University of Split,
Split, Croatia

FD analysis of wire antennas

- Vertical wire above a real ground

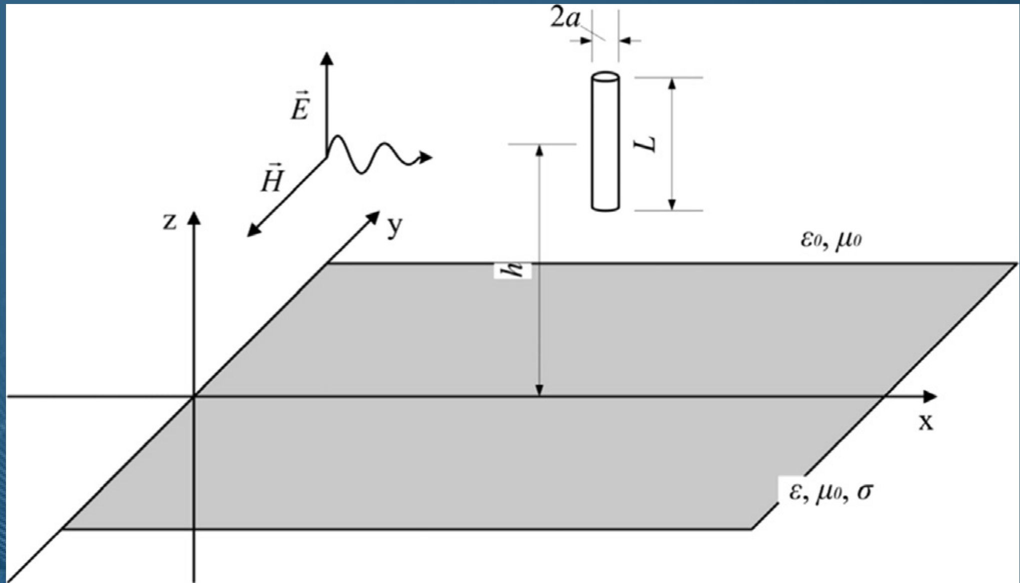

- Integro-differential equation (IDE) for vertical wire

$$\left[\frac{\partial^2}{\partial z^2}+k^2\right]\int_{h-(L/2)}^{h+(L/2)} I(z')g(z,z')dz' = -j4\pi\frac{k}{Z_0}E_z^{exc}$$

The propagation constant k is given by

$$k=\omega\sqrt{\mu_0\varepsilon_0}$$

and Z_0 is the free space impedance

$$Z_0=\sqrt{\frac{\mu_0}{\varepsilon_0}}$$

The total Green function is, as follows

$$g(z,z')=g_0(z,z')-\Gamma_{Fr}^{ref}g_i(z,z')$$

Department of Electronics
University of Split,
Split, Croatia

FD analysis of wire antennas

- Vertical wire penetrating the ground

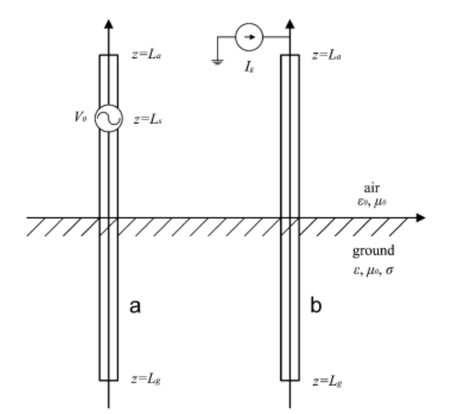

Fig. 4. Vertical antenna penetrating the ground excited by a voltage source (a) and by a current source (b).

with

$$\mu=\sqrt{\lambda^2-k^2};\ \mu_E=\sqrt{\lambda^2-k_2^2};\ k_2^2=\underline{n}k^2 \qquad (21)$$

where $\underline{n}$ is the relative complex permittivity of the air–ground interface given by (14), while ε_{eff} is the complex permittivity of the ground determined by (15), and k is wave propagation of free space

- Integro-differential equation for vertical wire penetrating the ground

$$E_z^{inc}=-\frac{1}{j4\pi\omega\varepsilon_{eff}}\left[\begin{array}{l}\int_{-L_g}^{0}\left(\frac{\partial^2}{\partial z^2}+k_2^2\right)G^{22}(\rho,z,z')I(z')dz'+\\ \int_{0}^{L_a}\left(\frac{\partial^2}{\partial z^2}+k_2^2\right)G^{12}(\rho,z,z')I(z')dz'\end{array}\right];\quad z\le 0,$$

$$E_z^{inc}=-\frac{1}{j4\pi\omega\varepsilon_0}\left[\begin{array}{l}\int_{-L_g}^{0}\left(\frac{\partial^2}{\partial z^2}+k_1^2\right)G^{21}(\rho,z,z')I(z')dz'+\\ \int_{0}^{L_a}\left(\frac{\partial^2}{\partial z^2}+k_1^2\right)G^{11}(\rho,z,z')I(z')dz'\end{array}\right];\quad z>0,$$

where

$$G^{11}(\rho,z,z')=\frac{g_0(z,z')}{-g_i(z,z')+g_{Sa}(\rho,z,z')},\ \text{for points } z>0 \text{ and } z'>0$$

while g_0, g_i are defined by (13) and g_{Sa} is given by

$$g_{Sa}(\rho,z,z')=2\int_0^\infty J_0(\lambda\rho)e^{-\mu(z+z')}\frac{\varepsilon_{eff}}{\varepsilon_{eff}\mu+\varepsilon_0\mu_E}\lambda d\lambda$$

Furthermore

$$G^{22}(\rho,z,z')=\frac{g_0(z,z')}{-g_i(z,z')+g_{Su}(\rho,z,z')},\ \text{for points } z<0 \text{ and } z'<0 \qquad (22)$$

while g_0, g_i, g_{Su} are defined, as follows:

$$g_0(z,z')=\frac{e^{-jk_2R}}{R},\quad g_i(z,z')=\frac{e^{-jk_2R_i}}{R_i} \qquad (23)$$

$$g_{Su}(\rho,z,z')=2\int_0^\infty J_0(\lambda\rho)e^{-\mu_E(z+z')}\frac{\varepsilon_0}{\varepsilon_0\mu_E+\varepsilon_{eff}\mu}\lambda d\lambda \qquad (24)$$

The Green functions related to transmitted field are given by:

$$G^{12}(\rho,z,z')=2\int_0^\infty J_0(\lambda\rho)e^{-\mu_E|z|}e^{-\mu|z'|}\frac{\varepsilon_{eff}}{\varepsilon_{eff}\mu+\varepsilon_0\mu_E}\lambda d\lambda \qquad (25)$$

for points $z<0$ and $z'>0$, and

$$G^{21}(\rho,z,z')=2\int_0^\infty J_0(\lambda\rho)e^{-\mu_E|z|}e^{-\mu|z'|}\frac{\varepsilon_0}{\varepsilon_{eff}\mu+\varepsilon_0\mu_E}\lambda d\lambda \qquad (26)$$

for points $z>0$ and $z'<0$:

Sommerfeld integrals (20), (24)–(28) are evaluated numerically using Simpson adaptive quadrature in complex plane [21].

Furthermore, certain continuity conditions have to be satisfied at the air–ground interface, i.e.:

$$I(z=0^+)=I(z=0^-) \qquad (27)$$

$$\frac{\partial I(z=0^+)}{\partial z}\varepsilon_{eff}=\frac{\partial I(z=0^-)}{\partial z}\varepsilon_0 \qquad (28)$$

where $(+)$ and $(-)$ denote above and below the interface, respectively.

UNIVERSITÉ Clermont Auvergne

FD analysis of wire antennas

Department of Electronics
University of Split,
Split, Croatia

- An extension to the wire array is straightforward and results in the the set of coupled Pocklington integral equations:

$$E_x^{exc} = -\frac{1}{j4\pi\omega\varepsilon_0}\sum_{n=1}^{M}\int_{-L_n/2}^{L_n/2}\left[\frac{\partial^2}{\partial x^2}+k_1^2\right]\left[g_{0mn}(x,x') - R'_{TM}\, g_{imn}(x,x')\right] I_n(x')\,dx'$$

$$m = 1, 2, \ldots M$$

where $I_n(x')$ is the unknown current distribution induced on the n-th wire axis, $g_{0mn}(x,x`)$ is the free space Green function, while $g_{imn}(x,x`)$ *arises from* the image theory:

$$g_{0mn}(x,x') = \frac{e^{-jk_1R_{1mn}}}{R_{1mn}}$$

$$g_{0mn}(x,x') = \frac{e^{-jk_1R_{1mn}}}{R_{1mn}}$$

FD analysis of wire antennas

Department of Electronics
University of Split,
Split, Croatia

- The wires are excited by a plane wave of arbitrary incidence

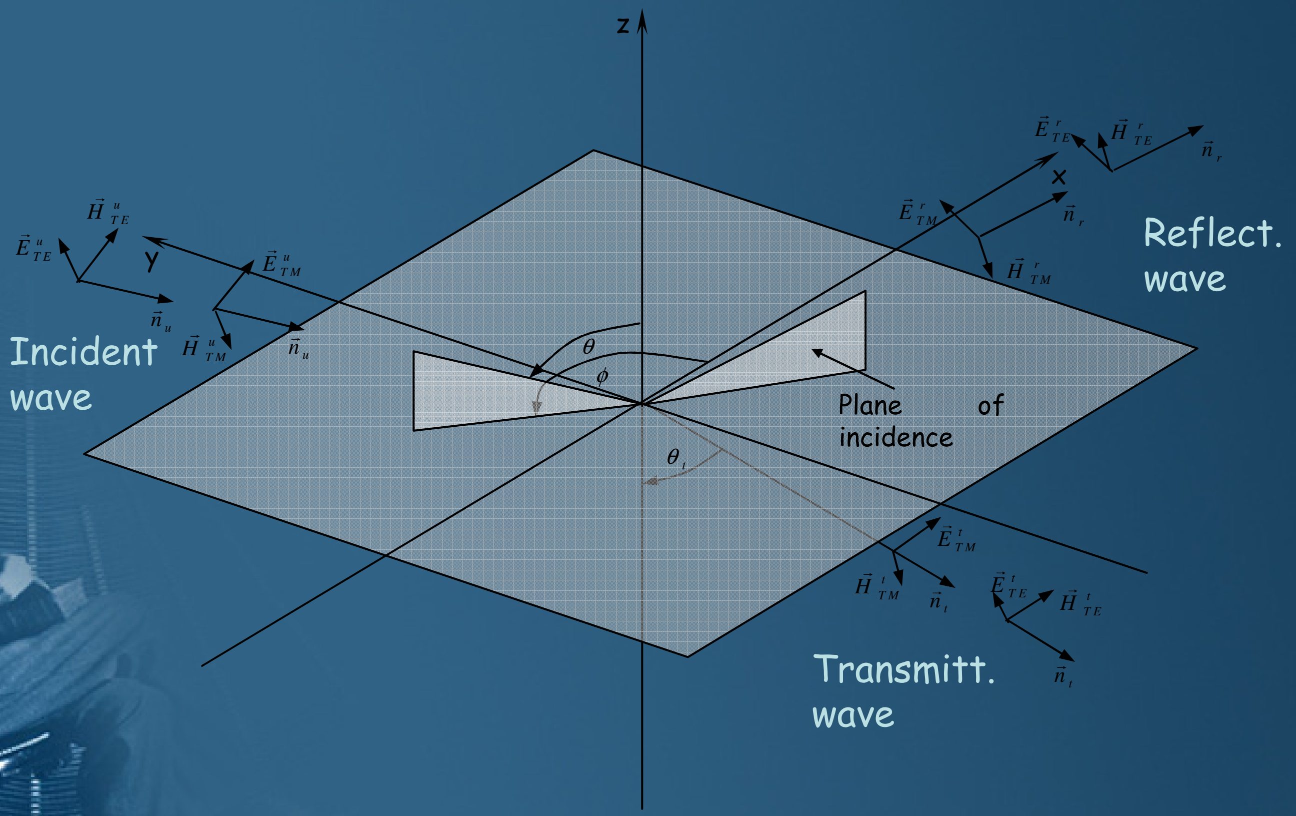

Incident, reflected and transmitted wave

Clermont-Ferrand, 03 April 2018

FD analysis of wire antennas

Department of Electronics
University of Split,
Split, Croatia

- The tangential component of an incident plane wave can be represented in terms of its vertical E_V and horizontal E_H component:

$$
\begin{aligned}
E_x^{exc} &= E_x^i + E_x^r = \\
&E_0(\sin\alpha\sin\phi - \cos\alpha\cos\theta\cos\phi)e^{-jk_1\vec{n}_i\cdot\vec{r}} + \\
&+E_0\left(R_{TE}\sin\alpha\sin\phi + R_{TM}\cos\alpha\cos\theta\cos\phi\right)e^{-jk_1\vec{n}_r\cdot\vec{r}}
\end{aligned}
$$

where α is an angle between *E-field* vector and the plane of incidence.

R_{TM} and R_{TE} are the vertical and horizontal Fresnel reflection coefficients at the air-earth interface given by:

$$R_{TM} = \frac{\underline{n}\cos\theta - \sqrt{\underline{n} - \sin^2\theta}}{\underline{n}\cos\theta + \sqrt{\underline{n} - \sin^2\theta}} \qquad R_{TE} = \frac{\cos\theta - \sqrt{\underline{n} - \sin^2\theta}}{\cos\theta + \sqrt{\underline{n} - \sin^2\theta}}$$

$$
\begin{aligned}
\vec{n}_i\cdot\vec{r} &= -x\sin\theta\cos\phi - y\sin\theta\sin\phi - z\cos\theta \\
\vec{n}_r\cdot\vec{r} &= -x\sin\theta\cos\phi - y\sin\theta\sin\phi + z\cos\theta
\end{aligned}
$$

FD analysis of wire antennas

Department of Electronics
University of Split,
Split, Croatia

- The *E*-field components are given, as follows:

$$E_x = \frac{1}{j4\pi\omega\varepsilon_0}\sum_{n=1}^{M}\left[-\int_{-L_n}^{L_n}\frac{\partial I_n(x')}{\partial x'}\frac{\partial G_{nm}(x,x')}{\partial x'}dx' + k^2\int_{-L_n}^{L_n}G_{nm}(x,x')I_n(x')dx'\right]$$

$$E_y = \frac{1}{j4\pi\omega\varepsilon_0}\sum_{n=1}^{M}\int_{-L_n}^{L_n}\frac{\partial I_n(x')}{\partial x'}\frac{\partial G_{nm}(x,x')}{\partial y}dx'$$

$$E_z = \frac{1}{j4\pi\omega\varepsilon_0}\sum_{n=1}^{M}\int_{-L_n}^{L_n}\frac{\partial I_n(x')}{\partial x'}\frac{\partial G_{nm}(x,x')}{\partial z}dx'$$

where $m=1, 2, \ldots, M$ and Green function *G* is given by:

$$G_{nm}(x,x') = g_{0nm}(x,x') - R_{TM}\, g_{inm}(x,x')$$

Department of Electronics
University of Split,
Split, Croatia

FD analysis of wire antennas

BEM solution of Pocklington equation system

- The BEM procedure starts, as follows:

$$I(x') = I_{1i}\frac{x_{2i}-x'}{\Delta x} + I_{2i}\frac{x'-x_{1i}}{\Delta x}$$

- Performing certain mathematical manipulations and BEM discretisation results in the following matrix equation:

$$\sum_{k=1}^{N_e}[Z]_{pk}\{I\}_k = \{V\}_p$$

N_e - the total number of elements

$p=1,2,\ldots,M$

$[Z]_{pk}$ - the interaction matrix:

$$[Z]_{pk}^{e} = -\int_{\Delta l_p}\int_{\Delta l_k}\{D\}_p\{D'\}_k^T g_{ji}(x,x')dx'dx + k^2\int_{\Delta l_p}\int_{\Delta l_k}\{f\}_l\{f'\}_k^T g_{ji}(x,x')dx'dx$$

- Vectors $\{f\}$ and $\{f'\}$ contain shape functions $f_n(x)$ and $f_n(x')$, while $\{D\}$ and $\{D'\}$ contain their derivatives.

- The vector $\{V\}_p$ represents the voltage along the segment:

$$\{V\}_p = -j4\pi\omega\varepsilon_0\int_{\Delta l_p}E_x^{inc}(x)\{f\}_p dx$$

FD analysis of wire antennas

Department of Electronics
University of Split,
Split, Croatia

UNIVERSITÉ Clermont Auvergne

The BEM field calculation

- Applying the BEM formalism to field expressions it follows:

$$E_x = \frac{1}{j4\pi\omega\varepsilon_0}\sum_{n=1}^{M}\sum_{i=1}^{N_j}\left[-\frac{I_{i+1,n}-I_{i,n}}{\Delta x}\int_{x_{i,n}}^{x_{i+1,n}}\frac{\partial G_{nm}(x,x')}{\partial x'}dx' + k^2\int_{x_{i,n}}^{x_{i+1,n}} G_{nm}(x,x')I_{in}(x')dx'\right];$$

$$m = 1,2,\ldots,M$$

$$E_y = \frac{1}{j4\pi\omega\varepsilon_0}\sum_{n=1}^{M}\sum_{i=1}^{N_j}\frac{I_{i+1,n}-I_{i,n}}{\Delta x}\int_{x_{i,n}}^{x_{i+1,n}}\frac{\partial G_{nm}(x,x')}{\partial y}dx'; \quad m = 1,2,\ldots,M$$

$$E_z = \frac{1}{j4\pi\omega\varepsilon_0}\sum_{n=1}^{M}\sum_{i=1}^{N_j}\frac{I_{i+1,n}-I_{i,n}}{\Delta x}\int_{x_{i,n}}^{x_{i+1,n}}\frac{\partial G_{nm}(x,x')}{\partial z}dx'; \quad m = 1,2,\ldots,M$$

- N_j is the total number of boundary elements on the j-th wire

FD analysis of wire antennas

Department of Electronics
University of Split,
Split, Croatia

UNIVERSITÉ Clermont Auvergne

Computational examples

Vertical wire:

- Single wire above a lossy ground

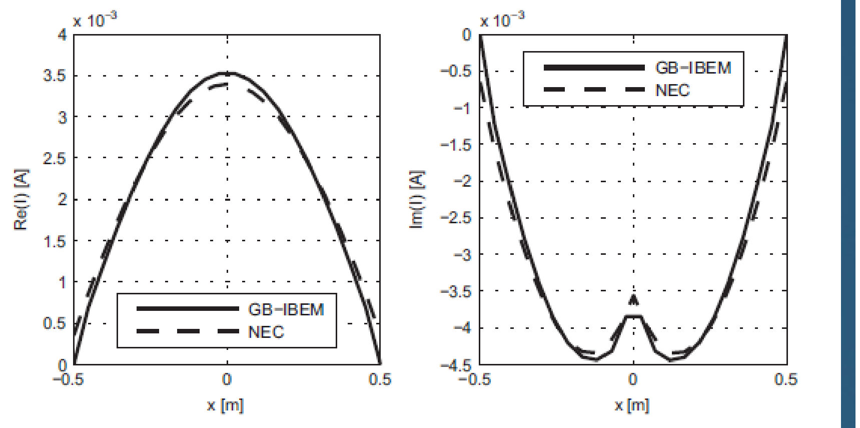

Fig. 2. Current distribution (L=1 m, a=0.005 m, h=2 m, σ=1 mS/m, ε_r=10, V_0=1 V, f=168.2 MHz).

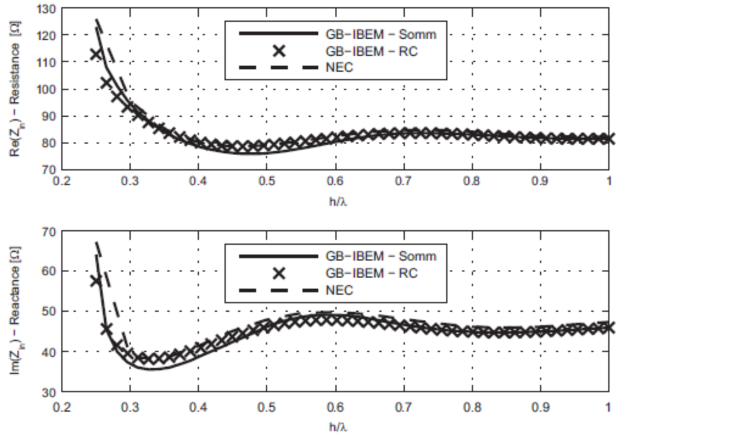

Fig. 3. Impedance (real and imaginary part) of vertical dipole above a real ground (L=1 m, a/λ=0.0005, σ=3 mS/m, ε_r=10, f=3 MHz).

- Wire penetrating the interface

24 D. Poljak et al. / Engineering Analysis with Boundary Elements 50 (2015) 19–28

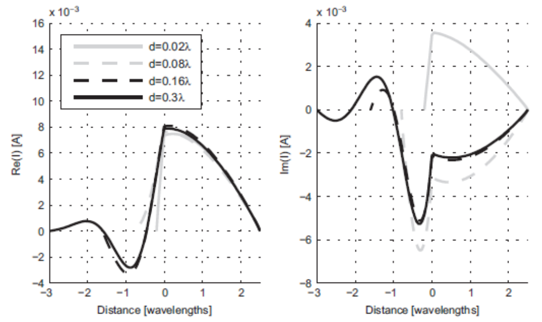

Fig. 5. Current distribution induced along the vertical wire penetrating a ground for various lengths of ground stake and voltage source at bottom end of the air stake.

FD analysis of wire antennas

Computational examples

Numerical results are obtained via TWiNS code for:

- Single wire above a lossy ground
- Wire array above a lossy ground
- Practical example: Yagi-Uda array for VHF TV applications
- Practical example: single LPDA for ILS

FD analysis of wire antennas

Department of Electronics
University of Split,
Split, Croatia

h=1m

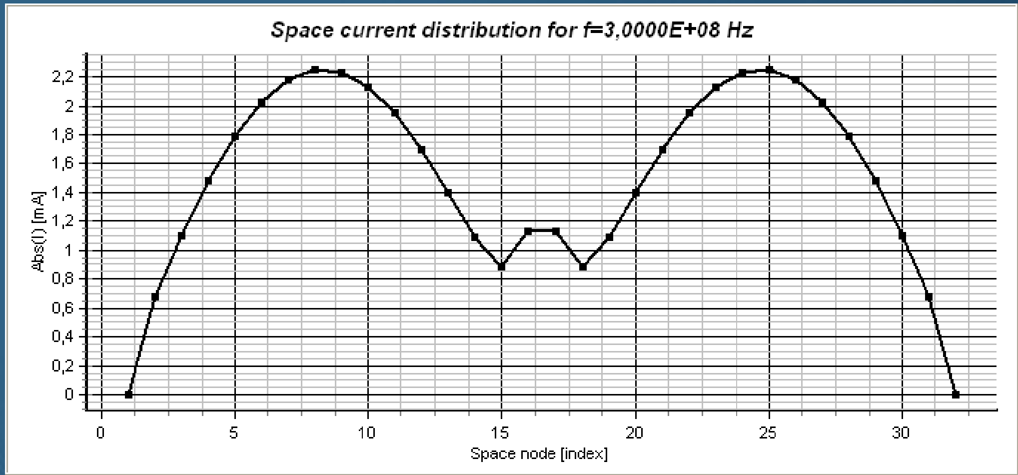

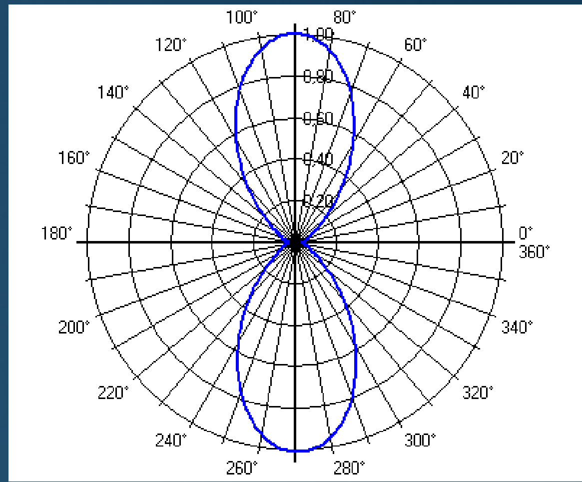

h=0.2m

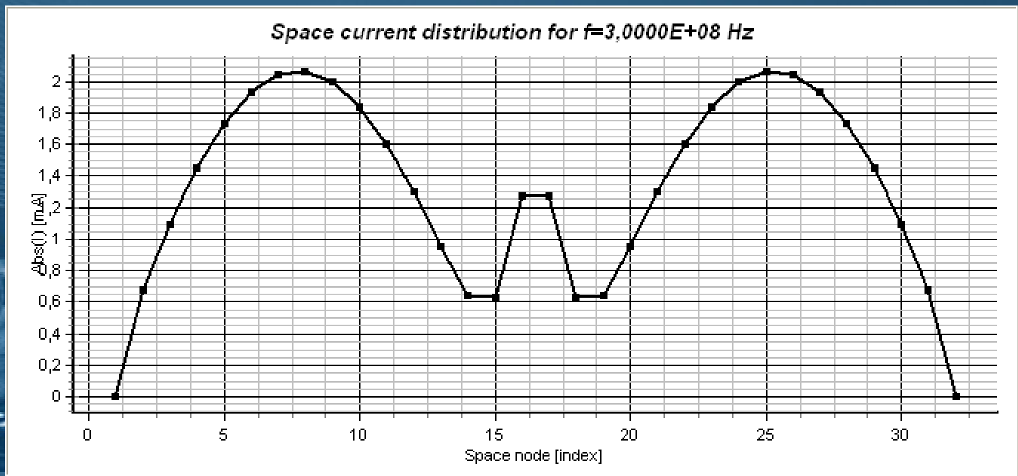

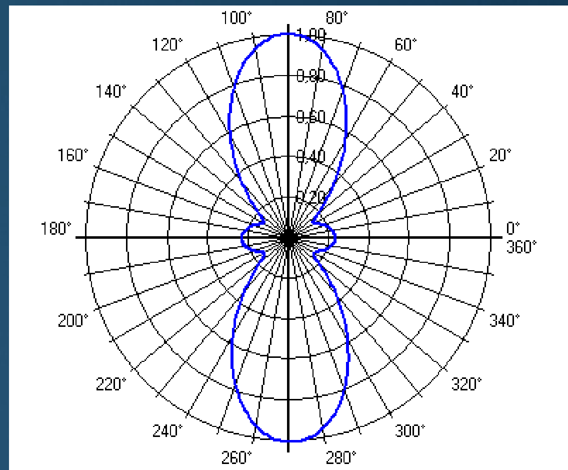

Dipole above a PEC ground, f=300MHz, L=λ

FD analysis of wire antennas

Department of Electronics
University of Split,
Split, Croatia

h=1m

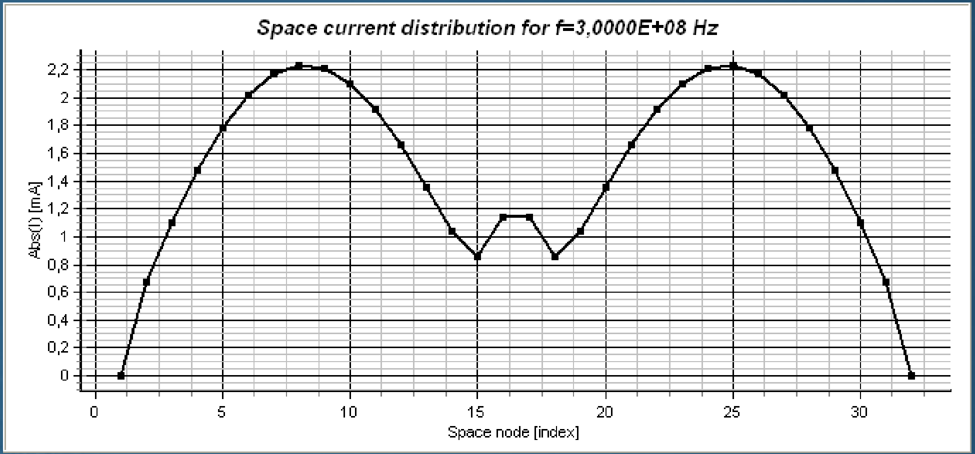

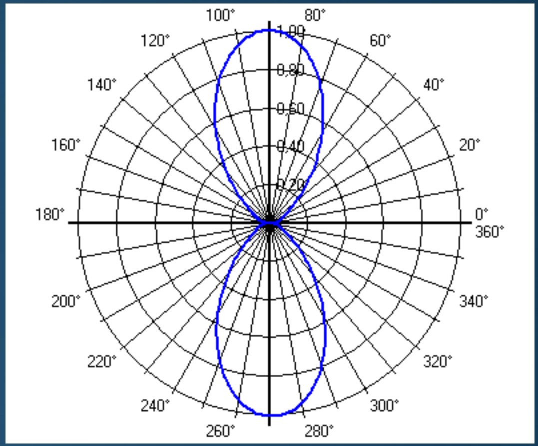

h=0.2m

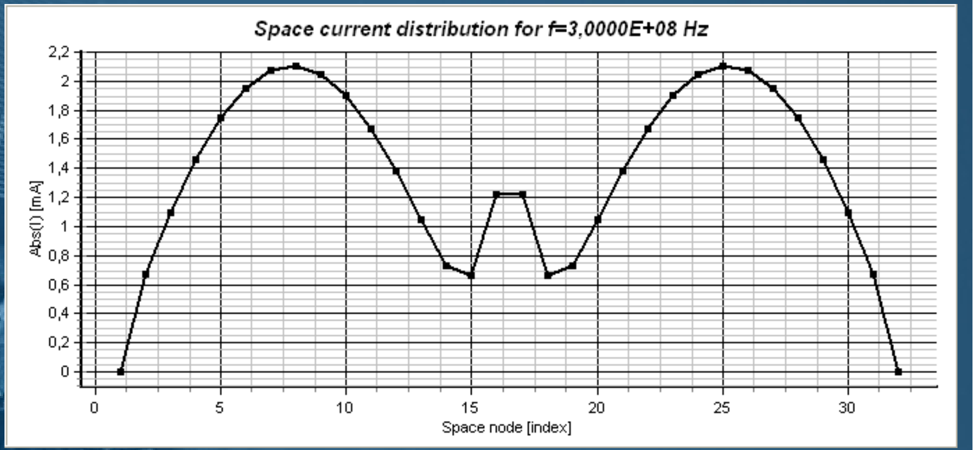

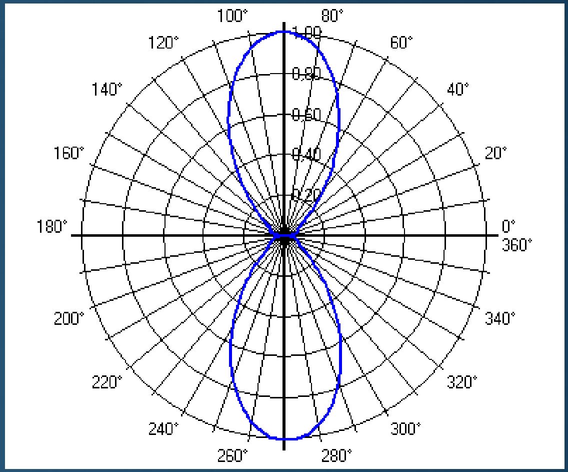

Dipole above a *<u>lossy ground</u>*, *f=300MHz, L=λ/2, ε_r= 30, σ=0.04 S/m*

FD analysis of wire antennas

Department of Electronics
University of Split,
Split, Croatia

h=1m

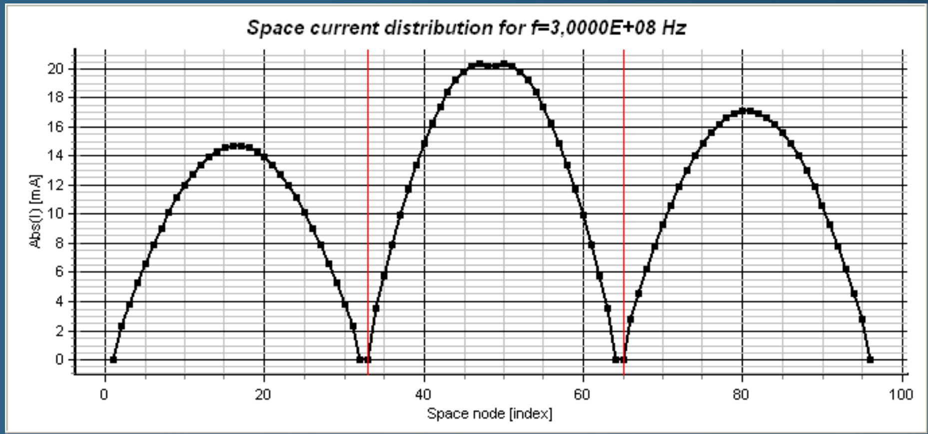

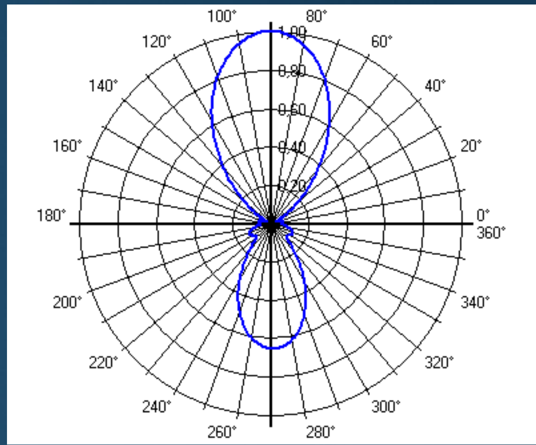

h=0.2m

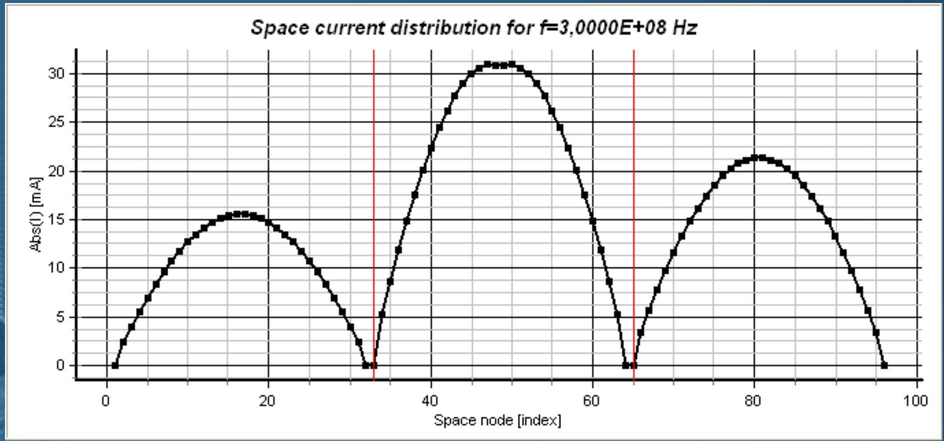

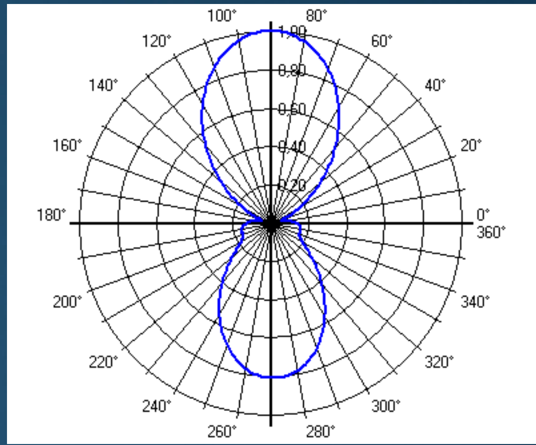

XYplane: Currents and far-field pattern for the Yagi-Uda array above a PEC ground (reflector, fed element + director), $a=0.0025m$, $L_r=0.479m$, $L_f=0.453m$ i $L_d=0.451m$, $d=0.25m$ $V_g=1V$

FD analysis of wire antennas

Department of Electronics
University of Split,
Split, Croatia

h=1m

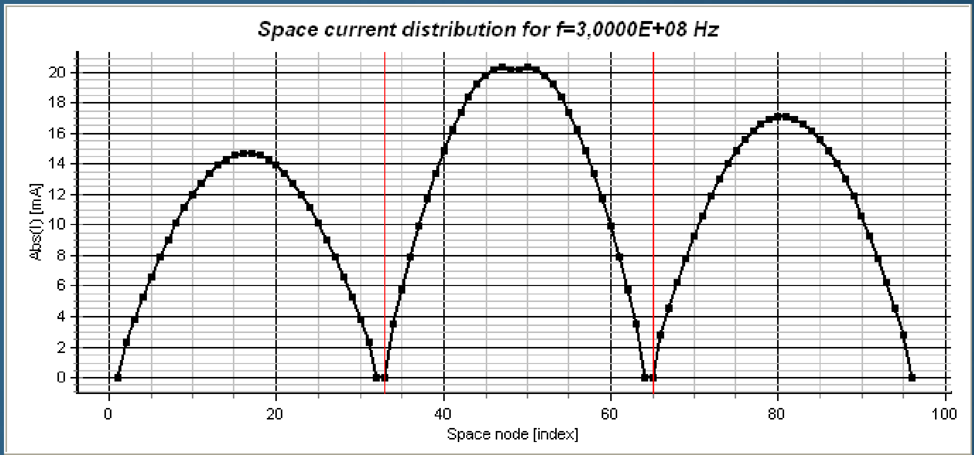

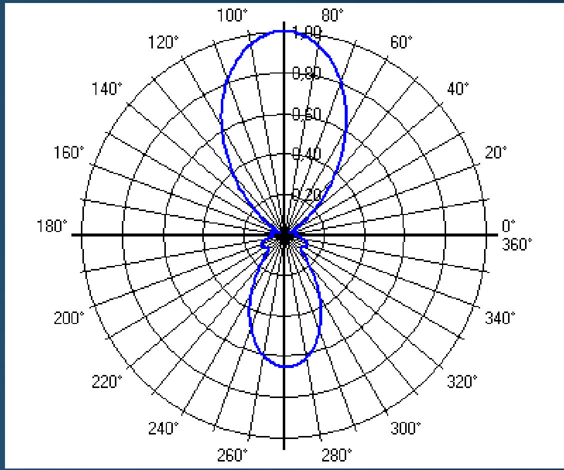

h=0.2m

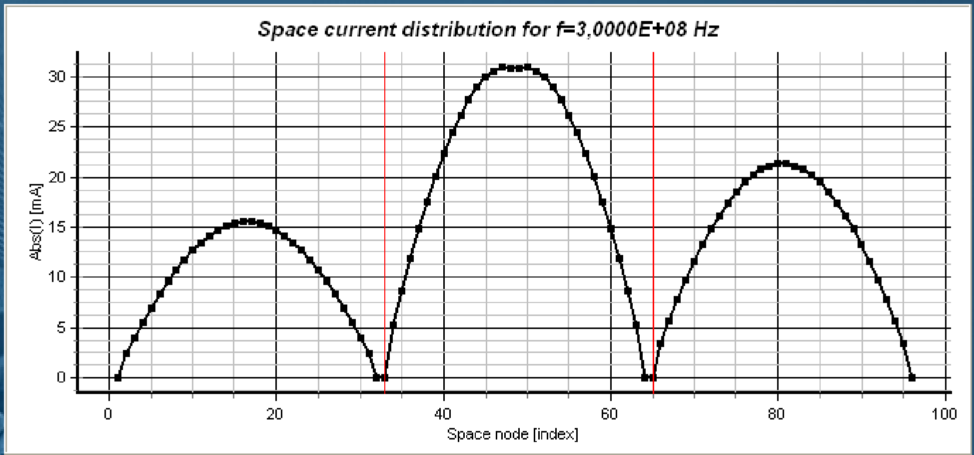

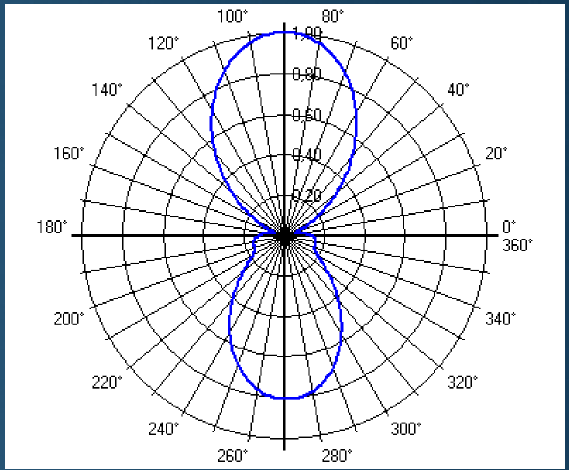

XYplane: Currents and far-field pattern for the Yagi-Uda array above a <u>real ground</u> (reflector, fed element + director),
a=0.0025m, L_r=0.479m, L_f=0.453m i L_d=0.451m, d=0.25m V_g=1V

Clermont-Ferrand, 03 April 2018

FD analysis of wire antennas

Department of Electronics
University of Split,
Split, Croatia

- Dipole antenna for Ground Penetrating Radar (GPR) applications

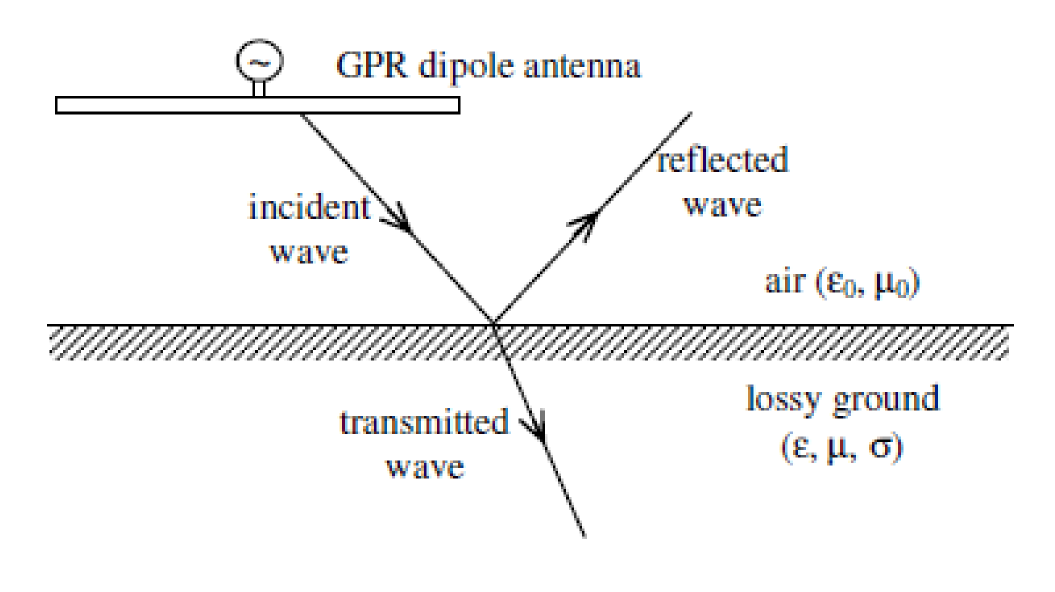

GPR dipole antenna above a lossy half-space

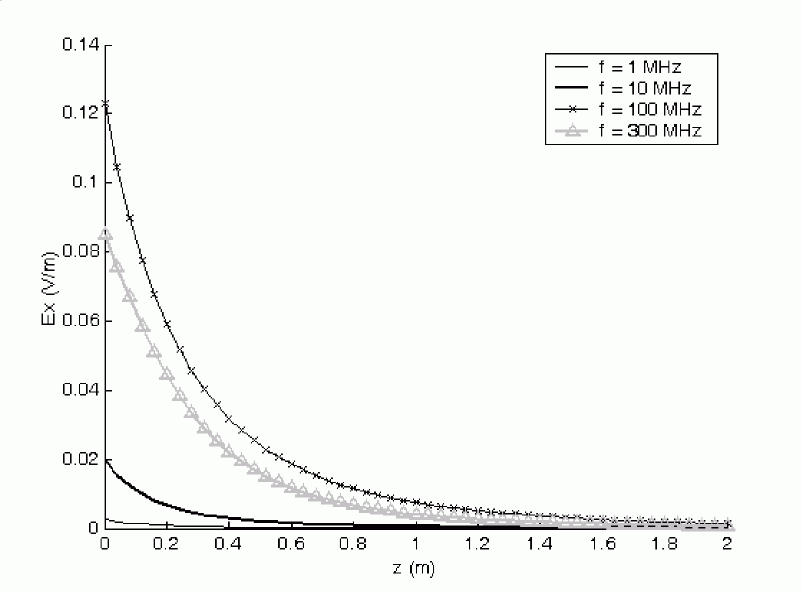

Broadside transmitted field (V/m) into the ground for different frequencies (L=1 m, a=2 mm, h=0.25 m, V_T=1 V, ε_{rg}=10, σ=10 mS/m)

FD analysis of wire antennas

Department of Electronics
University of Split,
Split, Croatia

Yagi-Uda array for VHF TV applications

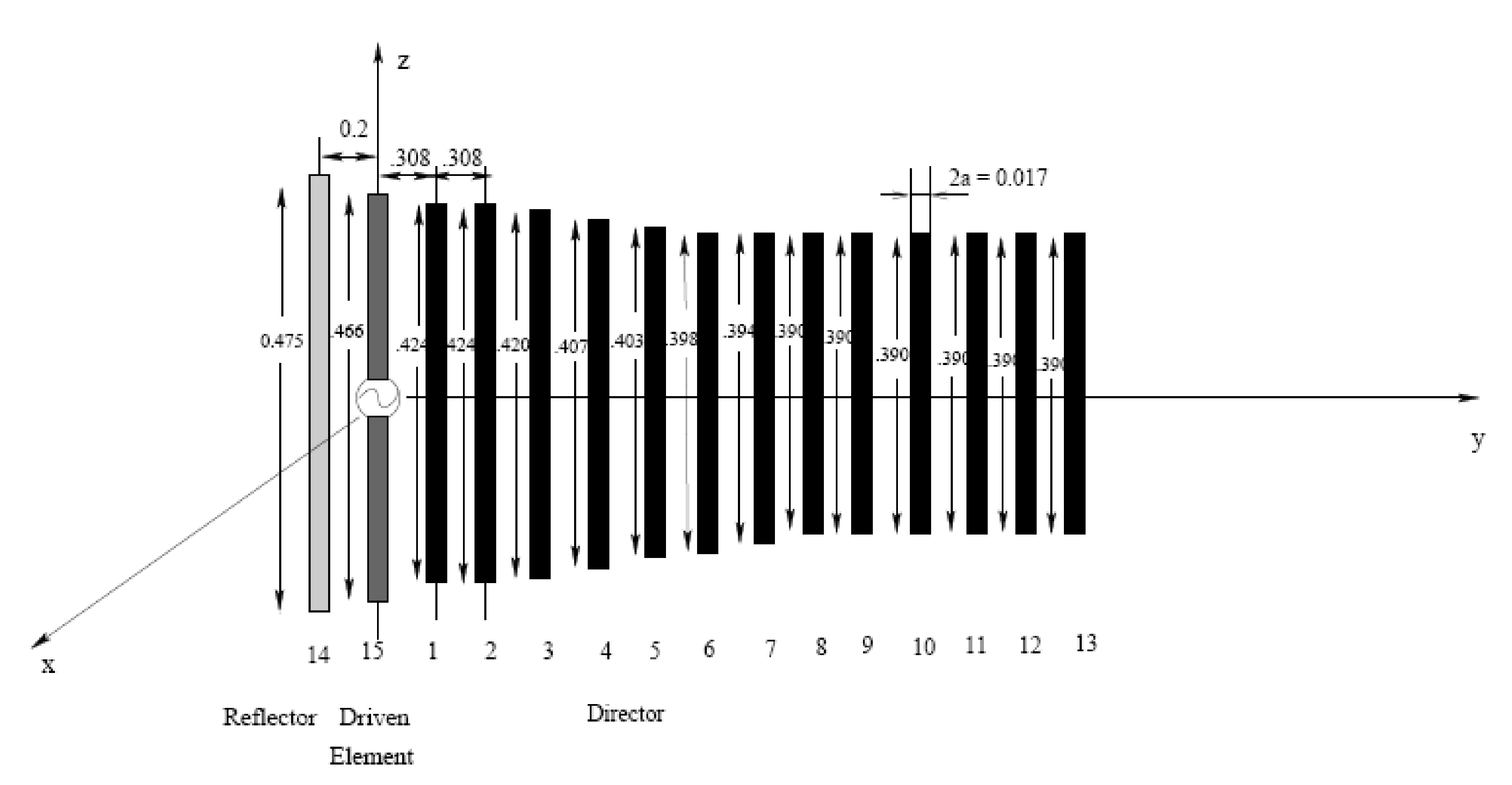

Geometry of Yagi-Uda array with 15 elements

FD analysis of wire antennas

Department of Electronics
University of Split,
Split, Croatia

Yagi-Uda array: technical parameters

- Number of wires N=15
- Number of directors 13
- Operating frequency f=216MHz (frequency of 13th TV channel)
- Wire radius: a= 0.0085λ=0.0118m
- *Director lengths* $l_1=l_2=0.424\lambda=0.589$m, $l_3=0.420\lambda=0.583$m,
- $l_4=0.407\lambda=0.565$m, $l_5=0.403\lambda=0.56$m, $l_6=0.398\lambda=0.553$m,
- $l_7=0.394\lambda=0.547$m, l_8- $l_{13}=0.390\lambda=0.542$m
- *Reflector lengths* $l_{14}=0.475\lambda=0.66$m
- *fed-element length* $l_{15}=0.466\lambda=0.647$m
- *Distance between directors* $d_d=0.308\lambda=0.427$m
- *Distance between reflector and fed-element* $d_r=0.2\lambda=0.278$m

Computational aspects

- $\Delta l \geq 2a$
- L_{tot}= 5.83m, N_{tot}=225

UNIVERSITÉ Clermont Auvergne

FD analysis of wire antennas

Department of Electronics
University of Split,
Split, Croatia

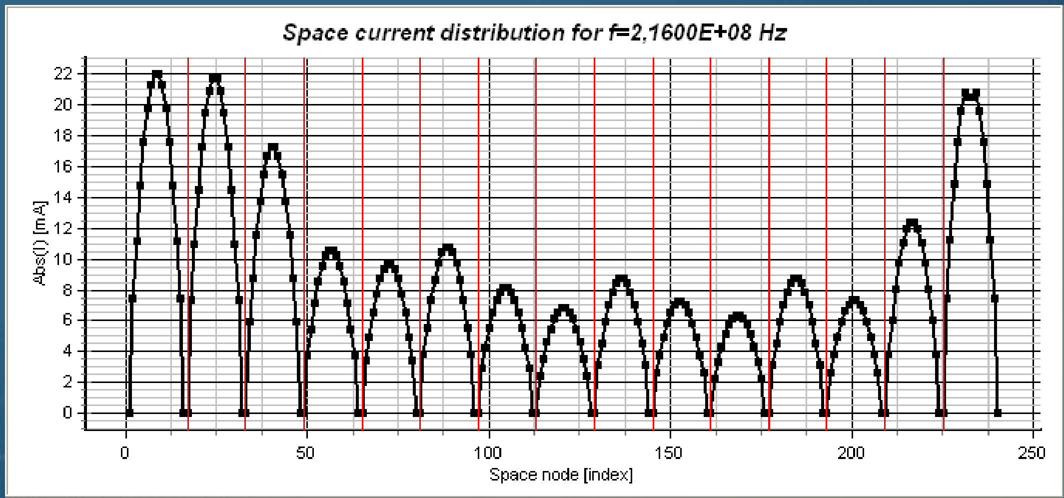

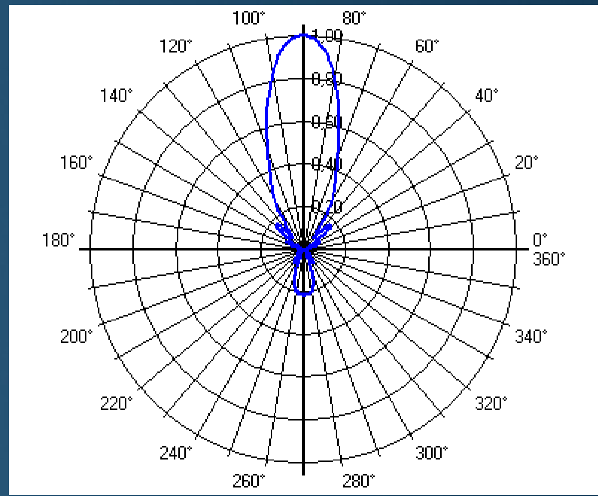

free space

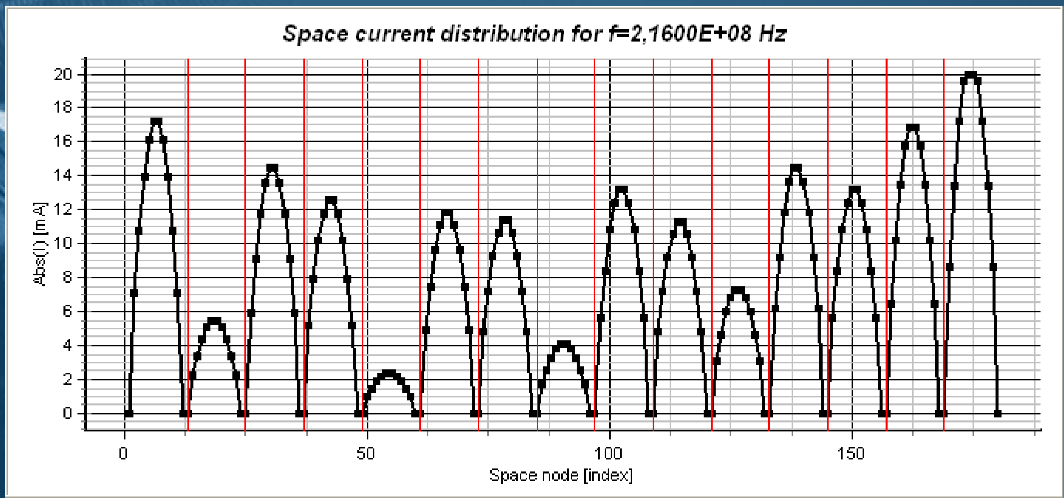

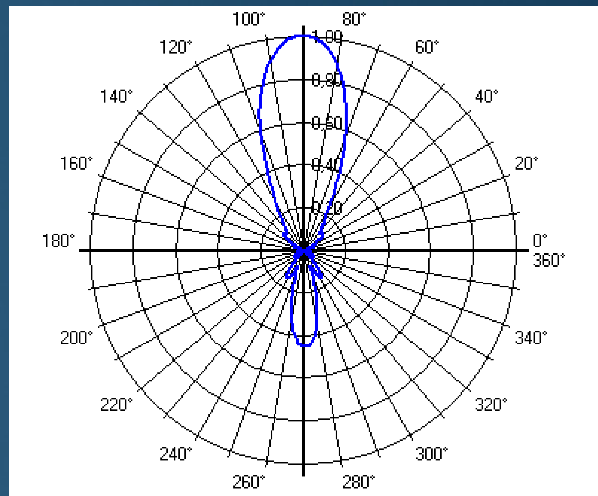

real ground

XYplane: Currents and far-field pattern for the Yagi-Uda array

Department of Electronics
University of Split,
Split, Croatia

FD analysis of wire antennas

Log-periodic dipole array

- LPDA impedance and radiation properties repeat periodically as the logarithm of frequency (VHF and UHF bands; 30MHz to 3GHz).
- The LPDA antennas are easy to optimize, while the crossing of the feeder between each dipole element leads to a mutual cancellation of backlobe components from the individual elements yielding to a very low level of backlobe radiation (around 25dB below main lobe gain at HF and 35dB at VHF and UHF).

The cutoff frequencies of the truncated structure is determined by the electrical lengths of the largest and shortest elements of the structure.

- The use of logarithmic antenna arrays is very often related with electronic beam steering. An important application of LPDA antennas is in air traffic, as it an essential part of localizer antenna array.
- A typical localizer antenna system is a part of the electronic systems known as *Instrumental Landing System* (ILS). Localizer shapes a radiation pattern providing lateral guidance to the aircraft beginning its descent, intercepting the projected runway center line, and then making a final approach.

FD analysis of wire antennas

Department of Electronics
University of Split,
Split, Croatia

The length of actual wire is obtained by multiplying the previous length and factor T:

$$\tau = \frac{L_{n+1}}{L_n}$$

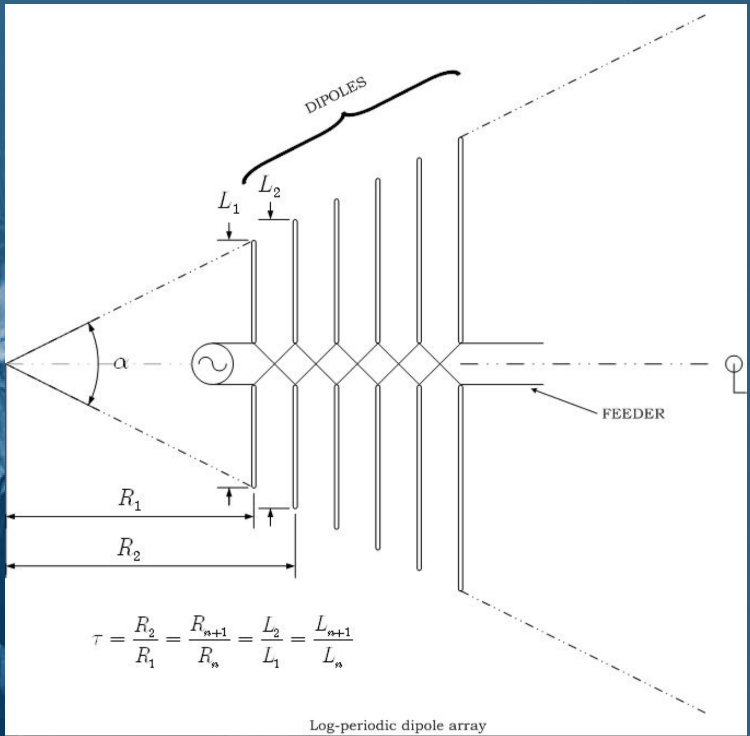

LPDA geometry

A look at a real localizer antenna element geometry...

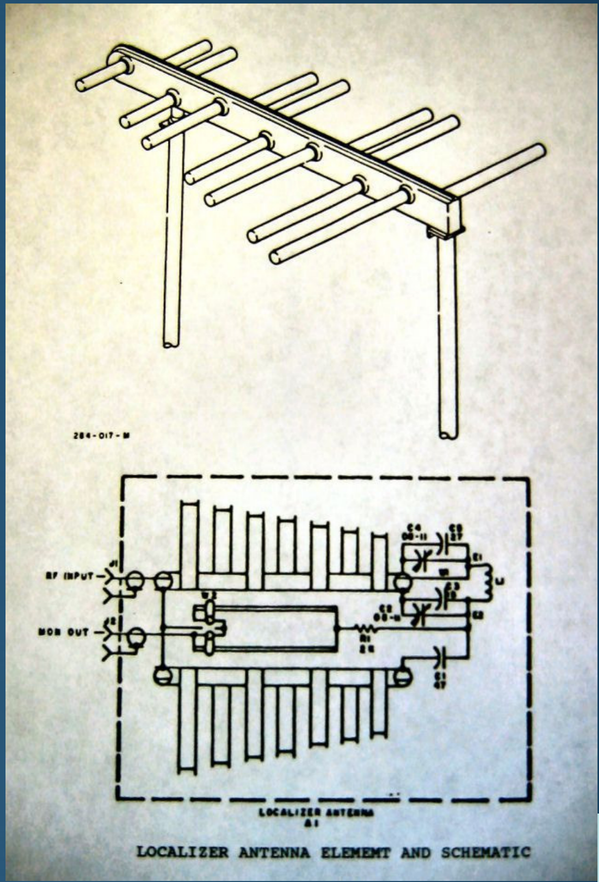

Department of Electronics
University of Split,
Split, Croatia

FD analysis of wire antennas

LPDA in free space

- LPDA is composed from 12 dipoles insulated in free space.
- The radius of all wires is a=0.004m while the length of wires are determined by the length of 1st wire L_1=1.5m, and factor T=0.9.
- All dipoles are fed by the voltage generator V_g=1V with variable phase (each time phase is changed for 180°).
- The operating frequency is varied from 100 MHz to 300 MHz.

FD analysis of wire antennas

Department of Electronics
University of Split,
Split, Croatia

LPDA in free space

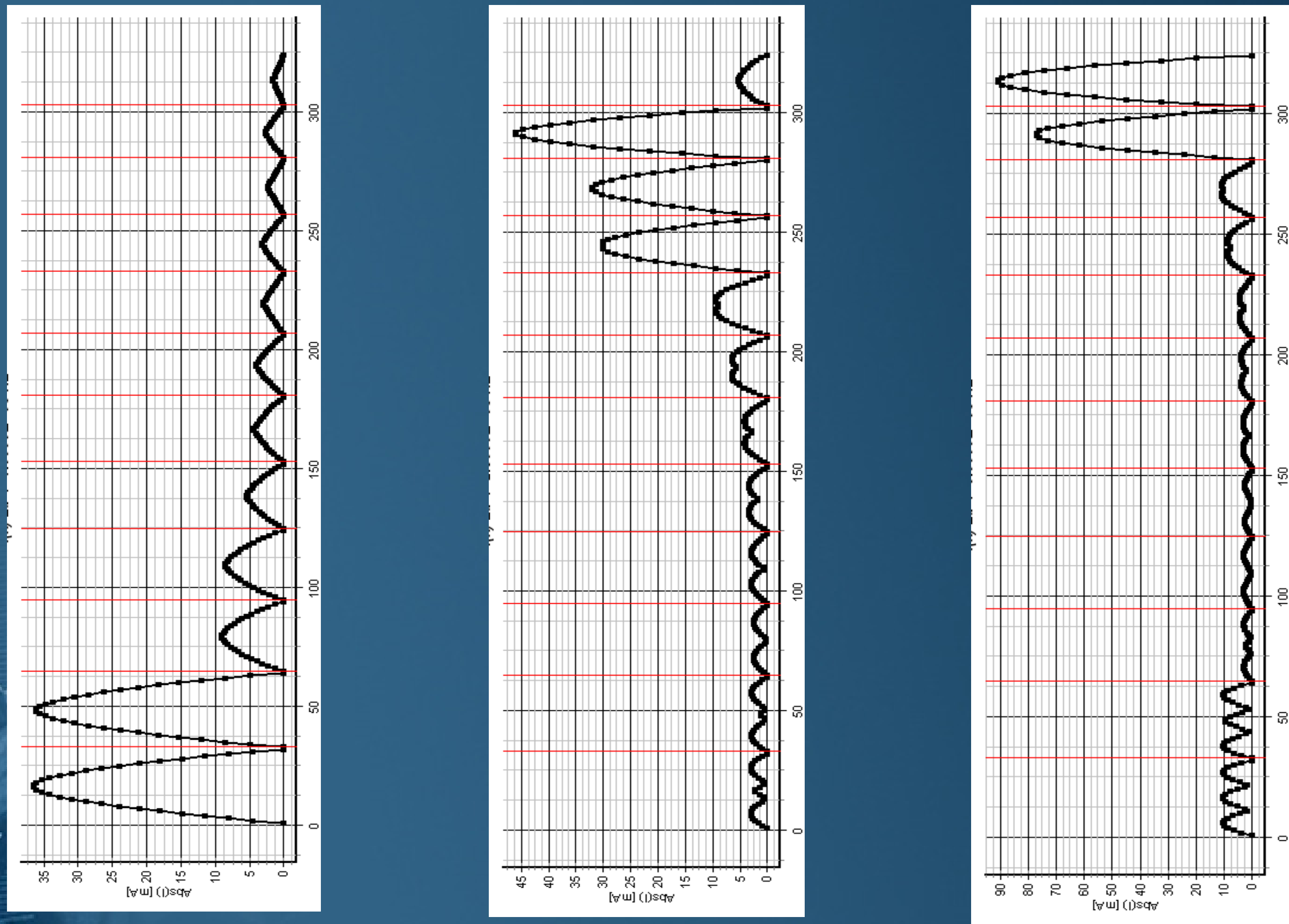

Absolute value of Current distribution along 12 dipoles versus BEM nodes at f=100MHz, f=250MHz and f=300MHz

UNIVERSITÉ Clermont Auvergne

FD analysis of wire antennas

Department of Electronics
University of Split,
Split, Croatia

LPDA in free space

Radiation pattern

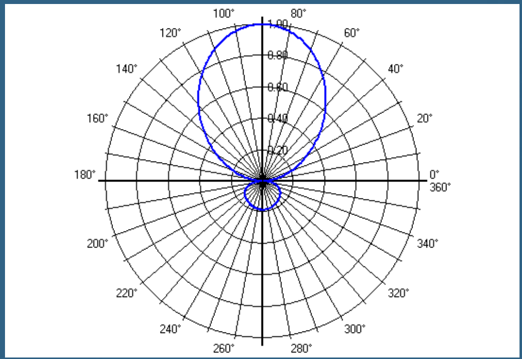
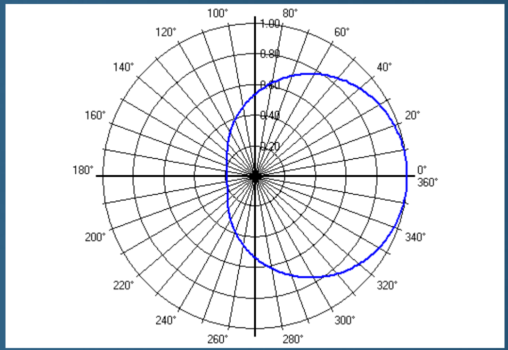

f=100MHz

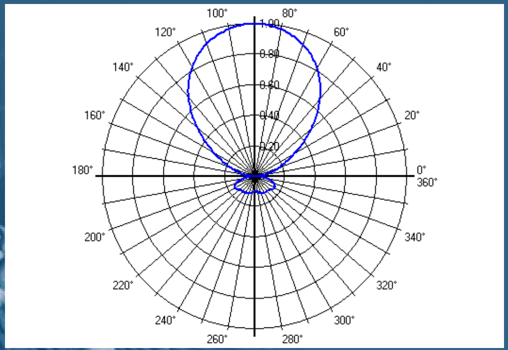
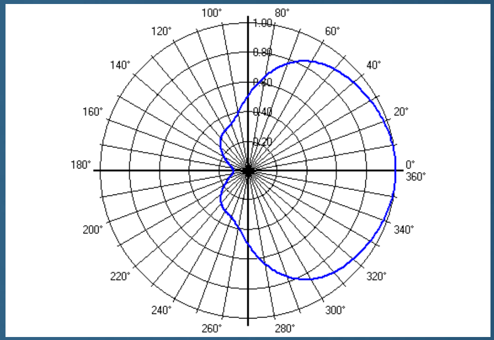

f=250MHz

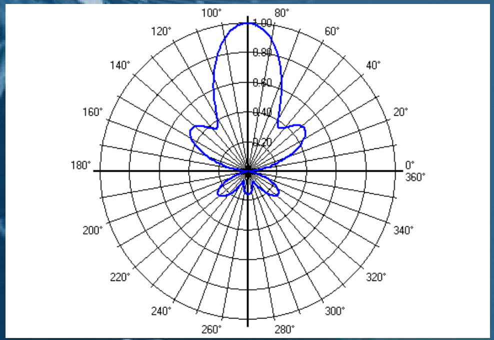
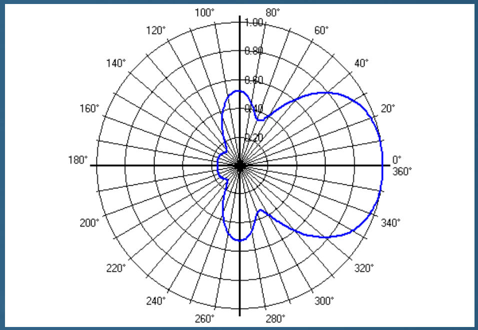

f=300MHz

(XY plane)

(YZ plane)

FD analysis of wire antennas

Department of Electronics
University of Split,
Split, Croatia

LPDA above a PEC ground

Radiation pattern (XY plane)

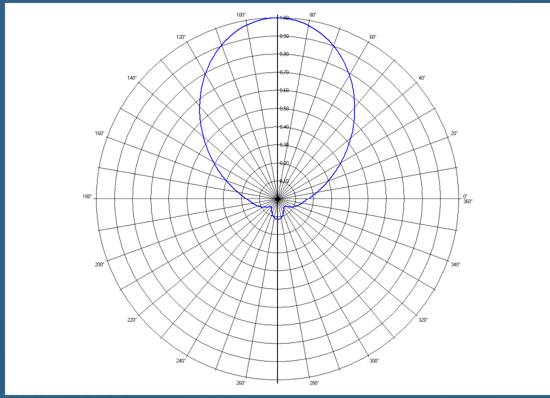
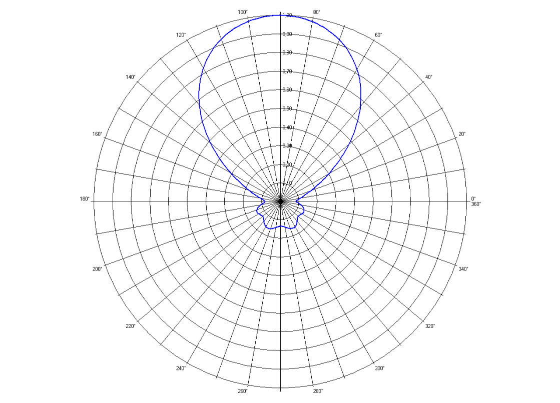
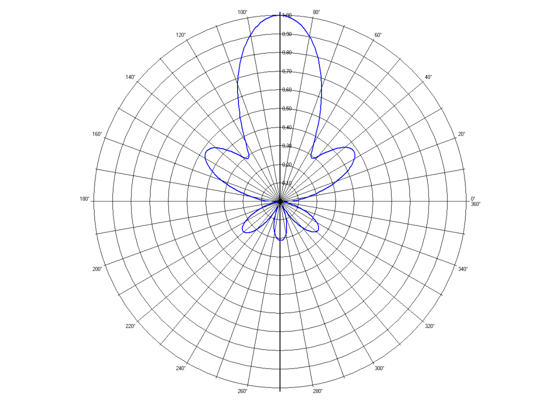

LPDA above a real ground

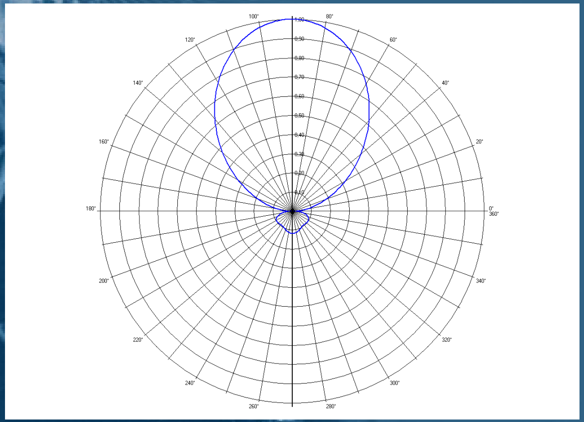
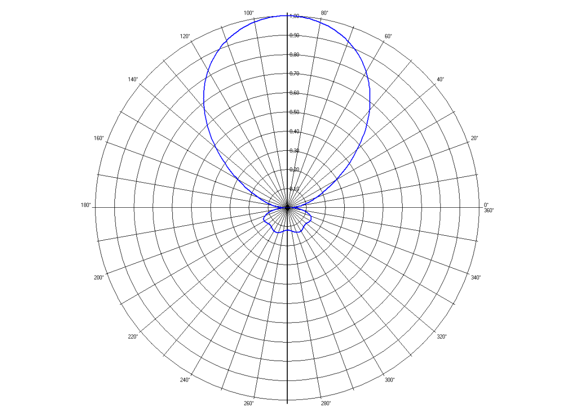
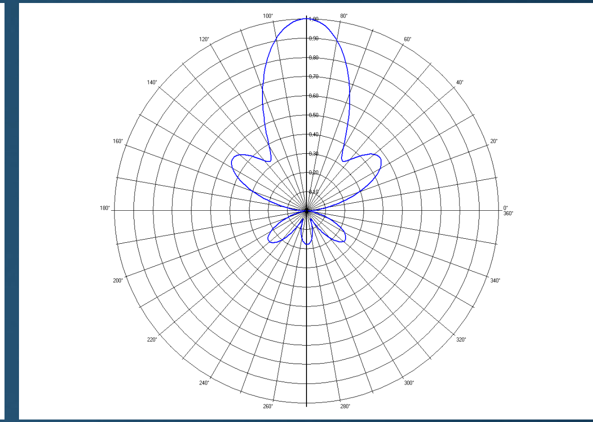

f=100MHz   *f*=250MHz   *f*=300MHz

UCA UNIVERSITÉ Clermont Auvergne

FD analysis of wire antennas

Department of Electronics
University of Split,
Split, Croatia

- realistic geometries of localizer antenna systems.

$f=110MHz$
$T=0.983$
$\sigma=0.1876$
$L_1=1.27m$
$d_1=0.4765m$
$n=7$ –wires per LPDA
$a=0.002$
$N_{seg}=11$ - segments per wire
$N_{LPDA}=14$
$h=1.82m$
$\sigma=0.005$
$\varepsilon_r=13$

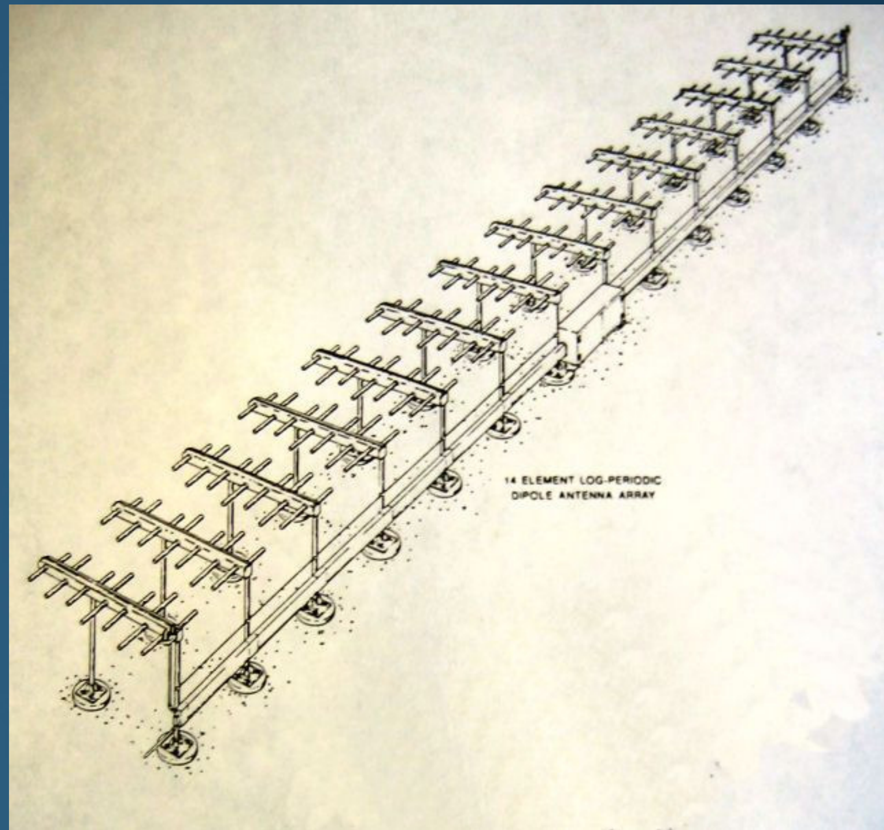

UNIVERSITÉ Clermont Auvergne

FD analysis of wire antennas

Department of Electronics
University of Split,
Split, Croatia

- realistic geometries of localizer antenna systems.

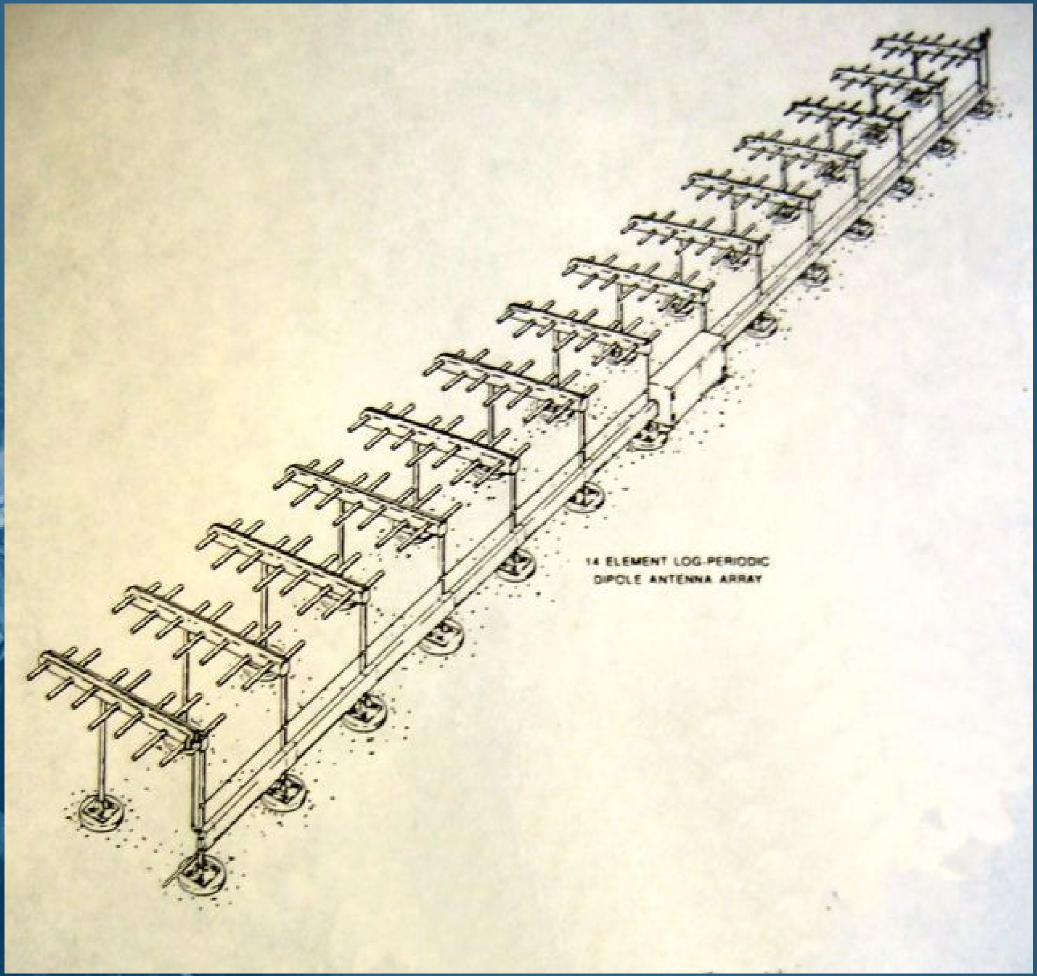

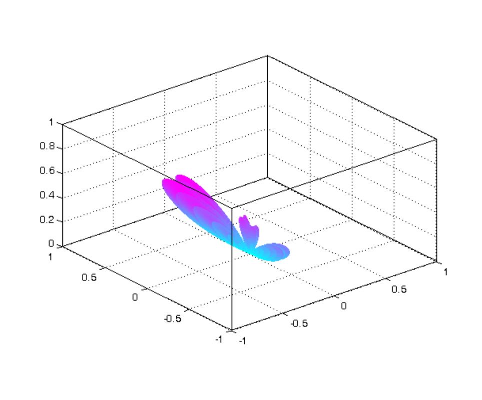

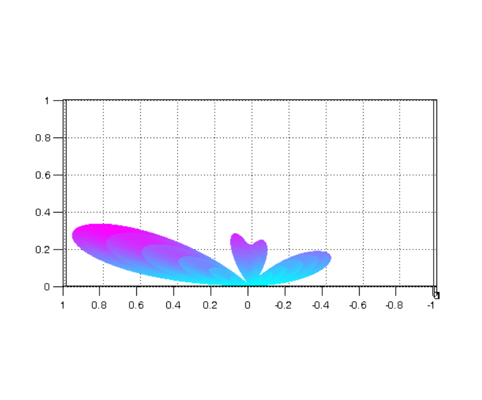

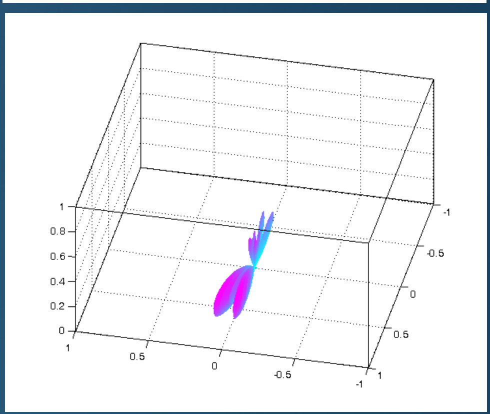

Department of Electronics
University of Split,
Split, Croatia

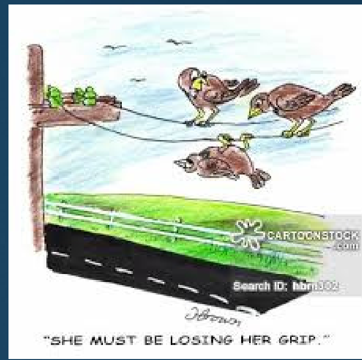

TRANSMISSION LINES

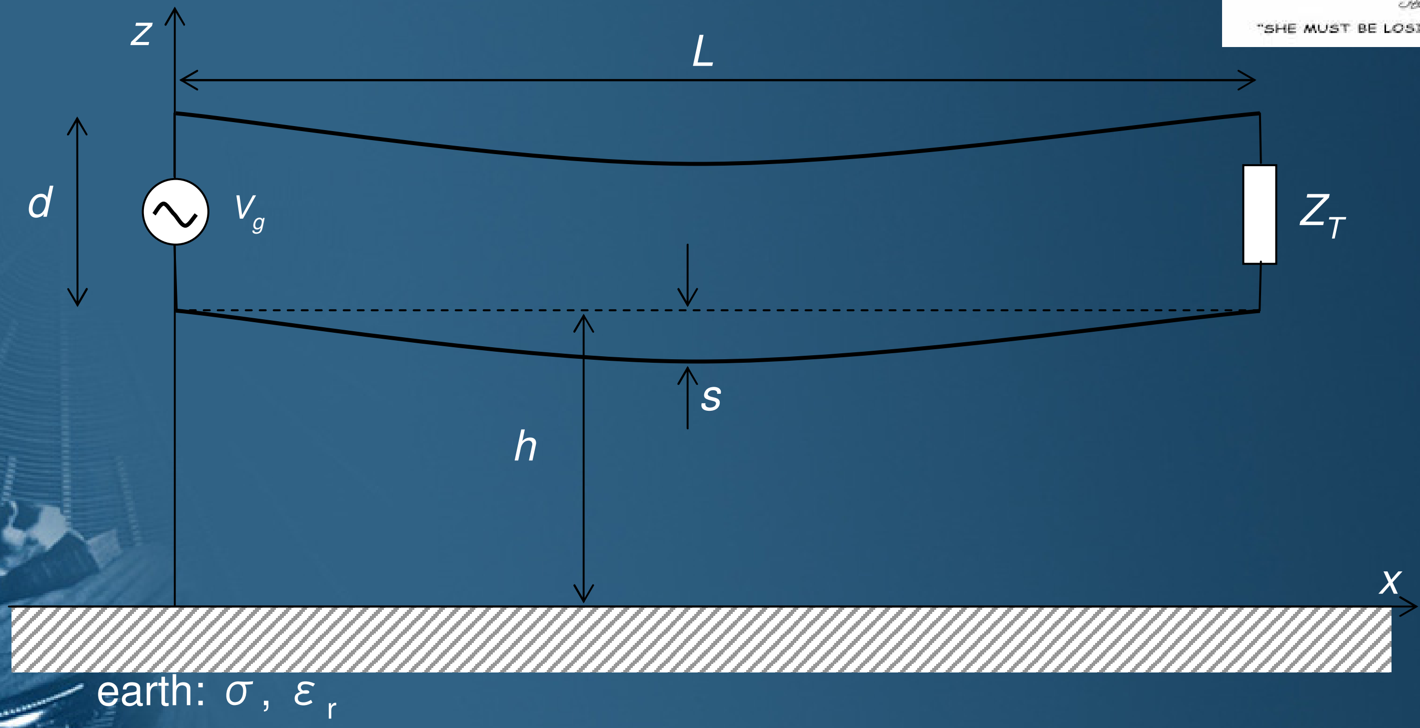

Clermont-Ferrand, 03 April 2018

UNIVERSITÉ Clermont Auvergne

Department of Electronics
University of Split,
Split, Croatia

Electromagnetic Field Coupling to Overhead Wires

•The EM field coupling to lines or cables can be analyzed by using the ***antenna theory***, or ***TL model***.

•The TL theory does not provide a complete solution if the wavelength of the field coupling to a line is comparable to, or less than, dimensions of the line.

•The TL approach is sufficient approximation for long lines with electrically-small cross sections, but is not valid for lines of finite length, particularly for the case of high frequency excitations.

•***The principal feature of TL approach is simplicity and relatively low computational cost.***

UNIVERSITÉ Clermont Auvergne

Department of Electronics
University of Split,
Split, Croatia

EM Field Coupling to Overhead Wires

•The analysis of the finite length lines requires the antenna theory approach.

•The main restriction of the wire antenna model applied to longer lines is a high computational cost.

• FD antenna theory formulation is based on the **Pocklington integro-differential equation.** The numerical solution is carried out via the corresponding **Galerkin-Bubnov** scheme of the **Indirect Boundary Element Method** (GB-IBEM).

• FD transmission line model is based on the corresponding **Telegrapher's equations.**

• The transmission line equations are treated using the chain matrix approach.

Department of Electronics
University of Split,
Split, Croatia

EM Field Coupling to Overhead Wires

- The PEC overhead wire of length *L* and radius *a*, at height *h* above a lossy ground, illuminated by an incident E-field, is of interest.

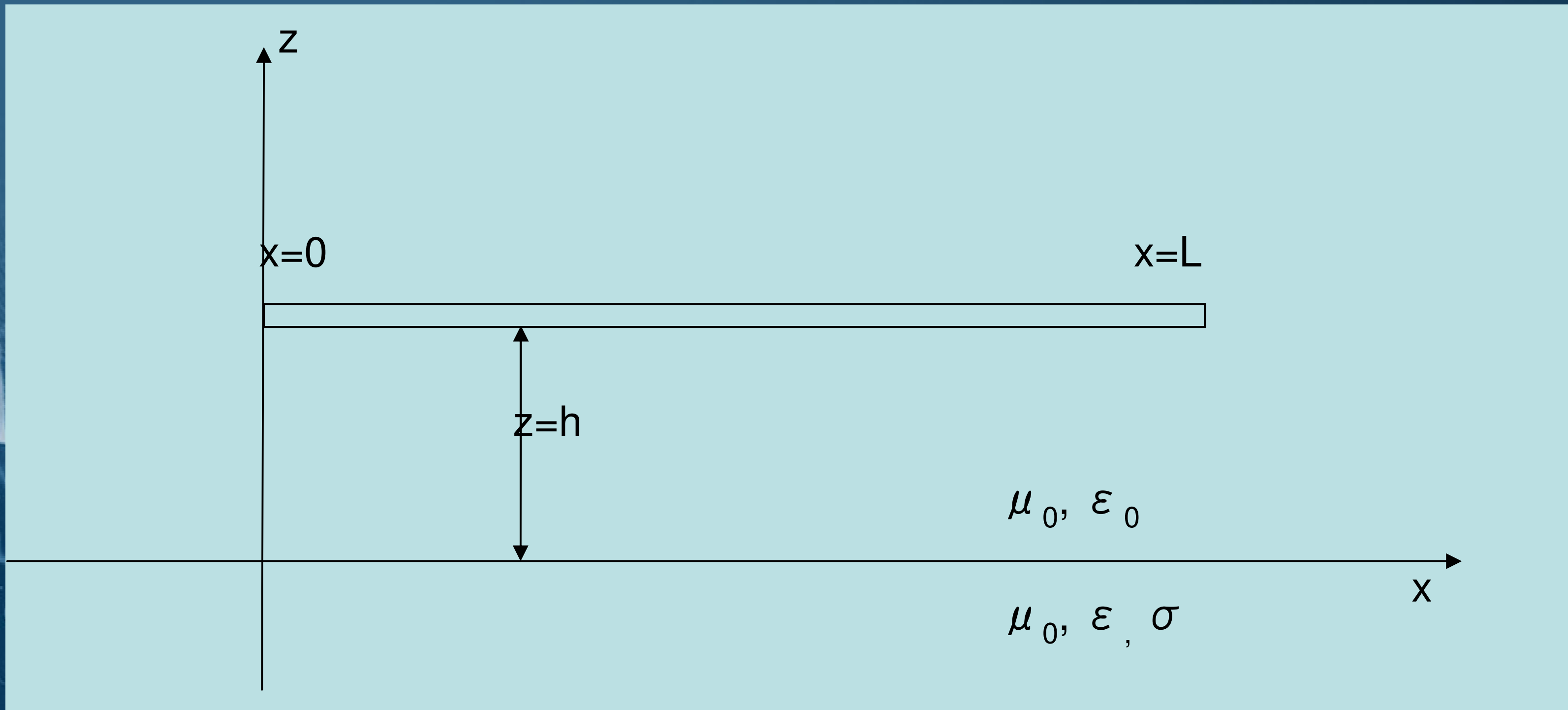

Finite length line above a lossy ground

UNIVERSITÉ Clermont Auvergne

Department of Electronics
University of Split,
Split, Croatia

EM Field Coupling to Overhead Wires

The antenna model: FD analysis of single wire

• The spatial current distribution along the wire is governed by the Pocklington integro-differential equation:

$$E_x^{exc} = j\omega\frac{\mu}{4\pi}\int_0^L I(x')g(x,x')\,dx' - \frac{1}{j4\pi\omega\varepsilon}\frac{\partial}{\partial x}\int_0^L \frac{\partial I(x')}{\partial x'}g(x,x')\,dx' + Z_s(x)I(x)$$

$$g(x,x') = g_0(x,x') - R_{TM}\, g_i(x,x')$$

$$n = \varepsilon_r - j\frac{\sigma}{\omega\varepsilon_0}$$

$$g_o(x,x') = \frac{e^{-jk_o R_o}}{R_o}$$

$$\Theta = \operatorname{arctg}\frac{|x-x'|}{2h}$$

$$g_i(x,x') = \frac{e^{-jk_o R_i}}{R_i}$$

$$R_{TM} = \frac{n\cos\Theta - \sqrt{n-\sin^2\Theta}}{n\cos\Theta + \sqrt{n-\sin^2\Theta}}$$

The transmission line model: FD analysis of single wire

• Voltages and currents along the line induced by an external field excitation can be obtained using the FD field-to-transmission line matrix equations.

$$\frac{d\hat{V}(z)}{dz} + \hat{Z}\,\hat{I}(z) = \hat{V}_F(z)$$

$$\frac{d\hat{I}(z)}{dz} + \hat{Y}\hat{V}(z) = \hat{I}_F(z)$$

$$\hat{Z} = j\omega L + \hat{Z}_w + \hat{Z}_g$$

$$\hat{Y} = j\omega C + G$$

UNIVERSITÉ Clermont Auvergne

Department of Electronics
University of Split,
Split, Croatia

EM Field Coupling to Overhead Wires

Computational examples: Wire above a PEC ground

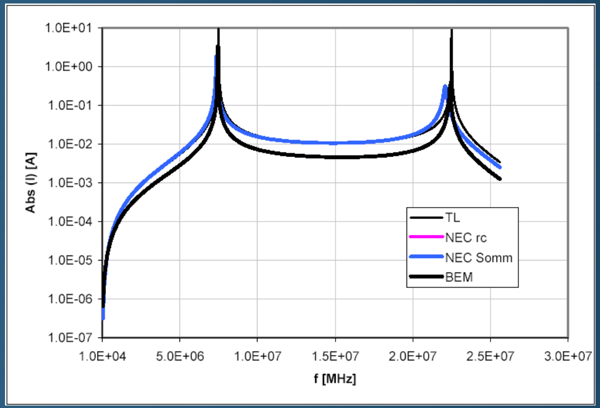

Université Clermont Auvergne

Computational examples: Wire above a lossy ground

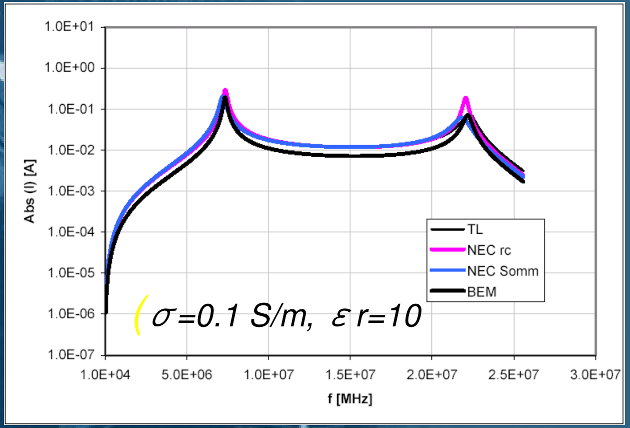

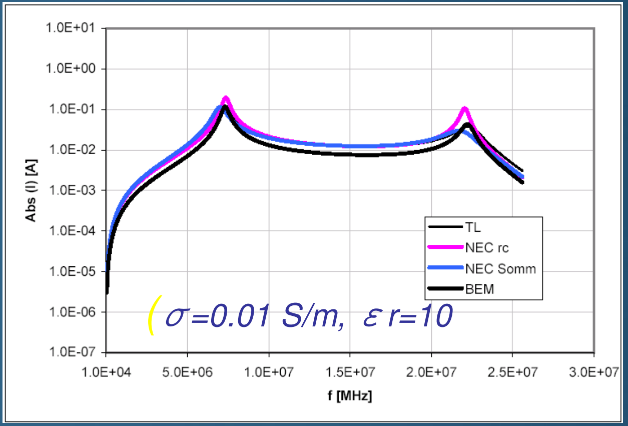

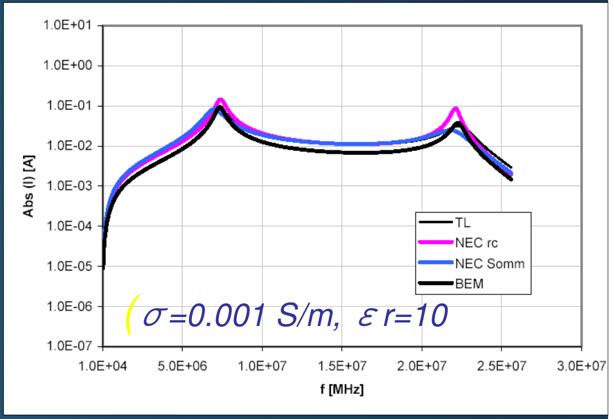

Current induced at the center of the line above a PEC ground versus frequency (L=20m, a=0.005m, h=1m E_0=1V/m – normal incidence)

Department of Electronics
University of Split,
Split, Croatia

EM Field Coupling to Overhead Wires

The antenna model: FD analysis of multiple wires

- The currents along the wire array is governed by the set of coupled Pocklington equations

$$E_x^{exc} = -\frac{1}{j4\pi\omega\varepsilon_0}\sum_{n=1}^{M}\int_{-L_n/2}^{L_n/2}\left[\frac{\partial^2}{\partial x^2}+k_1^2\right]\left[g_{0mn}(x,x')-R'_{TM}g_{imn}(x,x')\right]I_n(x')dx' \qquad m=1,2,\ldots M$$

- The Green functions for the source and image wires, respectively is given by:

$$g_{0mn}(x,x') = \frac{e^{-jk_1R_{1mn}}}{R_{1mn}} \qquad g_{imn}(x,x') = \frac{e^{-jk_1R_{2mn}}}{R_{2mn}}$$

Department of Electronics
University of Split,
Split, Croatia

EM Field Coupling to Overhead Wires

Computational example: Current distribution along two coupled wires over imperfect ground

f=20MHz, ε_r=10, σ=0.001mho/m, h=1m, D=0.5m, L=30m, a=0.15cm, ϕ=180°, θ=30°, α=0°

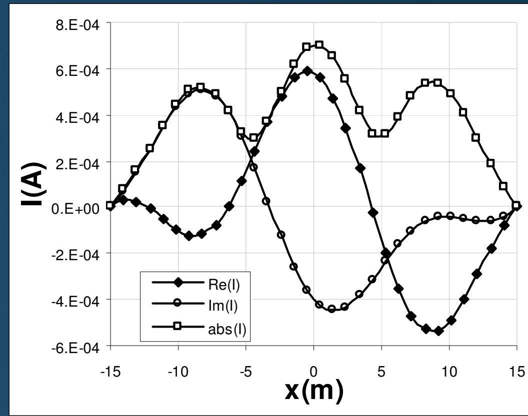

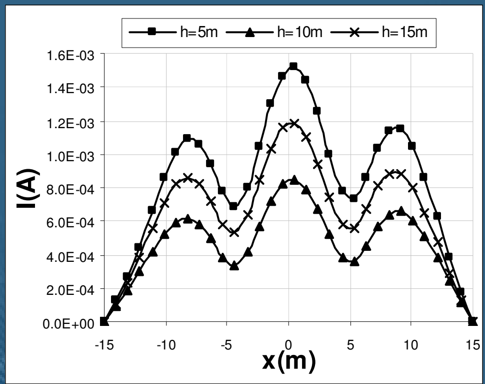

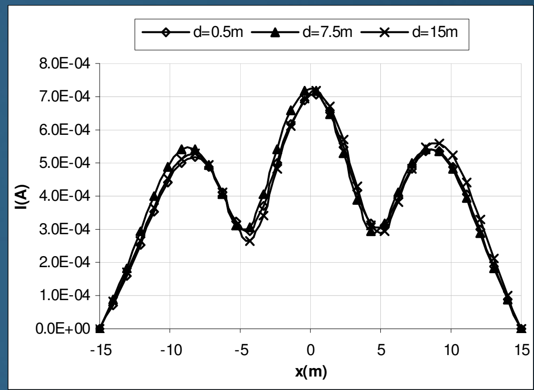

Current magnitudes for a different values of height h and separation D between wires

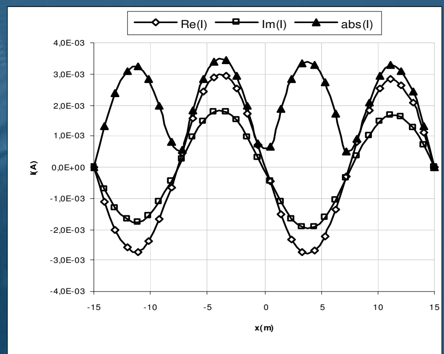

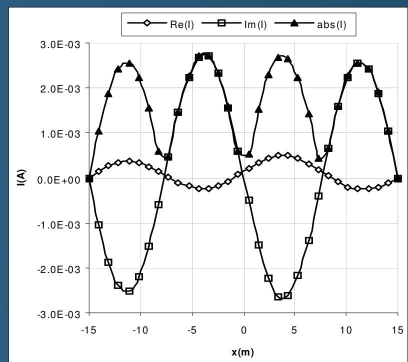

Current distribution along the wire for angle of incidence ϕ=120°, θ=30°, α=0° on (a) first wire, y=0 (b) second wire, y=D

Department of Electronics
University of Split,
Split, Croatia

EM Field Coupling to Overhead Wires

Computational example: Coupling from HF Transmitter to PLC System

- PLC systems aim to provide users with communications means using the already existed power line network.
- One of the principal disadvantages of this technology is related to EMI problems, as overhead power lines at the frequency range from 1 to 30 MHz behave as transmitting antennas or receiving antennas.
- An analysis of overhead power line as an EMI victim is undertaken using the wire antenna theory approach.

Department of Electronics
University of Split,
Split, Croatia

EM Field Coupling to Overhead Wires

Computational example: Coupling from HF Transmitter to PLC System

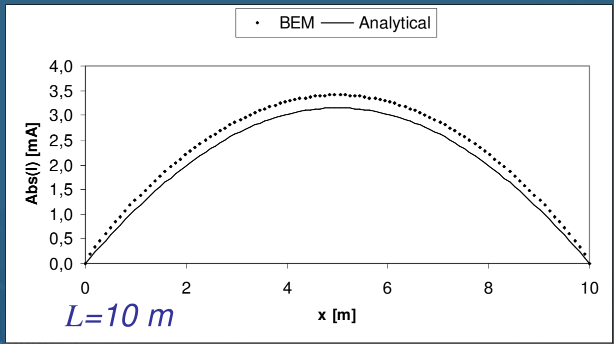

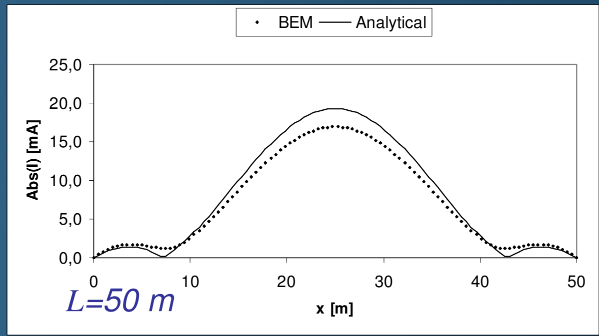

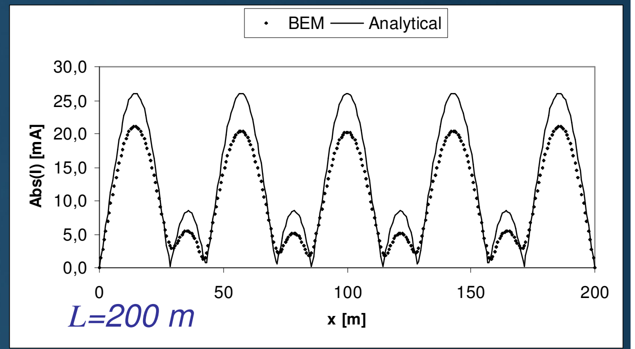

Absolute value of the current distribution along the overhead wire
f=7 MHz, a=6.35 mm, h=1 m, σ=0.005 S/m, ε_r=20

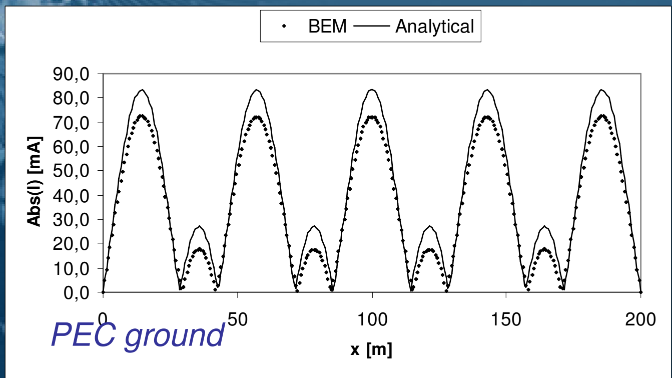

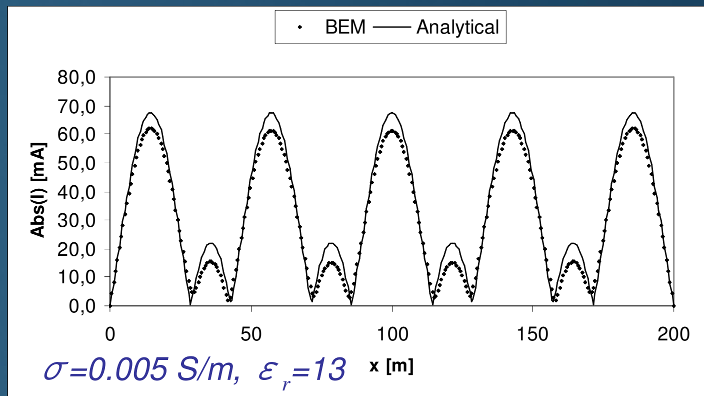

Absolute value of the current distribution along the overhead wire
(f=7 MHz, L=200 m, a=6.35 mm, h=10 m)

Clermont-Ferrand, 03 April 2018

Department of Electronics
University of Split,
Split, Croatia

EM Field Coupling to Overhead Wires

Power Line Communications System as EMI source

- A simple PLC system consisting of curved wires excited by the voltage source V_g is of interest.

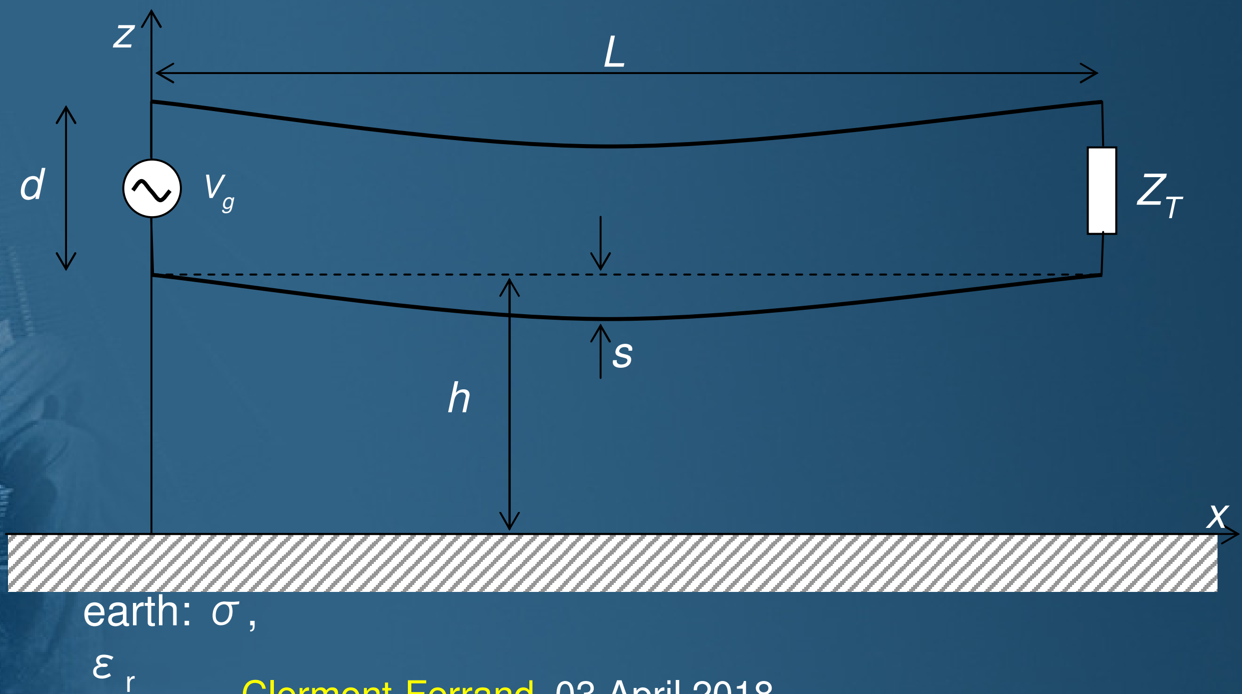

EM Field Coupling to Overhead Wires

Department of Electronics
University of Split,
Split, Croatia

PLC System as EMI source

The spatial current distribution along the curved wire

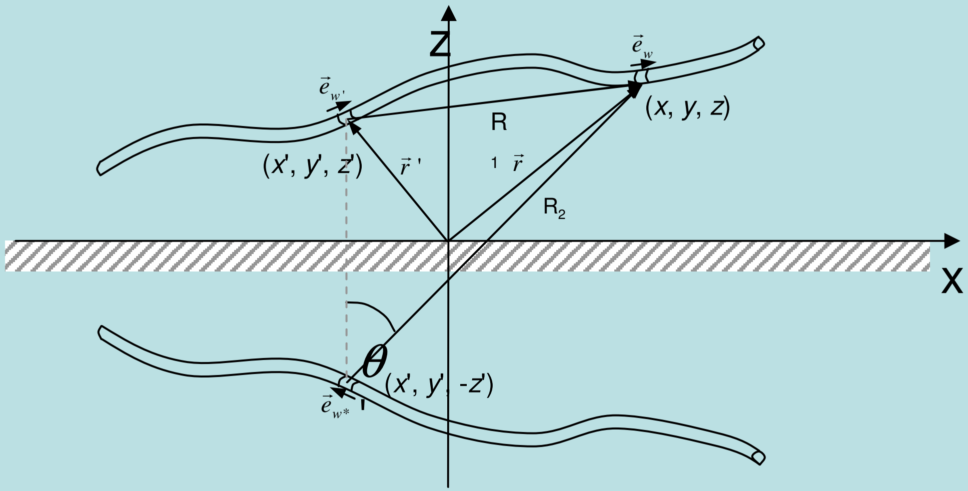

is governed by the following Pocklington integro-differential equation:

$$E^{exc}(s) = -\frac{1}{j4\pi\omega\varepsilon_0}\int_0^L \left\{ \left[k_1^2 \vec{e}_s \vec{e}_{s'} - \frac{\partial^2}{\partial s \partial s'} \right] g_0(s,s') + R_{TM} \left[k_1^2 \vec{e}_s \vec{e}_{s*} - \frac{\partial^2}{\partial s \partial s*} \right] g_i(s,s*) \right\} ds' + Z_T' I(s')$$

UNIVERSITÉ Clermont Auvergne

Department of Electronics
University of Split,
Split, Croatia

EM Field Coupling to Overhead Wires

PLC System as EMI source

For the case of multiple wires of arbitray shape the current distribution along the structure is governed by corresponding set of Pocklington integro-differential equation:

$$E^{exc}(s_n) = -\frac{1}{j4\pi\omega\varepsilon_0}\sum_{m=1}^{M}\int_0^{L_m}\left\{\left[k_1^2\vec{e}_{s_n}\vec{e}_{s_m} - \frac{\partial^2}{\partial s_n \partial s_m'}\right] g_{0nm}(s_n, s_m') + \right.$$

$$\left. + R_{TM}\left[k_1^2\vec{e}_{s_n}\vec{e}_{s_m^*} - \frac{\partial^2}{\partial s \partial s_m^*}\right] g_{inm}(s_n, s_m^*)\right\} I(s_m')ds_m'$$

$$n = 1 \ldots M$$

Department of Electronics
University of Split,
Split, Croatia

EM Field Coupling to Overhead Wires

PLC System as EMI source

BEM solution of the set of Pocklington integro-differential equation:

- The matrix equation

$$\sum_{n=1}^{M}\sum_{i=1}^{N_n}[Z]_{ji}^{e}\{I\}_{i}^{e}=\{V\}_{j}^{e}, \qquad \begin{array}{l} m=1,2,\ldots,M \\ j=1,2,\ldots,N_m \end{array}$$

- The voltage vector

$$\{V\}_{j}^{n}=-j4\pi\omega\varepsilon_0\int_0^{L_n}E_{s_n}^{inc}(s_n)f_{jn}(s_n)\frac{ds_n}{d\xi}d\xi_n$$

$$n=1,\ 2,\ \ldots,\ M$$

$$j=1,\ 2,\ \ldots,\ N_n$$

$$\frac{dw}{d\xi}=\sqrt{\left(\frac{dx}{d\xi}\right)^2+\left(\frac{dz}{d\xi}\right)^2}$$

- The mutual impedance matrix

$$\begin{aligned}
[Z]_{ij}^{e}=&-\int_{-1}^{1}\int_{-1}^{1}\{D\}_j\{D'\}_i^T g_{0nm}(s_n,s_m')\frac{ds_m'}{d\xi'}d\xi'\frac{ds_n}{d\xi}d\xi+\\
&+k_1^2\vec{e}_{s_n}\vec{e}_{s_m}\int_{-1}^{1}\int_{-1}^{1}\{f\}_j\{f'\}_i^T g_{0nm}(s_n,s_m')\frac{ds_m'}{d\xi'}d\xi'\frac{ds_n}{d\xi}d\xi-\\
&-R_{TM}\int_{-1}^{1}\int_{-1}^{1}\{D\}_j\{D'\}_i^T g_{inm}(s_n,s_m^*)\frac{ds_m'}{d\xi'}d\xi'\frac{ds_n}{d\xi}d\xi+\\
&+R_{TM}k_1^2\vec{e}_{s_n}\vec{e}_{s_m^*}\int_{-1}^{1}\int_{-1}^{1}\{f\}_j\{f'\}_i^T g_{inm}(s_n,s_m^*)\frac{ds_m'}{d\xi'}d\xi'\frac{ds_n}{d\xi}d\xi\\
&+\frac{j}{4\pi\omega\varepsilon_0}\int_{-1}^{1}Z_T'\{f\}_j\{f'\}_j^T\frac{ds_n}{d\xi}d\xi
\end{aligned}$$

Department of Electronics
University of Split,
Split, Croatia

EM Field Coupling to Overhead Wires

PLC System as EMI source

The radiated electric field is given by:

$$\vec{E} = \vec{E}_S + R_{TM}\vec{E}_I + \left(R_{TE} - R_{TM}\right)\left(\vec{E}_I \cdot \vec{e}_p\right)\vec{e}_p$$

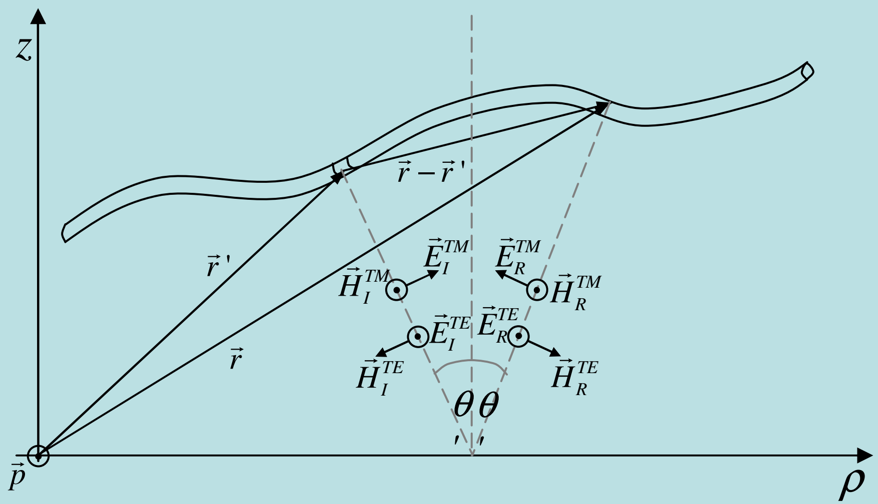

where:

$$\vec{E}_S = \frac{1}{j4\pi\omega\varepsilon_0}\left[k_1^2\int_0^L \vec{e}_{s'} I(s') g_0(\vec{r},\vec{r}\,')ds' + \int_0^L \frac{\partial I(s')}{\partial s'}\nabla g_0(\vec{r},\vec{r}\,')ds'\right]$$

$$\vec{p} = \left(\vec{r} - \vec{r}\,'\right)\times\vec{e}_z$$

$$\vec{E}_I = \frac{1}{j4\pi\omega\varepsilon_0}\left[k_1^2\int_0^L \vec{e}_{s*} I(s') g_i(\vec{r},\vec{r}\,*)ds' - \int_0^L \frac{\partial I(s')}{\partial s'}\nabla g_i(\vec{r},\vec{r}\,*)ds'\right]$$

$$\vec{e}_p = \frac{\vec{p}}{\left|\vec{p}\right|}$$

Department of Electronics
University of Split,
Split, Croatia

EM Field Coupling to Overhead Wires

PLC System as EMI source

BEM solution of the electric field

The total field is given by:

$$\vec{E} = \sum_{k=1}^{N} \left[\vec{E}^{e}_{Sk} + R_{TM} \vec{E}^{e}_{Ik} + \left(R_{TE} - R_{TM} \right) \left(\vec{E}^{e}_{I} \cdot \vec{e}_{p} \right) \vec{e}_{p} \right]$$

where the field components due to a wire segment are given by:

$$\vec{E}^{e}_{S} = \frac{1}{j4\pi\omega\varepsilon_0} \sum_{i=1}^{n} \left[k_1^2 \int_{-1}^{1} \vec{e}_{s'} I_i^e f_i(\xi) g_0(\vec{r},\vec{r}') \frac{ds'}{d\xi} d\xi + \int_{-1}^{1} I_i^e \frac{\partial f_i(\xi)}{\partial \xi} \nabla g_0(\vec{r},\vec{r}') d\xi \right]$$

$$\vec{E}^{e}_{I} = \frac{1}{j4\pi\omega\varepsilon_0} \sum_{i=1}^{n} \left[k_1^2 \int_{-1}^{1} \vec{e}_{s*} I_i^e f_i(\xi) g_i(\vec{r},\vec{r}^*) \frac{ds'}{d\xi} d\xi - \int_{-1}^{1} I_i^e \frac{\partial f_i(\xi)}{\partial \xi'} \nabla g_i(\vec{r},\vec{r}^*) d\xi \right]$$

Department of Electronics
University of Split,
Split, Croatia

EM Field Coupling to Overhead Wires

PLC System as EMI source

The radiated magnetic field is given by: $\vec{H} = \vec{H}_S + R_{TE}\vec{H}_I + \left(R_{TM} - R_{TE}\right)\left(\vec{H}_I \cdot \vec{e}_p\right)\vec{e}_p$

where:

$$\vec{H}_S = -\frac{1}{4\pi}\int_0^L I(s')\vec{e}_{s'} \times \nabla g_0(\vec{r},\vec{r}')ds'$$

$$\vec{H}_I = -\frac{1}{4\pi}\int_0^L I(s')\vec{e}_{s*} \times \nabla g_i(\vec{r},\vec{r}^*)ds'$$

BEM solution of the magnetic field

The total field is given by:

$$\vec{H} = \sum_{k=1}^{N}\left[\vec{H}^e_{Sk} + R_{TE}\vec{H}^e_{Ik} + \left(R_{TM} - R_{TE}\right)\left(\vec{H}^e_{Ik} \cdot \vec{e}_p\right)\vec{e}_p\right]$$

where the field components due to a wire segment are given by:

$$\vec{H}^e_S = -\frac{1}{4\pi}\sum_{i=1}^{n}\int_{-1}^{1} I_i f_i(\xi)\vec{e}_{s'} \times \nabla g_0(\vec{r},\vec{r}')\frac{ds'}{d\xi}d\xi$$

$$\vec{H}^e_I = -\frac{1}{4\pi}\sum_{i=1}^{n}\int_{-1}^{1} I^e_i f_i(\xi)\vec{e}_{s*} \times \nabla g_i(\vec{r},\vec{r}^*)\frac{ds'}{d\xi}d\xi$$

Department of Electronics
University of Split,
Split, Croatia

EM Field Coupling to Overhead Wires

Computational example: PLC System with curved wires as EMI source

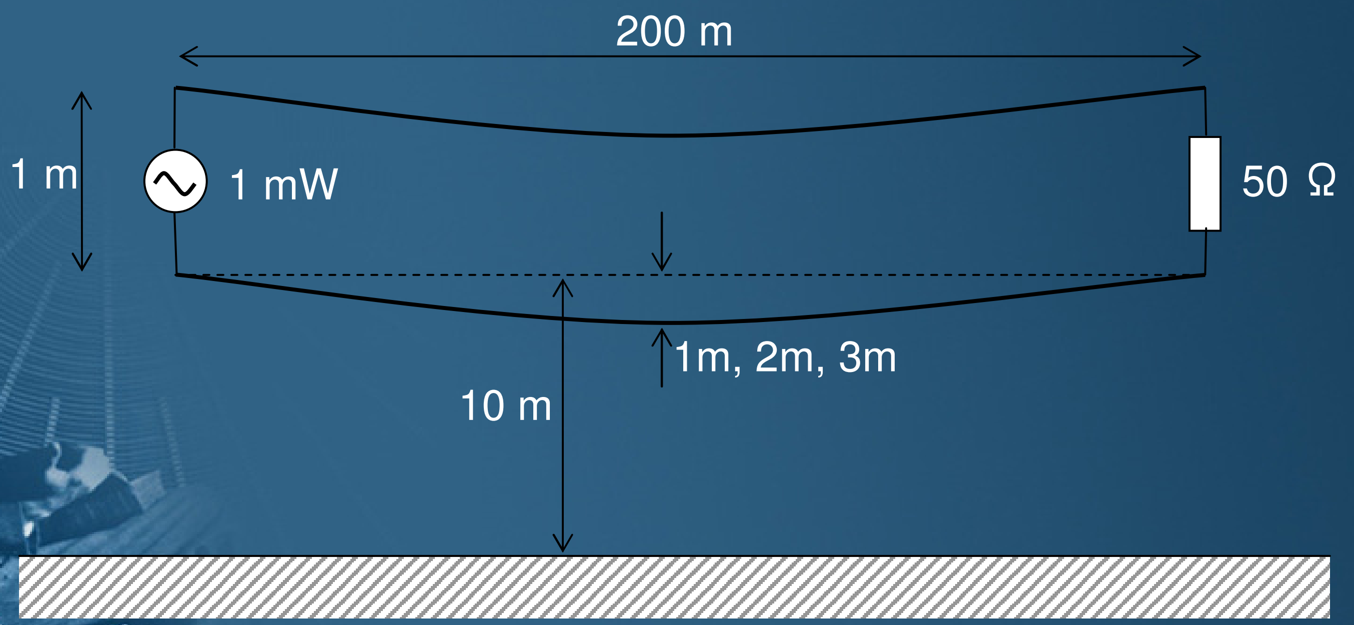

UNIVERSITÉ Clermont Auvergne

Department of Electronics
University of Split,
Split, Croatia

EM Field Coupling to Overhead Wires

Computational example: PLC System with curved wires as EMI source

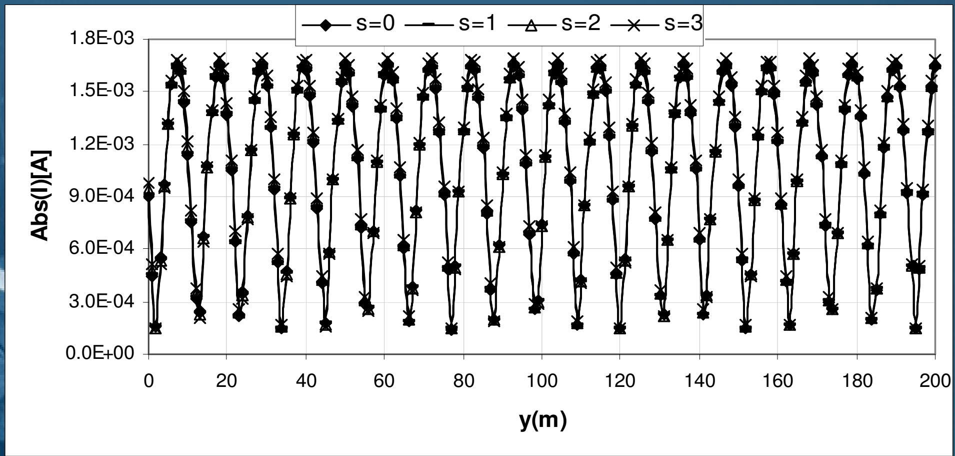

Current distribution along the upper conductor (σ=0.005S/m, ε_r=13)

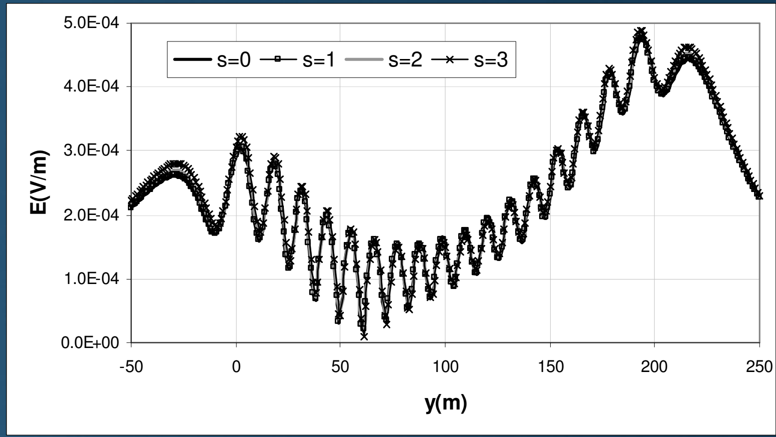

Axial component of the radiated E-field (x=30m, z=10m, σ=0.005S/m, ε_r=13)

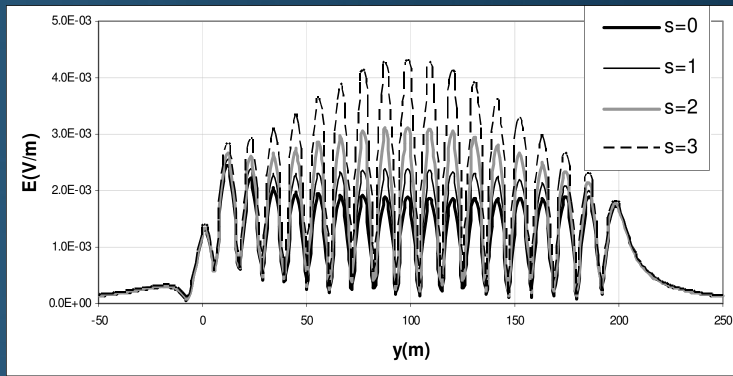

Axial component of the radiated E-field (x=30m, z=1.5m, σ=0.005S/m, ε_r=13)

Department of Electronics
University of Split,
Split, Croatia

EM Field Coupling to Overhead Wires

The antenna model: TD analysis of single wire

The PEC overhead wire of length *L* and radius *a*, at height *h* above a lossy ground, illuminated by an incident E-field, is of interest.

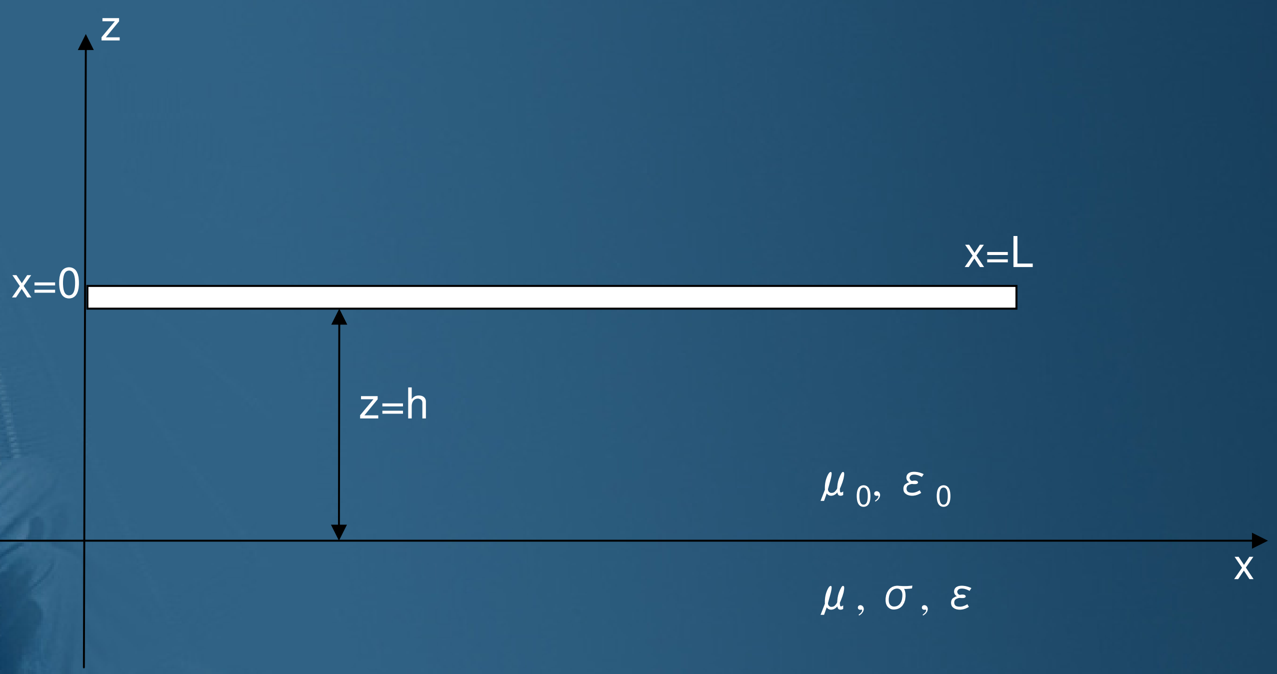

Finite length line above a lossy ground

Department of Electronics
University of Split,
Split, Croatia

EM Field Coupling to Overhead Wires

- The integral equation for the transient current along the **wire** is obtained by enforcing the condition for the tangential field at the wire surface:

$$E_z^{inc} + E_z^{sct} = 0$$

where E_z^{inc} is the incident electric field and the scattered electric field E_z^{inc} is expressed in terms of potentials:

$$\vec{E}^{sct}\Big|_{tan} = -\left(\frac{\partial \vec{A}}{\partial t} + \nabla \varphi\right)\Big|_{tan}$$

The vector and scalar potential, respectively, are given by:

$$\vec{A} = \frac{\mu}{4\pi} \iint_{S'} \frac{\vec{J}(\vec{r}', t-R/c)}{R} dS' \qquad \varphi = \frac{1}{4\pi\varepsilon} \iint_{S'} \frac{\rho(\vec{r}', t-R/c)}{R} dS'$$

where charge and current densities, respectively, are related with the continuity equation:

$$\nabla \vec{J}_s = -\frac{\partial \rho_s}{\partial t}$$

UNIVERSITÉ Clermont Auvergne

Department of Electronics
University of Split,
Split, Croatia

EM Field Coupling to Overhead Wires

Combining previous equations leads to the integral equation for the transient current along the wire in free space:

$$-\varepsilon \frac{\partial E_z^{inc}}{\partial t} = \left[\frac{\partial^2}{\partial z^2} - \frac{1}{c^2} \frac{\partial^2}{\partial t^2} \right] \int_0^L \frac{I(z',t - R/c)}{4\pi R} dz'$$

Integrating the Pocklington equation yields the Hallen integral equation:

$$\int_0^L \frac{I(z',t - R/c)}{4\pi R} dz' = F_0(t - \frac{z}{c}) + F_L(t - \frac{L - z}{c}) + \frac{1}{2Z_0} \int_0^L E_{\check{z}}^{inc}(z',t - \frac{|z - z'|}{c}) dz'$$

- $I(z', t-R/c)$ is the unknown current to be determined,
- c is the velocity of light,
- Z_0 is the wave impedance of a free space
- $F_0(t)$; $F_L(t)$ are related with the reflections from wire ends

UNIVERSITÉ Clermont Auvergne

Department of Electronics
University of Split,
Split, Croatia

EM Field Coupling to Overhead Wires

Performing certain mathematical manipulations one obtains the Hallen integral equation for wire above a lossy half-space:

$$\int_0^L \frac{I(x',t-R/c)}{4\pi R}dx' - \int_{-\infty}^{t}\int_0^L r(\theta,\tau)\frac{I(x',t-R^*/c-\tau)}{4\pi R^*}dx'\,d\tau =$$

$$= F_0\left(t-\frac{x}{c}\right) + F_L\left(t-\frac{L-x}{c}\right) + \frac{1}{2Z_0}\int_0^L E_x^{exc}\left(x',t-\frac{|x-x'|}{c}\right)dx'$$

where the influence of the interface is taken into account via the space-time reflection coefficient:

$$r(\theta',t) = A\delta(t) + \frac{4\beta}{1-\beta^2}\frac{e^{-at}}{t}\sum_{m=1}^{\infty}(-1)^{m+1} m A^m I_m(\alpha t)$$

The time domain Hallen equation is solved via the Galerkin-Bubnov indirect boundary element approach.

Department of Electronics
University of Split,
Split, Croatia

EM Field Coupling to Overhead Wires

The antenna model: TD analysis of multiple wires

- The PEC wires of length *L* and radius *a*, at different heights *h* above a dielectric half-space, illuminated by an incident *E*-field, are of interest.

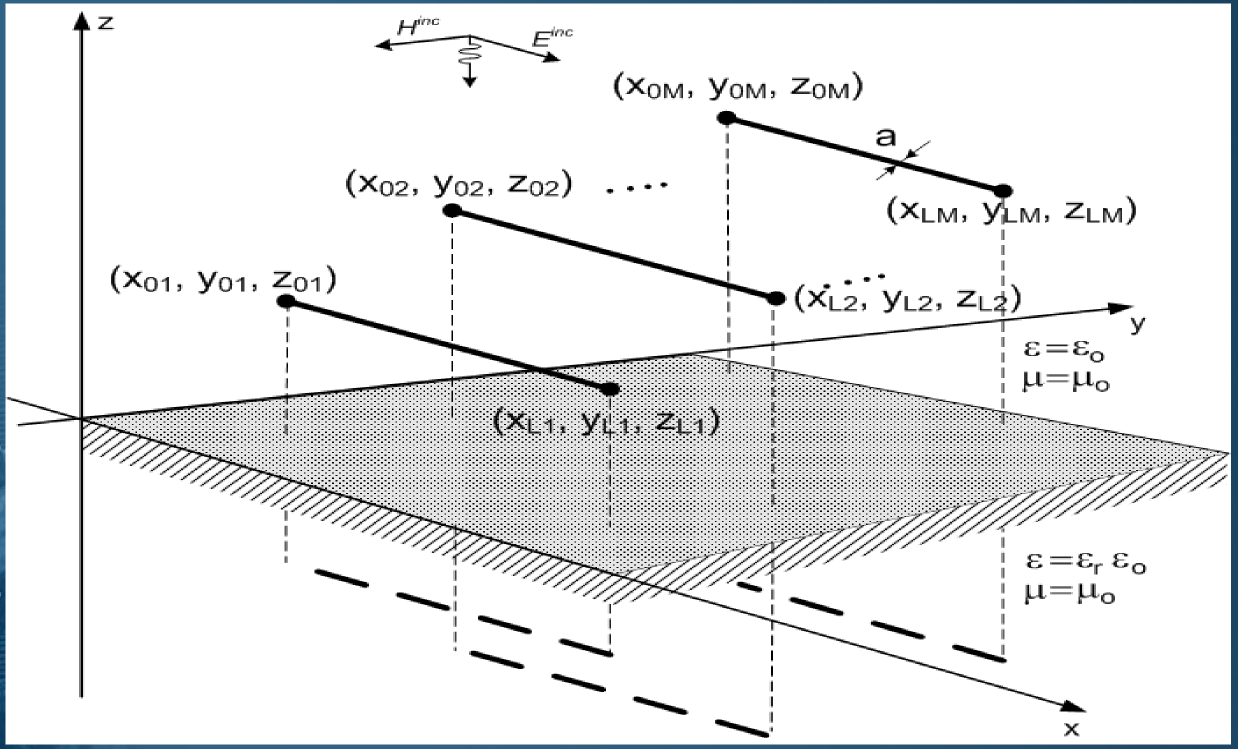

Straight thin wires at various heights above a dielectric half - space

Department of Electronics
University of Split,
Split, Croatia

EM Field Coupling to Overhead Wires

Transient response of *M* parallel wires above a real ground is governed by the set of the coupled space-time Hallen integral equations:

$$\sum_{s=1}^{M}\int_0^{L_s}\frac{I_s(x',t-\frac{R_{vs}}{c})}{4\pi R_{vs}}dx'-\sum_{s=1}^{M}\int_{-\infty}^{t}\int_0^{L_s}r_{vs}(\theta,\tau)\frac{I_s(x',t-\frac{R^*_{vs}}{c}-\tau)}{4\pi R^*_{vs}}dx'd\tau$$

$$=F_{0v}(t-\frac{x-x_{0v}}{c})+F_{Lv}(t-\frac{x_{Lv}-x}{c})+\frac{1}{2Z_0}\int_0^{L_s}E^{exc}_{xv}(x',t-\frac{|x-x'|}{c})dx'$$

Unknown time signals $F_{0v}(t)$ and $F_L(t)$ related to the multiple reflections of transient currents at the wires free ends are given by:

$$F_{0v}(t)=\sum_{n=0}^{\infty}K_{0v}(t-\frac{2nL_v}{c})-\sum_{n=0}^{\infty}K_{Lv}(t-\frac{(2n+1)L_v}{c})$$

$$F_{Lv}(t)=\sum_{n=0}^{\infty}K_{Lv}(t-\frac{2nL_v}{c})-\sum_{n=0}^{\infty}K_{0v}(t-\frac{(2n+1)L_v}{c})$$

The auxilliary functions *K* are defined:

$$K_{0v}(t)=\sum_{s=1}^{M}\int_0^{L_s}\frac{I_s(x',t-\frac{R^{(0)}_{vs}}{c})}{4\pi R^{(0)}_{vs}}dx'-\sum_{s=1}^{M}\int_{-\infty}^{t}\int_0^{L_s}r_{vs}(\theta,\tau)\frac{I_s(x',t-\frac{R^{*(0)}_{vs}}{c}-\tau)}{4\pi R^{*(0)}_{vs}}dx'd\tau-$$
$$-\frac{1}{2Z_0}\int_0^{L_s}E^{exc}_x(x',t-\frac{|x-x'|}{c})dx'$$

$$K_{Lv}(t)=\sum_{s=1}^{M}\int_0^{L_s}\frac{I_s(x',t-\frac{R^{(L)}_{vs}}{c})}{4\pi R^{(L)}_{vs}}dx'-\sum_{s=1}^{M}\int_{-\infty}^{t}\int_0^{L_s}r_{vs}(\theta,\tau)\frac{I_s(x',t-\frac{R^{*(L)}_{vs}}{c}-\tau)}{4\pi R^{*(L)}_{vs}}dx'd\tau-$$
$$-\frac{1}{2Z_0}\int_0^{L_s}E^{exc}_x(x',t-\frac{|x-x'|}{c})dx'$$

Department of Electronics
University of Split,
Split, Croatia

EM Field Coupling to Overhead Wires

For the case of a dielectric half-space the set of Hallen integral equations simplifies into:

$$\sum_{s=1}^{M}\int_{0}^{L_s}\frac{I_s(x',t-\frac{R_{vs}}{c})}{4\pi R_{vs}}dx'-\sum_{s=1}^{M}\int_{0}^{L_s}r_{vs}(\theta)\frac{I_s(x',t-\frac{R_{vs}^*}{c})}{4\pi R_{vs}^*}dx'=$$

$$F_{0v}(t-\frac{x-x_{0v}}{c})+F_{Lv}(t-\frac{x_{Lv}-x}{c})+\frac{1}{2Z_0}\int_{0}^{L_s}E_{xv}^{exc}(x',t-\frac{|x-x'|}{c})dx'$$

Space dependent reflection coefficient is:

$$r_{vs}(\theta)=\frac{1-\beta}{1+\beta},\quad \beta=\frac{\sqrt{\varepsilon_r-\sin^2\theta'}}{\varepsilon_r\cos\theta'},\qquad \theta'_{vs}=Arctg\frac{\sqrt{(x'-x)^2+(y'-y)^2_{vs}}}{z'+z}$$

- For the normal incidence the total *E* - field is given by:

$$E_{xv}^{exc}(x',z,t)=E_{xv}^{inc}(x',t-T)+E_{xv}^{ref}(x',t-T)$$

T - the time required for the wave to travel from the highest wire to the height *z* of the observed *v-th* wire.

- The reflected field:

$$E_{xv}^{ref}(x',t-T)=r_{|\theta=0}\cdot E_{xv}^{inc}(x',t-T-\frac{2z}{c})$$

Department of Electronics
University of Split,
Split, Croatia

UNIVERSITÉ Clermont Auvergne

EM Field Coupling to Overhead Wires

Numerical solution

The set of Hallen integral equations is handled via the TD scheme of the **Galerkin-Bubnov Indirect Boundary Element Method** (GB-IBEM).

- local approximation for the current on a wire: $I(x',t') = \{f\}^T \{I\}$

- space-domain shape functions given by: $f_r(x') = \dfrac{x_{r+1} - x'}{x_{r+1} - x_r} \quad f_{r+1}(x') = \dfrac{x' - x_r}{x_{r+1} - x_r}$

Applying the BEM discretisation leads to a local system of linear equations for the vth observed wire:

$$\sum_{s=1}^{M} \left[\int_{\Delta l_i} \int_{\Delta l_j} \frac{1}{4\pi R_{vs}} \{f\}_j \{f\}_i^T \, dx' dx \{I_s\} \Big|_{t-\frac{R_{vs}}{c}} - \int_{\Delta l_i} \int_{\Delta l_j} \frac{r_{vs}(\theta)}{4\pi R_{vs}^*} \{f\}_j \{f\}_i^T \, dx' dx \{I_s\} \Big|_{t-\frac{R_{vs}^*}{c}} \right]$$

$$= \frac{1}{2Z_0} \int_{\Delta l_i} \int_{\Delta l_j} E_{xv}^{exc}\left(x', t - \frac{|x - x'|}{c}\right) \{f\}_j \, dx' dx$$

$$+ \int_{\Delta l_j} F_0\left(t - \frac{x - x_{0v}}{c}\right) \{f\}_j \, dx + \int_{\Delta l_j} F_L\left(t - \frac{x_{Lv} - x}{c}\right) \{f\}_j \, dx$$

i,j=1,2..*N* - index of the elements (*s*-th source and the *v*-th observed wire, respectively *N* - total number of segments, *M* - actual number of wires.

Department of Electronics
University of Split,
Split, Croatia

EM Field Coupling to Overhead Wires

the matrix equation:

$$\sum_{s=1}^{M}\left[A_{vs}\right]\left\{I_s\right\}\Big|_{t-\frac{R_{vs}}{c}}-\sum_{s=1}^{M}\left[A_{vs}^{*}\right]\left\{I_s\right\}\Big|_{t-\frac{R_{vs}^{*}}{c}}=$$

$$=\left[B_v\right]\left\{E_v\right\}\Big|_{t-\frac{|x-x'|}{c}}+\sum_{s=1}^{M}\left[C_{vs}\right]\left\{\sum_{n=0}^{\infty}I_s^n\right\}\Big|_{t-\frac{x-x_{0v}}{c}-\frac{2n}{c}L_v-\frac{R_{vs}^{(0)}}{c}}-\sum_{s=1}^{M}\left[C_{vs}^{*}\right]\left\{\sum_{n=0}^{\infty}I_s^n\right\}\Big|_{t-\frac{x-x_{0v}}{c}-\frac{2n}{c}L_v-\frac{R_{vs}^{*(0)}}{c}}-\left[D_v\right]\left\{\sum_{n=0}^{\infty}E_v^n\right\}\Big|_{t-\frac{x-x_{0v}}{c}-\frac{2n}{c}L_v-\frac{|x'-x_{0v}|}{c}}-$$

$$-\sum_{s=1}^{M}\left[E_{vs}\right]\left\{\sum_{n=0}^{\infty}I_s^n\right\}\Big|_{t-\frac{x-x_{0v}}{c}-\frac{2n+1}{c}L_v-\frac{R_{vs}^{(L)}}{c}}+\sum_{s=1}^{M}\left[E_{vs}^{*}\right]\left\{\sum_{n=0}^{\infty}I_s^n\right\}\Big|_{t-\frac{x-x_{0v}}{c}-\frac{2n+1}{c}L_v-\frac{R_{vs}^{*(L)}}{c}}+\left[D_v\right]\left\{\sum_{n=0}^{\infty}E_v^n\right\}\Big|_{t-\frac{x-x_{0v}}{c}-\frac{2n+1}{c}L_v-\frac{|x_{Lv}-x'|}{c}}+\sum_{s=1}^{M}\left[E_{vs}\right]\left\{\sum_{n=0}^{\infty}I_s^n\right\}\Big|_{t-\frac{x_{Lv}-x}{c}-\frac{2n}{c}L_v-\frac{R_{vs}^{(L)}}{c}}-$$

$$-\sum_{s=1}^{M}\left[E_{vs}^{*}\right]\left\{\sum_{n=0}^{\infty}I_s^n\right\}\Big|_{t-\frac{x_{Lv}-x}{c}-\frac{2n}{c}L_v-\frac{R_{vs}^{*(L)}}{c}}-\left[D_v\right]\left\{\sum_{n=0}^{\infty}E_v^n\right\}\Big|_{t-\frac{x_{Lv}-x}{c}-\frac{2n}{c}L_v-\frac{|x_{Lv}-x'|}{c}}-\sum_{s=1}^{M}\left[C_{vs}\right]\left\{\sum_{n=0}^{\infty}I_s^n\right\}\Big|_{t-\frac{x_{Lv}-x}{c}-\frac{2n+1}{c}L_v-\frac{R_{vs}^{(0)}}{c}}+\sum_{s=1}^{M}\left[C_{os}^{*}\right]\left\{\sum_{n=0}^{\infty}I_s^n\right\}\Big|_{t-\frac{x_{Lo}-x}{c}-\frac{2n+1}{c}L_o-\frac{R_{os}^{*(0)}}{c}}+$$

$$+\left[D_o\right]\left\{\sum_{n=0}^{\infty}E_o^n\right\}\Big|_{t-\frac{x_{Lo}-x}{c}-\frac{2n+1}{c}L_o-\frac{|x'-x_{0o}|}{c}}$$

the space dependent matrices:

$$\left[A_{vs}\right]=\int_{\Delta l_j}\int_{\Delta l_i}\frac{1}{4\pi R_{vs}}\{f\}_j\{f\}_i^T\,dx'dx\;;\quad\left[A_{vs}^{*}\right]=\int_{\Delta l_j}\int_{\Delta l_i}\frac{r_{vs}(\theta)}{4\pi R_{vs}^{*}}\{f\}_j\{f\}_i^T\,dx'dx$$

$$\left[B_v\right]=\frac{1}{2Z_0}\int_{\Delta l_j}\int_{\Delta l_i}\{f\}_j\{f\}_i^T\,dx'dx\quad,\left[C_{vs}\right]=\int_{\Delta l_j}\int_{\Delta l_i}\frac{1}{4\pi R_{vs}^{(0)}}\{f\}_j\{f\}_i^T\,dx'dx$$

$$\left[C_{vs}^{*}\right]=\int_{\Delta l_j}\int_{\Delta l_i}\frac{r_{vs}(\theta)}{4\pi R_{vs}^{*(0)}}\{f\}_j\{f\}_i^T\,dx'dx\quad\left[D_v\right]=\frac{1}{2Z_0}\int_{\Delta l_j}\int_{\Delta l_i}\{f\}_j\{f\}_i^T\,dx'dx$$

$$\left[E_{vs}\right]=\int_{\Delta l_j}\int_{\Delta l_i}\frac{1}{4\pi R_{vs}^{(L)}}\{f\}_j\{f\}_i^T\,dx'dx\;,\left[E_{vs}^{*}\right]=\int_{\Delta l_j}\int_{\Delta l_i}\frac{r_{vs}(\theta)}{4\pi R_{vs}^{*(L)}}\{f\}_j\{f\}_i^T\,dx'dx$$

Department of Electronics
University of Split,
Split, Croatia

EM Field Coupling to Overhead Wires

TD antenna model

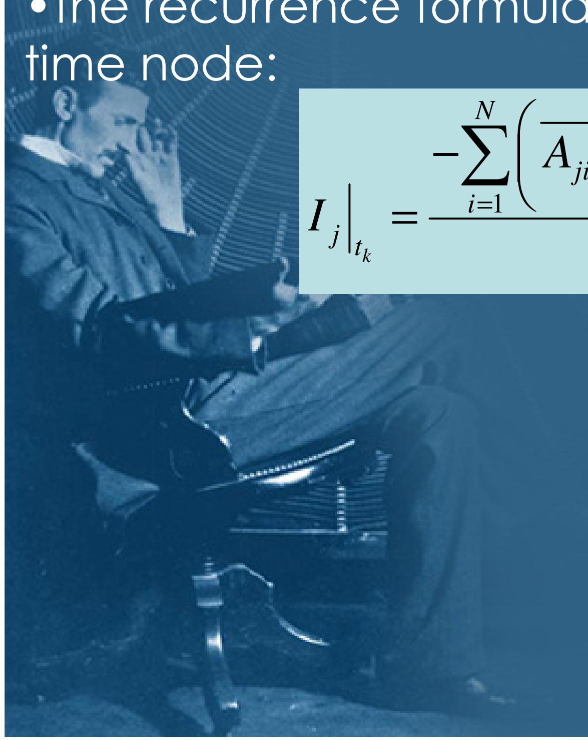

- The weighted residual approach in the time domain:

$$\int_{t_k}^{t_k+\Delta t}\left(\left[A\right]\{I\}\Big|_{t-\frac{R_{vs}}{c}} - \left[A^*\right]\{I\}\Big|_{t-\frac{R_{vs}^*}{c}} - \{g\}\theta_k\right)dt = 0;\ k=1,2,\ldots,N_t$$

- the recurrence formula for the transient current at *j*-th space node and *k*-th time node:

$$I_j\Big|_{t_k} = \frac{-\sum_{i=1}^{N}\left(\overline{A_{ji}}\, I_i\Big|_{t_k-\frac{R_{vs}}{c}} + A_{ji}^*\, I_i\Big|_{t_k-\frac{R_{vs}^*}{c}}\right) + g_j\Big|_{all\ previous\ discrete\ instants}}{A_{jj}}$$

Department of Electronics
University of Split,
Split, Croatia

EM Field Coupling to Overhead Wires

TD antenna model: Inclusion of ground conductivity

Geometry observed –a thin wire above lossy ground:

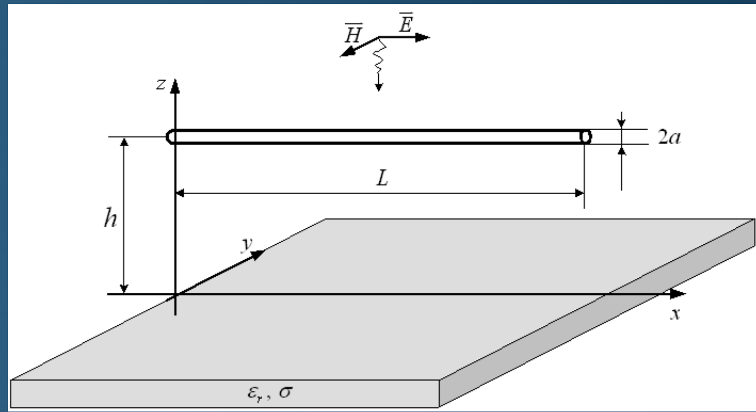

- The space-time RC can be written, as follows:

$$r(\theta,\tau) = r'(\theta,\tau) + r''(\theta,\tau)$$

where:

$$r'(\theta,t) = K\delta(t)$$

$$r''(\theta,t) = \frac{4\beta}{1-\beta^2}\frac{e^{-\alpha t}}{t}\sum_{n=1}^{\infty}(-1)^{n+1} nK^n I_n(\alpha t)$$

$$K = \frac{1-\beta}{1+\beta}$$

Department of Electronics
University of Split,
Split, Croatia

EM Field Coupling to Overhead Wires

TD antenna model: Inclusion of ground conductivity

- Inclusion of $r''(\theta, t)$ into the model leads to the following matrix equation:

$$[A]\{I\}_i\Big|_{t-\frac{R}{c}} - \left[A^*\right]\{I\}_i\Big|_{t-\frac{R^*}{c}} - \left\{\hat{A}\right\}\Big|_{t-\frac{R^*}{c}} = [B]\{E\}\Big|_{t-\frac{|x-x'|}{c}}$$

$$+[C]\left\{\sum_{n=0}^{\infty} I^n\right\}_i\Bigg|_{t-\frac{R_0}{c}-\frac{2nL}{c}-\frac{x}{c}} - \left[C^*\right]\left\{\sum_{n=0}^{\infty} I^n\right\}_i\Bigg|_{t-\frac{R_0^*}{c}-\frac{2nL}{c}-\frac{x}{c}} - \left\{\sum_{n=0}^{\infty} \hat{C}^n\right\}\Bigg|_{t-\frac{R_0^*}{c}-\frac{2nL}{c}-\frac{x}{c}}$$

$$-[B]\left\{\sum_{n=0}^{\infty} E^n\right\}\Bigg|_{t-\frac{x'}{c}-\frac{2nL}{c}-\frac{x}{c}} - [D]\left\{\sum_{n=0}^{\infty} I^n\right\}_i\Bigg|_{t-\frac{R_L}{c}-\frac{(2n+1)L}{c}-\frac{x}{c}}$$

$$+\left[D^*\right]\left\{\sum_{n=0}^{\infty} I^n\right\}_i\Bigg|_{t-\frac{R_L^*}{c}-\frac{(2n+1)L}{c}-\frac{x}{c}} + [B]\left\{\sum_{n=0}^{\infty} E^n\right\}\Bigg|_{t-\frac{L-x'}{c}-\frac{(2n+1)L}{c}-\frac{x}{c}} + \left\{\sum_{n=0}^{\infty} \hat{D}^n\right\}\Bigg|_{t-\frac{R_L^*}{c}-\frac{(2n+1)L}{c}-\frac{x}{c}}$$

$$+[D]\left\{\sum_{n=0}^{\infty} I^n\right\}_i\Bigg|_{t-\frac{R_L}{c}-\frac{2nL}{c}-\frac{L-x}{c}} - \left[D^*\right]\left\{\sum_{n=0}^{\infty} I^n\right\}_i\Bigg|_{t-\frac{R_L^*}{c}-\frac{2nL}{c}-\frac{L-x}{c}} + \left\{\sum_{n=0}^{\infty} \hat{D}^n\right\}\Bigg|_{t-\frac{R_L^*}{c}-\frac{2nL}{c}-\frac{L-x}{c}}$$

$$-[B]\left\{\sum_{n=0}^{\infty} E^n\right\}\Bigg|_{t-\frac{L-x'}{c}-\frac{2nL}{c}-\frac{L-x}{c}} - [C]\left\{\sum_{n=0}^{\infty} I^n\right\}_i\Bigg|_{t-\frac{R_0}{c}-\frac{(2n+1)L}{c}-\frac{L-x}{c}}$$

$$+\left[C^*\right]\left\{\sum_{n=0}^{\infty} I^n\right\}_i\Bigg|_{t-\frac{R_0^*}{c}-\frac{(2n+1)L}{c}-\frac{L-x}{c}} + [B]\left\{\sum_{n=0}^{\infty} E^n\right\}\Bigg|_{t-\frac{x'}{c}-\frac{(2n+1)L}{c}-\frac{L-x}{c}} - \left\{\sum_{n=0}^{\infty} \hat{C}^n\right\}\Bigg|_{t-\frac{R_0^*}{c}-\frac{(2n+1)L}{c}-\frac{L-x}{c}}$$

Department of Electronics
University of Split,
Split, Croatia

EM Field Coupling to Overhead Wires

TD antenna model: Inclusion of ground conductivity

- Additional vectors are expressed as follows:

$$\left\{\hat{A}\right\} = \int_{0}^{t-\frac{R^*}{c}} \int_{\Delta l_j} \int_{\Delta l_i} \{f\}_j \{f\}_i^T \, H_1 dx' dx \left\{I(\tau)\right\}_i d\tau$$

$$\left\{\hat{C}^n\right\} = \int_{0}^{t-\frac{R_0^*}{c}-\frac{2nL}{c}-\frac{x}{c}} \int_{\Delta l_j} \int_{\Delta l_i} \{f\}_j \{f\}_i^T \, H_2 dx' dx \left\{I(\tau)\right\}_i d\tau$$

$$\left\{\hat{D}^n\right\} = \int_{0}^{t-\frac{R_L^*}{c}-\frac{(2n+1)L}{c}-\frac{x}{c}} \int_{\Delta l_j} \int_{\Delta l_i} \{f\}_j \{f\}_i^T \, H_3 dx' dx \left\{I(\tau)\right\}_i d\tau$$

where:

$$H_1 = \frac{r''(\theta, t - \frac{R^*}{c} - \tau)}{4\pi R^*}; \quad H_2 = \frac{r''(\theta, t - \frac{R_0^*}{c} - \frac{2nL}{c} - \frac{x}{c} - \tau)}{4\pi R_0^*}; \quad H_3 = \frac{r''(\theta, t - \frac{R_L^*}{c} - \frac{(2n+1)L}{c} - \frac{x}{c} - \tau)}{4\pi R_0^*}$$

EM Field Coupling to Overhead Wires

TD antenna model: Inclusion of ground conductivity

- Assembly into global matrix system yields:

$$\left[A\right]\{I\}\Big|_{t-\frac{R}{c}} = \{g\}\Big|_{\substack{\text{previous time}\\ \text{instants}}} + \{\hat{g}\}\Big|_{\substack{\text{previous time}\\ \text{instants}}}$$

where:

$$\{\hat{g}\} = \{\hat{A}\}\Big|_{t-\frac{R^*}{c}} - \left\{\sum_{n=0}^{\infty}\hat{C}^n\right\}\Bigg|_{t-\frac{R_0^*}{c}-\frac{2nL}{c}-\frac{x}{c}} + \left\{\sum_{n=0}^{\infty}\hat{D}^n\right\}\Bigg|_{t-\frac{R_L^*}{c}-\frac{(2n+1)L}{c}-\frac{x}{c}}$$
$$+ \left\{\sum_{n=0}^{\infty}\hat{D}^n\right\}\Bigg|_{t-\frac{R_L^*}{c}-\frac{2nL}{c}-\frac{L-x}{c}} - \left\{\sum_{n=0}^{\infty}\hat{C}^n\right\}\Bigg|_{t-\frac{R_0^*}{c}-\frac{(2n+1)L}{c}-\frac{L-x}{c}}$$

$$\{g\} = \left[A^*\right]\{I\}\Big|_{t-\frac{R^*}{c}} + [B]\{E\}\Big|_{t-\frac{|x-x'|}{c}}$$
$$+[C]\left\{\sum_{n=0}^{\infty}I^n\right\}\Bigg|_{t-\frac{R_0}{c}-\frac{2nL}{c}-\frac{x}{c}} - \left[C^*\right]\left\{\sum_{n=0}^{\infty}I^n\right\}\Bigg|_{t-\frac{R_0^*}{c}-\frac{2nL}{c}-\frac{x}{c}}$$
$$-[B]\left\{\sum_{n=0}^{\infty}E^n\right\}\Bigg|_{t-\frac{x'}{c}-\frac{2nL}{c}-\frac{x}{c}} - [D]\left\{\sum_{n=0}^{\infty}I^n\right\}\Bigg|_{t-\frac{R_L}{c}-\frac{(2n+1)L}{c}-\frac{x}{c}}$$
$$+\left[D^*\right]\left\{\sum_{n=0}^{\infty}I^n\right\}\Bigg|_{t-\frac{R_L^*}{c}-\frac{(2n+1)L}{c}-\frac{x}{c}} + [B]\left\{\sum_{n=0}^{\infty}E^n\right\}\Bigg|_{t-\frac{L-x'}{c}-\frac{(2n+1)L}{c}-\frac{x}{c}}$$
$$+[D]\left\{\sum_{n=0}^{\infty}I^n\right\}\Bigg|_{t-\frac{R_L}{c}-\frac{2nL}{c}-\frac{L-x}{c}} - \left[D^*\right]\left\{\sum_{n=0}^{\infty}I^n\right\}\Bigg|_{t-\frac{R_L^*}{c}-\frac{2nL}{c}-\frac{L-x}{c}}$$
$$-[B]\left\{\sum_{n=0}^{\infty}E^n\right\}\Bigg|_{t-\frac{L-x'}{c}-\frac{2nL}{c}-\frac{L-x}{c}} - [C]\left\{\sum_{n=0}^{\infty}I^n\right\}\Bigg|_{t-\frac{R_0}{c}-\frac{(2n+1)L}{c}-\frac{L-x}{c}}$$
$$+\left[C^*\right]\left\{\sum_{n=0}^{\infty}I^n\right\}\Bigg|_{t-\frac{R_0^*}{c}-\frac{(2n+1)L}{c}-\frac{L-x}{c}} + [B]\left\{\sum_{n=0}^{\infty}E^n\right\}\Bigg|_{t-\frac{x'}{c}-\frac{(2n+1)L}{c}-\frac{L-x}{c}}$$

Department of Electronics
University of Split,
Split, Croatia

EM Field Coupling to Overhead Wires

TD antenna model: Inclusion of ground conductivity

- After time sampling, recurrent formula for the unknown current:

$$I_j\Big|_{t_k} = \frac{\sum_{i=1}^{N^s} a_{ji} \, I_j\Big|_{t_k - \frac{R}{c}} - g_j\Big|_{\substack{previous\ time\\ instants}} - \widehat{g}_j\Big|_{\substack{previous\ time\\ instants}}}{a_{jj}}$$

where:

$I_j\Big|_{t_k}$ - current for the *j*-th space node and *k*-th time node

N^S - number of space elements

a_{ji} - member of matrix *[A]* for *i*-th source space node and *j*-th observation space node, where $i \neq j$

$g_j, \widehat{g}_j$ - member of vectors $\{g\}, \{\widehat{g}\}$ for *j* *j*-th observation space node

Department of Electronics
University of Split,
Split, Croatia

EM Field Coupling to Overhead Wires

TD transmission line model

• Voltages and currents along the lines due to an external field can be obtained using the matrix equations.

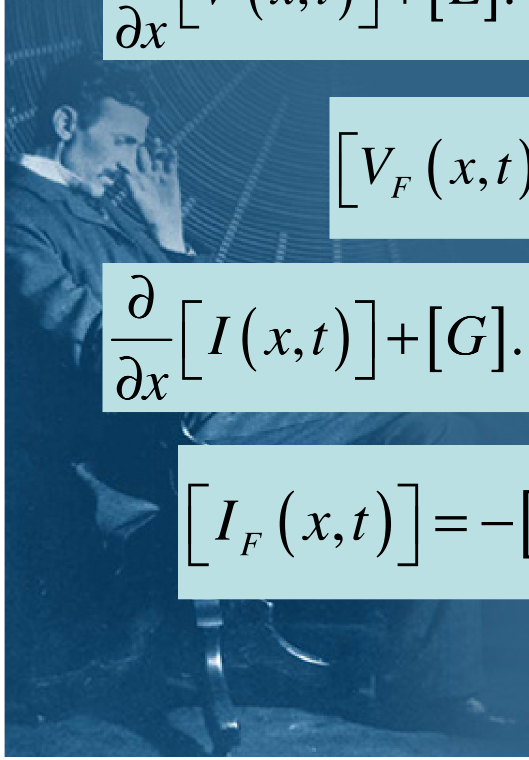

$$\frac{\partial}{\partial x}\left[V(x,t)\right]+[L].\,\frac{\partial}{\partial t}\left[I(x,t)\right]+\left[z'(t)\right]*\left[I(x,t)\right]=\left[V_F(x,t)\right]$$

$$\left[V_F(x,t)\right]=-\frac{\partial}{\partial x}\left[E_T(x,t)\right]+\left[E_L(x,t)\right]$$

$$\frac{\partial}{\partial x}\left[I(x,t)\right]+[G].\left[V(x,t)\right]+[C].\,\frac{\partial}{\partial t}\left[V(x,t)\right]=\left[I_F(x,t)\right]$$

$$\left[I_F(x,t)\right]=-[G].\left[E_T(x,t)\right]-[C].\frac{\partial}{\partial t}.\left[E_T(x,t)\right]$$

Department of Electronics
University of Split,
Split, Croatia

EM Field Coupling to Overhead Wires

TD transmission line model

•The solution of the TD **transmission line equations** is carried out via the **FDTD** method.

•The solutions of MTL equations by FDTD:

$$[V_1^{n+1}]=\left(\frac{\Delta x}{\Delta t}[R_S][C]+1\right)^{-1}\left[\left(\frac{\Delta x}{\Delta t}[R_S][C]-1\right)[V_1^n]-2[R_S][I_1^{n+1/2}]+[V_S^n]+[V_S^{n+1}]+\frac{\Delta x}{\Delta t}[R_S][C]\left([E_{T,1}^n]-[E_{T,1}^{n+1}]\right)\right]$$

$$[V_k^{n+1}]=[V_k^n]-\frac{\Delta x}{\Delta t}[C]^{-1}\left([I_k^{n+1/2}]-[I_{k-1}^{n+1/2}]\right)+[E_{T,k}^n]-[E_{T,k}^{n+1}] \qquad k=2....N_x$$

$$[V_{Nx+1}^{n+1}]=\left(\frac{\Delta x}{\Delta t}[R_L][C]+1\right)^{-1}\left[\left(\frac{\Delta x}{\Delta t}[R_L][C]-1\right)[V_{Nx+1}^n]+[V_L^n]+[V_L^{n+1}]+2[R_L][I_{Nx+1}^{n+1/2}]+\frac{\Delta x}{\Delta t}[R_L][C]\left([E_{T,Nx+1}^n]-[E_{T,Nx+1}^{n+1}]\right)\right]$$

$$[I_k^{n+3/2}]=[I_k^{n+1/2}]-\frac{\Delta t}{\Delta x}[L]^{-1}\left([V_{k+1}^{n+1}]-[V_k^{n+1}]\right)-[L]^{-1}\left(\frac{\Delta t}{\Delta x}([E_{T,k+1}^{n+1}]-[E_{T,k}^{n+1}])-\frac{\Delta t}{2}([E_{L,k}^{n+3/2}]+[E_{L,k}^{n+1/2}])\right) k=1......N_x$$

UNIVERSITÉ Clermont Auvergne

Department of Electronics
University of Split,
Split, Croatia

EM Field Coupling to Overhead Wires

Computational example: Transient response of GPR dipole antenna at the center of the line

The excitation: Gaussian pulse

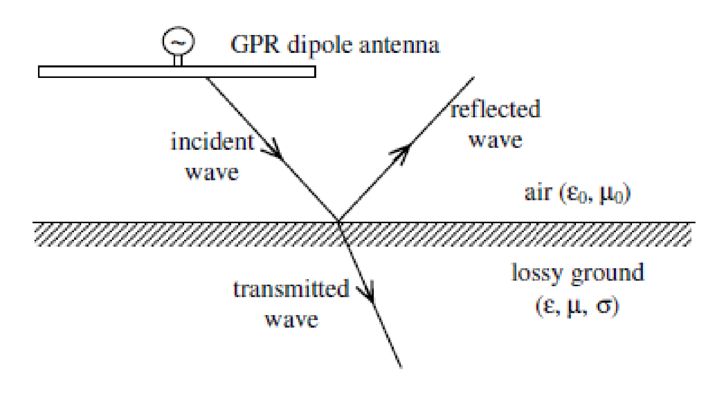

GPR dipole antenna above a lossy half-space

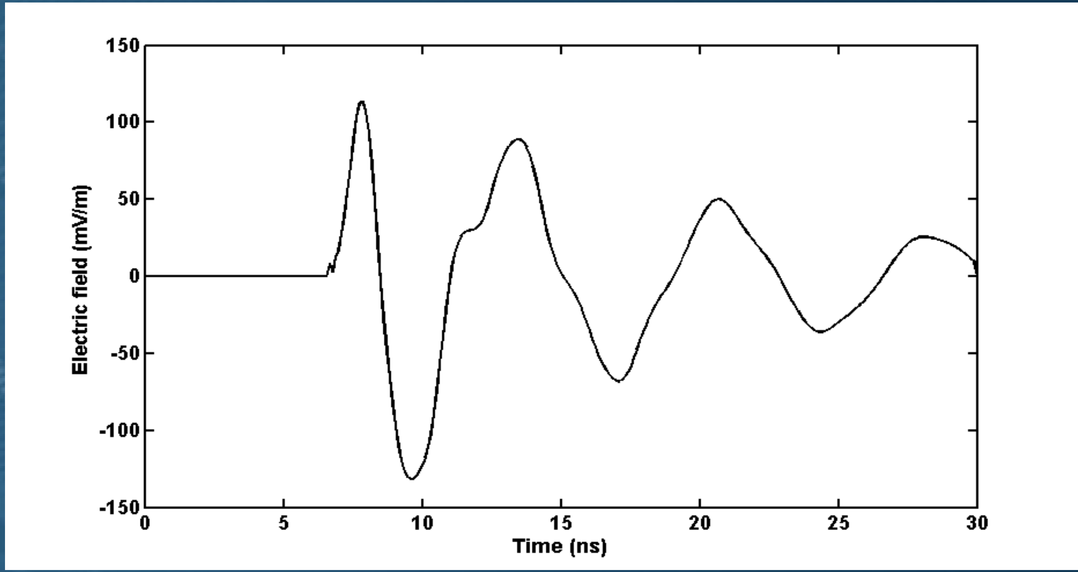

Transmitted electric field in the dielectric half-space (ε_r=10)

$$\int_0^L \frac{I(x',t-\frac{R}{c})}{4\pi R}dx' - \int_{-\infty}^{t}\int_0^L r(\theta,\tau)\frac{I(x',t-\frac{R^*}{c}-\tau)}{4\pi R^*}dx'd\tau = \frac{1}{2Z_0}\int_0^L E_x^{inc}(x',t-\frac{|x-x'|}{c})dx' + F_0(t-\frac{x}{c}) + F_L(t-\frac{L-x}{c})$$

$$E_x^{tr}(r,t) = \frac{\mu_0}{4\pi}\int_{-\infty}^{t}\int_0^L \Gamma_{tr}^{MIT}(\theta,\tau)\frac{\partial I(x',t-R''/v-\tau)}{\partial t}\frac{e^{-\frac{1}{\tau_g}\frac{R''}{v}}}{R''}dx'd\tau$$

Department of Electronics
University of Split,
Split, Croatia

EM Field Coupling to Overhead Wires

Computational example: Transient response of GPR dipole antenna at the center of the line

The excitation: Gaussian pulse

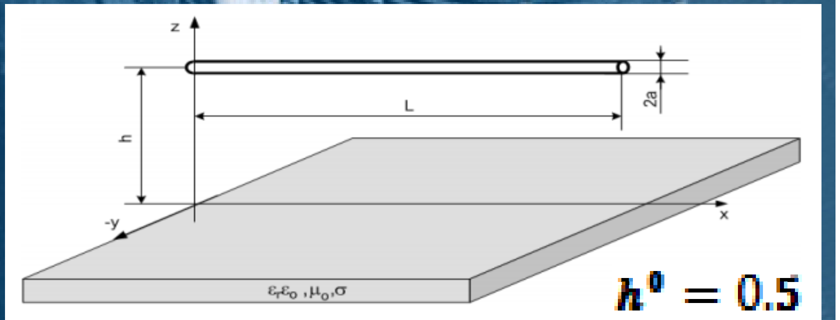

Deterministic thin wires above lossy ground.

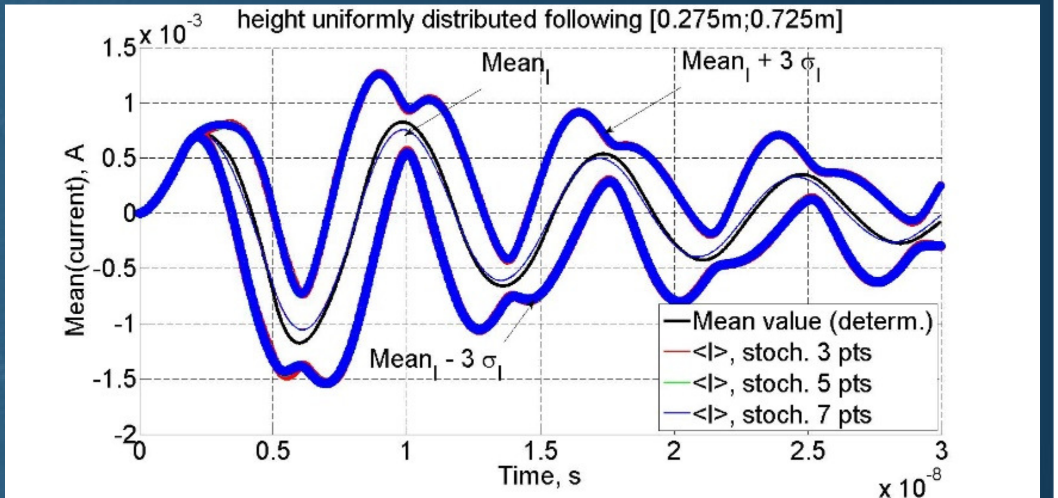

Stochastic case #2: wire height uniformly distributed between 0.275 and 0.725 m

Department of Electronics
University of Split,
Split, Croatia

EM Field Coupling to Overhead Wires

Computational example: Transient response at the center of the line

The excitation: EMP
normal incidence

$$E_x^{inc} = E_0\left(e^{-at} - e^{-bt}\right)$$

E_0=1.1V/m, a=7.92*$10^4$$s^{-1}$, b=4*$10^4$$s^{-1}$

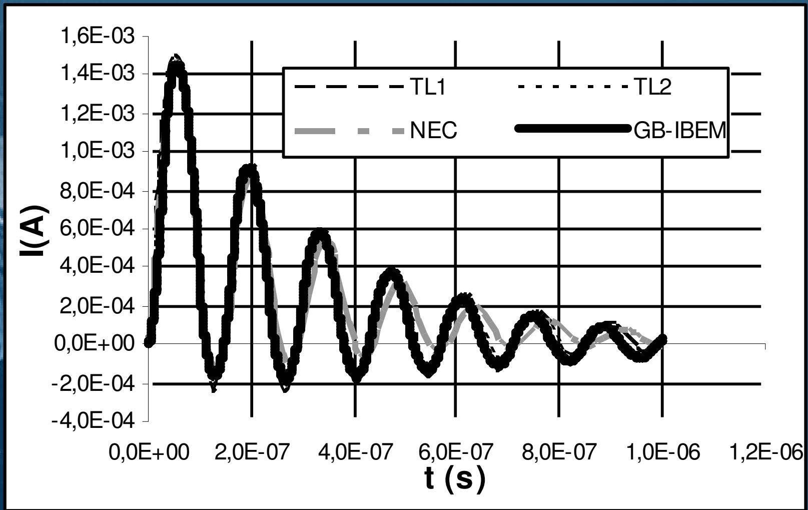

Transient current at the center of the line above dielectric half-space (L=20m,h=1m, ε_r=10)

The excitation: Gaussian pulse

$$E_x^{inc} = E_0 e^{-g^2(t-t_0)^2}$$

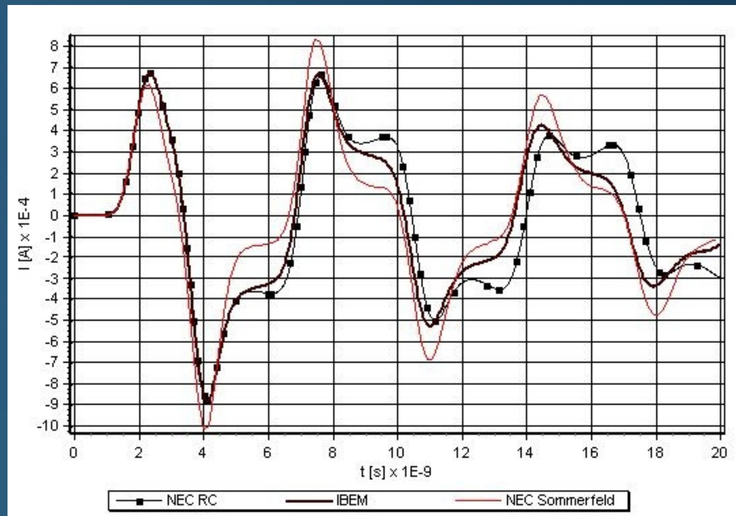

Transient current induced at the center of the wire above a lossy ground (*L*=1m, ε_r=10, σ=10mS/m)

Department of Electronics
University of Split,
Split, Croatia

EM Field Coupling to Overhead Wires

Computational example: Transient response at the center of the line

Configuration:

- L=1 m, a=2 mm, ε_r=10
- Incident electric field:

$$E_x^{inc}(t) = E_0(e^{-at} - e^{-bt})$$

E_0=1 V/m, a=4*10^7 s^{-1},b=6*10^8 s^{-1}

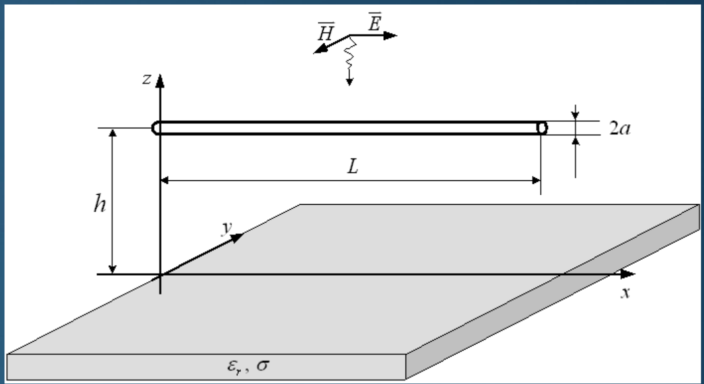

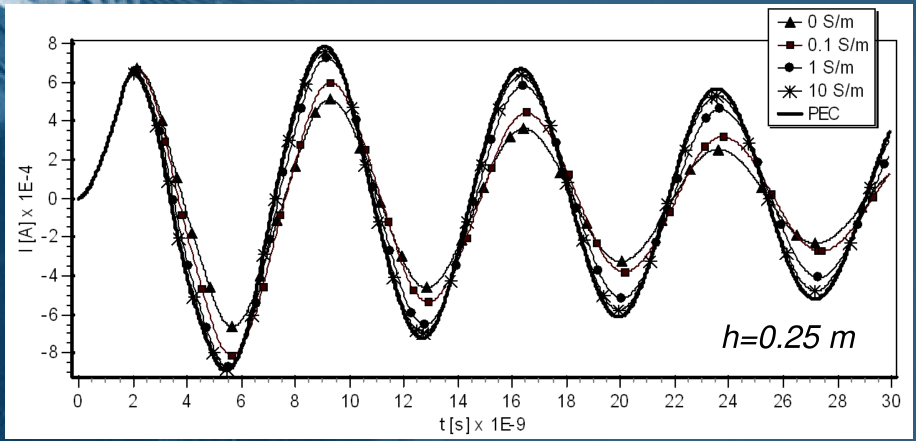

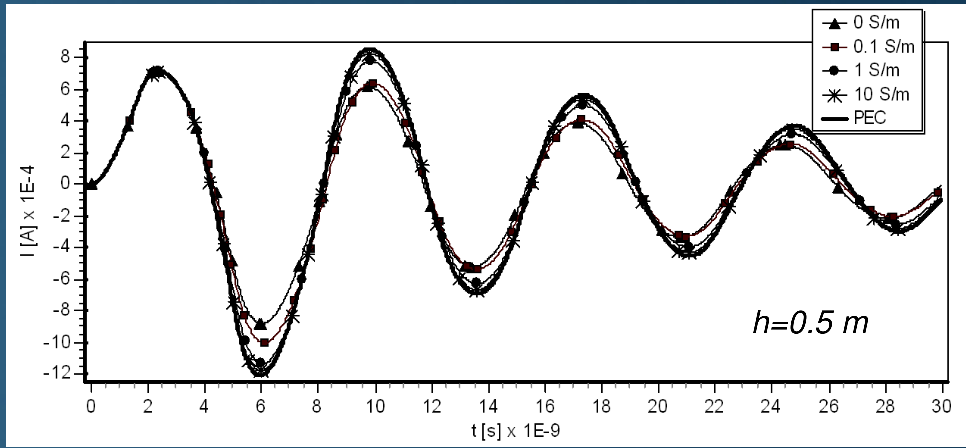

Transient current at the wire center, various conductivities:

Department of Electronics
University of Split,
Split, Croatia

EM Field Coupling to Overhead Wires

TD antenna model: Inclusion of ground conductivity

- Notes

- GB-IBEM expanded to numerically model ground conductivity
- Time dependent part of the reflection coefficient is modeled via additional vectors
- Convolutions integrals highly computationally inefficient
- Further modifications regarding computational efficiency necessary

UNIVERSITÉ Clermont Auvergne

Department of Electronics
University of Split,
Split, Croatia

EM Field Coupling to Overhead Wires

Computational example: *Transient response of a two -wire array above a PEC ground - comparison between IFFT-NEC2, GB-IBEM and TL*

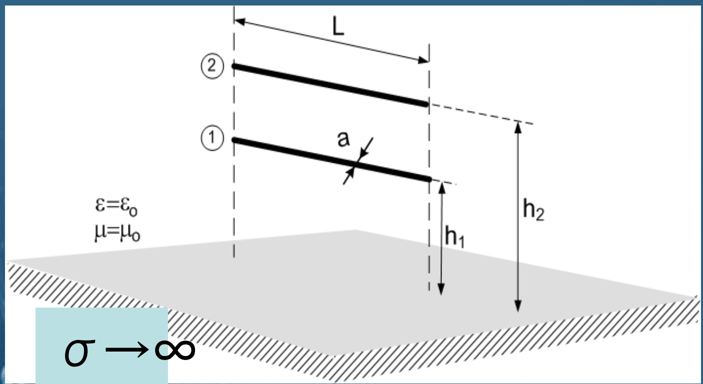

L=10m, a=2cm
h_1=1m, h_2=2m

Excitation: EMP
E_0=1V/m, a=4*$10^7 s^{-1}$, b=6*$10^8 s^{-1}$

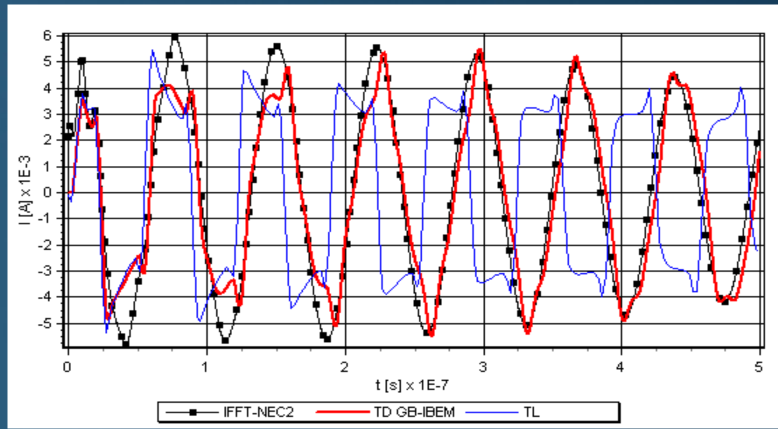

Transient current induced at the center of wire 1

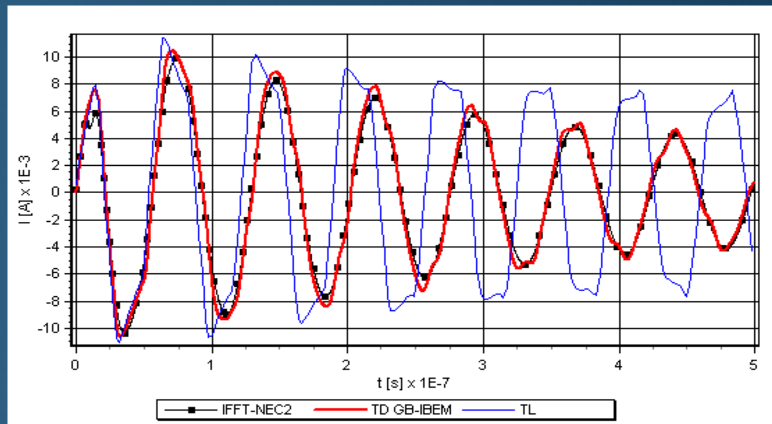

Transient current induced at the center of wire 2

Department of Electronics
University of Split,
Split, Croatia

EM Field Coupling to Overhead Wires

Computational example: *Transient response of a two -wire array above a PEC ground - comparison between IFFT-NEC2, GB-IBEM and TL*

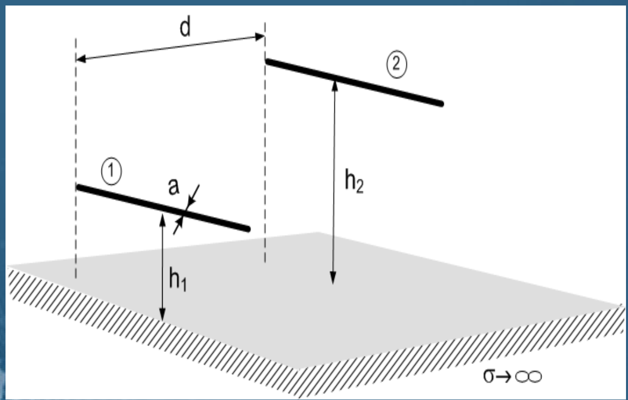

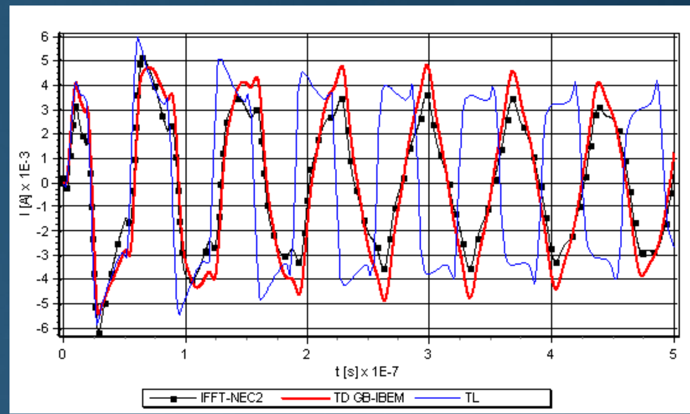

Transient current induced at the center of wire 1

L=10m, a=2cm,
h_1=1m, h_2=2m, d=1m

Excitation: EMP
E_0=1V/m, $a=4*10^7 s^{-1}$, $b=6*10^8 s^{-1}$

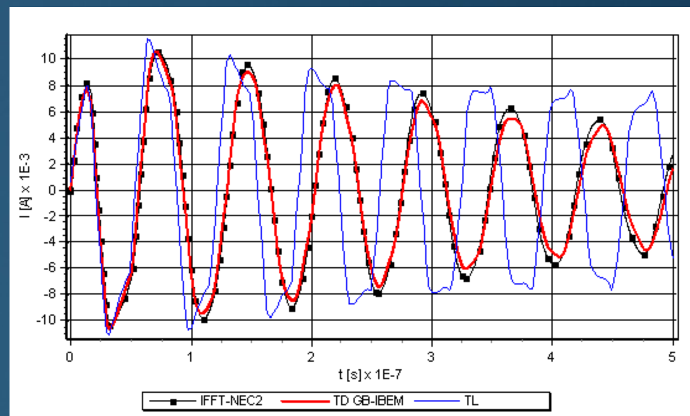

Transient current induced at the center of wire 2

Department of Electronics
University of Split,
Split, Croatia

EM Field Coupling to Overhead Wires

Computational example: *Transient response of a three -wire array above a PEC ground - comparison between IFFT-NEC2, GB-IBEM and TL*

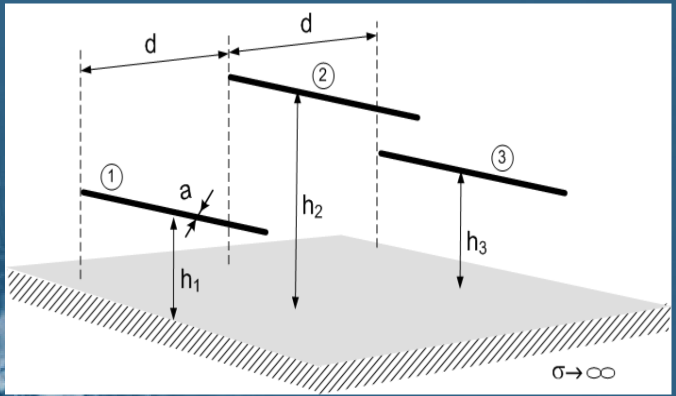

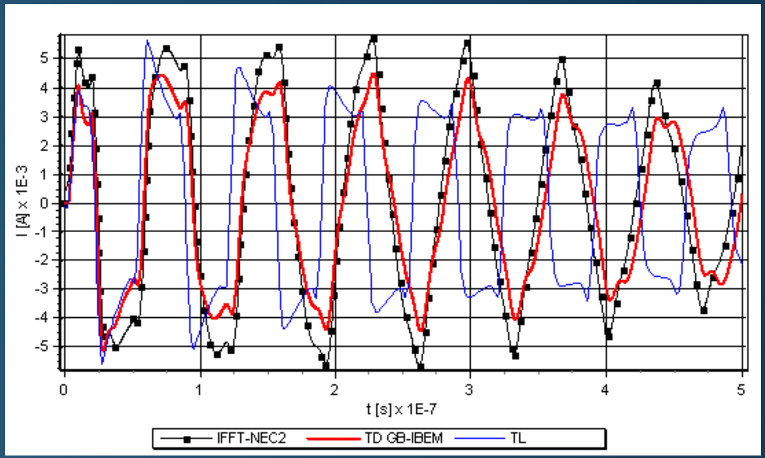

Transient current induced at the center of wires 1 and 3

L=10m, a=2cm,
$h_1=h_3$=1m, h_2=2m, d=1m

Excitation: EMP
E_0=1V/m, $a=4{*}10^7 s^{-1}$, $b=6{*}10^8 s^{-1}$

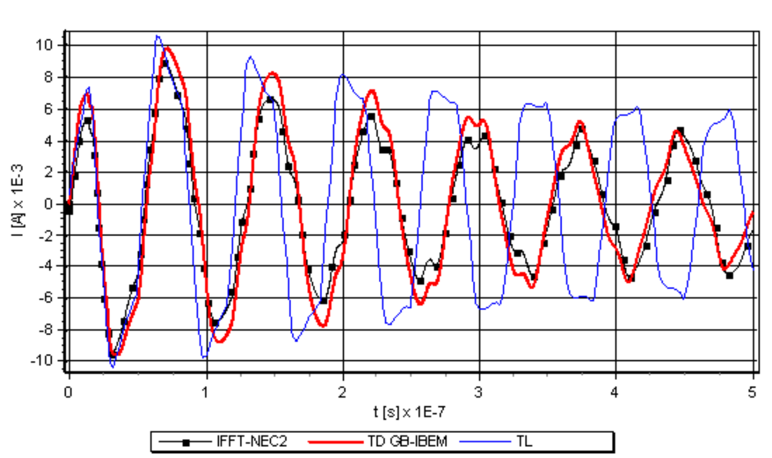

Transient current induced at the center of wire 2

Université Clermont Auvergne

Department of Electronics
University of Split,
Split, Croatia

EM Field Coupling to Overhead Wires

Computational example: *Transient response of a two-wire array above a PEC ground - comparison between IFFT-NEC2, GB-IBEM and TL*

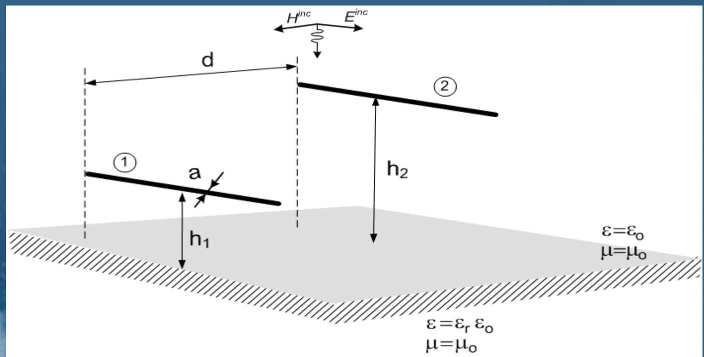

L=10m, *a*=2cm,
h_1=1m, h_2=2m, d=1m

Excitation: EMP
E_0=1V/m, *a*=$4*10^7 s^{-1}$, *b*=$6*10^8 s^{-1}$

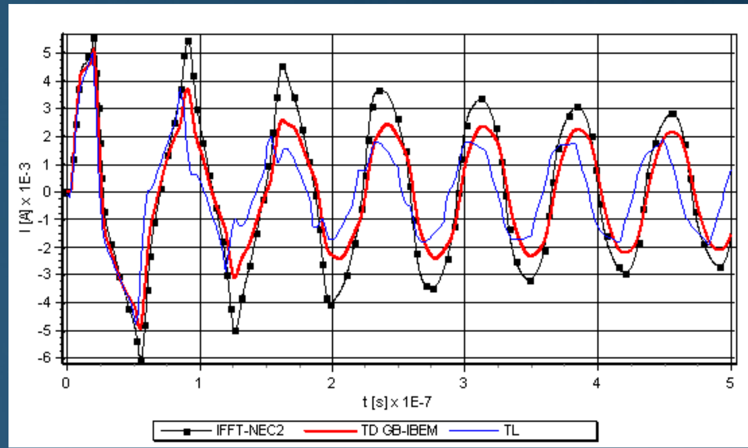

Transient current induced at the center of wires 1 and 3

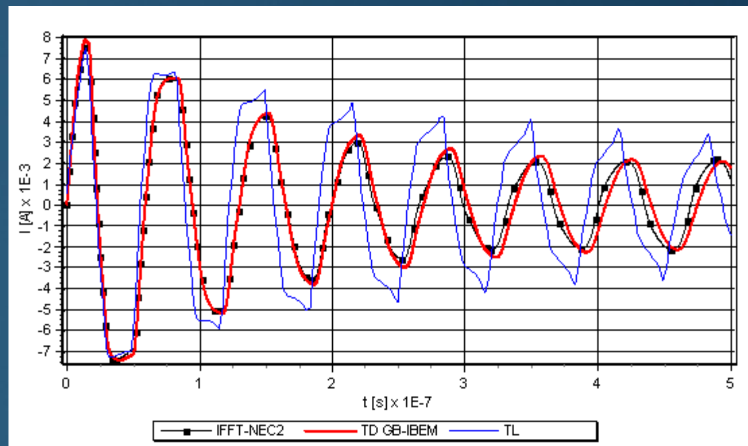

Transient current induced at the center of wire 2

UNIVERSITÉ Clermont Auvergne

Department of Electronics
University of Split,
Split, Croatia

EM Field Coupling to Overhead Wires

Computational example: *Transient response of a three -wire array above a PEC ground - comparison between IFFT-NEC2, GB-IBEM and TL*

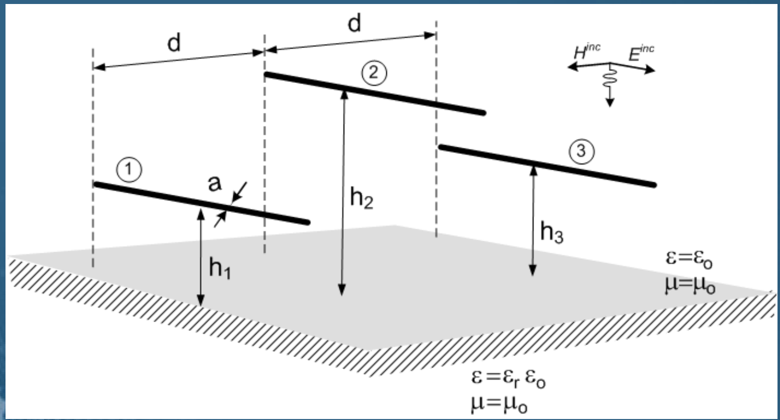

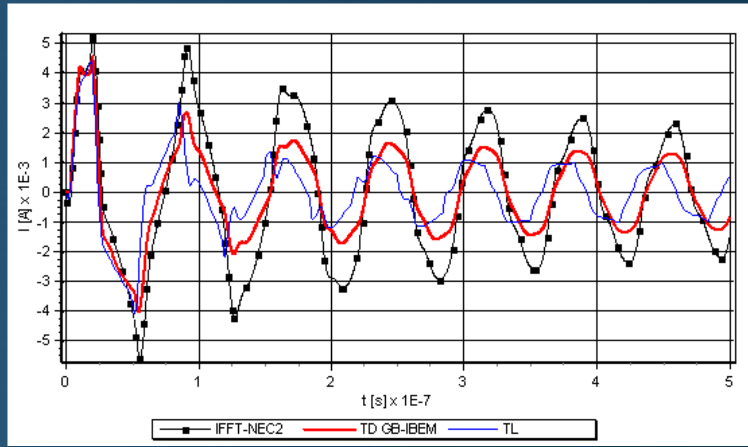

Transient current induced at the center of wires 1 and 3

L=10m, a=2cm,
$h_1=h_3$=1m, h_2=2m, d=1m
E_r=10

Excitation: EMP
E_0=1V/m, $a=4*10^7 s^{-1}$, $b=6*10^8 s^{-1}$

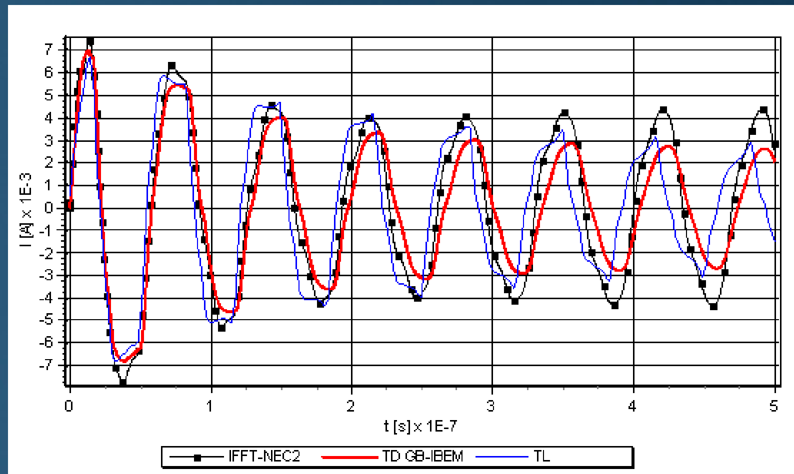

Transient current induced at the center of wire 2

UNIVERSITÉ Clermont Auvergne

Department of Electronics
University of Split,
Split, Croatia

EM Field Coupling to Overhead Wires

Computational example: *Two wire array: PEC and dielectric half space comparisons*

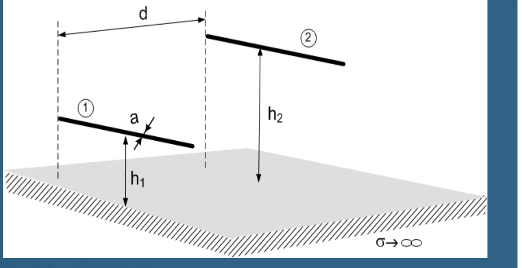

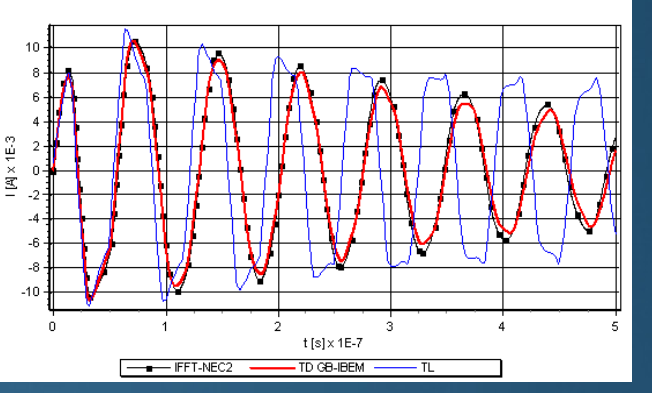

Transient current induced at the center of wire 2 – <u>PEC ground</u>

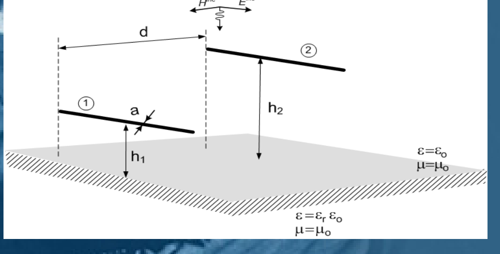

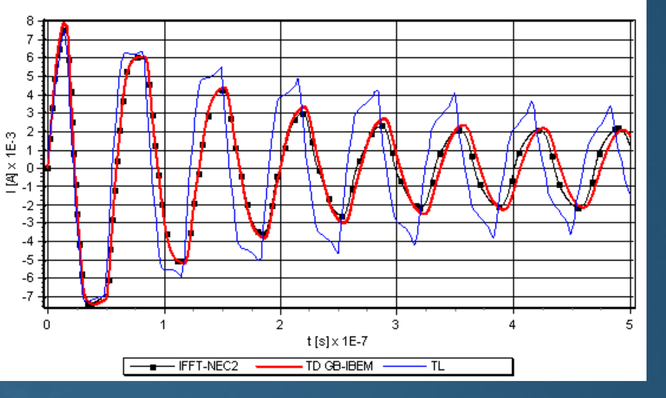

Transient current induced at the center of wire 2 – <u>dielectric half-space</u>

The results obtained via different approaches agree for early time instants in both cases.

At later times TL fails to ensure valid results due to limitations of the model itself (radiation effects).

Department of Electronics
University of Split,
Split, Croatia

EM Field Coupling to Overhead Wires

Computational example: *Two wire array: PEC and dielectric half space comparisons*

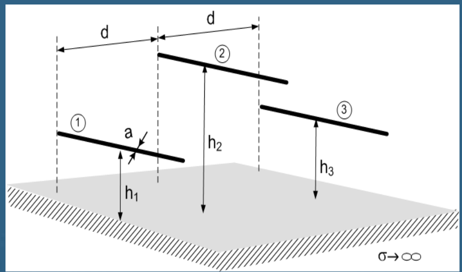

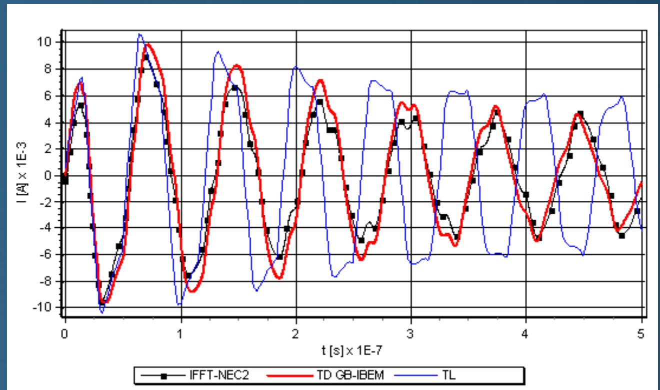

Transient current induced at the center of wire 2 – PEC ground

The behaviour of 3-wires above PEC ground is similar to a two-wire array.

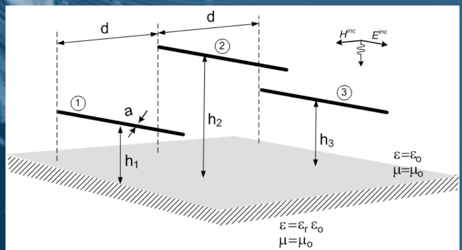

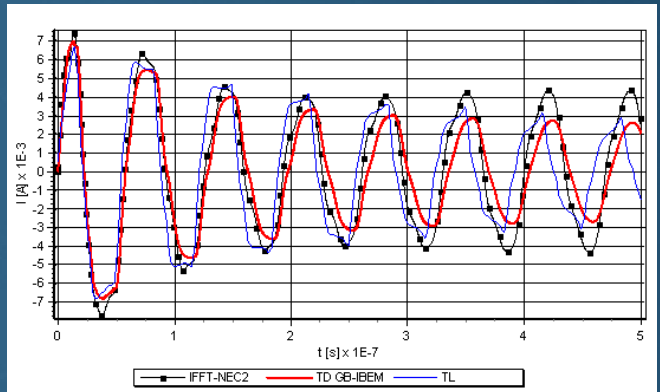

Transient current induced at the center of wire 2 – dielectric half-space

For dielectric half-space NEC 2 produces non-physical solution (magnitude increase) at later times.

Department of Electronics
University of Split,
Split, Croatia

Electromagnetic Field Coupling to Buried Wires

- EM field coupling buried wires in frequency domain has been studied using the wire antenna theory (set of the Pocklington equations) and Transmission line method (Telegrapher's equations).

- The Pocklington equation is solved via the Galerkin-Bubnov scheme of the Indirect Boundary Element Method (GB-IBEM), while the transmission line equations are treated using the chain matrix method and modal equation to derive per unit length parameters.

UNIVERSITÉ Clermont Auvergne

Department of Electronics
University of Split,
Split, Croatia

EM Field Coupling to Buried Wires

The antenna model: FD analysis of a single wire

• The spatial current distribution along the wire is governed by the Pocklington integro-differential equation:

$$E_x^{exc} = j\omega\frac{\mu}{4\pi}\int_0^L I(x')g(x,x')dx' - \frac{1}{j4\pi\omega\varepsilon_{eff}}\frac{\partial}{\partial x}\int_0^L \frac{\partial I(x')}{\partial x'}g(x,x')dx'$$

$$g(x,x') = g_0(x,x') - R_{TM}\, g_i(x,x')$$

$$g_0(x,x') = \frac{e^{-jk_2R_1}}{R_1} \qquad g_i(x,x') = \frac{e^{-jk_2R_2}}{R_2}$$

$$\varepsilon_{eff} = \varepsilon_r\varepsilon_0 - j\frac{\sigma}{\omega}$$

$$R_1 = \sqrt{(x-x')^2 + a^2}, \quad R_2 = \sqrt{(x-x')^2 + 4d^2}$$

$$\Gamma_{TM} = \frac{2\sqrt{\underline{n}}\cos\theta}{\underline{n}\cos\theta + \sqrt{\underline{n} - \sin^2\theta}}$$

$$E_x^{exc} = E_x^{tr} = E_0\Gamma_{TM}e^{-jk_2d}$$

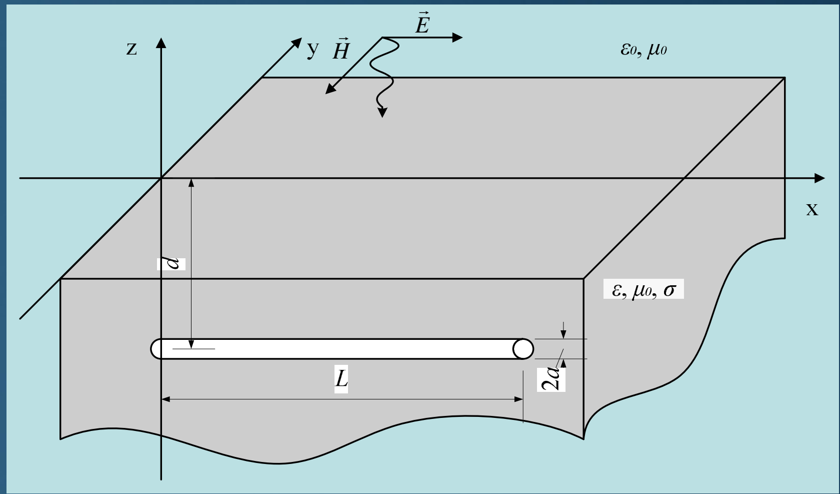

The straight wire buried in a lossy earth, illuminated by the transmitted E-Field

Department of Electronics
University of Split,
Split, Croatia

The geometry of horizontal buried thin wires

The antenna model: FD analysis of multiple buried wires

- The FD analysis of multiple wire array buried in a lossy ground is carried out via the set of Pocklington integro-differential equation:

$$E_x^{exc} = -\frac{1}{j4\pi\omega\varepsilon_{eff}} \sum_{n=1}^{M} \int_{-L_n}^{L_n} \left[\frac{\partial^2}{\partial x^2} + k_2^2 \right] \left[g_{0mn}(x,x') - R'_{TM}\, g_{imn}(x,x') \right] I_n(x')\, dx'$$
$$m = 1,2,\ldots,M$$

- The Green's functions

$$g_{0mn}(x,x') = \frac{e^{-jk_2 R_{1mn}}}{R_{1mn}}, \quad g_{imn}(x,x') = \frac{e^{-jk_2 R_{2mn}}}{R_{2mn}}$$

$$R_{1mn} = \sqrt{(x-x')^2 + a_m^2}, \quad R_{2mn} = \sqrt{(x-x')^2 + 4d_m^2} \quad m = n$$

$$R_{1mn} = \sqrt{(x-x')^2 + D_{mn}^2}, \quad R_{2mn} = \sqrt{R_{1mn}{}^2 + 4d_m^2} \quad m \neq n$$

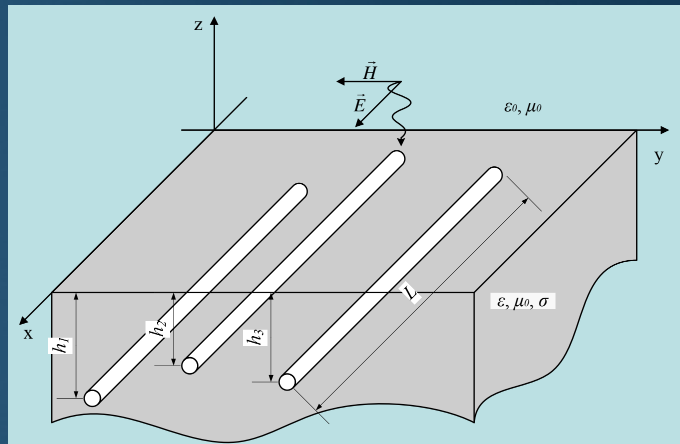

The geometry of horizontal buried thin wires

Department of Electronics
University of Split,
Split, Croatia

EM Field Coupling to Buried Wires

The antenna model: TD analysis of single wire

• The transient current distribution along the wire is governed by the space-time integro-differential equation of the Pocklington type:

$$\left[\frac{\sigma}{\varepsilon}+\frac{\partial}{\partial t}\right]E_x^{tr}=\left[-v^2\frac{\partial^2}{\partial x^2}+\frac{\partial^2}{\partial t^2}+\frac{\sigma}{\varepsilon}\frac{\partial}{\partial t}\right]\cdot\left[\frac{\mu}{4\pi}\int_0^L I(x',t-R/v)\frac{e^{-\frac{t}{\tau_g}\frac{R}{v}}}{R}dx'-\int_{-\infty}^{t}\int_0^L\Gamma_{ref}(\theta,\tau)\frac{I(x',t-R^*/v-\tau)}{4\pi R^*}\frac{e^{-\frac{t}{\tau_g}\frac{R^*}{v}}}{R^*}dx'd\tau\right]$$

The transmitted electric field is defined by the convolution integral:

$$E_x^{tr}(x,t)=\int_{-\infty}^{t}E_x^{inc}(x,t-\tau)\Gamma_{tr}^{Fr,MIT}(\theta_{tr},\tau)d\tau$$

The reflection and transmission coefficient, respectively, is given by:

$$\Gamma_{ref}^{MIT}(t)=-\left[\frac{\tau_1}{\tau_2}\delta(t)+\frac{1}{\tau_2}\left(1-\frac{\tau_1}{\tau_2}\right)e^{-t/\tau_2}\right]$$

$$\Gamma_{tr}^{MIT}(t)=\frac{\tau_3}{\tau_2}\delta(t)+\frac{1}{\tau_2}\left(1-\frac{\tau_3}{\tau_2}\right)e^{-t/\tau_2}$$

Department of Electronics
University of Split,
Split, Croatia

EM Field Coupling to Buried Wires

The antenna model: TD analysis of single wire

• Analytical solution: The Pocklington equations can be transformed into a differential equation of the form:

$$\left(\mu\varepsilon\frac{\partial}{\partial t}+\mu\sigma\right)E_x^{tr}(t)=-\left(\frac{\partial^2}{\partial x^2}-\mu\sigma\frac{\partial}{\partial t}-\mu\varepsilon\frac{\partial^2}{\partial t^2}\right)\left[\frac{\mu}{4\pi}I\left(x,t-\frac{a}{v}\right)\int_0^L\frac{e^{-\frac{1}{\tau_g}\frac{R}{v}}}{R}dx'-\frac{\mu}{4\pi}\int_0^t\Gamma_{ref}^{MIT}(\tau)\,I\left(x,t-\frac{a}{v}-\tau\right)\int_0^L\frac{e^{-\frac{1}{\tau_g}\frac{R^*}{v}}}{R^*}dx'd\tau\right]$$

Undertaking certain mathematical manipulations the solution can be obtained in the close form:

$$I(x,t)=\frac{4\pi}{\mu}\left\{R(s_\Psi)\left[1-\frac{\cosh\left(\gamma_\Psi\left(\frac{L}{2}-x\right)\right)}{\cosh\left(\gamma_\Psi\frac{L}{2}\right)}\right]e^{\left(t+\frac{a}{v}\right)s_\Psi}-\frac{\pi}{\mu\varepsilon L^2}\sum_{n=1}^{\infty}\frac{2n-1}{\pm\sqrt{b^2-4c_n}\,s_{1,2n}\Psi\left(s_{1,2n}\right)}\sin\frac{(2n-1)\pi x}{L}e^{\left(t+\frac{a}{v}\right)s_{1,2n}}\right\}$$

where:

$$R(s_\Psi)=\frac{1}{2\ln\frac{L}{2d}\frac{s_\Psi}{s_\Psi\tau_2+1}\left(\tau_1-\tau_2\frac{s_\Psi\tau_1+1}{s_\Psi\tau_2+1}\right)},\quad s_\Psi=-\frac{\ln\frac{L}{a}+\ln\frac{L}{2d}}{\tau_1\ln\frac{L}{a}+\tau_2\ln\frac{L}{2d}}$$

$$\gamma_\Psi=\sqrt{\mu\varepsilon\left(s_\Psi^2+bs_\Psi\right)},\quad s_{1,2n}=\frac{1}{2}\left(-b\pm\sqrt{b^2-4c_n}\right),\quad b=\frac{\sigma}{\varepsilon}$$

$$c_n=\frac{(2n-1)^2\pi^2}{\mu\varepsilon L^2},\quad n=1,2,3,\ldots$$

Department of Electronics
University of Split,
Split, Croatia

EM Field Coupling to Buried Wires

The TL model: FD analysis of multiple bureid wires

- Field-to-transmission line matrix equations are given by:

$$\frac{d}{dx}\left[\hat{V}(x)\right]+\left[\hat{Z}\right]\cdot\left[\hat{I}(x)\right]=\left[\hat{V}_F(x)\right]$$

$$\frac{d}{dx}\left[\hat{I}(x)\right]+\left[\hat{Y}\right]\cdot\left[\hat{V}(x)\right]=\left[\hat{I}_F(x)\right]$$

- The Longitudinal impedance matrix is of the form:

$$\left[\hat{Z}\right]=j\omega[L]+\left[\hat{Z}_w\right]+\left[\hat{Z}_g\right]$$

and the transversal admittance matrix is given by:

$$\left[\hat{Y}\right]=j\omega[C]+[G]$$

Department of Electronics
University of Split,
Split, Croatia

EM Field Coupling to Buried Wires

Computational example: Current distribution along the wire immersed into the sea water.

Wire geometry: L=120m, a=0.6m; L=160m, a=0.8m; f=1MHz
The sea waterparameters: ε_r=80 and σ=4S/m.

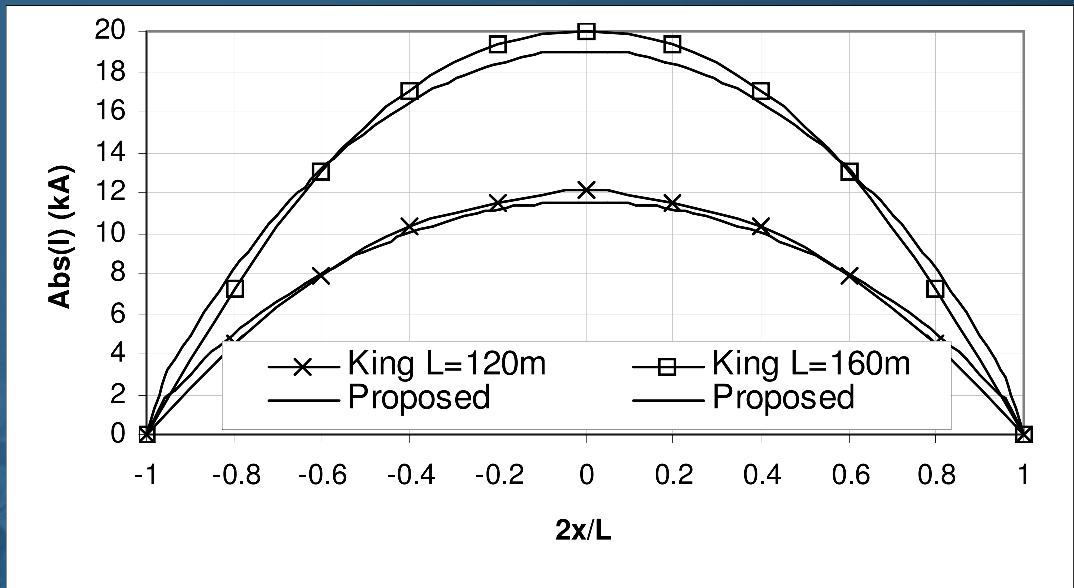

Current distribution along the wire

Department of Electronics
University of Split,
Split, Croatia

EM Field Coupling to Buried Wires

Computational example: Current induced at the center of the wire buried in a lossy ground versus frequency

The wire (L=20m, a=0.005m), buried at depth d=1m in the lossy ground Is excited by the plane wave E_0=1V/m (normal incidence).

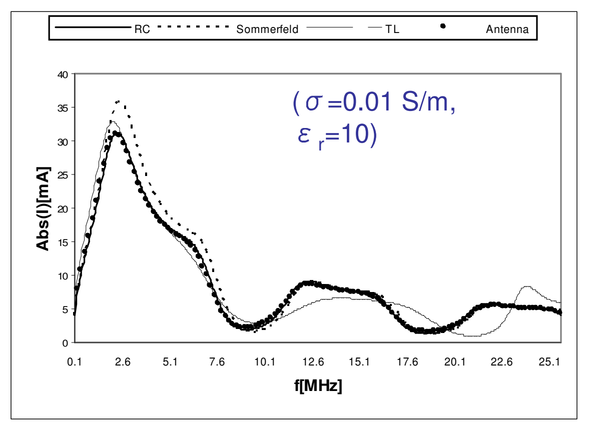

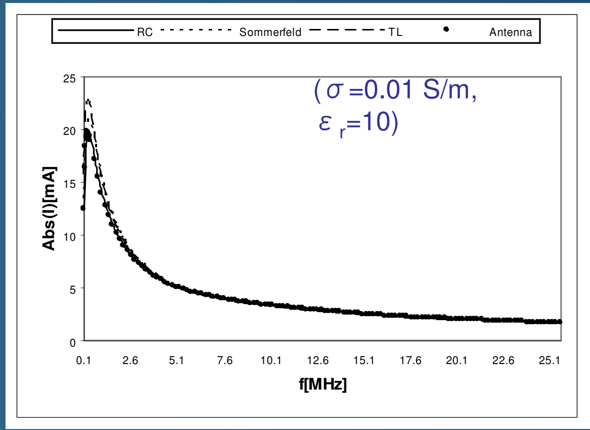

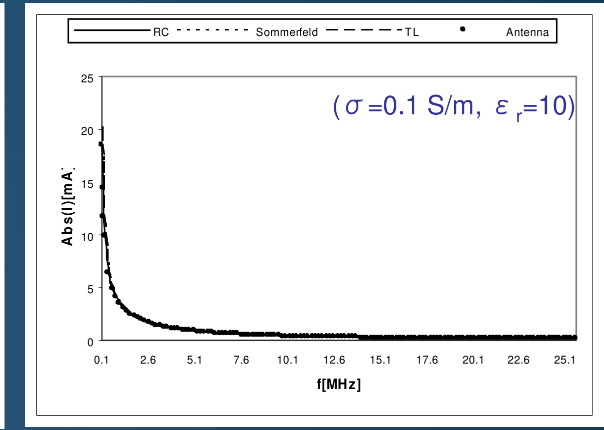

Current induced at the center of the wire buried in a lossy ground versus frequency

Department of Electronics
University of Split,
Split, Croatia

EM Field Coupling to Buried Wires

Computational example: Transient response at the center of the line

The L=5m long wire with a radius of a=1cm is buried at depth d=1m in dielectric ground with ε_r=10.

The wire is illuminated by the transmitted EMP: $E^{inc}(t) = E_0(e^{-at} - e^{-bt})$

E_0=52.5kV/m, $a=4 \cdot 10^6 s^{-1}$, $b=4.78 \cdot 10^8 s^{-1}$

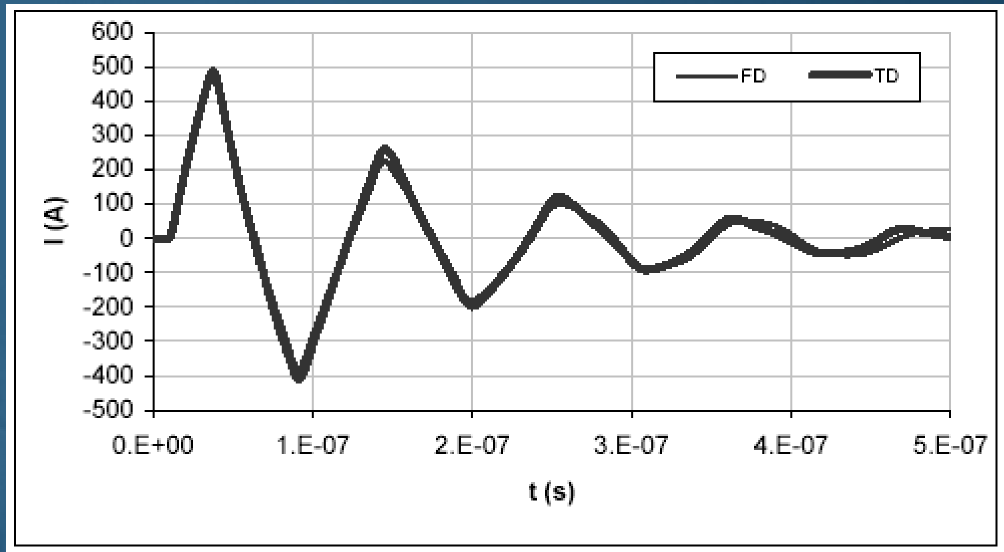

Transient currrent induced at the center of the straight wire: Comparison of direct TD approach to an indirect FD approach+IFFT

UNIVERSITÉ Clermont Auvergne

EM Field Coupling to Buried Wires

Department of Electronics
University of Split,
Split, Croatia

Computational example: Transient response at the center of the line

The transmission lines buried in a lossy ground with permittivity $\varepsilon_r=10$ and conductivity $\sigma=0.001$S/m are of interest.

Conductor radius is a=1cm while length L and burial depth d are varied.

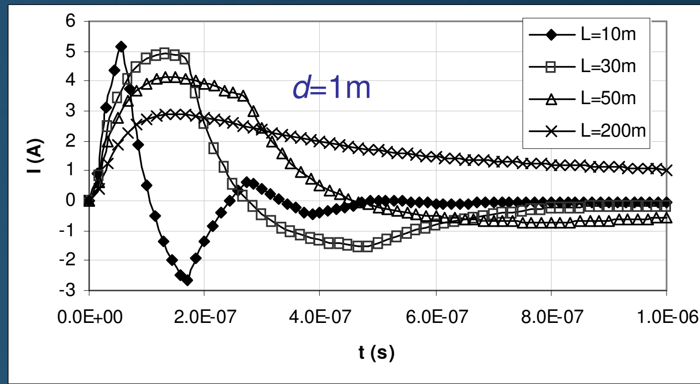

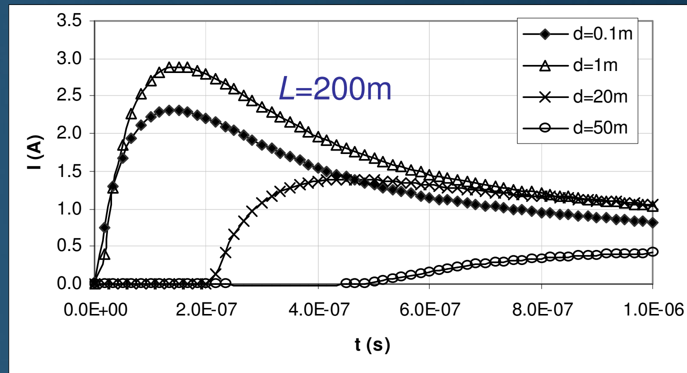

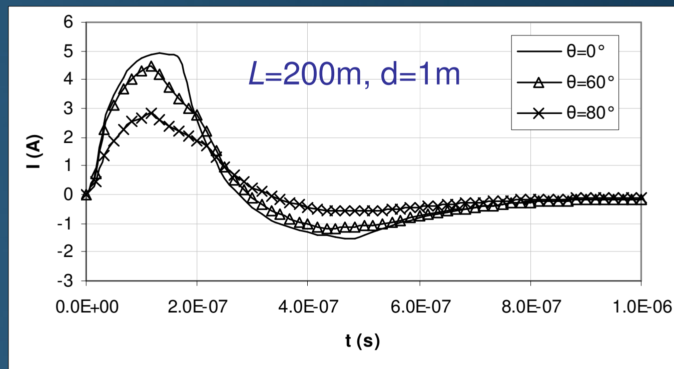

The excitation:

$$E_x^{tr}(t)=E_0 e^{-at}$$

$a=(8.85410^{-8}\mathrm{s})^{-1}$

Université Clermont Auvergne

EM Field Coupling to Buried Wires

Department of Electronics
University of Split,
Split, Croatia

Computational example: Frequency response at the center of the line

- Current induced at the centre of the wire
  - ε_r=10
  - plane wave excitation E_0=1 V/m

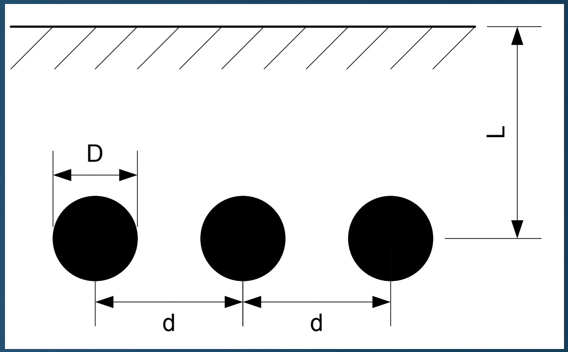

D=20.5 mm, d=36 mm, L=1 m

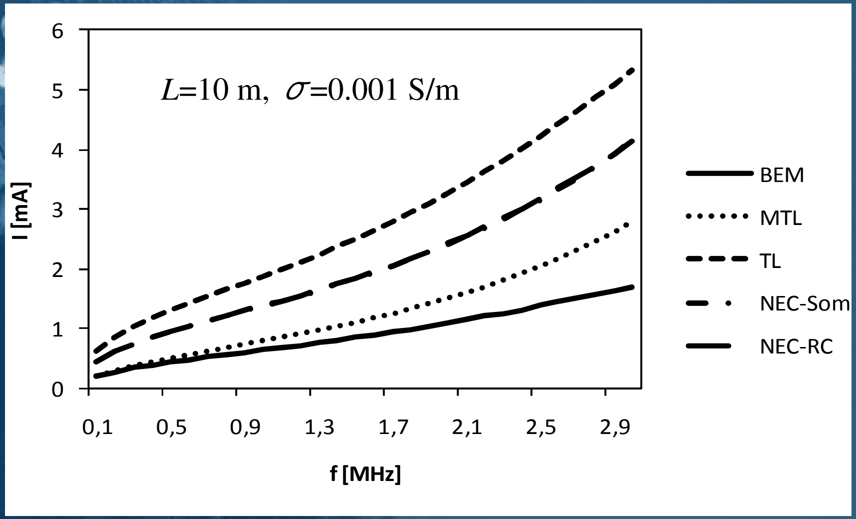

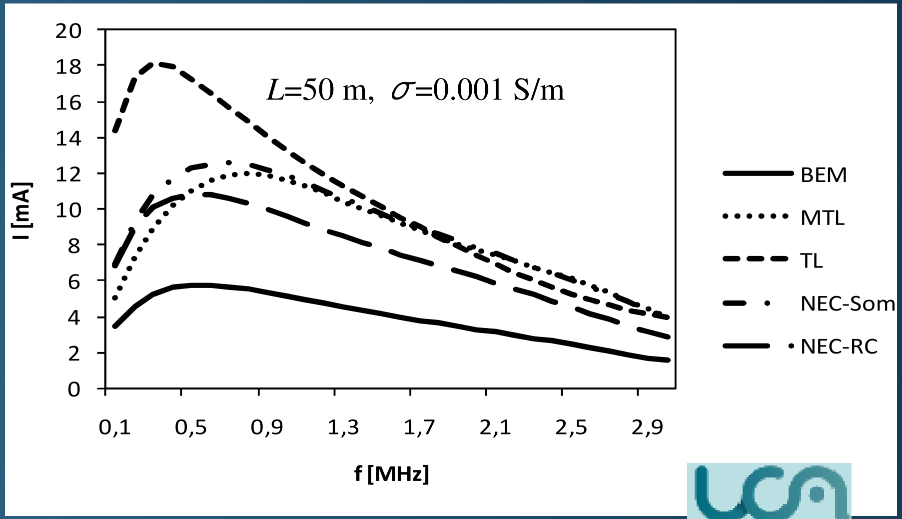

Université Clermont Auvergne

Department of Electronics
University of Split,
Split, Croatia

EM Field Coupling to Buried Wires

Computational example: Frequency response at the center of the line

- Current induced at the centre of the wire
  - $\varepsilon_r=10$
  - plane wave excitation $E_0=1$ V/m

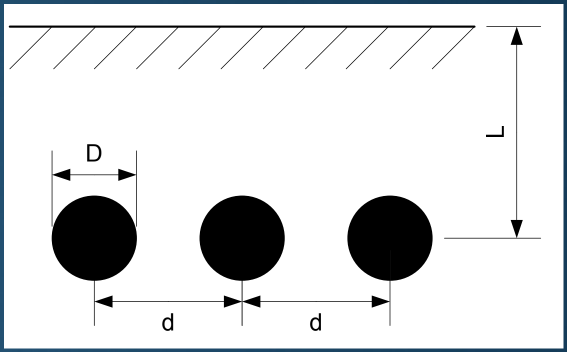

D=20.5 mm, d=36 mm, L=1 m

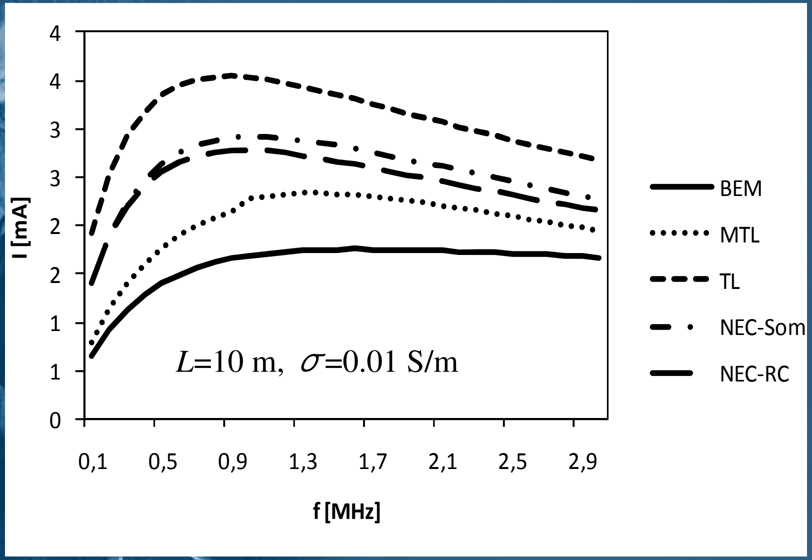

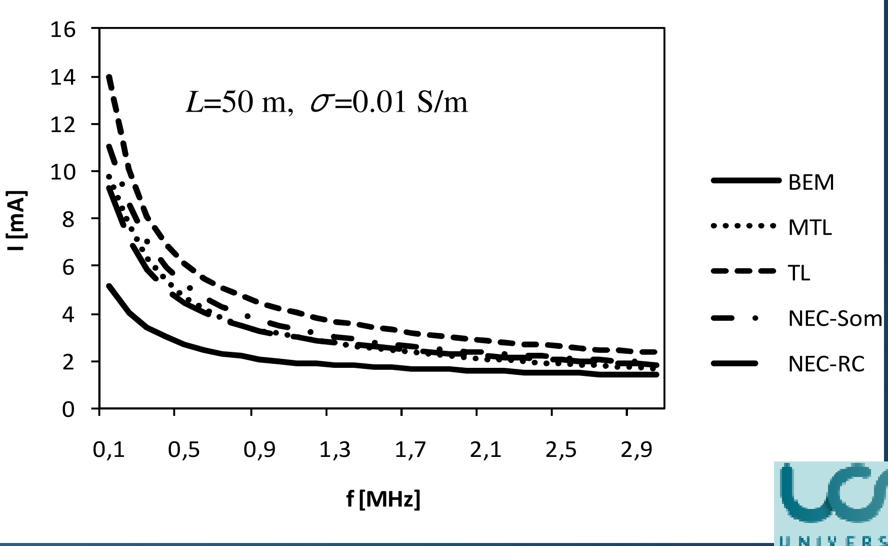

EM Field Coupling to Buried Wires

Department of Electronics
University of Split,
Split, Croatia

Computational example: Frequency response at the center of the line

- Current induced at the centre of the wire
  - $\varepsilon_r=10$
  - plane wave excitation $E_0=1$ V/m

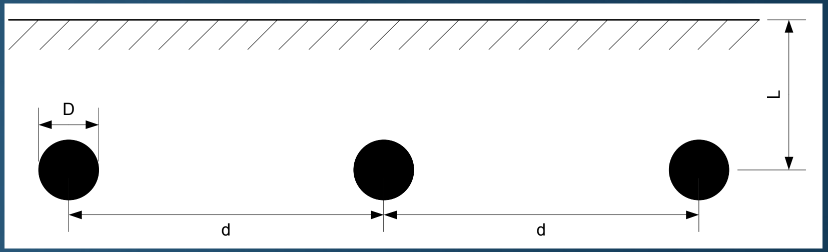

D=20.5 mm, d=106 mm, L=1 m

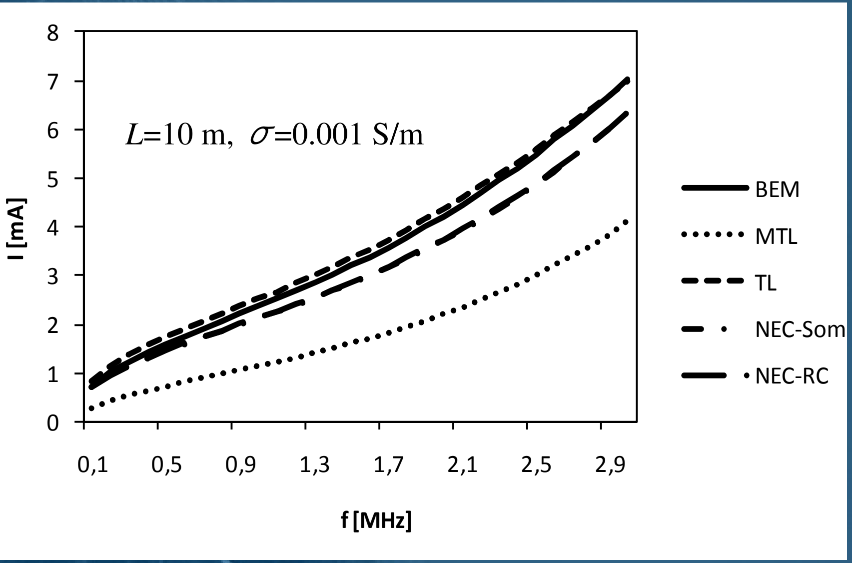

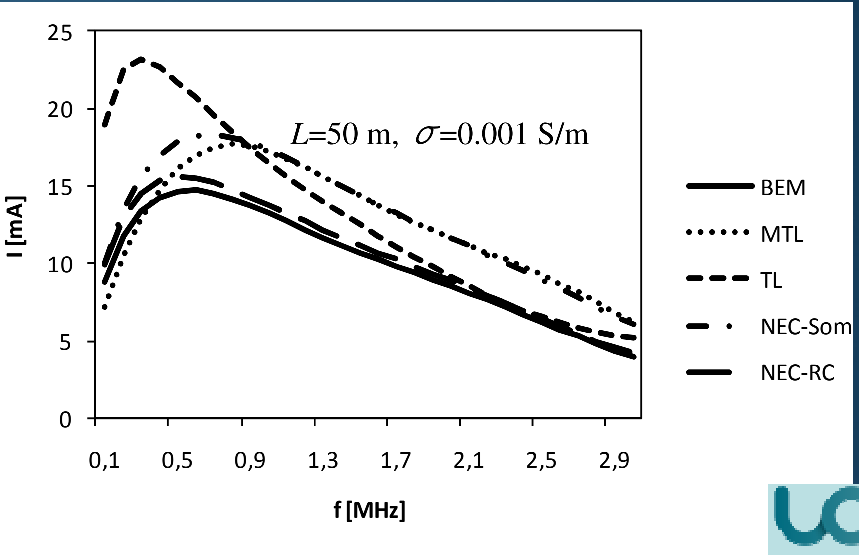

EM Field Coupling to Buried Wires

Department of Electronics
University of Split,
Split, Croatia

Computational example: Frequency response at the center of the line

- Current induced at the centre of the wire
  - ε_r=10
  - plane wave excitation E_0=1 V/m

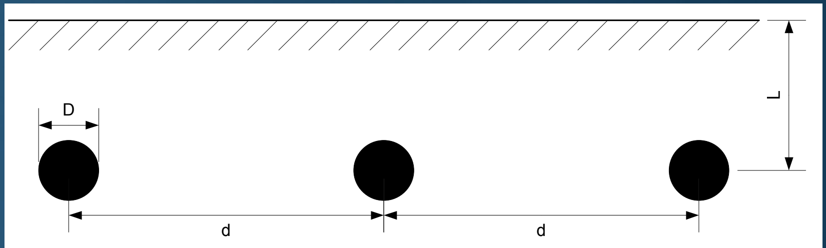

D=20.5 mm, d=106 mm, L=1 m

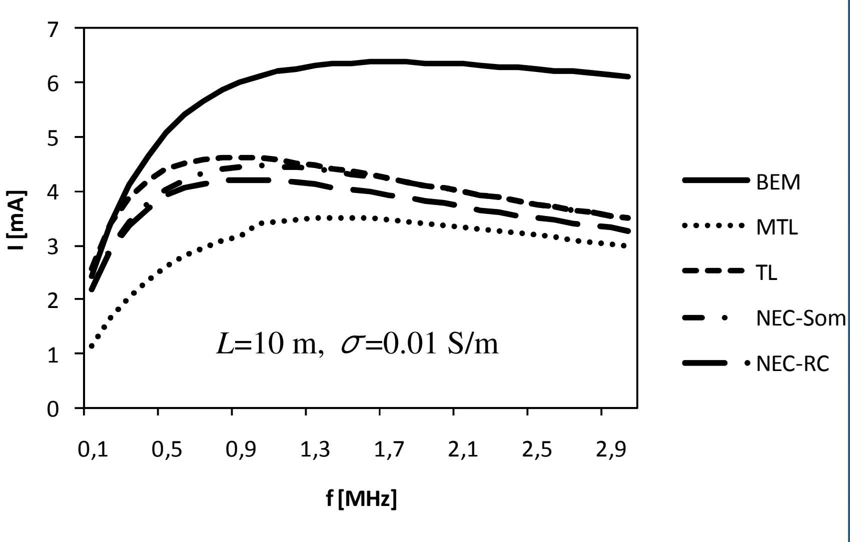

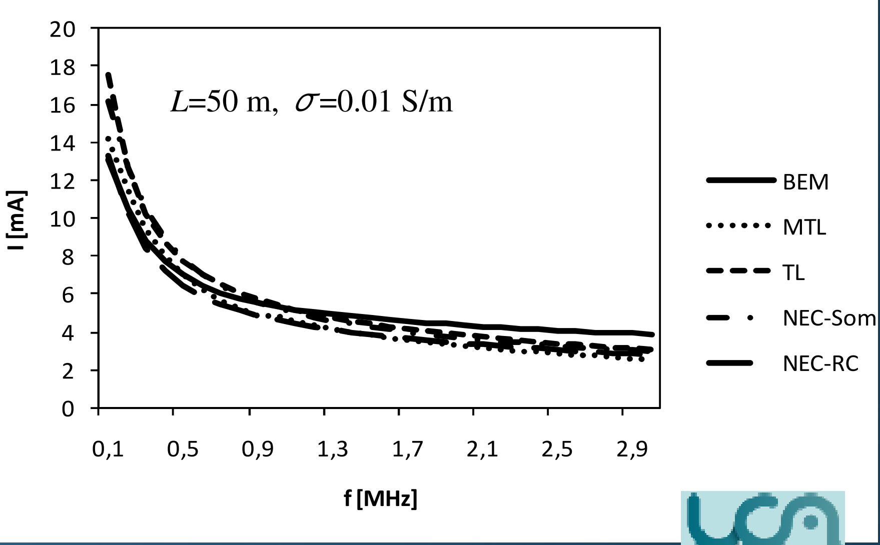

EM Field Coupling to Buried Wires

Department of Electronics
University of Split,
Split, Croatia

Computational example: Frequency response at the center of the line

- Current induced at the centre of the wire
  - $\varepsilon_r=10$
  - plane wave excitation $E_0=1$ V/m

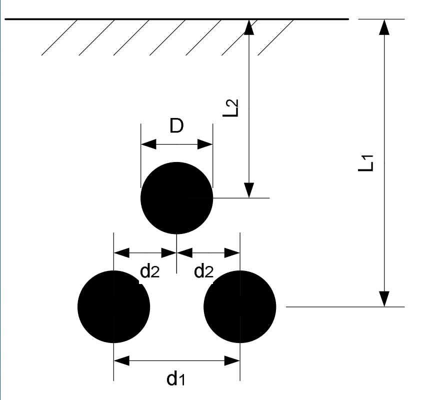

D=20.5 mm, d_1=36 mm, d_2=18 mm, L_1=1 m, L_2=0.97 m

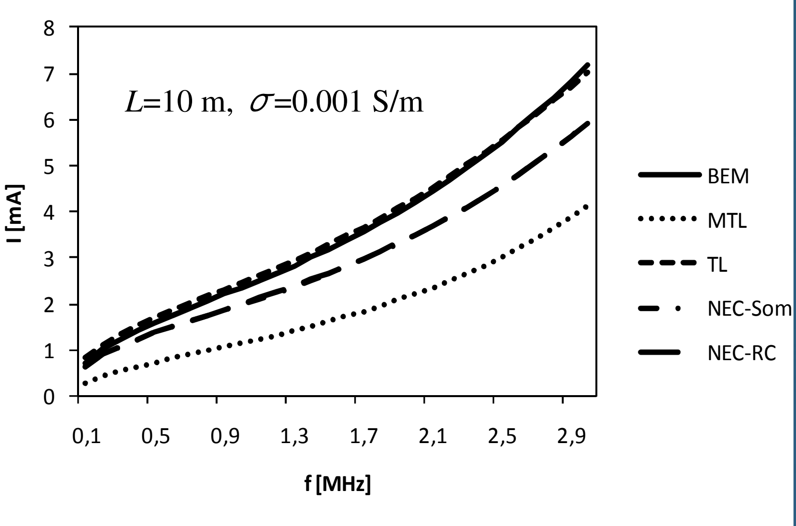

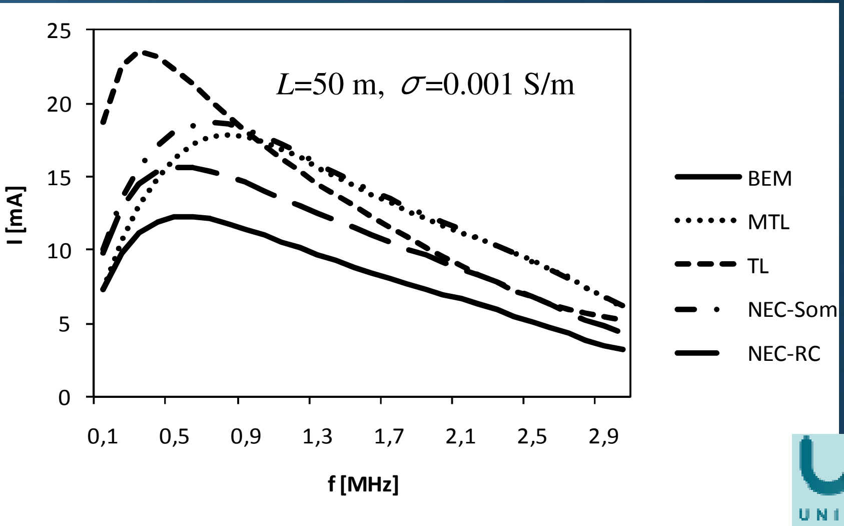

EM Field Coupling to Buried Wires

Department of Electronics
University of Split,
Split, Croatia

Computational example: Frequency response at the center of the line

- Current induced at the centre of the wire
  - $\varepsilon_r=10$
  - plane wave excitation E_0=1 V/m

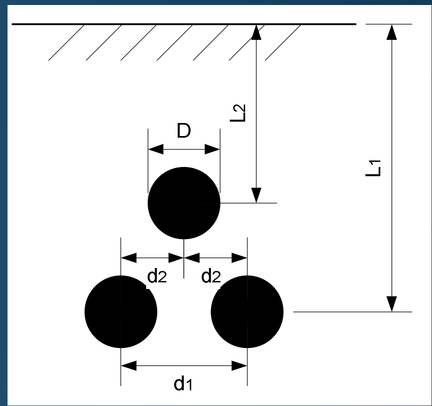

D=20.5 mm, d_1=36 mm, d_2=18 mm, L_1=1 m, L_2=0.97 m

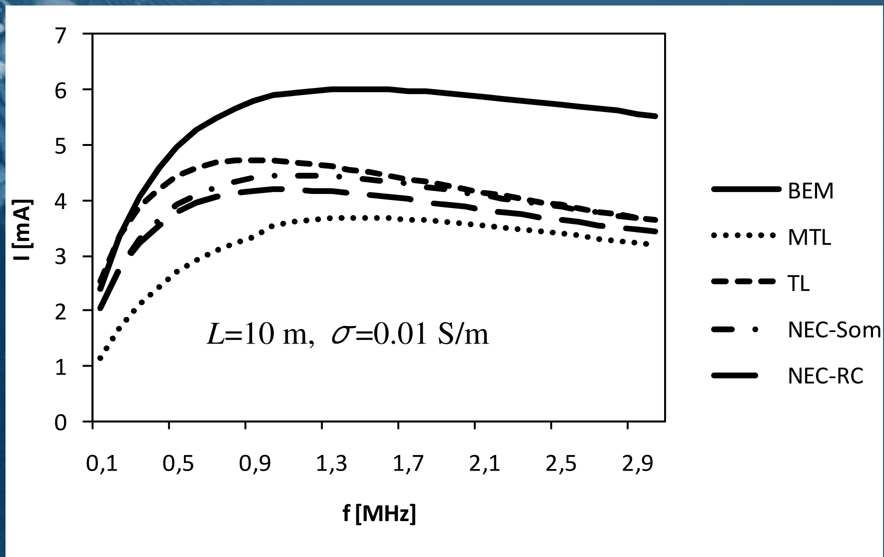

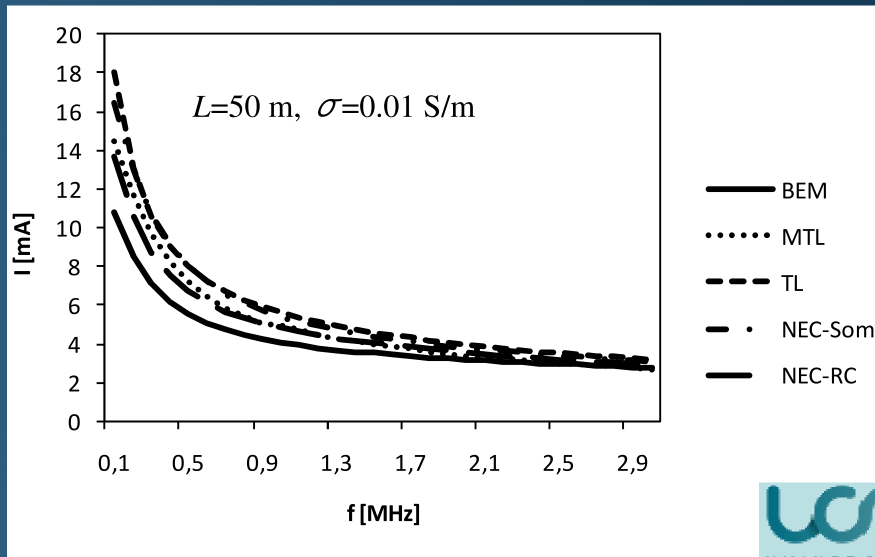

EM Field Coupling to Buried Wires

Department of Electronics
University of Split,
Split, Croatia

Computational example: Transient response at the center of the line

- direct TD method of solution

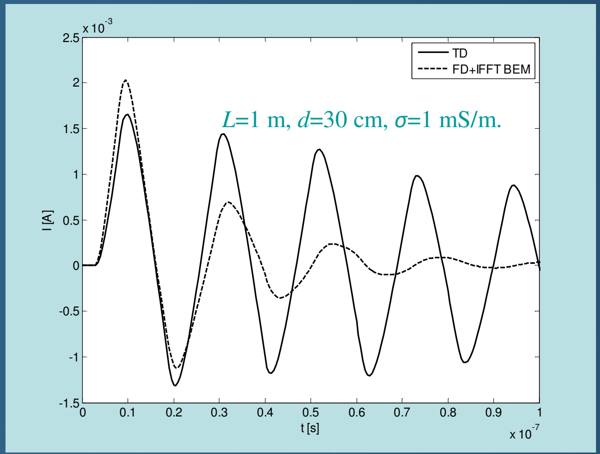

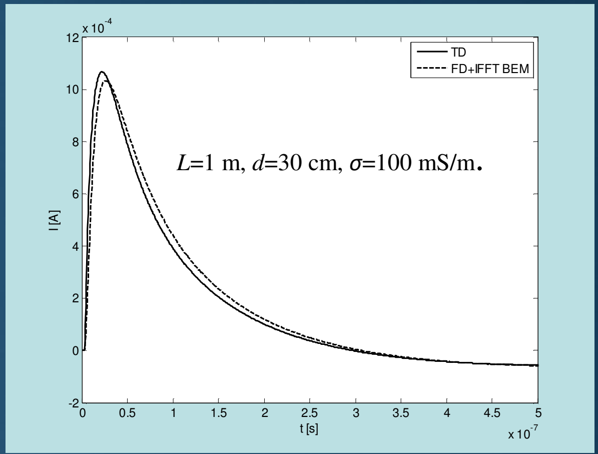

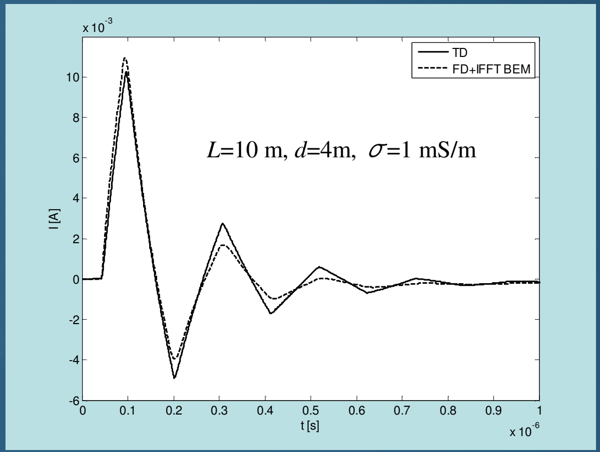

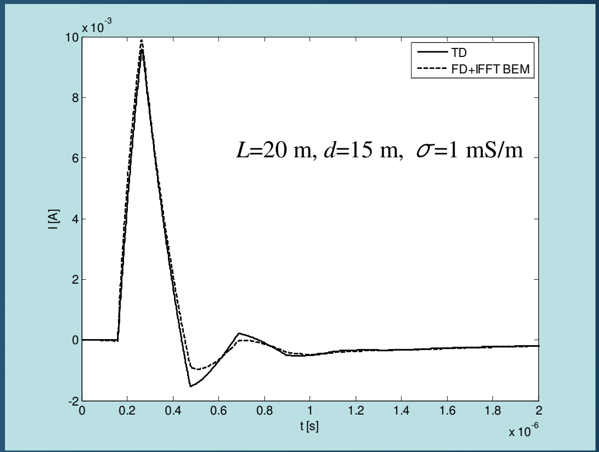

Department of Electronics
University of Split,
Split, Croatia

LIGHTNING ELECTROMAGNETICS

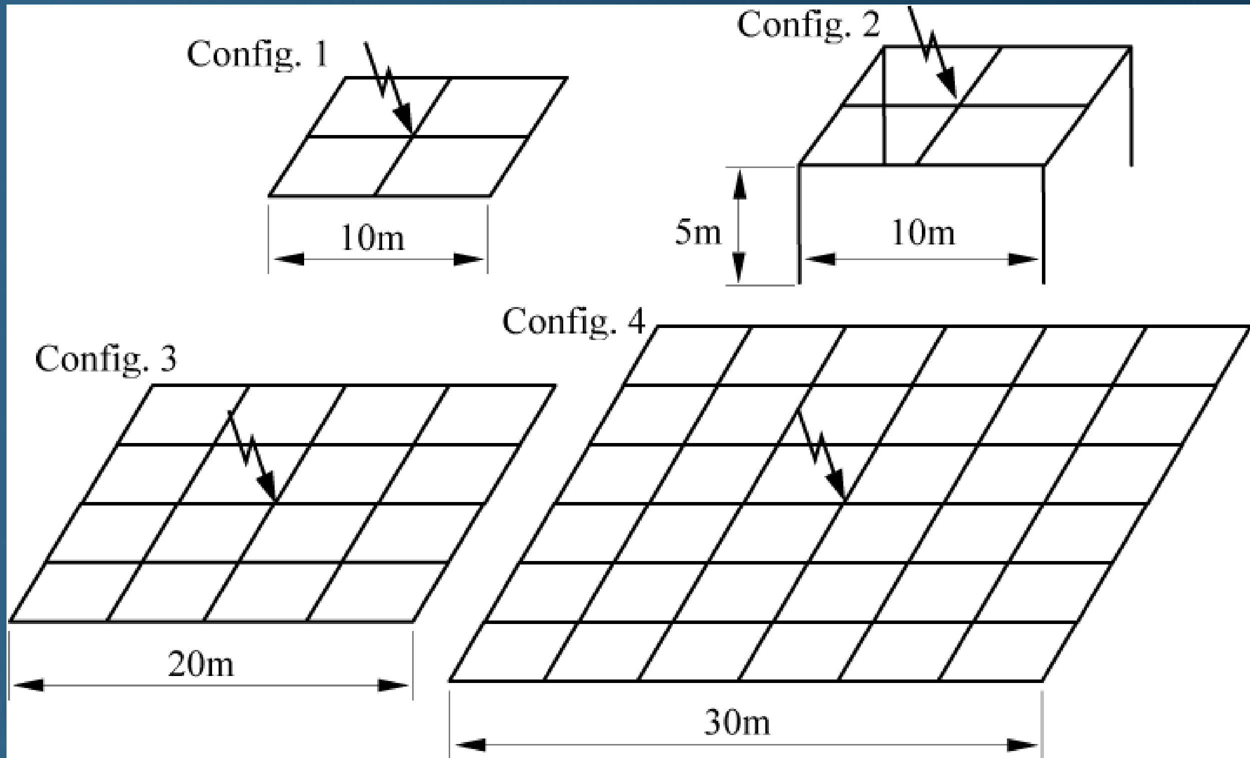

Clermont-Ferrand, 03 April 2018

UNIVERSITÉ Clermont Auvergne

Department of Electronics
University of Split,
Split, Croatia

Transient Analysis of Groundig Electrodes

- Grounding systems, (vertical or horizontal electrodes, large grounding grids) are a fundamental part of lightning protection systems (LPS).
- The principal task of such grounding systems is to ensure the safety of personnel and prevent damage of installations and equipment.
- The secondary purpose of grounding systems is to provide common reference voltage for all interconnected electrical and electronic systems.
- While the steady state behaviour of grounding systems is well investigated and understood, the transients studies are more demanding.

Department of Electronics
University of Split,
Split, Croatia

Transient Analysis of Grounding Electrodes

- Transient analysis of grounding systems are related to analytical approaches, transmission line models or full wave (antenna) models..

- The antenna model is based on the Pocklington integral equation formulation featuring the rigorous Sommerfeld integral approach to account for the treatment of the half-space effect.

The frequency response is obtained multiplying the input impedance spectrum with Fourier transform of the current excitation waveform.

The transient response is computed by using the Inverse Fourier Transform (IFT).

The analysis has been undertaken for vertical, horizontal and complex grounding systems of arbitrary shape.

Department of Electronics
University of Split,
Split, Croatia

Transient Analysis of Grounding Electrodes

The antenna model: FD analysis of single grounding elecrode of arbitrary shape

- First the single wire grounding electrode of arbitrary shape is considered.

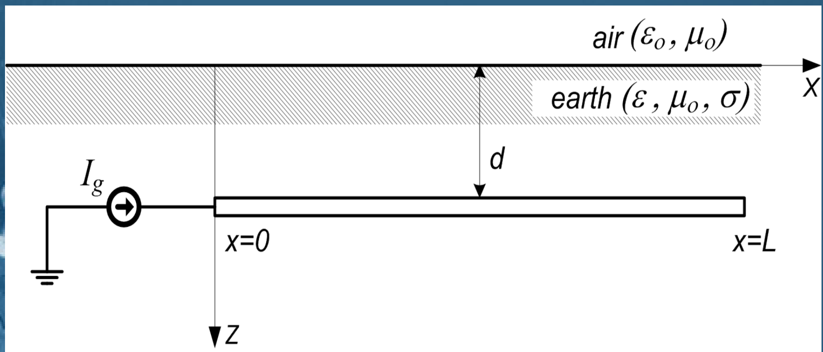

Horizontal electrode

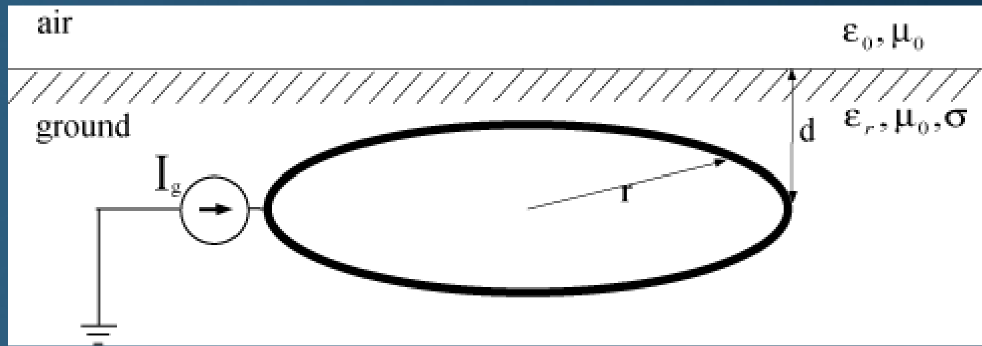

Ring electrode

- The spatial current distribution along the wire is governed by the homogeneous Pocklington integro-differential equation:

$$-\frac{1}{j4\pi\omega\varepsilon_{eff}}\left[\int_C I(s')\cdot\left[\vec{s}\cdot\vec{s}'\cdot k_1^2+\frac{\partial^2}{\partial s\partial s'}\right]g_0(s,s')ds'+\frac{k_0^2-k_1^2}{k_0^2+k_1^2}\int_C I(s')\cdot\left[\vec{s}\cdot\vec{s}^*\cdot k_1^2+\frac{\partial^2}{\partial s\partial s^*}\right]g_i(s,s^*)ds'+\int_C I(s')\cdot\vec{s}\cdot\vec{s}^*\cdot G_s(s,s')ds'\right]=0$$

Department of Electronics
University of Split,
Split, Croatia

Transient Analysis of Grounding Electrodes

The antenna model: FD analysis of single grounding elecrode of arbitrary shape

UNIVERSITÉ Clermont Auvergne

The Green function components:

$$g_0(s,s')=\frac{e^{-jk_1R_0}}{R_0}\qquad g_i(s,s^*)=\frac{e^{-jk_1R_1}}{R_1}$$

$$G_s(s,s')=(\vec{e}_x\cdot\vec{s}\,')\cdot\left(G_\rho^H\cdot\vec{e}_\rho+G_\phi^H\cdot\vec{e}_\phi+G_z^H\cdot\vec{e}_z\right)+(\vec{e}_z\cdot\vec{s}\,')\cdot\left(G_\rho^V\cdot\vec{e}_\rho+G_z^V\cdot\vec{e}_z\right)$$

$$G_z^V=\left(\frac{\partial^2}{\partial z^2}+k_1^2\right)k_0^2\,V^R\qquad G_\rho^V=\frac{\partial^2}{\partial\rho\partial z}k_0^2\,V^R\qquad G_\rho^H=\cos\varphi\left(\frac{\partial^2}{\partial\rho^2}k_1^2\,V^R+k_1^2\,U^R\right)\qquad D_1(\lambda)=\frac{2}{\gamma_0+\gamma_1}-\frac{2k_1^2}{\gamma_1\left(k_1^2+k_0^2\right)}$$

$$G_\phi^H=-\sin\phi\left(\frac{1}{\rho}\frac{\partial}{\partial\rho}k_1^2\,V^R+k_1^2\,U^R\right)\qquad U^R=\int_0^\infty D_1(\lambda)\,e^{-\gamma_1|z+z'|}\,J_0(\lambda\rho)\,\lambda\,d\lambda\qquad D_2(\lambda)=\frac{2}{k_1^2\gamma_0+k_0^2\gamma_1}-\frac{2}{\gamma_1\left(k_1^2+k_0^2\right)}$$

$$G_z^H=-j4\pi\omega\varepsilon_{eff}\cos\phi\,G_\rho^V\qquad V^R=\int_0^\infty D_2(\lambda)\,e^{-\gamma_1|z+z'|}\,J_0(\lambda\rho)\,\lambda\,d\lambda\qquad \gamma_0=\sqrt{\lambda^2-k_0^2};\quad \gamma_1=\sqrt{\lambda^2-k_1^2}$$

Department of Electronics
University of Split,
Split, Croatia

Transient Analysis of Grounding Electrodes

The antenna model: FD analysis of complex grounding systems

- There is a number of configurations of practical grounding systems:

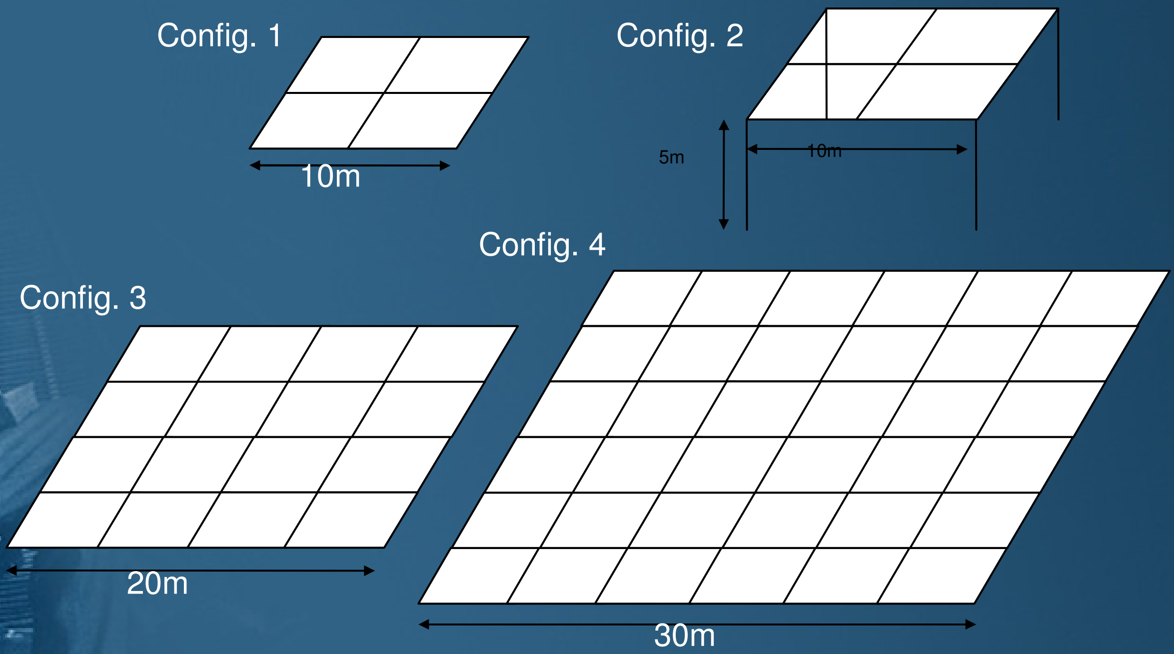

Different grounding grid configurations

Department of Electronics
University of Split,
Split, Croatia

Transient Analysis of Grounding Electrodes

- The spatial current distribution along the wire is governed by the set of coupled homogeneous Pocklington integro-differential equations:

$$-\frac{1}{j4\pi\omega\varepsilon_{eff}}\sum_{n=1}^{N_W}\left[\int_{C_n'} I_n(s')\cdot\left[\vec{s}_m\cdot\vec{s}_n'\cdot k_1^2+\frac{\partial^2}{\partial s_m \partial s_n'}\right]g_{0n}(s_m,s_n')ds'+\frac{k_0^2-k_1^2}{k_0^2+k_1^2}\int_{C_n'} I(s_n')\cdot\left[\vec{s}_m\cdot\vec{s}_n^{\,*}\cdot k_1^2+\frac{\partial^2}{\partial s_m \partial s_n^{\,*}}\right]g_{in}(s_m,s_n^{\,*})ds'+\int_{C_n'} I_n(s')\cdot\vec{s}_m\cdot\vec{s}_n^{\,*}\cdot G_s(s_m,s_n')ds'\right]=0$$

$$m=1,2,\ldots N_W$$

- The excitation is incorporated into formulation through the boundary condition:

$$I_1 = I_g$$

where I_g denotes current generator and I_1 current in the injection node.

At a junction consisting of two or more segments the continuity properties of the field must be satisfied, which is ensured by the Kirchhoff current law:

$$\sum_{k=1}^{n} I_k = 0$$

and the equation of continuity:

$$\nabla\vec{J} = -j\omega\rho \qquad \frac{\partial I}{\partial s} = -j\omega q_l \qquad \left[\frac{\partial I_1}{\partial s_1'}\right]\Bigg|_{na\ spoju} = \left[\frac{\partial I_2}{\partial s_2'}\right]\Bigg|_{na\ spoju} = \cdots = \left[\frac{\partial I_n}{\partial s_n'}\right]\Bigg|_{na\ spoju}$$

Department of Electronics
University of Split,
Split, Croatia

Transient Analysis of Grounding Electrodes

Numerical solution

- The set of Pocklington equations is handled via the (GB-IBEM).

- local approximation for the current:

$$I_n^e(\zeta)=\sum_{i=1}^{n} I_{ni} f_{ni}(\zeta)=\{f\}_n^T\{I\}_n$$

- the system of equations:

$$f_1=\frac{1-\zeta}{2} \qquad f_2=\frac{1+\zeta}{2}$$

$$\sum_{n=1}^{N_w}\sum_{i=1}^{N_n}[Z]_{ji}^e\{I_n\}_i = 0,$$

$$\mathrm{m}=1,2,\ldots,N_w; \qquad \mathrm{j}=1,2,\ldots,N_m$$

- the mutual impedance matrix:

$$\begin{aligned}
[Z]_{ji}^e = &-\int_{-1}^{1}\int_{-1}^{1}\{D\}_j\{D'\}_i^T g_{0nm}(s_m,s'_n)\frac{ds_n}{d\zeta'}d\zeta'\frac{ds_m}{d\zeta}d\zeta \\
&+k_1^2\cdot\hat{s}_m\cdot\hat{s}_n'\int_{-1}^{1}\int_{-1}^{1}\{f\}_j\{f'\}_i^T g_{0nm}(s_m,s'_n)\frac{ds_n}{d\zeta'}d\zeta'\frac{ds_m}{d\zeta}d\zeta+ \\
&+\frac{k_0^2-k_1^2}{k_0^2+k_1^2}\left[\begin{aligned}&-\int_{-1}^{1}\int_{-1}^{1}\{D\}_j\{D'\}_i^T g_{inm}(s_m,s^*_n)\frac{ds_n}{d\zeta'}d\zeta'\frac{ds_m}{d\zeta}d\zeta+ \\ &+k_1^2\cdot\hat{s}_m\cdot\hat{s}_n^*\int_{-1}^{1}\int_{-1}^{1}\{f\}_j\{f'\}_i^T g_{inm}(s_m,s^*_n)\frac{ds_n}{d\zeta'}d\zeta'\frac{ds_m}{d\zeta}d\zeta\end{aligned}\right]+ \\
&+\hat{s}_m\cdot\hat{s}_n'\int_{-1}^{1}\int_{-1}^{1}\{f\}_j\{f'\}_i^T G_{snm}(s_m,s'_n)\frac{ds_n}{d\zeta'}d\zeta'\frac{ds_m}{d\zeta}d\zeta
\end{aligned}$$

FESB
Department of Electronics
University of Split,
Split, Croatia

UCA Université Clermont Auvergne

Transient Analysis of Grounding Electrodes

Numerical solution

- The calculation of transient response is carried out by means of Inverse Fourier Transform.

$$V(f)=I(f)\cdot Z(f)$$

$$z(t)=\frac{v(t)}{i(t)}$$

$$v(t)=\int_{-\infty}^{\infty} V(f)e^{j2\pi ft}d\omega$$

$$Z_{in}(f)=\frac{V_g(f)}{I_g}$$

$$V_g=-\int_{\infty}^{a}\overrightarrow{E}^{sct}d\vec{l}$$

$$E_{sm}^{sct}(s)=\frac{1}{j4\pi\omega\varepsilon_{eff}}\sum_{n=1}^{N_W}\left[\begin{array}{l}\int_{C_n'} I_n(s')\cdot\vec{s}\cdot\vec{s}'\cdot\left[k_1^2+\nabla\nabla\right]g_{0n}(s_m,s_n')ds'+\\ +\frac{k_0^2-k_1^2}{k_0^2+k_1^2}\int_{C_n'} I(s_n')\cdot\vec{s}\cdot\vec{s}^*\cdot\left[k_1^2+\nabla\nabla\right]g_{in}(s_m,s_n^*)ds'+\\ +\int_{C_n'} I_n(s')\cdot\vec{s}\cdot\vec{s}^*\cdot G_s(s_m,s_n')ds'\end{array}\right]\quad m=1,2,\ldots N_W$$

Department of Electronics
University of Split,
Split, Croatia

Transient Analysis of Grounding Electrodes

Transient voltage assessment

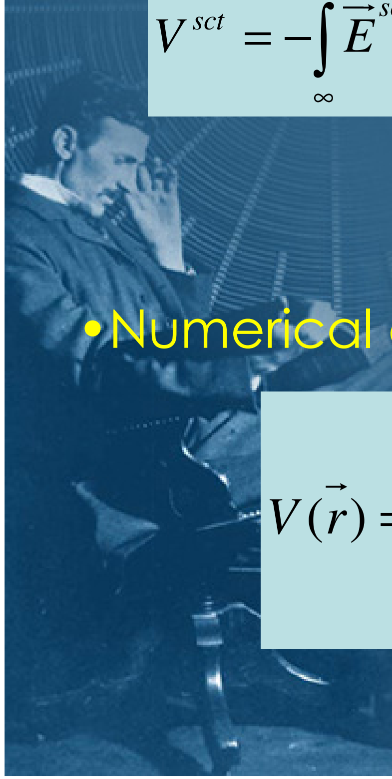

• Assuming the potential in the remote soil to be zero, the voltage between the point on the wire and remote soil is :

$$V^{sct} = -\int_{\infty}^{\vec{r}} \vec{E}^{sct} \, d\vec{l}$$

$$V\left(\vec{r}\right) \cong \varphi\left(\vec{r}\right) = -\frac{1}{j4\pi\omega\varepsilon_{eff}} \sum_{i=1}^{N_W} \left\{ \begin{array}{l} \displaystyle\int_{C'} \frac{\partial I(s')}{\partial s'} \cdot g_0(\vec{r}, s')ds' + \\ \displaystyle\frac{k_1^2 - k_2^2}{k_1^2 + k_2^2} \int_{C'} \frac{\partial I(s')}{\partial s^*} \cdot g_i(\vec{r}, s^*)ds' \end{array} \right\}$$

• Numerical evaluation:

$$V(\vec{r}) = -\frac{1}{j4\pi\omega\varepsilon_{eff}} \sum_{i=1}^{N_W} \sum_{n=1}^{N_g} \sum_{k=1}^{nl} \int_{-1}^{1} I_k^{ei} \frac{\partial f_k^e(\zeta')}{\partial \zeta'} \cdot \left[\begin{array}{l} g_0^i(\vec{r}, s') \\ \displaystyle -\frac{k_1^2 - k_2^2}{k_1^2 + k_2^2} g_i^i(\vec{r}, s^*) \end{array} \right] d\zeta'$$

UNIVERSITÉ Clermont Auvergne

Department of Electronics
University of Split,
Split, Croatia

Transient Analysis of Grounding Electrodes

Numerical results: Horizontal electrode

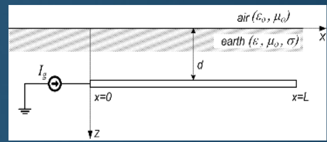

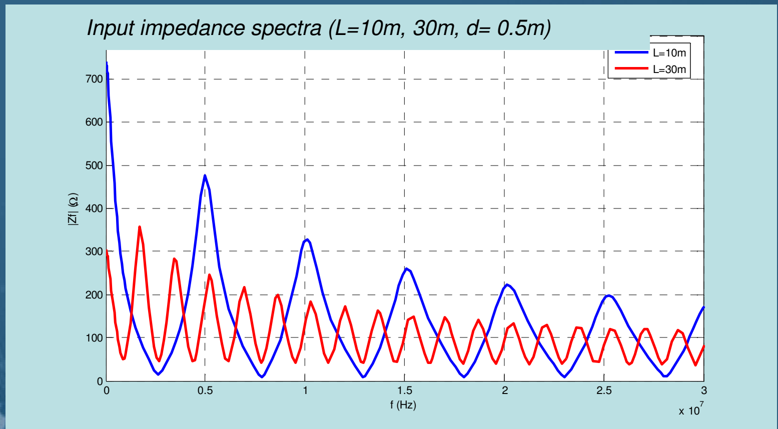

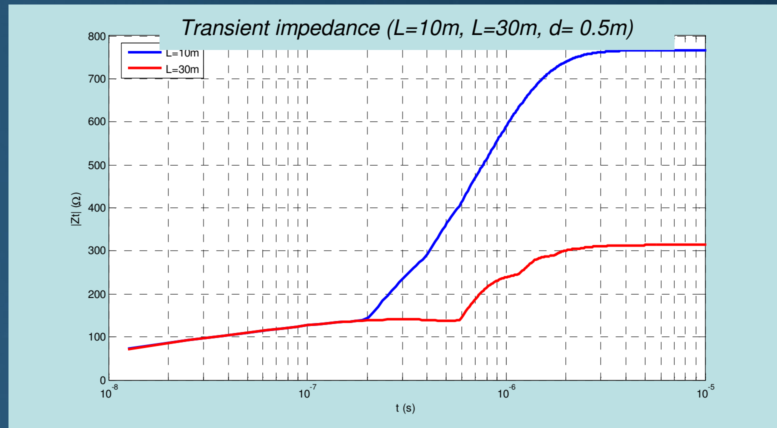

Numerical results: Vertical electrode

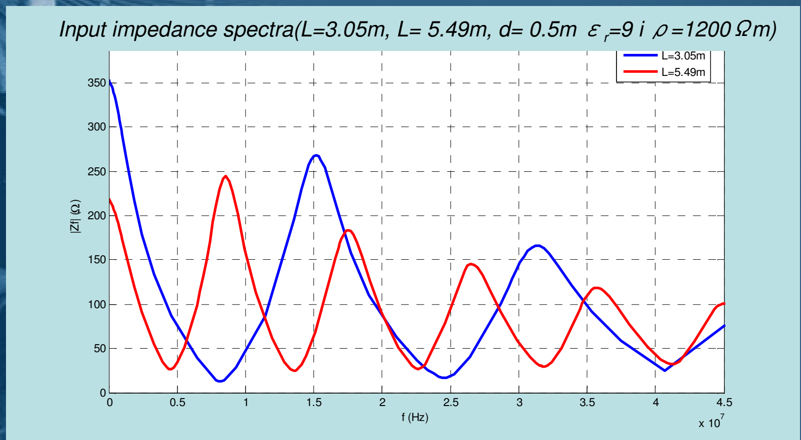

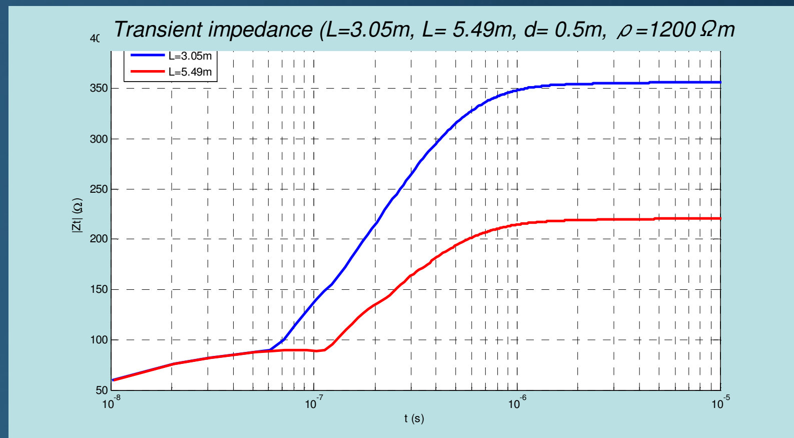

Department of Electronics
University of Split,
Split, Croatia

Transient Analysis of Grounding Electrodes

Numerical results: Ring electrode

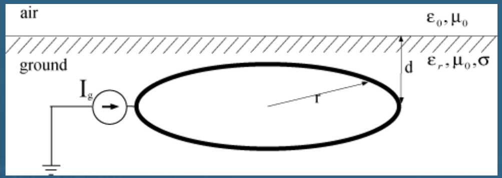

- local approximation for the current:

$$f_1(\xi) = \frac{1}{2}\xi(\xi - 1);$$

$$f_2(\xi) = 1 - \xi^2;$$

$$f_3(\xi) = \frac{1}{2}\xi(\xi + 1)$$

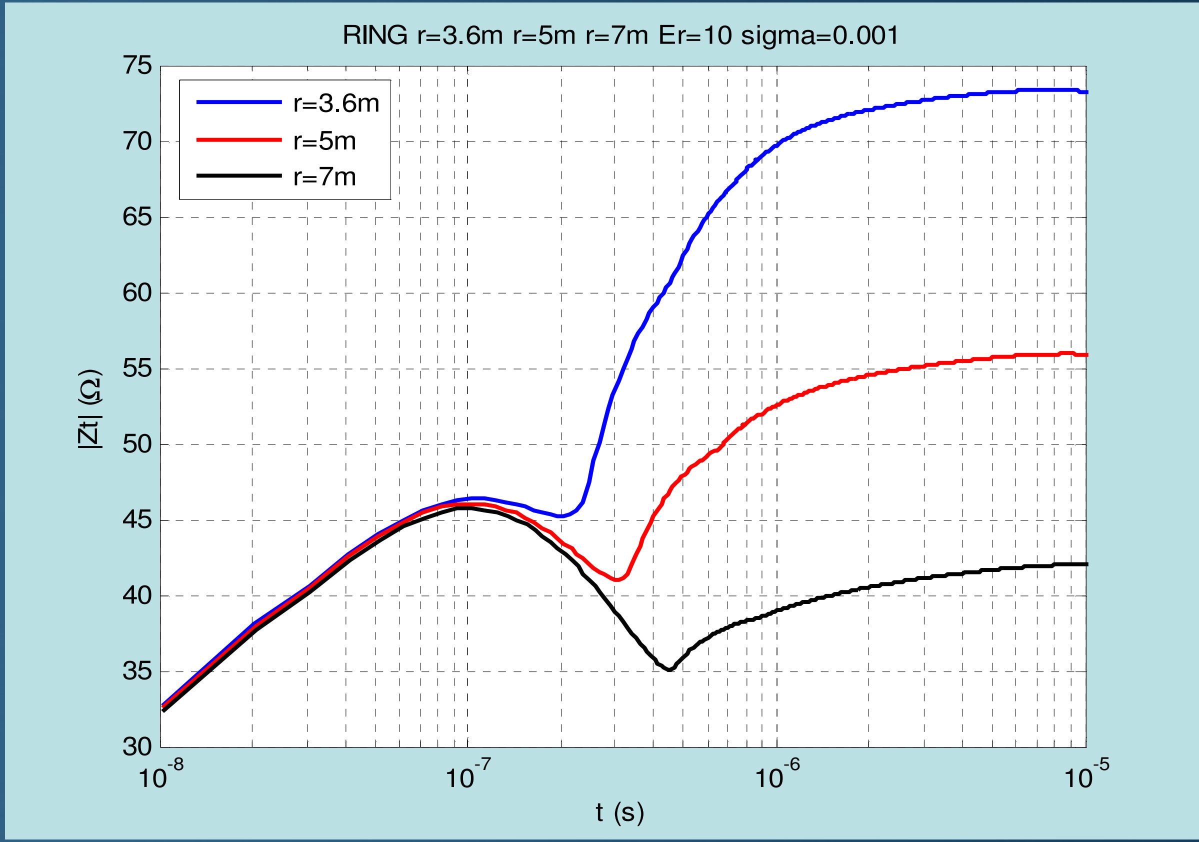

Transient impedance of ring grounding electrode for various radii

Department of Electronics
University of Split,
Split, Croatia

Transient Analysis of Grounding Electrodes

Numerical results: Ring electrode

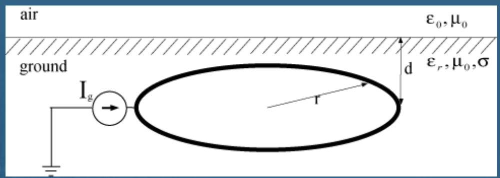

- local approximation for the current:

$$f_1(\xi) = \frac{1}{2}\xi(\xi - 1);$$

$$f_2(\xi) = 1 - \xi^2;$$

$$f_3(\xi) = \frac{1}{2}\xi(\xi + 1)$$

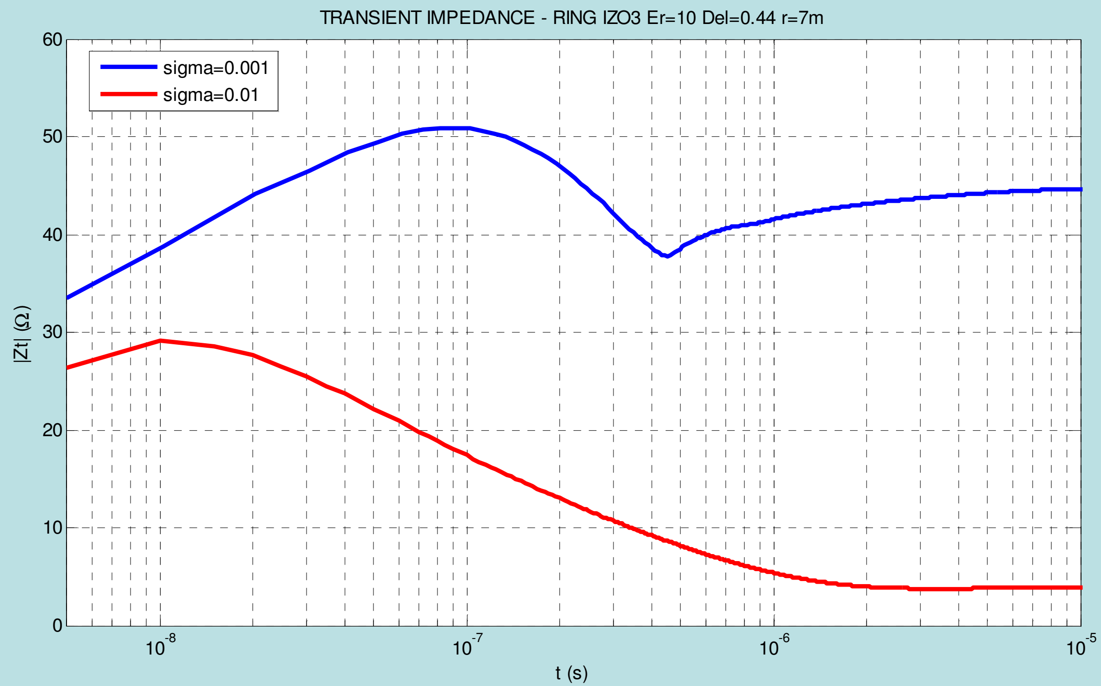

Transient impedance of ring electrode calculated for various soil conductivities

Clermont-Ferrand, 03 April 2018

Department of Electronics
University of Split,
Split, Croatia

Transient Analysis of Grounding Electrodes

A comparison of the transient impedances obtained via different approaches (AM versus TL)

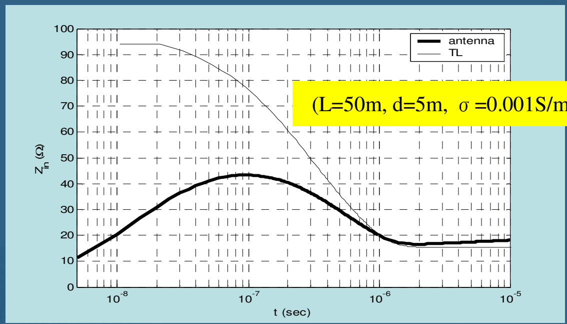

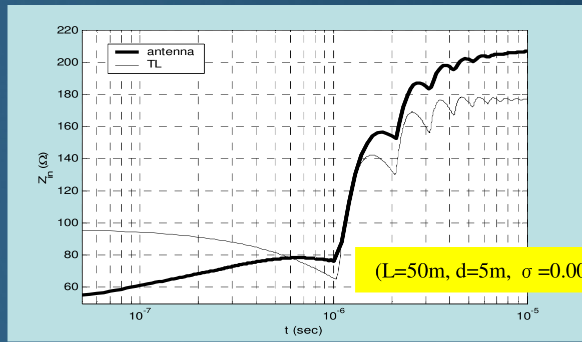

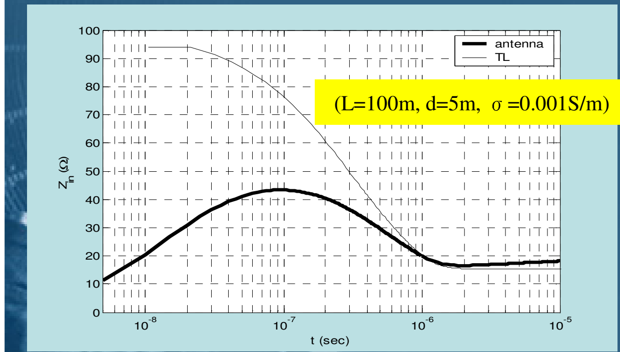

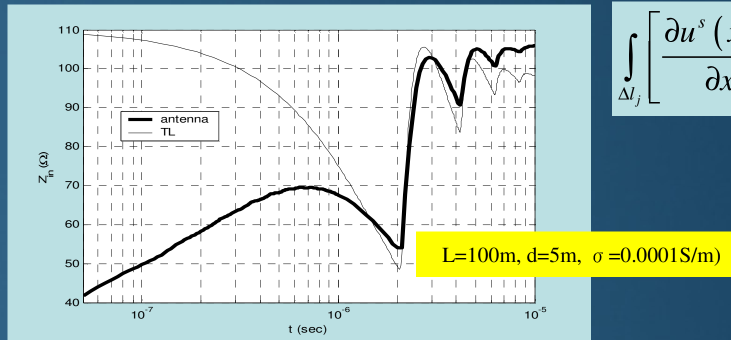

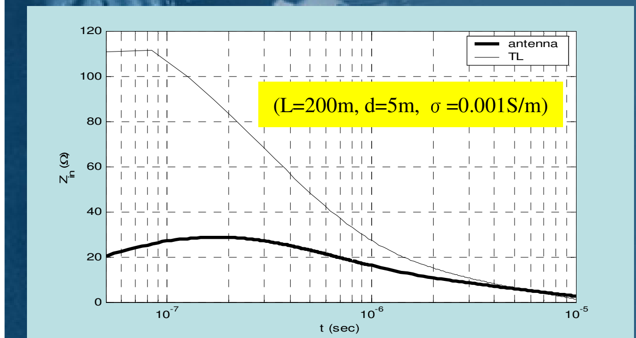

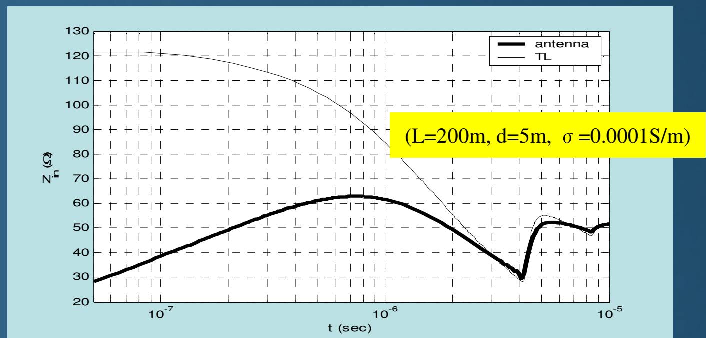

$$\frac{\partial u(x,t)}{\partial x} + L\frac{\partial i(x,t)}{\partial t} + Ri(x,t) = 0$$

$$\frac{\partial i(x,t)}{\partial x} + C\frac{\partial u(x,t)}{\partial t} + Gu(x,t) = 0$$

FEM solution

$$\int_{\Delta l_j}\left[\frac{\partial u^s(x,t)}{\partial x} + L\frac{\partial i(x,t)}{\partial x} + Ri(x,t)\right]W_j dx = 0$$

$$\int_{\Delta l}\left[\frac{\partial i(x,t)}{\partial x} + C\frac{\partial u^s(x,t)}{\partial x}\right]W_j dx = 0$$

$$u(x,t) = \{f\}^T\{u\}$$

$$i(x,t) = \{f\}^T\{i\}$$

Clermont-Ferrand, 03 April 2018

Department of Electronics
University of Split,
Split, Croatia

Transient Analysis of Grounding Electrodes

Numerical results: Grounding grid

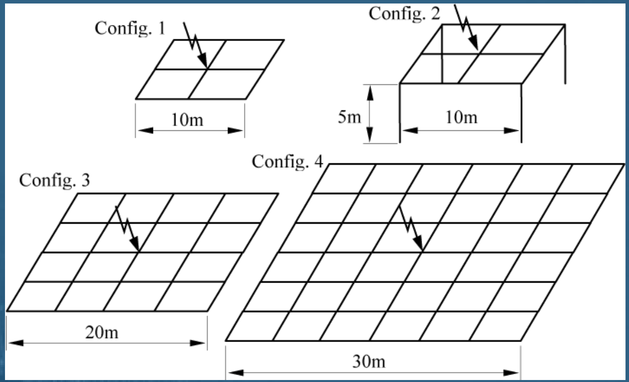

Various configurations of grounding grids

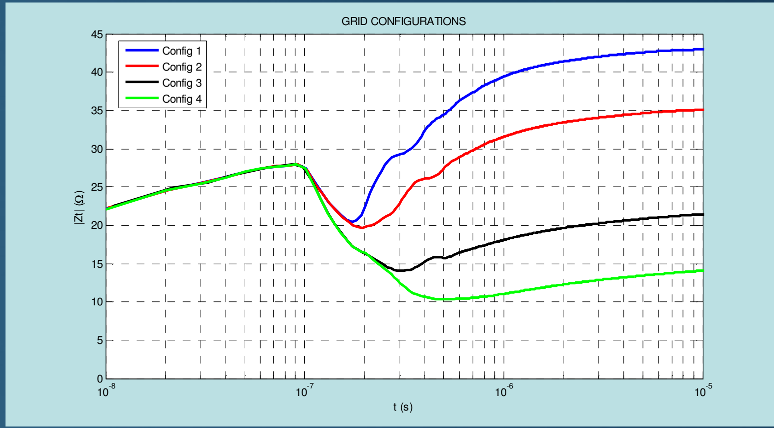

Transient impedance of grounding grid

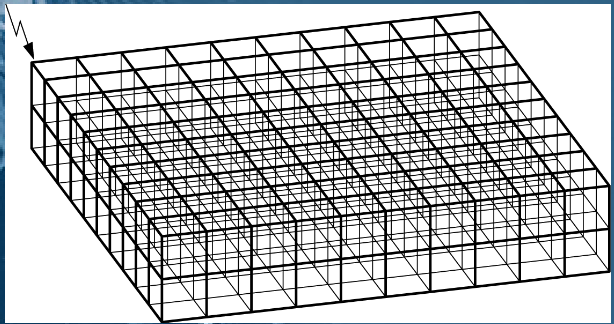

Configuration of multi-layered grounding grid

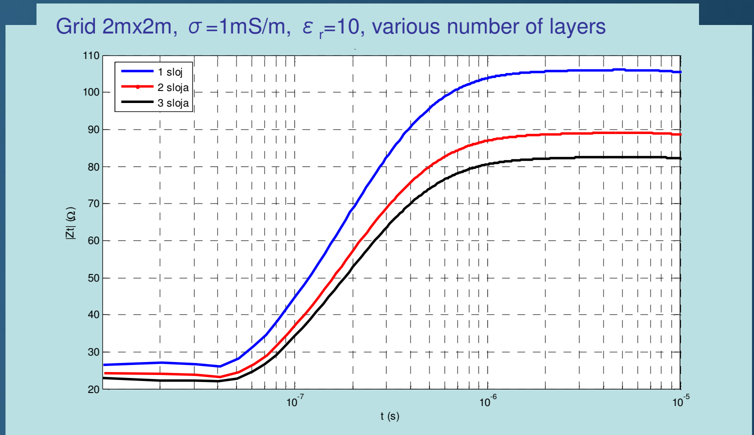

Transient impedance of complex grounding system

Department of Electronics
University of Split,
Split, Croatia

Transient Analysis of Grounding Electrodes

Numerical results: Grounding grid: AT versus TL approach

Grounding system of interest is composed of grid 60mx60m (6 by 6 10m square meshes); wire radius 0.007m; depth: 0.5m; ρ=100Ωm; ε_r=36. The grounding grid is energized at certain points by the double exponential current source:

$$i(t) = I_0\left(e^{-at} - e^{-bt}\right) \tag{32}$$

where $I_0 = 1.2kA$, $a = 0.0142\cdot 10^{-6}$, $b = 1.073\cdot 10^{-6}$.

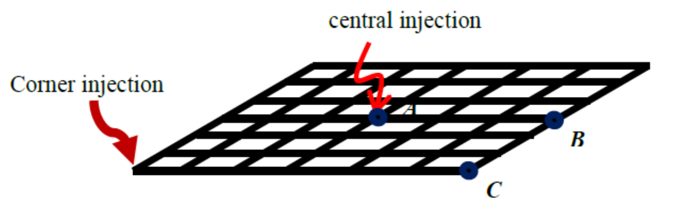

Fig. 2 Grounding grid under central injection of the current source (double exponential excitation)

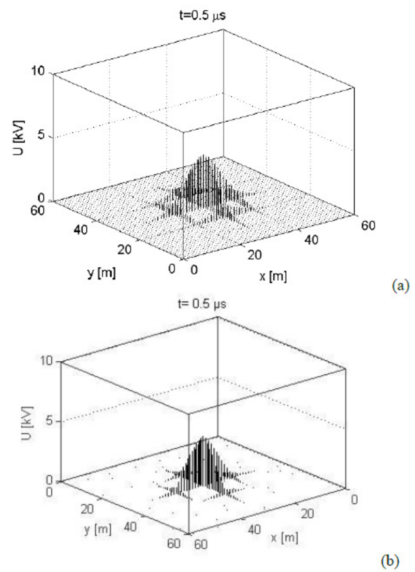

Fig. 3.Spatial distribution of the voltage induced along the grounding grid (center injection) at T=0.5µs computed via: (a) AT approach; (b) FDTD- TL approach

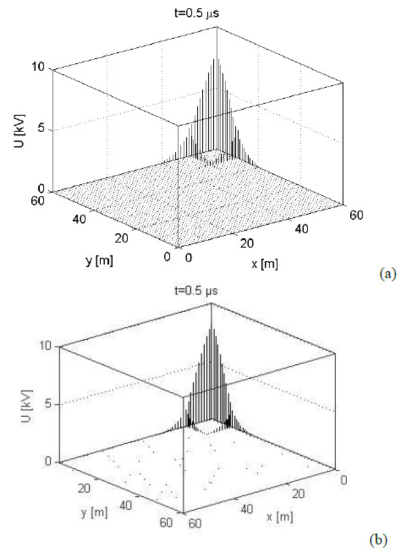

Fig. 4.Spatial distribution of the voltage induced along the grounding grid at T=0.5µs computed via: (a) Φ – matrix - TL approach; (b) FDTD- TL approach; (c) AT approach, corner injection.

Department of Electronics
University of Split,
Split, Croatia

Transient Analysis of Grounding Electrodes

Numerical results: Grounding grid: AT versus TL approach

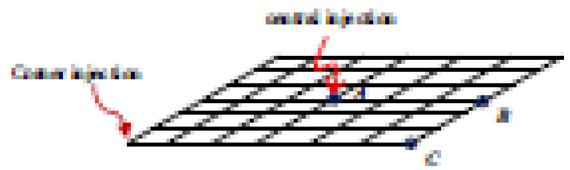

Fig. 9. Grounding grid under corner injection and central injection of the current source (double exponential excitation).

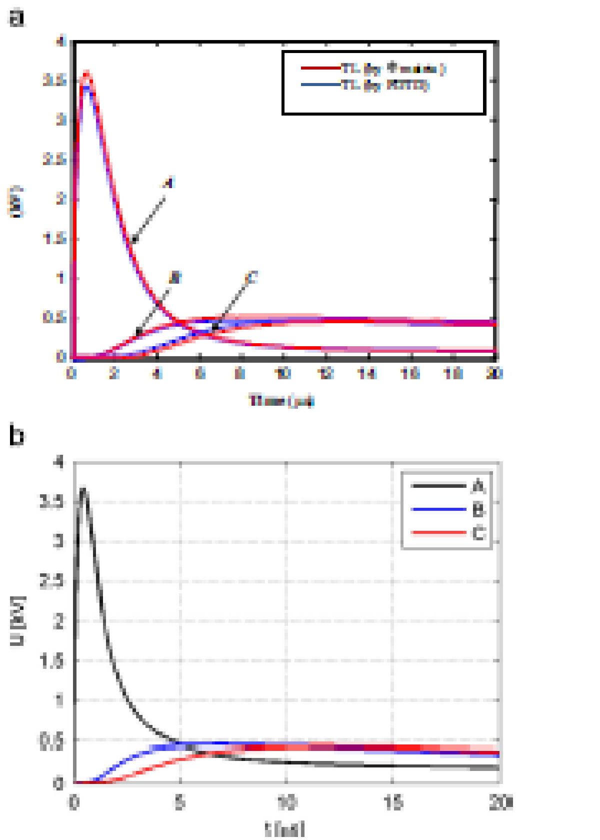

Fig. 10. (a) Transient voltage induced at the center of the grounding grid – TL approach. (b) Transient voltage induced at the center of the grounding grid – AT approach.

Department of Electronics
University of Split,
Split, Croatia

Transient Analysis of Grounding Electrodes

Numerical results: Multi-layered grounding grid

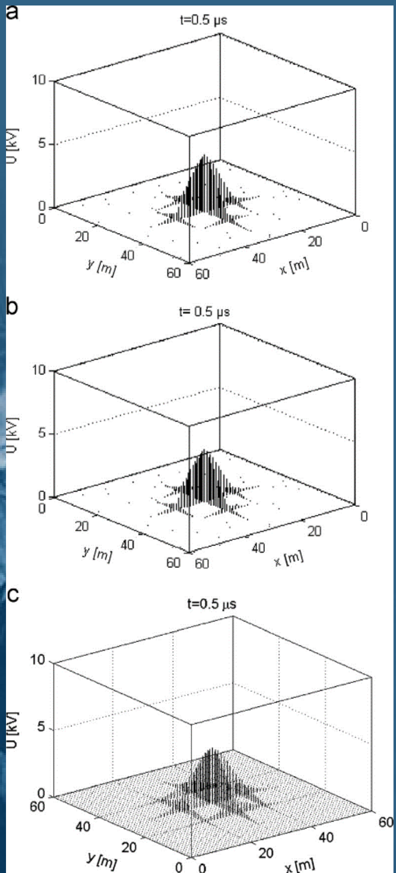

Fig. 11. Spatial distribution of the voltage induced along the grounding grid at T=0.5 μs computed via: (a) Φ-matrix – TL approach; (b) FDTD – TL approach; (c) AT approach – Central injection.

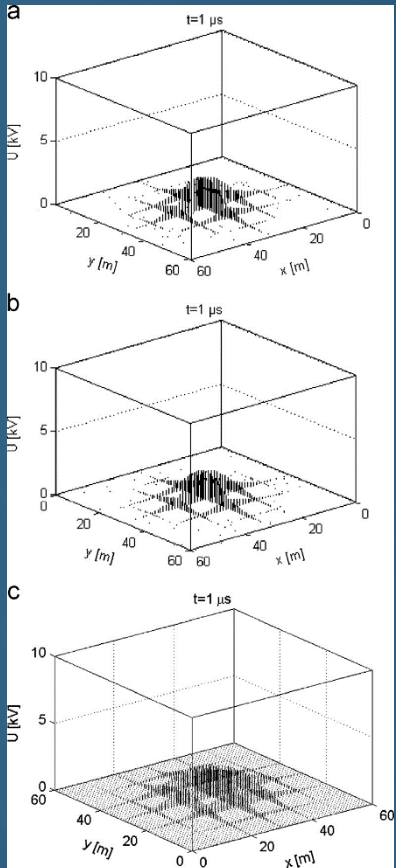

Fig. 12. Spatial distribution of the voltage induced along the grounding grid at T=1 μs computed via: (a) Φ-matrix – TL approach; (b) FDTD- TL approach; (c) AT approach – Central injection.

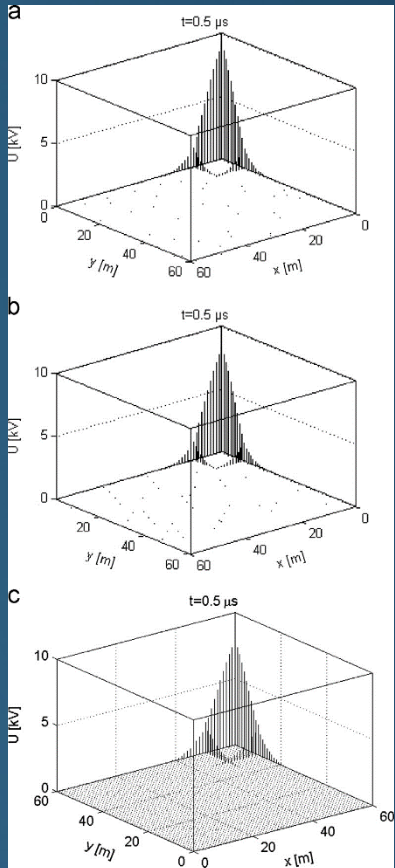

Fig. 13. Spatial distribution of the voltage induced along the grounding grid at T=0.5 μs computed via: (a) Φ-matrix – TL approach; (b) FDTD– TL approach; (c) AT approach – Corner injection.

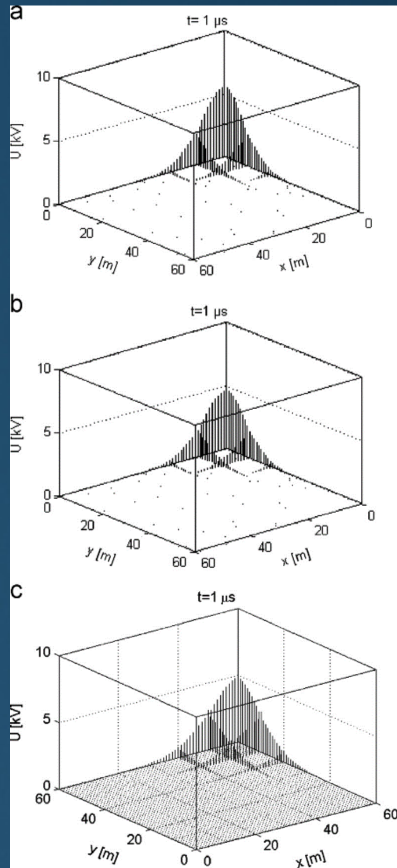

Fig. 14. Spatial distribution of the voltage induced along the grounding grid at T= 1 μs computed via: (a) Φ-matrix – TL approach; (b) FDTD – TL approach; (c) AT approach – Corner injection.

UNIVERSITÉ Clermont Auvergne

Department of Electronics
University of Split,
Split, Croatia

Transient Analysis of Grounding Electrodes

Numerical results: Complex grounding grid for wind-turbines

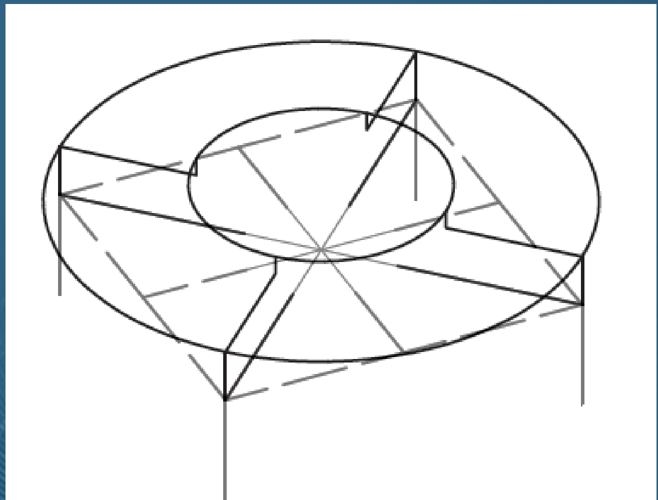

Configuration of practical wind-turbine grounding systems: 3D view

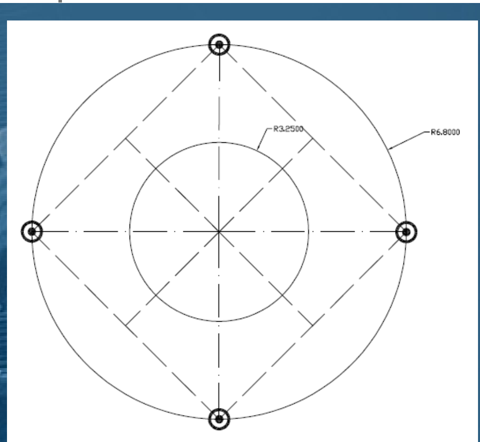

Configuration of practical wind-turbine grounding systems: Top view

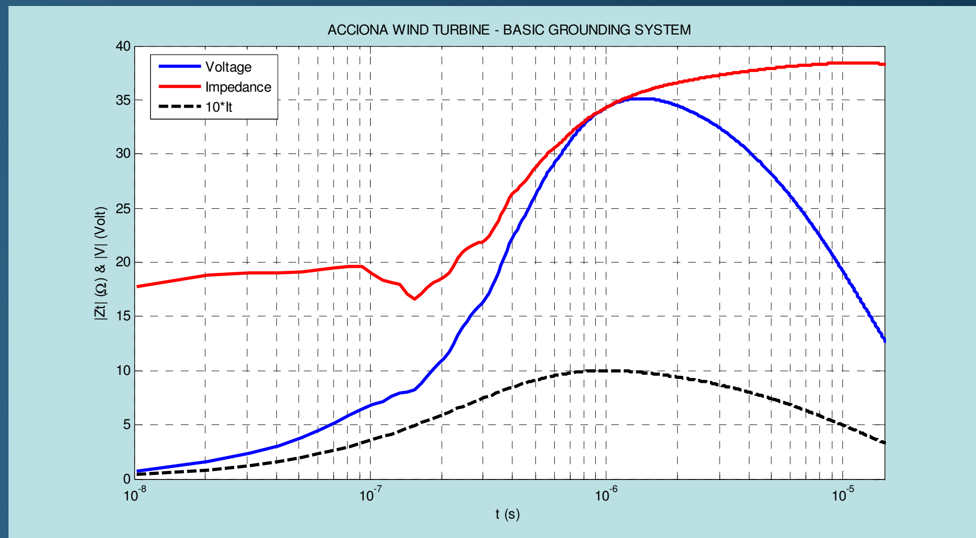

Transient response of complex grounding system

Department of Electronics
University of Split,
Split, Croatia

Transient Analysis of Grounding Electrodes

Numerical results: Complex grounding grid for wind-turbines

Configuration of practical wind-turbine grounding systems: 3D view

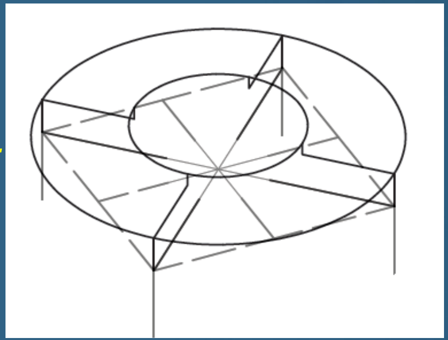

Configuration of practical wind-turbine grounding systems: Top view

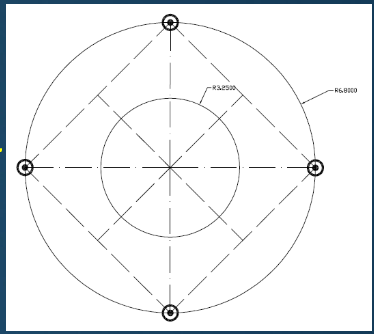

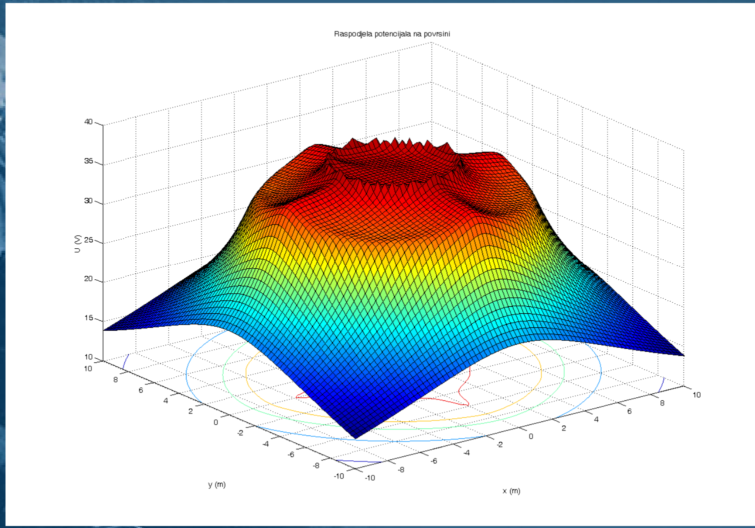

a) 3D view

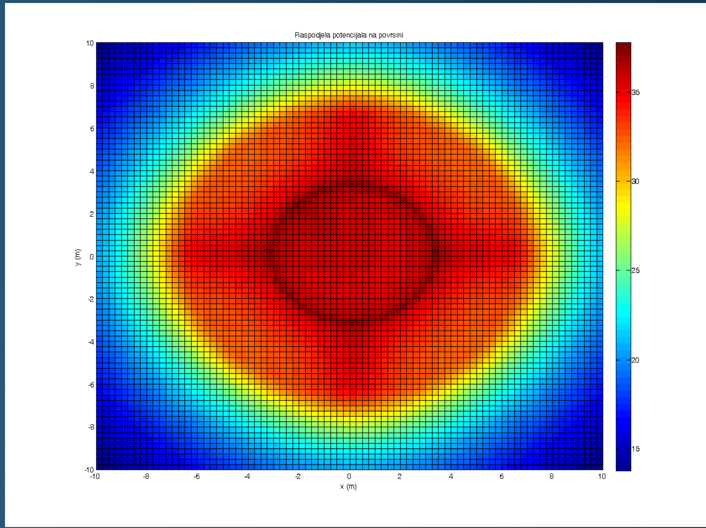

b) top wiew

Potential distribution along the surface above the grounding system for wind turbine

Department of Electronics
University of Split,
Split, Croatia

Transient Analysis of Grounding Electrodes

Numerical results: Complex grounding grid for wind-turbines

- Model of a WT grounding system

Figure shows a WT subjected to a lighting strike.

The influence of WT itself (tower, blades etc.) is neglected.

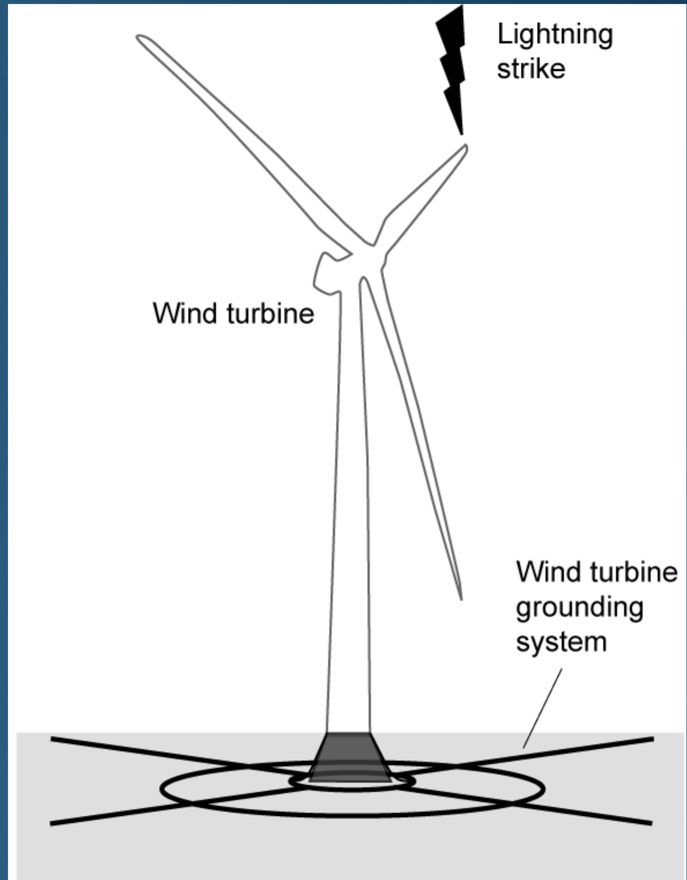

Wind turbine subjected to a lightning strike

Department of Electronics
University of Split,
Split, Croatia

Transient Analysis of Grounding Electrodes

Numerical results: Complex grounding grid for wind-turbines

- Typical grounding system (placed in a homogenous soil; ρ=1200Ω/m, ε_r=9) consists of:

  - a square of galvanized steel flanges (Fe/Zn 30x3.5mm – gray line) at the 2m depth,

  - 2 rings (Cu 70 mm^2 - black line) at different levels (smaller: 3.25m radius at 5cm depth, the larger with 6.8m radius buried at 55cm depth) and additional four copper wires.

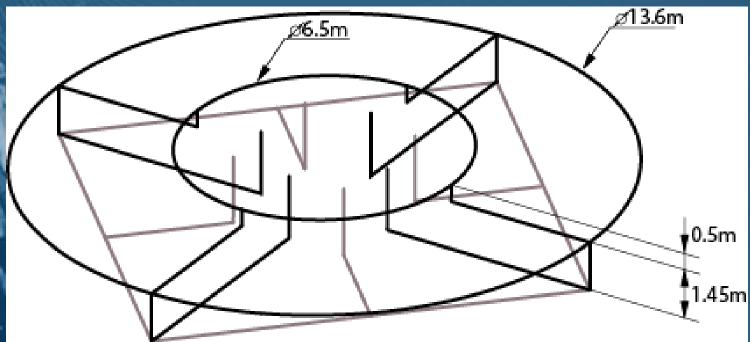

The lightning current is expressed by the double exponential function:

$$i(t) = I_0\left(e^{-\alpha t} - e^{-\beta t}\right)$$

with:

- All parts are connected by welding.

I_0=1.1043A, α=0.07924·10^{6}s^{-1}, β=0.07924·10^6 s^{-1}.

Department of Electronics
University of Split,
Split, Croatia

Transient Analysis of Grounding Electrodes

Numerical results: Complex grounding grid for wind-turbines

- Figure shows the transient response of the grounding system. Dashed line represents a ten times higher input current waveform for the comparison purpose.

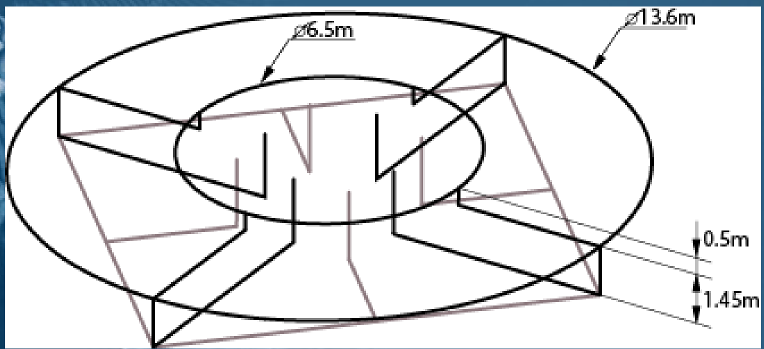

Basic grounding system

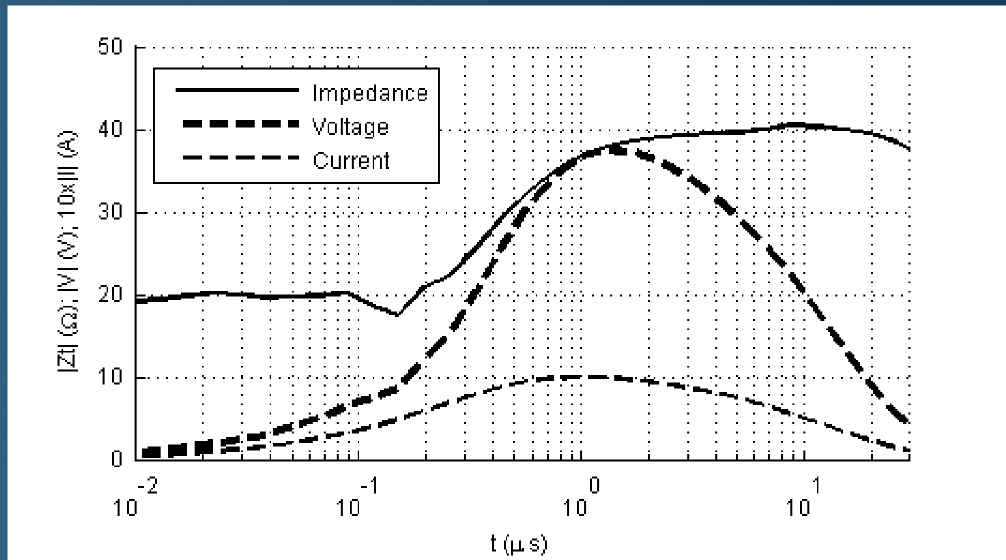

Transient behavior of the grounding system

Department of Electronics
University of Split,
Split, Croatia

Transient Analysis of Grounding Electrodes

Numerical results: Complex grounding grid for wind-turbines

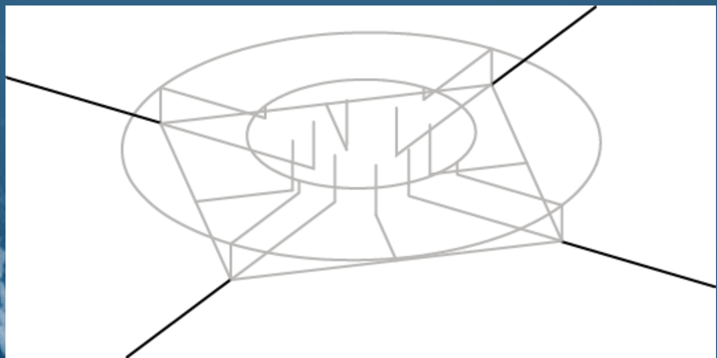

Additional horizontal electrodes on wind turbine grounding system

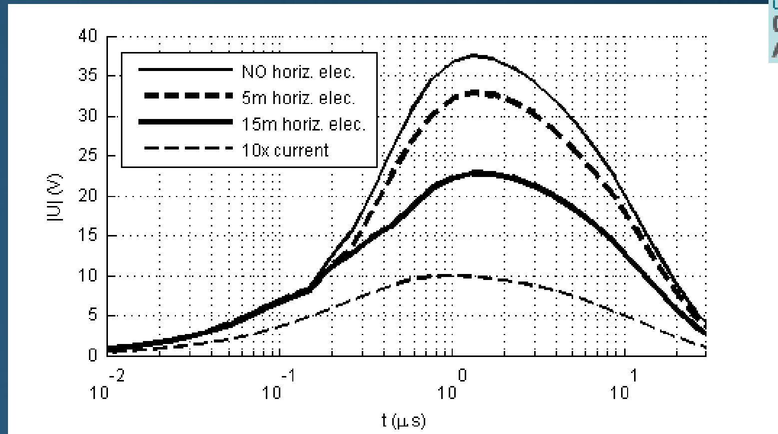

Induced feeding point transient voltage for different lengths of additional horizontal electrodes

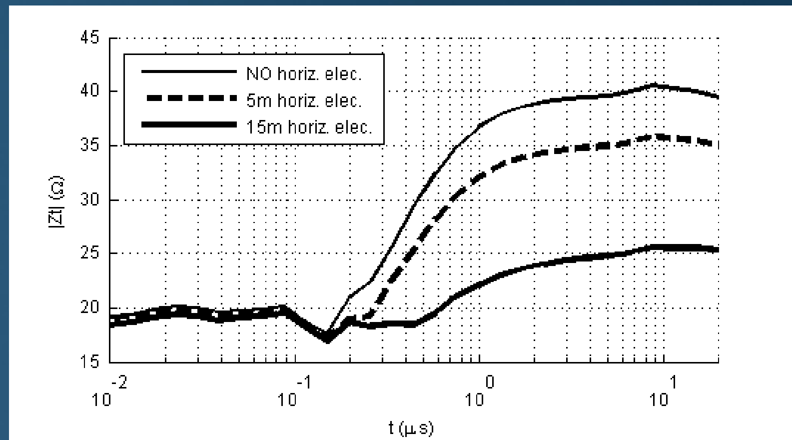

Transient impedance for different lengths of additional horizontal electrodes

The grounding system is upgraded with four 5m or 15 m long horizontal electrodes.

Department of Electronics
University of Split,
Split, Croatia

Transient Analysis of Grounding Electrodes

Numerical results: Complex grounding grid for wind-turbines

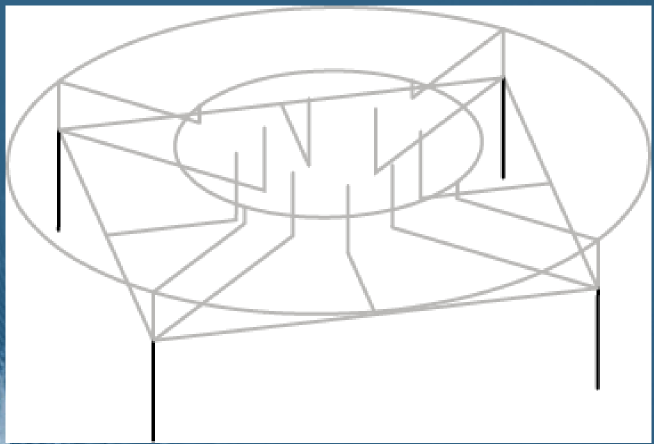

Additional vertical electrodes on wind turbine grounding system

The grounding system is upgraded with vertical electrodes of various lengths (3m, 5.5m and 15m).

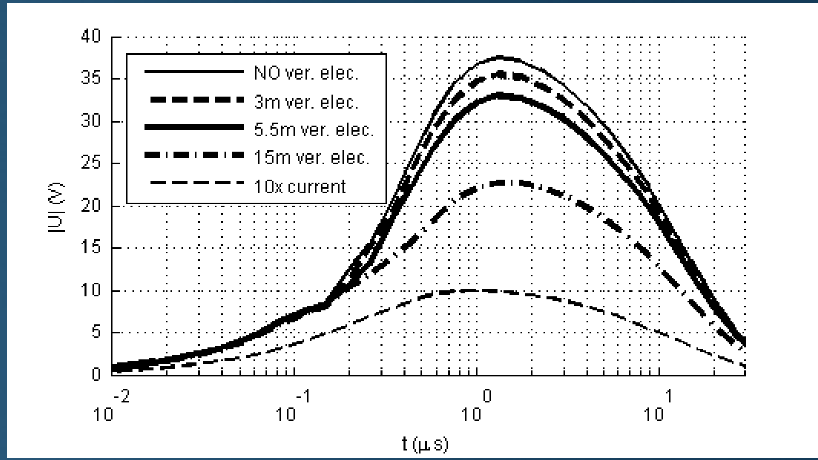

Induced feeding point transient voltage for different lengths of additional vertical electrodes

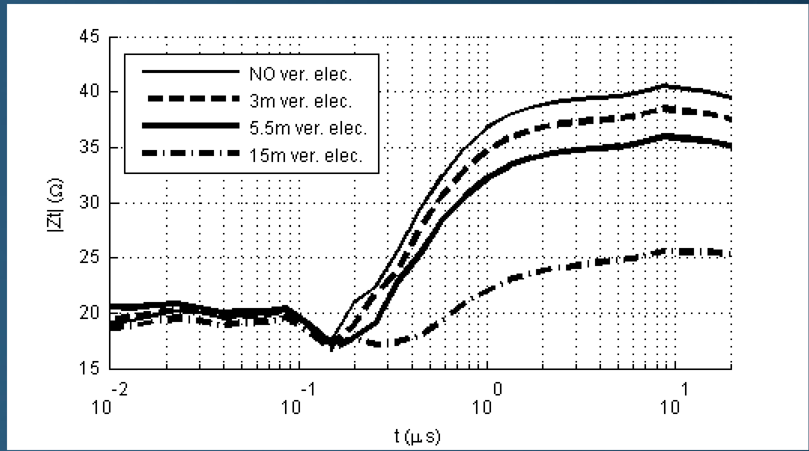

Transient impedance for different lengths of additional vertical electrodes

Department of Electronics
University of Split,
Split, Croatia

Transient Analysis of Grounding Electrodes

Numerical results: Complex grounding grid for wind-turbines

- The maximum step voltage - outside of the outer ring electrode (appx. at the point: (*5.5m, 5.5m*).

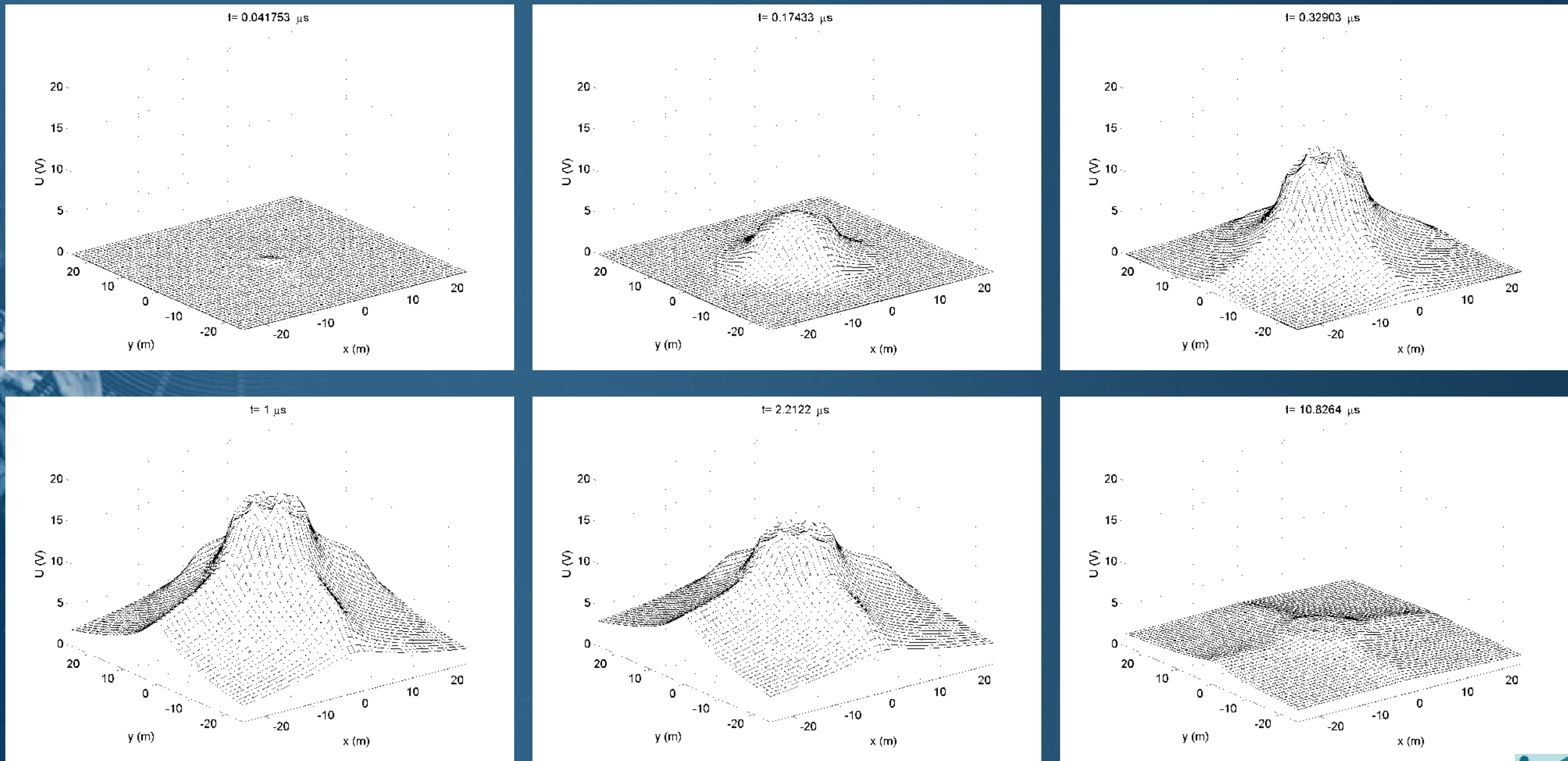

Transient GPR above the grounding system –spatial distribution

Department of Electronics
University of Split,
Split, Croatia

Transient Analysis of Grounding Electrodes

Numerical results: Complex grounding grid

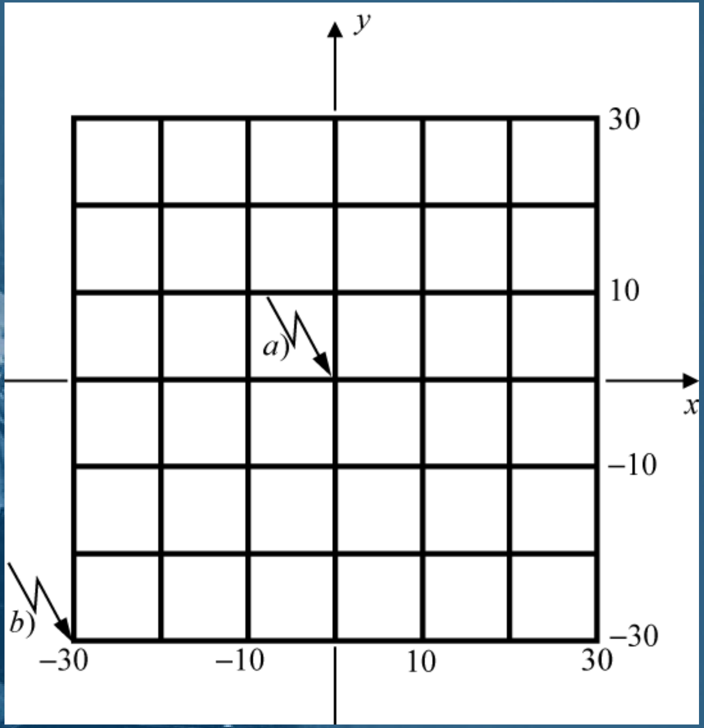

Configuration of grounding grid

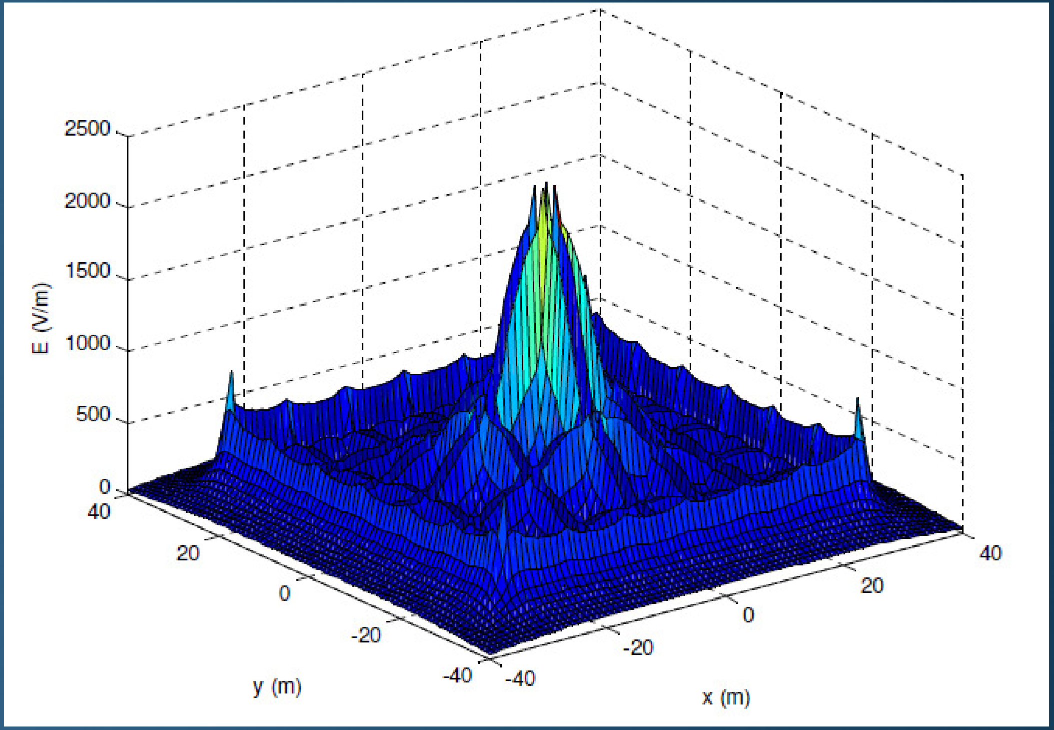

Electric field distribution on the earth surface

Department of Electronics
University of Split,
Split, Croatia

Transient Analysis of Grounding Electrodes

Frequency Domain Transmission Line Model

The field coupling to grounding grid due to indirect lightning strike is handled via transmission line (TL) approximation.

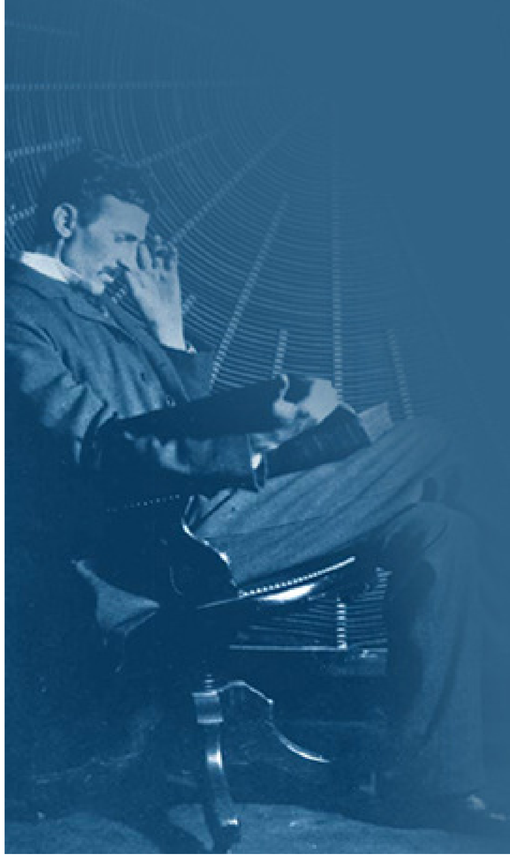

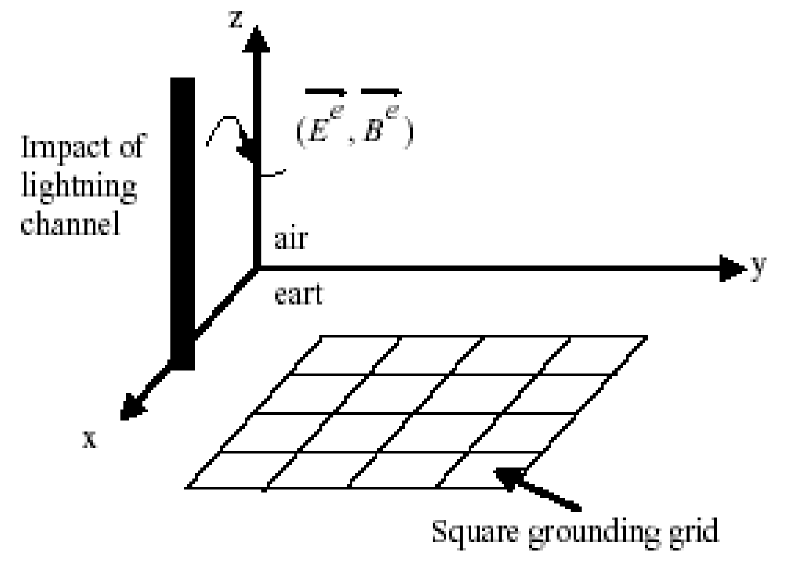

Figure 1. Illumination of grounding system by a lightning strike.

Department of Electronics
University of Split,
Split, Croatia

Transient Analysis of Grounding Electrodes

The field coupling to grounding grid due to indirect lightning strike is handled via transmission line (TL) approximation.

$$\begin{cases} \dfrac{\partial u^s}{\partial \eta} + (R + j\omega L)\, i = E_\eta^e \\ \dfrac{\partial i}{\partial \eta} + (G + j\omega C) u^s = 0 \end{cases} \qquad \eta = x \text{ or } y \qquad (1)$$

Where:

u^s : diffracted voltage.

i : total current.

E_η^e : is the tangential excitation component of the electric field.

If the propagation occurs in two-directions; x and y, the corresponding differential equation in scalar potential in two-dimensional (2D) is given by:

$$\frac{\partial^2 u^s}{\partial x^2} + \frac{\partial^2 u^s}{\partial y^2} - 2\left(RG + j\omega\left(RC + LG\right) - LC\omega^2\right)u^s = \frac{\partial E_x^e}{\partial x} + \frac{\partial E_y^e}{\partial y} \qquad (2)$$

R, L, C and G are per unit length parameters of the buried interconnected conductors.

Once the diffracted voltages is computed at a certain frequency has been obtained in all points of interest, the currents in interconnected conductors of the grounding grid are computed obtained by means of a numerical integration of the following line current equation:

$$\frac{\partial u^s}{\partial \eta} + (R + j\omega L)\, i = E_\eta^e \qquad \eta = x \text{ or } y \qquad (15)$$

UNIVERSITÉ Clermont Auvergne

Transient Analysis of Grounding Electrodes

The field coupling to grounding grid due to indirect lightning strike is handled via transmission line (TL) approximation.

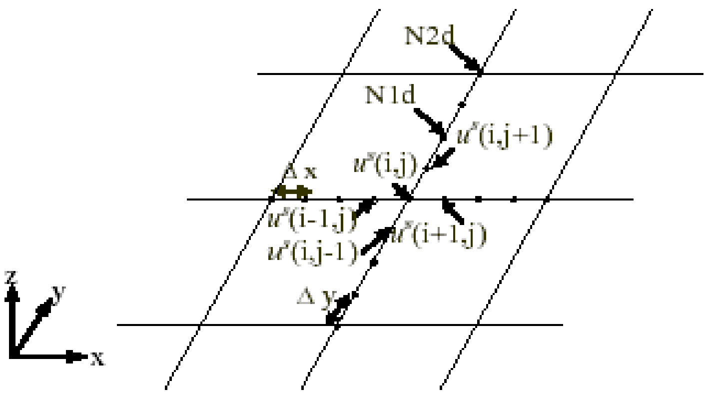

Figure 2. Spatial discretization of the square grid.

The spatial derivative approximation at point *(i, j)* using simple finites differences is given by:

$$\frac{\partial^2 u^s}{\partial x^2} = \frac{1}{\Delta x^2}\left(\left(u^s\right)_{i+1,j} - 2\left(u^s\right)_{i,j} + \left(u^s\right)_{i-1,j}\right) \quad (3)$$

$$\frac{\partial^2 u^s}{\partial y^2} = \frac{1}{\Delta y^2}\left(\left(u^s\right)_{i,j+1} - 2\left(u^s\right)_{i,j} + \left(u^s\right)_{i,j-1}\right) \quad (4)$$

$$\frac{\partial E_x^e}{\partial x} = \frac{1}{2\Delta x}\left(\left(E_x^e\right)_{i+1,j} - \left(E_x^e\right)_{i-1,j}\right) \quad (5)$$

$$\frac{\partial E_y^e}{\partial y} = \frac{1}{2\Delta y}\left(\left(E_y^e\right)_{i,j+1} - \left(E_y^e\right)_{i,j-1}\right) \quad (6)$$

Department of Electronics
University of Split,
Split, Croatia

Transient Analysis of Grounding Electrodes

Computational examples: Modeling of an indirect lightning strike

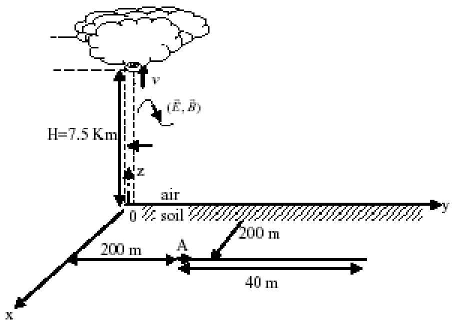

Figure 4. Buried horizontal electrode illuminated by lightning channel.

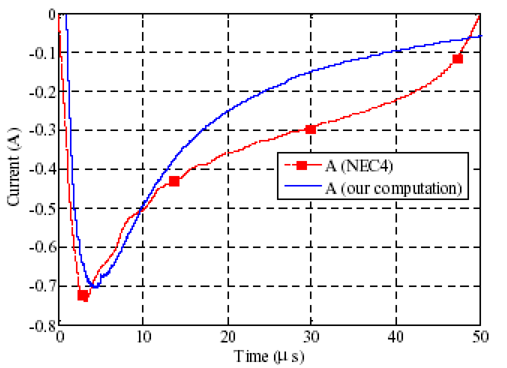

Figure 5. Transient induced current at electrode extremity (point A).

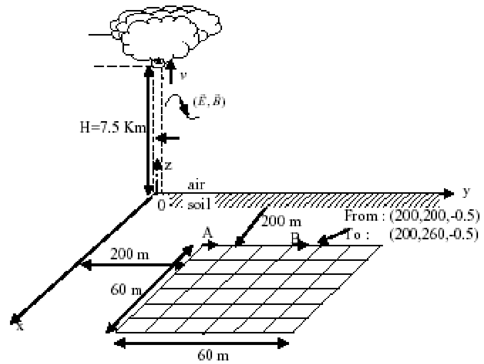

Figure 6. Grounding grid illuminated by lightning channel.

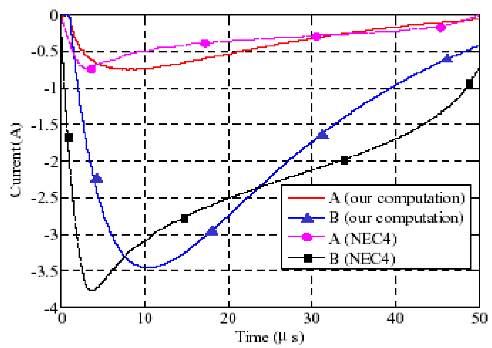

Figure 7. Induced current in branches A and B of the grounding grid.

UNIVERSITÉ Clermont Auvergne

Department of Electronics
University of Split,
Split, Croatia

Transient Analysis of Grounding Electrodes

Computational examples: Modeling of an indirect lightning strike

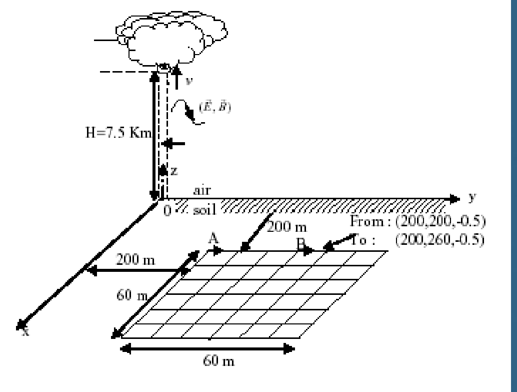

Figure 6. Grounding grid illuminated by lightning channel.

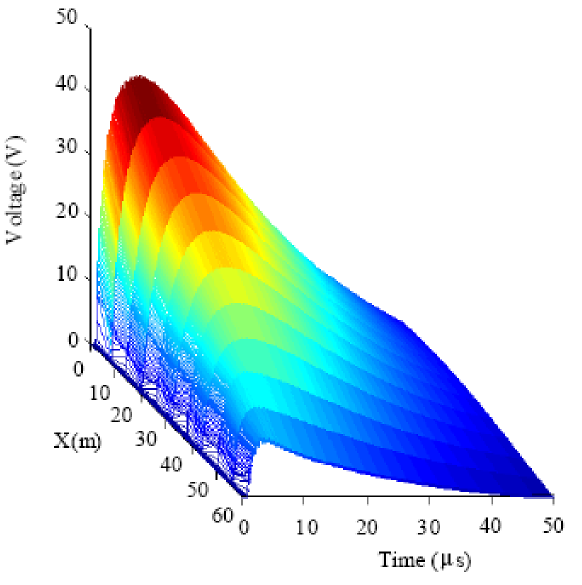

Figure 8. Induced voltages along profile 1.

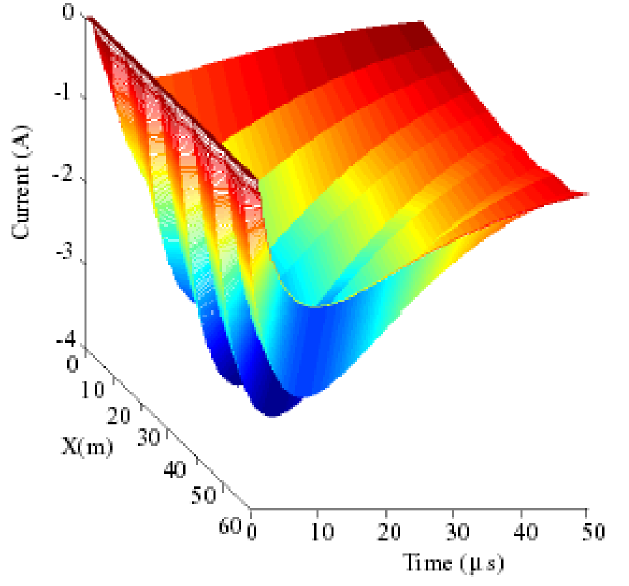

Figure 9. Induced cuurents along profile 1.

Université Clermont Auvergne

Department of Electronics
University of Split,
Split, Croatia

Transient Analysis of Grounding Electrodes

The antenna model: Direct TD analysis of single grounding elecrode

Generalized wave equation for lossy media is given by:

$$\frac{\sigma}{\varepsilon}E_x^{inc}+\frac{\partial E_x^{inc}}{\partial t}=-\frac{1}{\mu\varepsilon}\frac{\partial^2 A_x}{\partial x^2}+\frac{\partial^2 A_x}{\partial t^2}+\frac{\sigma}{\varepsilon}\frac{\partial A_x}{\partial t}$$

The magnetic vector potential is defined by a differential equation:

$$\nabla^2\vec{A}-\mu\sigma\frac{\partial\vec{A}}{\partial t}-\mu\varepsilon\frac{\partial^2\vec{A}}{\partial t^2}=-\mu\vec{J}_s$$

Green function is determined by a differential equation:

$$\left(\nabla^2-\mu\sigma\frac{\partial}{\partial t}-\mu\varepsilon\frac{\partial^2}{\partial t^2}\right)g(r,r',t)=\delta(r-r',t)$$

Department of Electronics
University of Split,
Split, Croatia

Transient Analysis of Grounding Electrodes

The antenna model: Direct TD analysis of single grounding elecrode

Green function is determined by a differential equation:

$$\left(\nabla^2 - \mu\sigma\frac{\partial}{\partial t} - \mu\varepsilon\frac{\partial^2}{\partial t^2}\right) g(r,r',t) = \delta(r-r',t)$$

and is given by:

$$g(r,r',t) = e^{-\frac{\sigma}{2\varepsilon v}R}\frac{\delta(t-R/v)}{4\pi R} + \frac{\sigma^2}{16\pi\varepsilon^2 v} e^{-\frac{\sigma}{2\varepsilon t}} \frac{I_1\left(\frac{\sigma}{2\varepsilon}\sqrt{t^2-(R/v)^2}\right)}{\frac{\sigma}{2\varepsilon}\sqrt{t^2-(R/v)^2}} U(t-R/v)$$

$$v = \frac{1}{\sqrt{\mu\varepsilon}}; \qquad R = \left|r-r'\right|$$

Adopting certain approximations yields:

$$g(r,r',t) = e^{-\frac{\sigma}{2\varepsilon v}R}\frac{\delta(t-R/v)}{4\pi R}$$

And the magnetic vector potential becomes:

$$A_x(x,t) = \frac{\mu}{4\pi}\int_0^L I(x',t-R/v)\frac{e^{-\frac{\sigma}{2\varepsilon v}R}}{R}dx'$$

Department of Electronics
University of Split,
Split, Croatia

Transient Analysis of Grounding Electrodes

The antenna model: Direct TD analysis of a single elecrode

Combining previous relations leads to the Pocklington equation for the grounding wire in a homogeneous lossy medium:

$$\frac{\sigma}{\varepsilon}E_x^{inc}+\frac{\partial E_x^{inc}}{\partial t}=\frac{\mu}{4\pi}\left(-\frac{1}{\mu\varepsilon}\frac{\partial^2}{\partial x^2}+\frac{\partial^2}{\partial t^2}+\frac{\sigma}{\varepsilon}\frac{\partial}{\partial t}\right)\cdot\int_0^L I(x',t-R/v)\frac{e^{-\frac{\sigma}{2\varepsilon v}R}}{R}dx'$$

The incident electric field along the electrode does not exist: $E_x^{inc}=0$

This results in a homogeneus TD integro-differential equation:

$$\frac{\mu}{4\pi}\left(-\frac{1}{\mu\varepsilon}\frac{\partial^2}{\partial x^2}+\frac{\partial^2}{\partial t^2}+\frac{\sigma}{\varepsilon}\frac{\partial}{\partial t}\right)\cdot\int_0^L I(x',t-R/v)\frac{e^{-\frac{\sigma}{2\varepsilon v}R}}{R}dx'=0$$

The current source is included into the integral equation through the boundary condition: $I(0)=I_g$

Université Clermont Auvergne

Department of Electronics
University of Split,
Split, Croatia

Transient Analysis of Grounding Electrodes

Numerical Procedure

The space-time dependent current along the electrode can be expressed, as follows:

$$I(x',t-R/v)=\sum_{i=1}^{N} I(t-R/v)N_i(x')$$

where $N_i(x')$ stands for the set of linear base functions.

Performing certain mathematical manipulations it follows::

$$\sum_{i=1}^{N} I_i(t-\tau_{ij})\left[\frac{\mu}{4\pi}\int_{\Delta l_j}\int_{\Delta l_i}\frac{\partial f_j(x)}{\partial x}\frac{\partial f_i(x')}{\partial x'}\frac{e^{-\frac{\sigma}{2\varepsilon v}R}}{R}dx'dx+\frac{1}{v^2}\frac{\partial^2}{\partial t^2}\int_{\Delta l_j}\int_{\Delta l_i}f_j(x)f_i(x')\frac{e^{-\frac{\sigma}{2\varepsilon v}R}}{R}dx'dx+\right.$$

$$\left.+\frac{\sigma}{\varepsilon}\frac{\partial}{\partial t}\int_{\Delta l_j}\int_{\Delta l_i}f_j(x)f_i(x')\frac{e^{-\frac{\sigma}{2\varepsilon v}R}}{R}dx'dx\right]=0 \qquad j=1,\ 2,\ \ldots,N$$

Université Clermont Auvergne

Department of Electronics
University of Split,
Split, Croatia

Transient Analysis of Grounding Electrodes

Numerical Procedure

In matrix form the following time domain differential equation is obtained:

$$[M]\frac{\partial^2}{\partial t^2}\{I(t')\}+[C]\frac{\partial}{\partial t}\{I(t')\}+[K]\{I(t')\}=0$$

… and carrying out the marching-on-in-time procedure:

$$\sum_{i=1}^{n}\left[M_{ji}+\gamma\Delta t C_{ji}+\beta\Delta t^2 K_{ji}\right]I_i^k=-\sum_{i=1}^{n}\left[-2M_{ji}+(1-2\gamma)\Delta t C_{ji}+\left(\frac{1}{2}-2\beta+\gamma\right)\Delta t^2 K_{ji}\right]I_i^{k-1}$$
$$-\sum_{n=1}^{n}\left[M_{ji}-(1-\gamma)\Delta t C_{ji}+\left(\frac{1}{2}+\beta-\gamma\right)\Delta t^2 K_{ji}\right]I_i^{k-2}$$

where the stability is achieved by choosing: $\gamma=\frac{1}{2};\quad \beta=\frac{1}{4}$

Université Clermont Auvergne

Transient Analysis of Grounding Electrodes

Numerical Example

Numerical example is related to the grounding electrode of length *L*=10m, radius *a*=5mm immersed in the lossy ground with $\varepsilon r=10$, $\sigma=0.001$S/m.

Grounding electrode is excited with the double exponential current pulse

$$i(t) = I_0 \cdot (e^{-at} - e^{-bt}), \quad t \geq 0;$$

defined with: I_0=1.1043A, a=0.07924·10^{7}s^{-1}, b=4.0011·10^{7}s^{-1}:

Université Clermont Auvergne

Department of Electronics
University of Split,
Split, Croatia

Transient Analysis of Grounding Electrodes

Numerical results

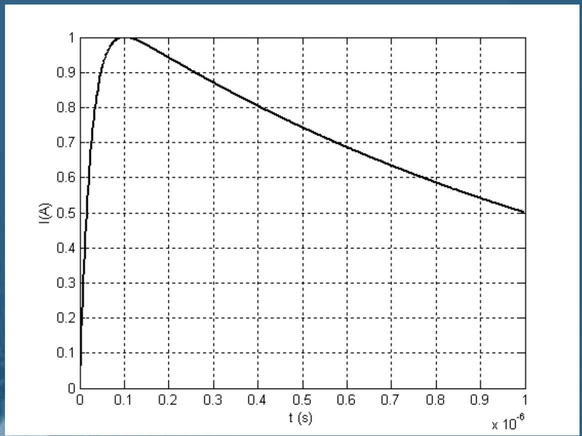

Double exponential current pulse

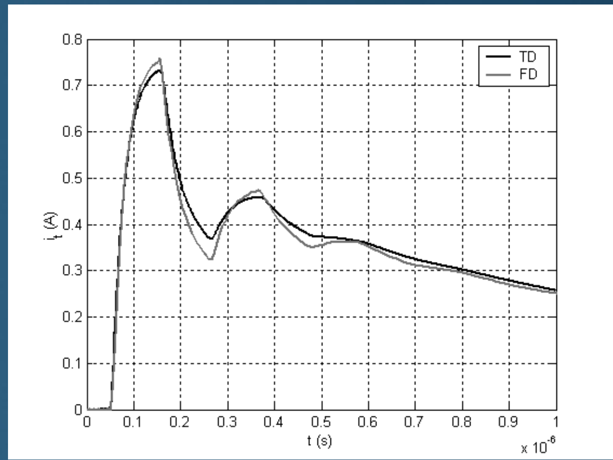

Current at the centre of the wire

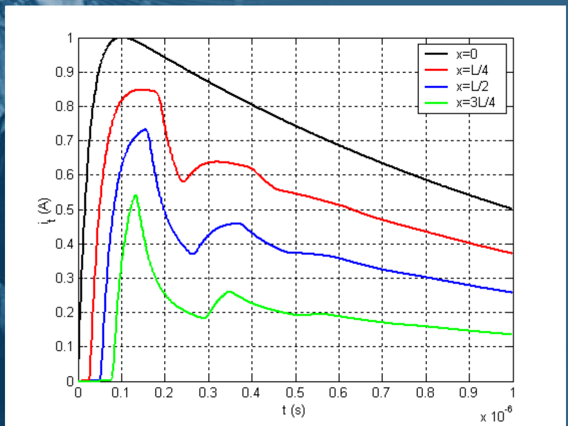

Current iat the different positions along the wire

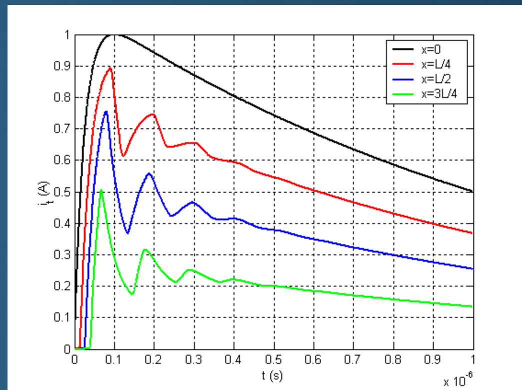

Current induced at the different distances over a 5m long wire

Department of Electronics
University of Split,
Split, Croatia

Transient Analysis of Grounding Electrodes

Analytical approach

Pocklington equation:

$$\left(\frac{\partial^2}{\partial x^2} - \mu\sigma\frac{\partial}{\partial t} - \mu\varepsilon\frac{\partial^2}{\partial t^2}\right)\cdot\left[\frac{\mu}{4\pi}\int_0^L I\left(x',t-\frac{R}{v}\right)\frac{e^{-\frac{1}{\tau_g}\frac{R}{v}}}{R}dx' - \frac{\mu}{4\pi}\int_0^t\int_0^L \Gamma_{ref}^{MIT}(\tau)\, I\left(x',t-\frac{R^*}{v}-\tau\right)\frac{e^{-\frac{1}{\tau_g}\frac{R^*}{v}}}{R^*}dx'd\tau\right]=0$$

$$\Gamma_{ref}^{MIT}(t) = -\left[\frac{\tau_1}{\tau_2}\delta(t) + \frac{1}{\tau_2}\left(1-\frac{\tau_1}{\tau_2}\right)e^{-\frac{t}{\tau_2}}\right]$$

$$\tau_1 = \frac{\varepsilon_0(\varepsilon_r - 1)}{\sigma}, \quad \tau_2 = \frac{\varepsilon_0(\varepsilon_r + 1)}{\sigma}$$

Impulse response:

$$I(x,t) = \frac{2\pi}{\mu\varepsilon L^2}\sum_{n=1}^{\infty}\frac{(-1)^{n-1} n}{\pm\sqrt{b^2-4c_n}}\sin\frac{n\pi(L-x)}{L}e^{ts_{1,2n}}$$

$$s_{1,2n} = \frac{1}{2}\left(-b \pm \sqrt{b^2-4c_n}\right), \quad b = \frac{\sigma}{\varepsilon}, \quad c_n = \frac{n^2\pi^2}{\mu\varepsilon L^2},\; n = 1,2,3,\ldots$$

Analytical solution:

$$I_g(t) = I_0\left(e^{-\alpha t} - e^{-\beta t}\right).$$

$$I(x,t) = \frac{2\pi I_0}{\mu\varepsilon L^2}\sum_{n=1}^{\infty}\frac{(-1)^{n-1} n}{\pm\sqrt{b^2-4c_n}}\sin\frac{n\pi(L-x)}{L}\cdot\left(\frac{e^{s_{1,2n}t}-e^{-\alpha t}}{s_{1,2n}+\alpha} - \frac{e^{s_{1,2n}t}-e^{-\beta t}}{s_{1,2n}+\beta}\right)$$

Department of Electronics
University of Split,
Split, Croatia

Transient Analysis of Grounding Electrodes

Analytical versus numerical results

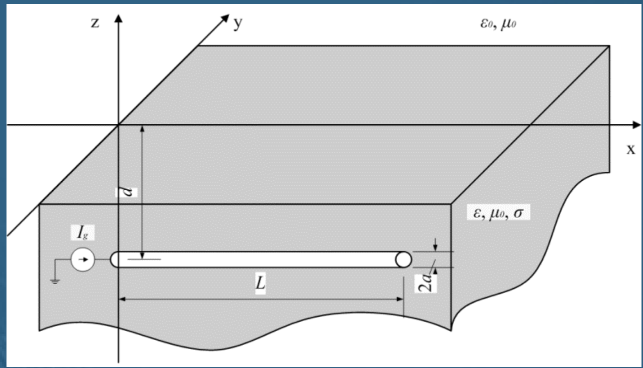

Horizontal straight thin wire buried in a lossy medium

Analytical results for the transient current induced at the center of the electrode are calculated with (43) and are compared to the results obtained via numerical approach. The results shown in Fig. 8 are calculated for the grounding electrode with L=10 m, buried in a lossy ground with the conductivity σ=1 mS/m. The agreement between the results is very good.

The results shown in Fig. 9 are related to calculations performed for electric properties of the ground σ=0.833 mS/m and ε_r=9. It is worth emphasizing that low ground conductivity is considered. The electrode is buried at depth d=0.5 m. Length of the grounding electrode is L=200 m. The agreement between analytical and numerical results for the current induced at the center of the electrodes is very good, especially for the longer electrode.

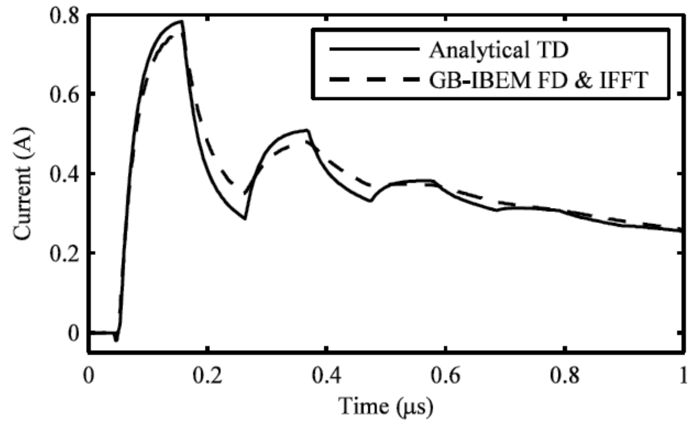

Fig. 8. Transient current at the center of the grounding electrode, 0.1/1 μs pulse

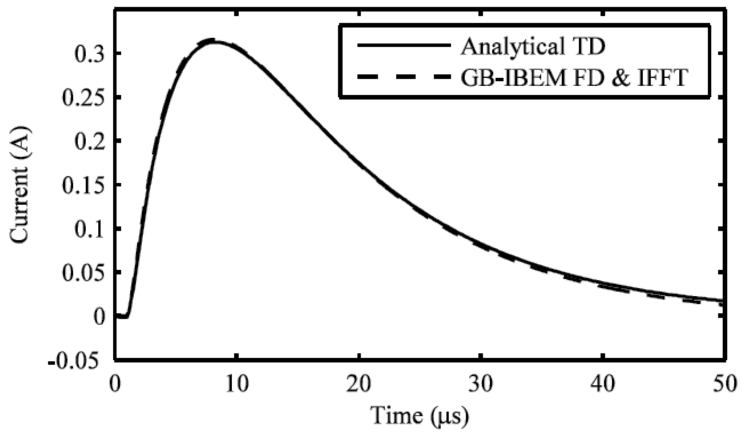

Fig. 9. Transient current at the center of the grounding electrode, 1/10 μs pulse

Department of Electronics
University of Split,
Split, Croatia

Transient Analysis of a Lightning Rod

- Lightning protection system (LPS) in terms of lightning rod aims to capture a direct lightning strike.
- The protection area around the rod can be determined by applying the scattering theory approach.
- The first step in the process is to obtain the current distribution along the rod.

According to the image theory lightning rod is modelled as a thin wire antenna excited with the current source at the both wire ends.

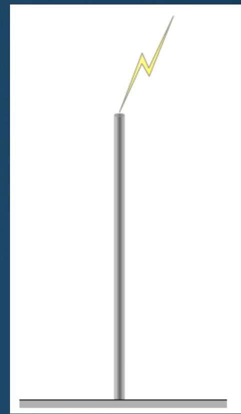

Lightning rod

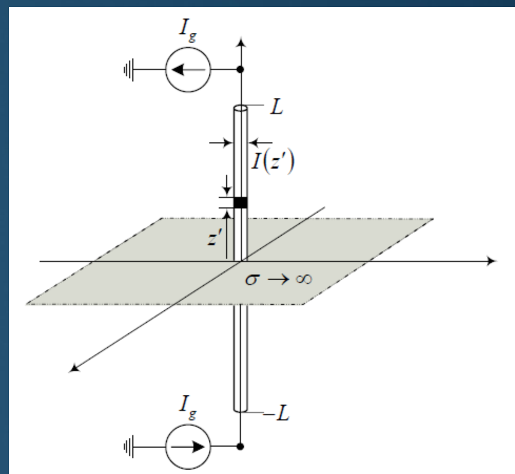

Antenna model of a lightning rod

UNIVERSITÉ
Clermont
Auvergne

Department of Electronics
University of Split,
Split, Croatia

Transient Analysis of a Lightning Rod

Time Domain Antenna Model

The corresponding wave equation in free space is given by:

$$\frac{\partial \vec{E}}{\partial t} = -\frac{\partial^2 \vec{A}}{\partial t^2} + \frac{1}{\mu_0 \varepsilon_0} \nabla \left(\nabla \vec{A} \right)$$

The magnetic vector potential is defined by relation:

$$A_z = \frac{\mu}{4\pi} \int_{-L}^{L} \frac{I(z', t - R/c)}{R} dz'$$

Combining previous relations leads to the corresponding Pocklington equation for the unknown current:

$$\frac{\partial E_z^{exc}}{\partial t} = \frac{\mu_0}{4\pi} \left[\frac{\partial^2}{\partial t^2} - c^2 \frac{\partial^2}{\partial z^2} \right] \int_{-L}^{L} \frac{1}{R_a} \cdot I\left(z', t - \frac{R_a}{c} \right) dz'$$

Department of Electronics
University of Split,
Split, Croatia

Transient Analysis of a Lightning Rod

Time Domain Antenna Model

The incident electric field along the electrode does not exist i.e.:

$$E_z^{exc} = 0$$

witch results in a homogeneus TD integro-differential equation:

$$\frac{\mu_0}{4\pi}\left[\frac{\partial^2}{\partial t^2} - c^2\frac{\partial^2}{\partial z^2}\right]\int_{-L}^{L}\frac{I\left(z',t-R_a/c\right)}{R_a}dz' = 0$$

The current source is included into the integral equation scheme through the symmetric boundary condition:

$$I(-L) = I(L) = I_g$$

Transient Analysis of a Lightning Rod

Time Domain Antenna Model

Charge Distribution

The current distribution and linear charge density along the rod are related through the continuity equation:

$$\frac{\partial I}{\partial z} = -\frac{\partial q}{\partial t}$$

Charge density along the rod at the any moment is readily computed by integrating the current derivation:

$$q(z,t) = -\int_0^t \frac{\partial I(z,t)}{\partial z}\, dt$$

Department of Electronics
University of Split,
Split, Croatia

Transient Analysis of a Lightning Rod

Numerical Procedure

The space-time dependent current along the rod can be expressed, as follows:

$$I\left(z',t-R_a/c\right)=\sum_{i=1}^{N} I_i\left(t-R_a/c\right) f_i^{g}(z')$$

where $f_i^{g}(z')$ stands for the set of linear base functions.

Performing certain mathematical manipulations it follows:

$$\sum_{i=1}^{N}\left[\frac{\partial^2}{\partial t^2}\int_{-L}^{L}\int_{L}^{L}\frac{1}{R_a}\cdot I_i\left(t-R_a/c\right) f_i^{g}(z')f_j^{g}(z)dz'dz+c^2\int_{-L}^{L}\int_{-L}^{L}\frac{1}{R_a}I_i\left(t-R_a/c\right)\frac{\partial f_i^{g}(z')}{\partial z'}\frac{\partial f_j^{g}(z)}{\partial z}dz'dz\right]=0;$$

$$j=1,2,\ldots N$$

Department of Electronics
University of Split,
Split, Croatia

Transient Analysis of a Lightning Rod

Numerical Procedure

Using BEM discretization, results in the linear equation system:

$$\sum_{i=1}^{2}\left[\frac{\partial^2}{\partial t^2}\int_{\Delta l_m}\int_{\Delta l_n}\frac{1}{R_a}\cdot I_i\left(t-R_a/c\right) f_i\,(z')\, f_j\,(z)\,dz'dz + c^2\int_{\Delta l_m}\int_{\Delta l_n}\frac{1}{R_a} I_i\left(t-R_a/c\right)\frac{\partial f_i\,(z')}{\partial z'}\frac{\partial f_j\,(z)}{\partial z}\,dz'dz\right]=0;$$

$$j=1,2;\quad m=1,2,\ldots N;\quad n=1,2,\ldots N$$

In matrix form the following TD differential equation is obtained:

$$[M]\frac{\partial^2}{\partial t^2}\{I(t')\}+[K]\{I(t')\}=0$$

… and carrying out the marching-on-in-time procedure:

$$\sum_{i=1}^{n}\left[M_{ji}+\beta\Delta t^2 K_{ji}\right]I_i^k=-\sum_{i=1}^{n}\left[-2M_{ji}+\left(\frac{1}{2}-2\beta+\gamma\right)\Delta t^2 K_{ji}\right]I_i^{k-1}-\sum_{n=1}^{n}\left[M_{ji}+\left(\frac{1}{2}+\beta-\gamma\right)\Delta t^2 K_{ji}\right]I_i^{k-2}$$

$$\gamma=\frac{1}{2};\quad \beta=\frac{1}{4}$$

Department of Electronics
University of Split,
Split, Croatia

Transient Analysis of a Lightning Rod

Numerical Procedure

The spatial derivation of the current is calculated using the FD scheme:

$$\frac{\partial I(z_i,t_k)}{\partial z} = \frac{I(z_{i+1},t_k) - I(z_i,t_k)}{\Delta z}$$

Time domain integration is preformed numerically using the trapezoidal rule:

$$q(z_i,t_k) = -\frac{\Delta t}{2}\sum_{j=0}^{k}\left[\frac{\partial I(z_i,t_j)}{\partial z} + \frac{\partial I(z_i,t_{j+1})}{\partial z}\right]$$

where Δt stands for time step.

UNIVERSITÉ Clermont Auvergne

Department of Electronics
University of Split,
Split, Croatia

Transient Analysis of a Lightning Rod

Numerical Results

Computational example is related to the single lightning rod of length *L*=10m and radius *a*=0.019m.

The rod is excited by the double exponential current pulse

$$i(t) = I_0 \cdot (e^{-at} - e^{-bt}), \quad t \geq 0;$$

with parameters I_0= 1.1043 A, α= 0.07924·10^7 s^{-1}, β= 4.0011·10^7 s^{-1}.

Transient Analysis of a Lightning Rod

Department of Electronics
University of Split,
Split, Croatia

Numerical Results

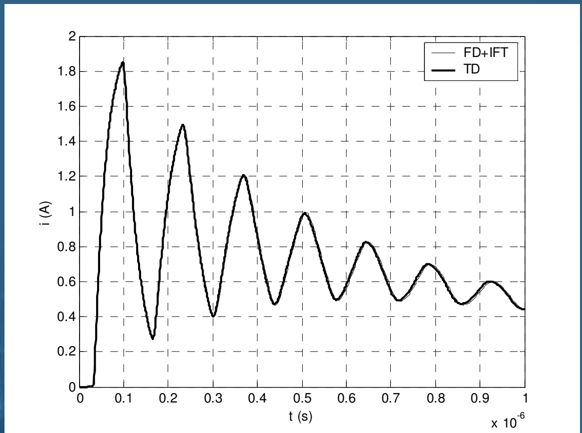

Induced current at the base of the rod obtained via different approaches

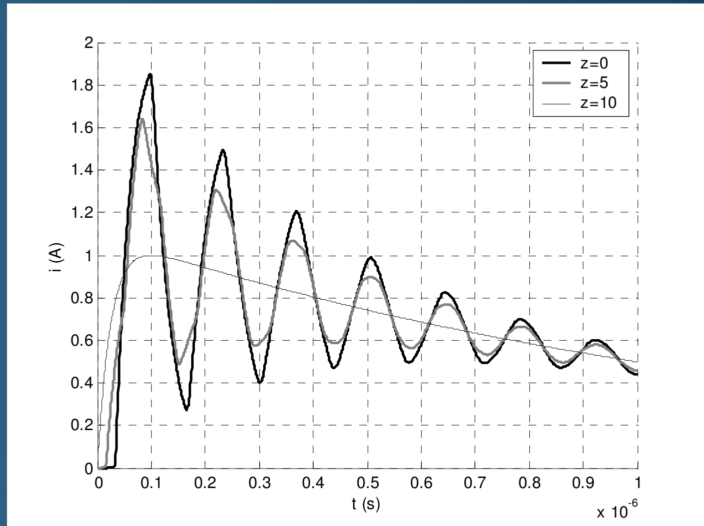

Current induced at the different distances over a wire

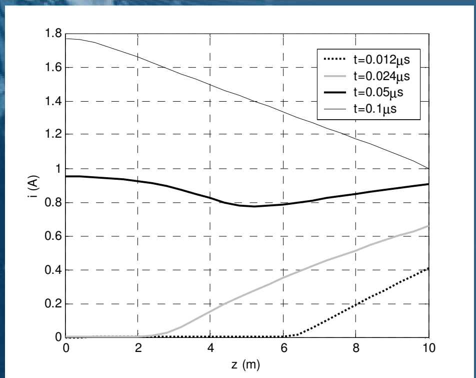

Current induced along the rod at different time instants

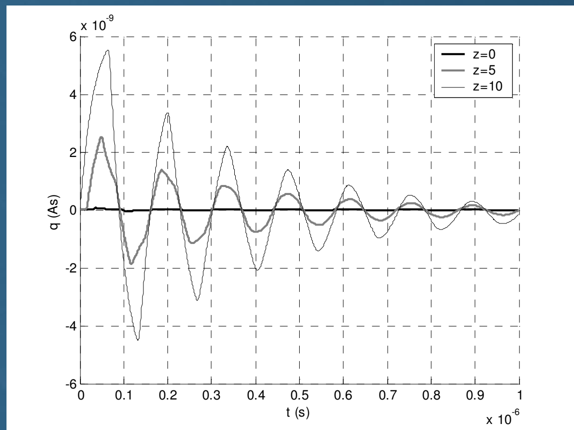

Induced charge at the different distances over a wire

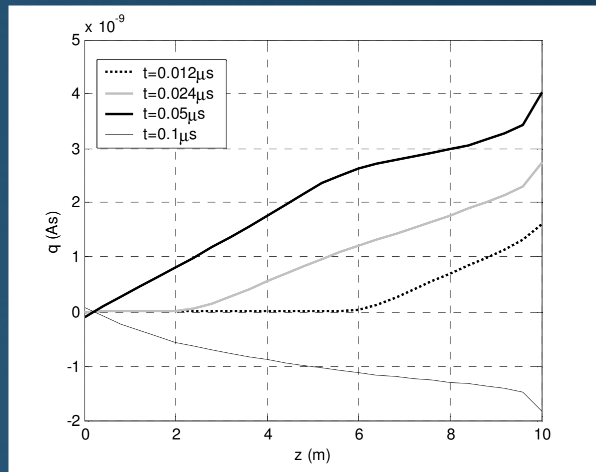

Induced charge along the rod at different time instants

Department of Electronics
University of Split,
Split, Croatia

Transient Analysis of a Lightning Strike

• The lightning strike, either direct or indirect, is a common cause of serious damages and malfunctions of power installations and telecommunication equipmnt.

• As measurements are usually difficult to perform and very expensive, it is essential to analyze this problem through numerical modeling.

• One of the possible approaches is ~~related to~~ based on transmission line (TL) approximation and the finite difference time domain (FDTD) method.

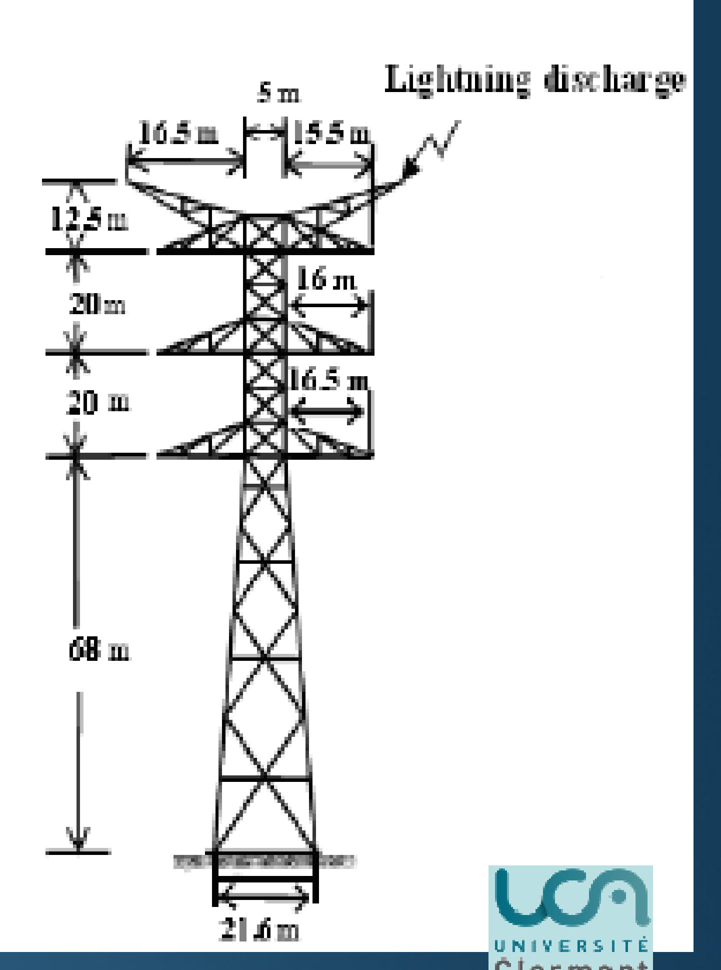

UNIVERSITÉ
Clermont
Auvergne

Department of Electronics
University of Split,
Split, Croatia

Transient Analysis of a Lightning Strike

Time Domain Transmission Line Model

The field coupling to electrical tower (pylon) due to indirect lightning strike is handled via transmission line (TL) approximation.

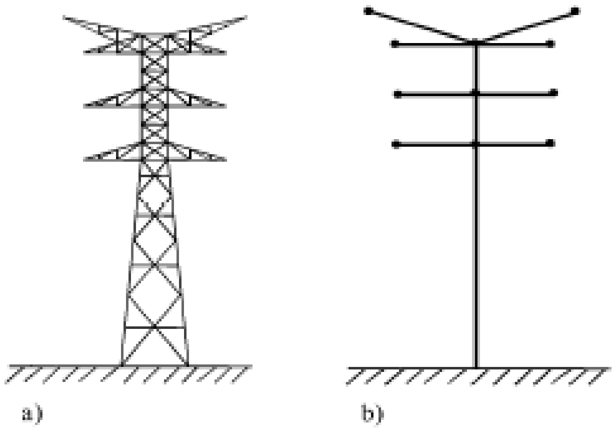

Figure 1. Electric tower and its equivalent representation by interconnected conductors.

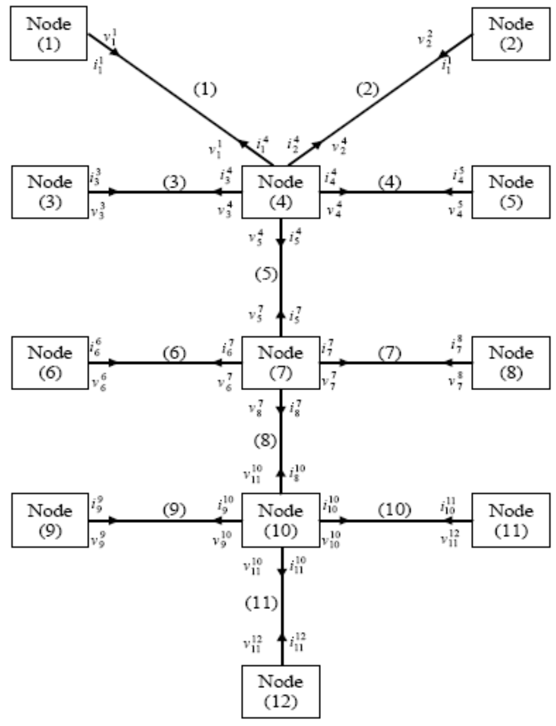

Figure 3. Topological approach of an electrical tower.

Department of Electronics
University of Split,
Split, Croatia

Transient Analysis of a Lightning Strike

Time Domain Transmission Line Model

$$\begin{cases} \dfrac{\partial v(x,t)}{\partial x} + R\,i(x,t) + L\dfrac{\partial i(x,t)}{\partial t} = v_S(x,t) \\ \dfrac{\partial i(x,t)}{\partial x} + C\dfrac{\partial v(x,t)}{\partial t} = i_S(x,t) \end{cases} \tag{2}$$

L, *R* and *C* the per unit lines parameters which can be calculated and derived from the formalism developed by A.Ametani et al [7] or by that of J.Gutierrez et al [8] for the vertical conductors, and for the horizontal ones the formalism described in [9] has been used,

$v_S(x,t)$ and $i_S(x,t)$ are the equivalent sources of voltage and current due to the lightning wave [5].

$$v_S(x,t) = -\frac{\partial \xi_T(x,t)}{\partial x} + \xi_L(x,t) \tag{3}$$

$$i_S(x,t) = -C.\frac{\partial \xi_T(x,t)}{\partial t} \tag{4}$$

with: $\xi_T(x,t) = \int_0^h E_z^e(x,z,t)dz$ and $\xi_L = E_x^e(x,h,t)$

$$\left(\frac{C}{\Delta t}\right)v_1^n = \left(\frac{C}{\Delta t}\right)v_1^{n-1} - \frac{i_1^{n-1/2} - i_0^{n-1/2}}{\Delta x/2} - C\frac{(\xi_T)_1^n - (\xi_T)_1^{n-1}}{\Delta t} \tag{9}$$

$$\left(\frac{C}{\Delta t}\right)v_{k_{\max}+1}^n = \left(\frac{C}{\Delta t}\right)v_{k_{\max}+1}^{n-1} - \frac{i_{k_{\max}+1}^{n-1/2} - i_{k_{\max}}^{n-1/2}}{\Delta x/2} - C\frac{(\xi_T)_{k_{\max}+1}^n - (\xi_T)_{k_{\max}+1}^{n-1}}{\Delta t} \tag{10}$$

UNIVERSITÉ Clermont Auvergne

Department of Electronics
University of Split,
Split, Croatia

UNIVERSITÉ Clermont Auvergne

Transient Analysis of a Lightning Strike

Computational examples: Modeling of a direct lightning strike

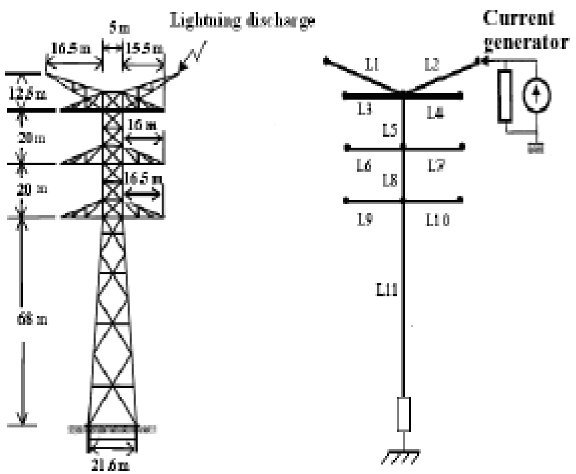

Figure 4. Configuration to study the direct impact (adopted model).

The direct impact is modeled by a biexponential current generator: $i(t) = I_0\left(e^{-\alpha t} - e^{-\beta t}\right)$ with $I_0 = 1.06537$ kA, $\alpha = 1.88\times10^4 s^{-1}$, and $\beta = 1.6\times10^6 s^{-1}$.

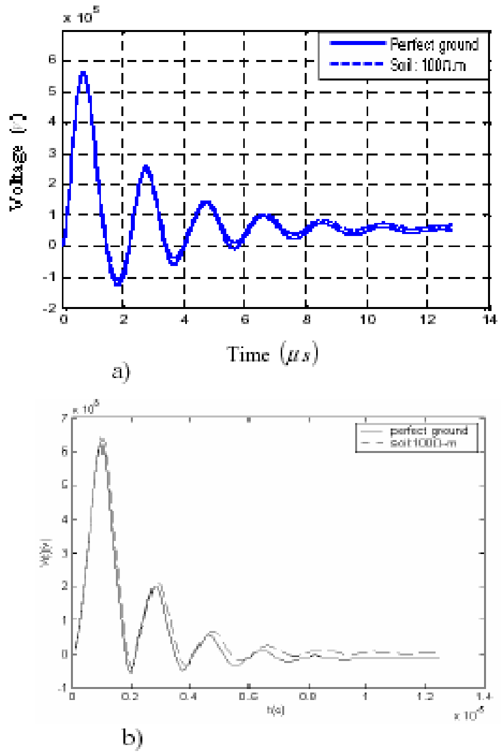

Figure 5. Voltage at the top of the tower
a-our calculation result, b- published results [3].

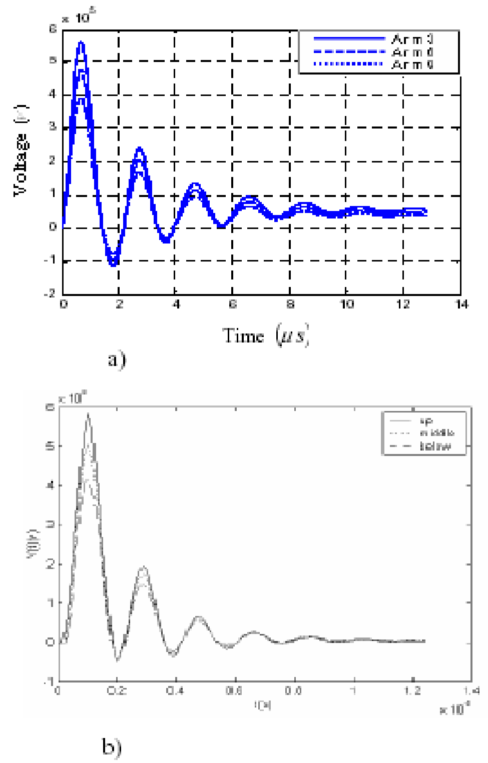

Figure 6. Voltage in different arms
a-our calculation result, b- published results [3]).

Department of Electronics
University of Split,
Split, Croatia

UNIVERSITÉ Clermont Auvergne

Transient Analysis of a Lightning Strike

Computational examples: Modeling of an indirect lightning strike

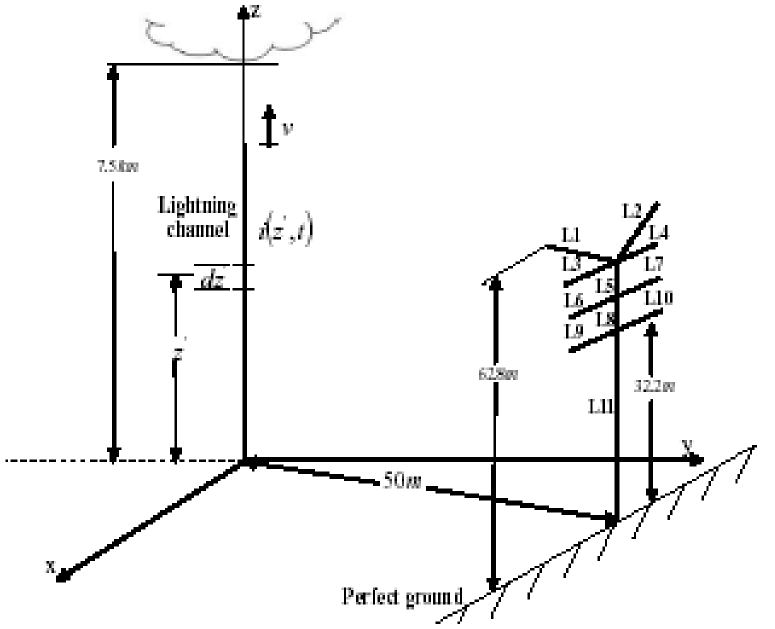

Figure 7. Geometry of the problem.

The channel base current is given by:

$i(t) = I_0\left(\exp(-\alpha t) - \exp(-\beta t)\right),$

With : $\alpha = 3\times10^4 s^{-1}, \beta = 10^7 s^{-1}$ and $I_0 = 10\ kA$.

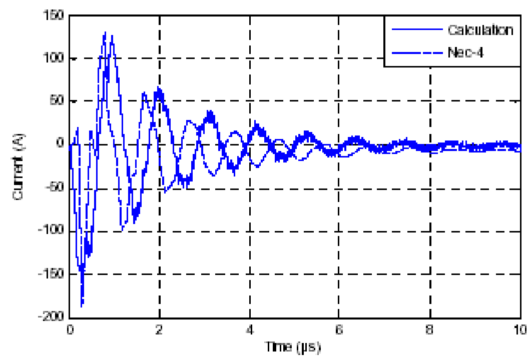

Figure 8. Current induced at the top of segment 5.

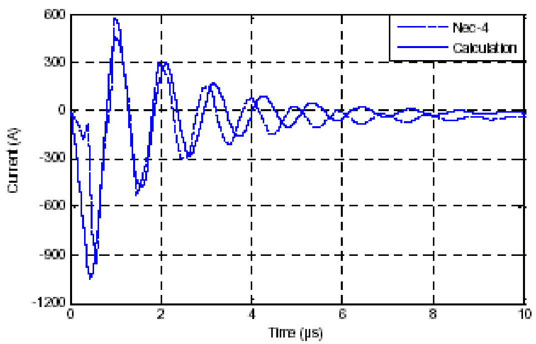

Figure 9. Current induced at the base of tower.

Department of Electronics
University of Split,
Split, Croatia

Transient Analysis of a Lightning Strike

Computational examples: Lightning channel current

Frequency Domain Antenna Model

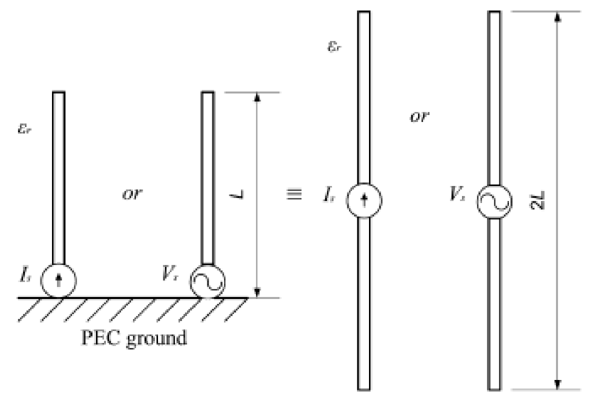

Fig. 6. Monopole and dipole antenna representation of the lightning channel energized by current or voltage source, respectively.

In the case of an equivalent voltage source the excitation is expressed in terms of the incident electric field $E_z^{inc}(z)$ and the unknown current distribution $I(z')$ along the channel is governed by the following integral equation [42]

$$E_z^{inc}(z) = -\frac{1}{j4\pi\omega\varepsilon_0\varepsilon_r}\int_{-L}^{L} I(z')\left[k^2 + \frac{d^2}{dz^2}\right]g_0(z,z')dz' + Z_S I(z) \qquad (29)$$

where $g_0(z,z')$ is the homogenous medium Green function, k is the propagation constant and Z_S is the impedance term to account for the losses.

On the other hand, if the current source is used the incident field $E_z^{inc}(z)$ is set to zero. Thus, in the case of a current source at the dipole center integral Eq. (29) simplifies to homogenous one.

$$-\frac{1}{j4\pi\omega\varepsilon_0\varepsilon_r}\int_{-L}^{L} I(z')\left[k^2 + \frac{d^2}{dz^2}\right]g_0(z,z')dz' + Z_S I(z) = 0 \qquad (30)$$

Note that the excitation is incorporated into the formulation through the forced condition within the numerical solution procedure [42].

Department of Electronics
University of Split,
Split, Croatia

Transient Analysis of a Lightning Strike

Computational examples: Modeling of a lightning channel current

Frequency Domain Antenna Model

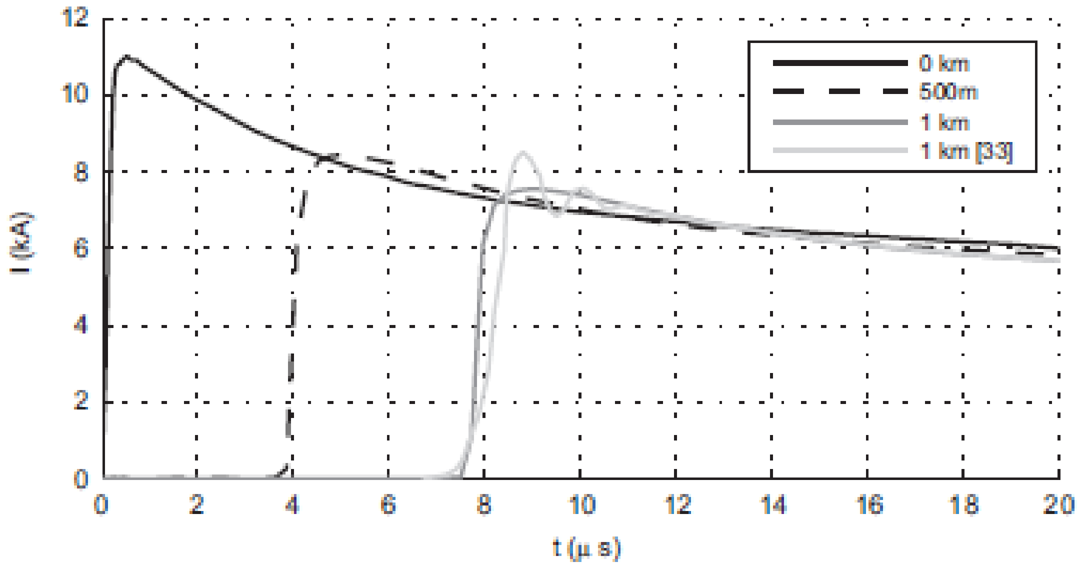

Fig. 7. Current waveforms at different heights along the channel.

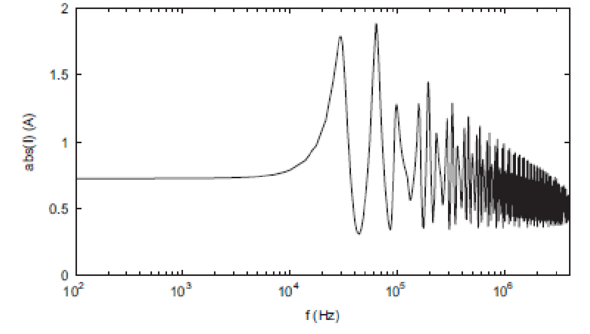

Fig. 8. Frequency spectrum of current at the height h=500 m (unit current source) – 2 km channel.

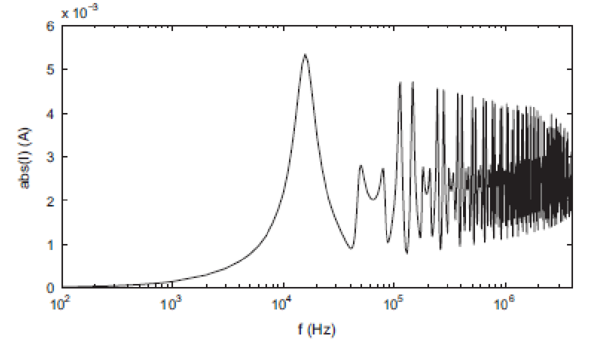

Fig. 9. Frequency spectrum of current at the height h=500 m (unit voltage source) – 2 km channel.

Department of Electronics
University of Split,
Split, Croatia

Transient Analysis of a Lightning Strike

Computational examples: Modeling of a lightning channel current

Frequency Domain Antenna Model

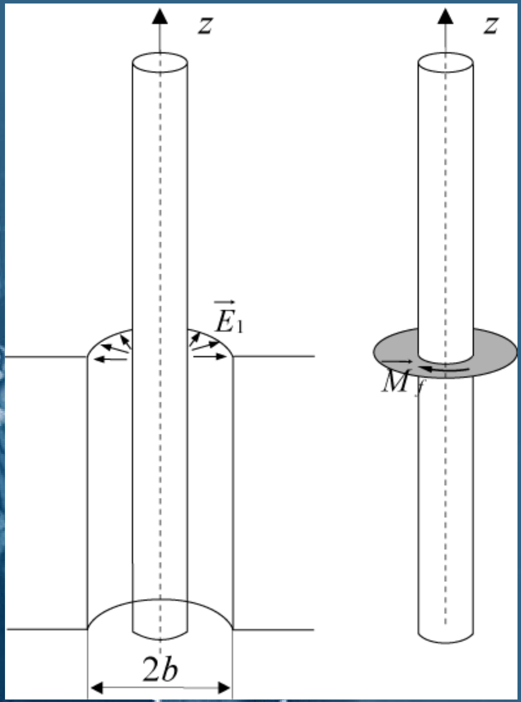

Magnetic frill concept:

$$\vec{E}_1 = \hat{e}_\rho \frac{1}{2}\frac{V_0}{\rho \ln\left(\frac{b}{a}\right)}$$

$$\vec{M}_f = -\hat{e}_\phi \frac{V_0}{\rho \ln\left(\frac{b}{a}\right)}$$

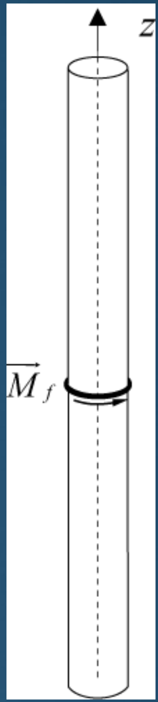

$$\vec{M}_f == \hat{e}_\phi \delta(\varphi' = a)$$

$$E_z(0,z) = \frac{1}{2}\frac{V_0}{\ln\left(\frac{b}{a}\right)}\left[\frac{e^{-jk\sqrt{a^2+(z-z')^2}}}{\sqrt{a^2+(z-z')^2}} - \frac{e^{-jk\sqrt{b^2+(z-z')^2}}}{\sqrt{b^2+(z-z')^2}}\right]$$

$$E_z(0,z) = \frac{a^2}{2}\left[jk + \frac{1}{\sqrt{a^2+(z-z')^2}}\right]\frac{e^{-jk\sqrt{a^2+(z-z')^2}}}{a^2+(z-z')^2}$$

Department of Electronics
University of Split,
Split, Croatia

Transient Analysis of a Lightning Strike

Computational examples: Modeling of a lightning channel current

$H = 7500m$

$R = 0.07\Omega / m$

$\varepsilon_r = 5.3$

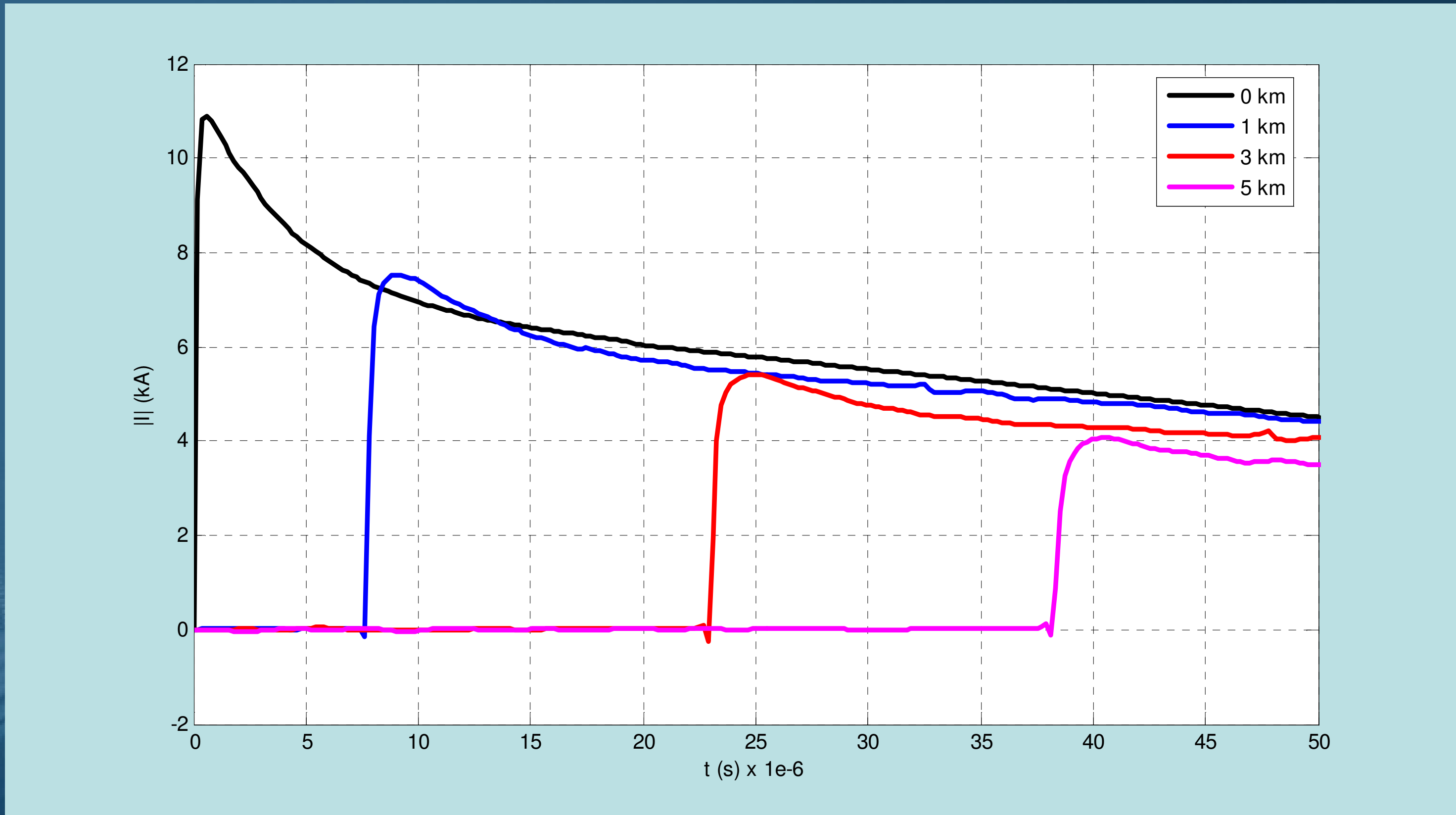

Lightnig channel current versus time for different heights along the PEC ground

Université Clermont Auvergne

Department of Electronics
University of Split,
Split, Croatia

HUMAN EXPOSURE TO ELECTROMAGNETIC FIELDS

DON'T BELIEVE EVERYTHING YOU READ ON YOUR WAP WRAPPER

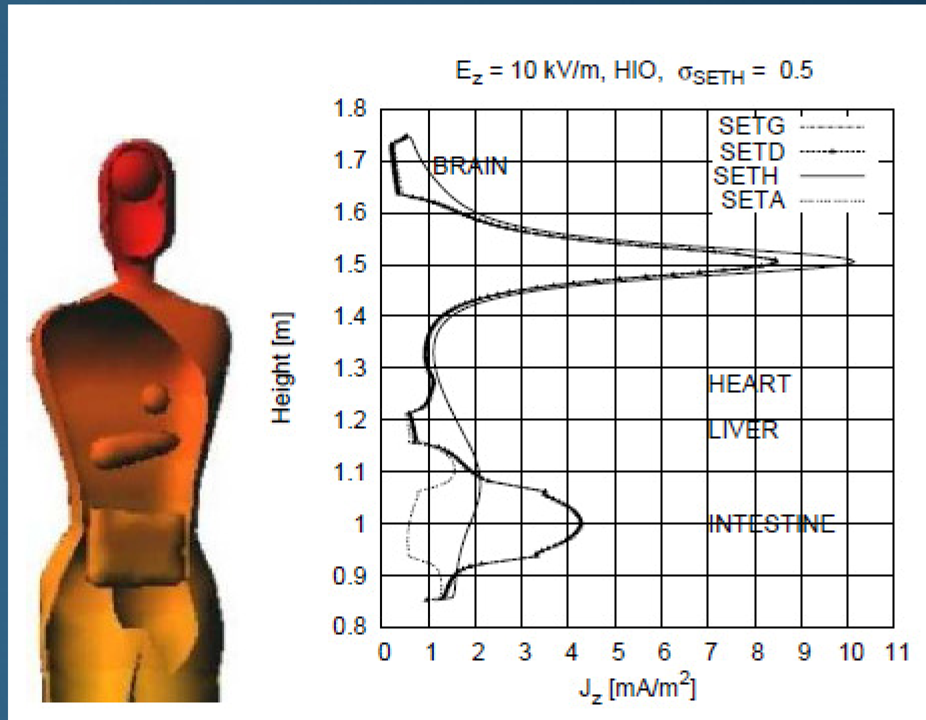

Clermont-Ferrand, 03 April 2018

UNIVERSITÉ Clermont Auvergne

Department of Electronics
University of Split,
Split, Croatia

Human Exposure to Electromagnetic Fields

In the 20th century, occurrence of EM fields in the environment has significantly increased.

There is also a continuing public concern associated with the possible adverse health effects due to human exposure to these fields, particularly exposure to HV power lines and radiation from cellular base stations and mobile phones.

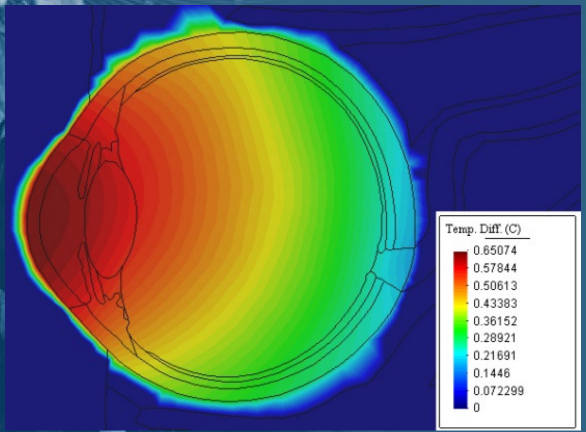

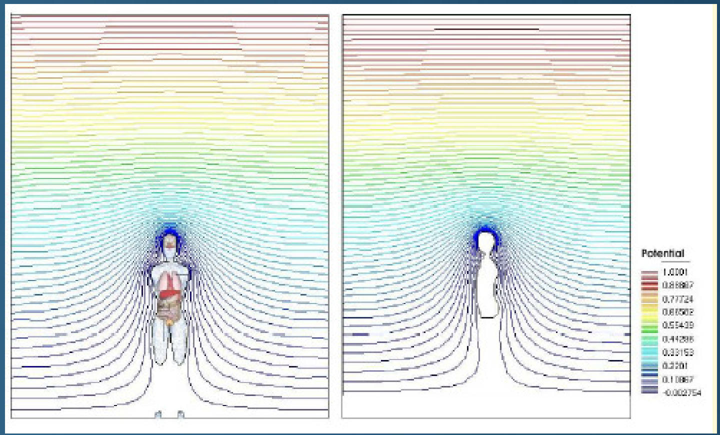

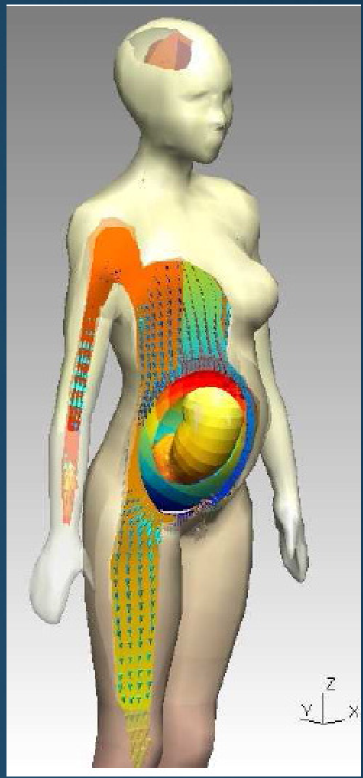

Department of Electronics
University of Split,
Split, Croatia

Human Exposure to Electromagnetic Fields

Non-ionizing radiation

- Non-ionizing fields are split into two main categories; LF (up to about 30 kHz) and HF frequencies (from 30 kHz to 300 GHz).
- At ELF (up to 3 kHz), the wavelengths are very long (6000 km at 50 Hz) so that there is no radiation and electric and magnetic fields are analyzed separately. <u>ELF fields</u> are generally used for power utilities (transmission, distribution and applications) and for strategic global communications with submarines submerged in conducting seawater.
- <u>RF fields</u> lie in the frequency range from 30kHz to 300 GHz and are used for RTV, radar, and other RF/microwave applications.

Department of Electronics
University of Split,
Split, Croatia

Human Exposure to Electromagnetic Fields

Interaction of humans with EM fields

- The LF fields may cause excitation of sensory, nerve and muscle cells.

- Humans are particularly sensitive to HF fields as the body absorbs the radiated energy, and the related heating effects become dominant.
- The humans absorb a great deal of energy at certain frequencies, since the body acts as an antenna if the body dimensions parts are comparable to the field wavelength.
- When the body size is half the wavelength, the resonant frequency is reached and a large amount of energy is absorbed from the field at frequencies between 30 MHz and 300 MHz.

- It is worth noting that children have a higher resonant frequency than adults.

Department of Electronics
University of Split,
Split, Croatia

Human Exposure to Electromagnetic Fields

Dosimetry

- Theoretical models are required to interpret and confirm the experiment, develop an extrapolation process, and thereby establish safety guidelines and exposure limits for humans.
- Sophisticated numerical modeling is required to predict distribution of internal fields.
- Today realistic computational models comprising of cubical cells are mostly related to applying of Finite Difference Time Domain (FDTD) methods.
- In certain studies, the Finite Element Method (FEM) is considered to be a more accurate method than the FDTD, and a more sophisticated tool when the treatment of irregular or curved shape domains is of interest.
- Some recent research has also demonstrated that the use of Boundary Element Method (BEM), fast multipole techniques and wavelet techniques can reduce the computational task.

Department of Electronics
University of Split,
Split, Croatia

Human Exposure to Electromagnetic Fields

Dosimetry: *Low and high frequencies*

- The induced currents and fields in human organs may give rise to thermal and nonthermal effects.
- When man is exposed to LF fields the thermal effects seem to be negligible, and possible nonthermal effects are related to the cellular level.
- The knowledge of the internal current density is the key to understanding the interaction of the human body with LF fields.
- The key point in HF dosimetry is how much EM energy is absorbed by a biological body and where it is deposited.
- The basic dosimetric quantity for HF fields is the specific absorption rate (SAR).

Department of Electronics
University of Split,
Split, Croatia

Human Exposure to Electromagnetic Fields

Dosimetry: Exposure to static fields

FORMULATION: Laplace equation

3D electrostatic field distribution between a VDU and the head is governed by the Laplace equation for electric potential ϕ:

$$\nabla^2 \varphi = 0$$

boundary conditions:

$\varphi = \varphi_s$ on the display

$\varphi = \varphi_h$ on the head

$\nabla \varphi \cdot \vec{n} = 0$ on the far field boundaries

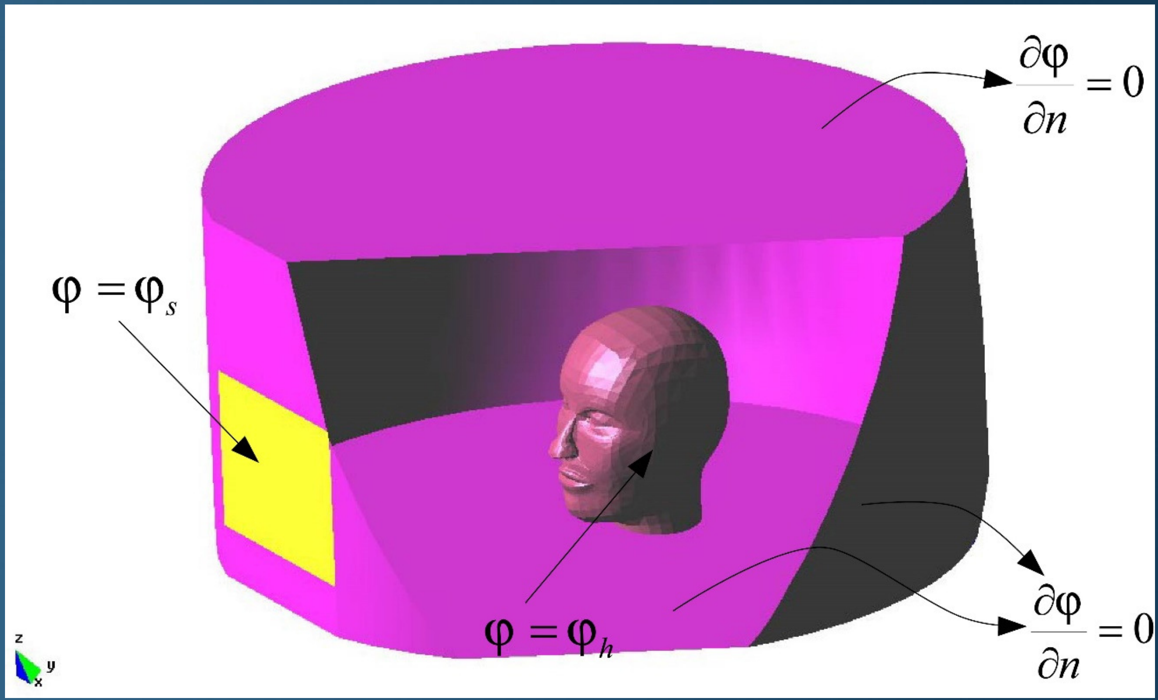

3D model of the head located in front of a VDU

Human Exposure to Electromagnetic Fields

Dosimetry: Exposure to static fields - FEM SOLUTION

Applying the weighted residual approach to Laplace equation yields:

$$\int_{\Omega} \nabla^2 \varphi W_j \, d\Omega = 0$$

Performing some mathematical manipulations gives:

$$\int_{\Omega} \nabla \varphi \nabla W_j \, d\Omega = \int_{\Gamma} \frac{\partial \varphi}{\partial n} W_j \, d\Gamma$$

The Galerkin-Bubnov procedure ($W_j = N_j$) it follows:

$$\int_{\Omega} \nabla \varphi \nabla N_j \, d\Omega = \int_{\Gamma} \frac{\partial \varphi}{\partial n} N_j \, d\Gamma$$

Neumann condition: $\frac{\partial \varphi}{\partial n} = 0$ $\quad \int_{\Omega} \nabla \varphi \nabla N_j \, d\Omega = 0$

The unknown potential over an element is expressed by linear combination of shape functions:

$$\varphi^e = \sum_{i=1}^{4} \alpha_i N_i$$

The shape functions:

$$N_i(x, y, z) = \frac{1}{D}\left(V_i + a_i x + b_i y + c_i z\right) \qquad i = 1, 2, 3, 4$$

The global matrix system:

$$[a] \; \{\alpha\} = \{Q\}$$

The electrostatic field from expression:

$$\vec{E} = -\nabla \varphi$$

Department of Electronics
University of Split,
Split, Croatia

Human Exposure to Electromagnetic Fields

Dosimetry: Exposure to static fields- Computational examples

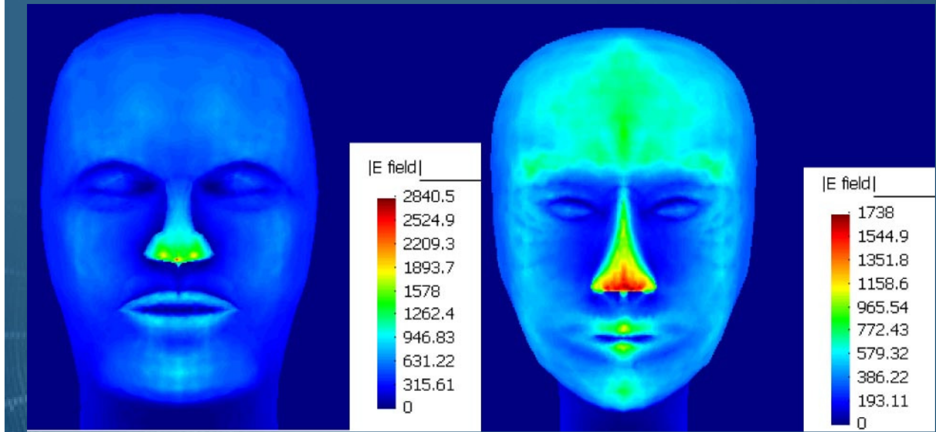

a)

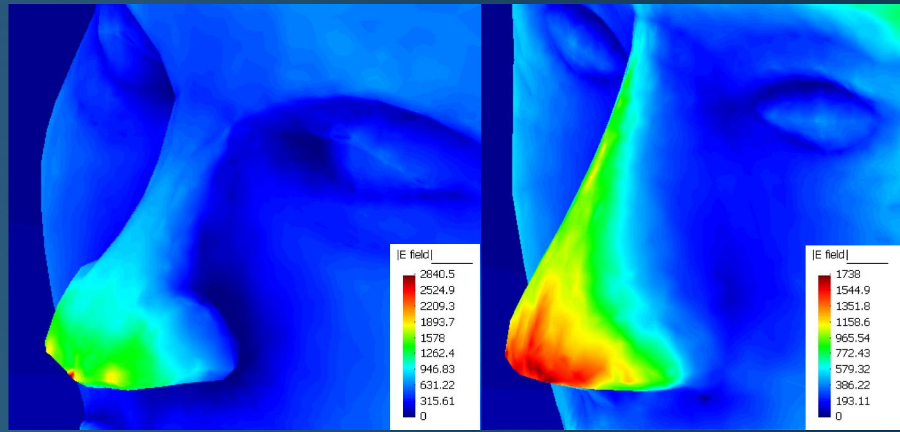

b)

Electrostatic field strength [V/cm] on the faces. a) Person 1; b) Person 2

Dosimetry: Exposure to LF fields: Cylindrical body model

$$E_z^{inc} = -\frac{1}{4j\pi\omega\varepsilon_0}\int_{-L}^{L}\left[\frac{\partial^2}{\partial z^2}+k^2\right]g_E(z,z')I(z')dz' + Z_L(z)I(z)$$

$$g_E(z,z') = \frac{1}{2\pi}\int_0^{2\pi}\frac{e^{-jkR}}{R}d\phi$$

$$R = \sqrt{(z-z')^2 + 4a^2\sin^2\frac{\phi}{2}}$$

FEM solution

$$\sum_{i=1}[Z]_{ji}\{I\}_i = \{V\}_j,$$

and $j = 1,2,\ldots,M$

$$[Z]_{ji} = -\frac{1}{4j\pi\omega\varepsilon}\left(\int_{\Delta l_j}\{D\}_j\int_{\Delta l_i}\{D'\}_i^T g_E(z,z')dz'dz + k^2\int_{\Delta l_j}\{f\}_j\int_{\Delta l_i}\{f\}_i^T g_E(z,z')dz'dz\right) + \int_{\Delta l_j} Z_L(z)\{f\}_j\{f\}_i^T dz$$

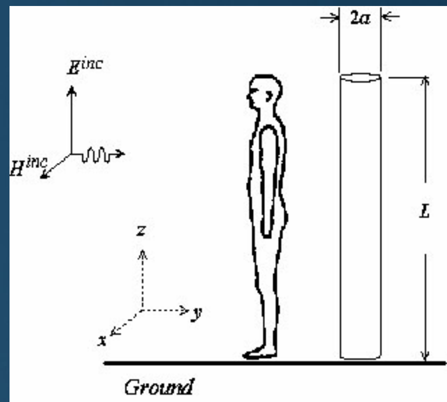

The equivalent antenna model of the human body

Department of Electronics
University of Split,
Split, Croatia

Human Exposure to Electromagnetic Fields

Dosimetry: Exposure to low frequency fields: Realistic approach: anatomically based body model

The Formulation:

The equation of continuity

$$\nabla \vec{J} + \frac{\partial \rho}{\partial t} = 0$$

$$\vec{J} = -\sigma \nabla \varphi \qquad \nabla(\varepsilon \nabla \varphi) = -\rho$$

For the time-harmonic ELF exposures it follows:

$$\nabla\left[(\sigma + j\omega\varepsilon)\nabla\varphi\right] = 0$$

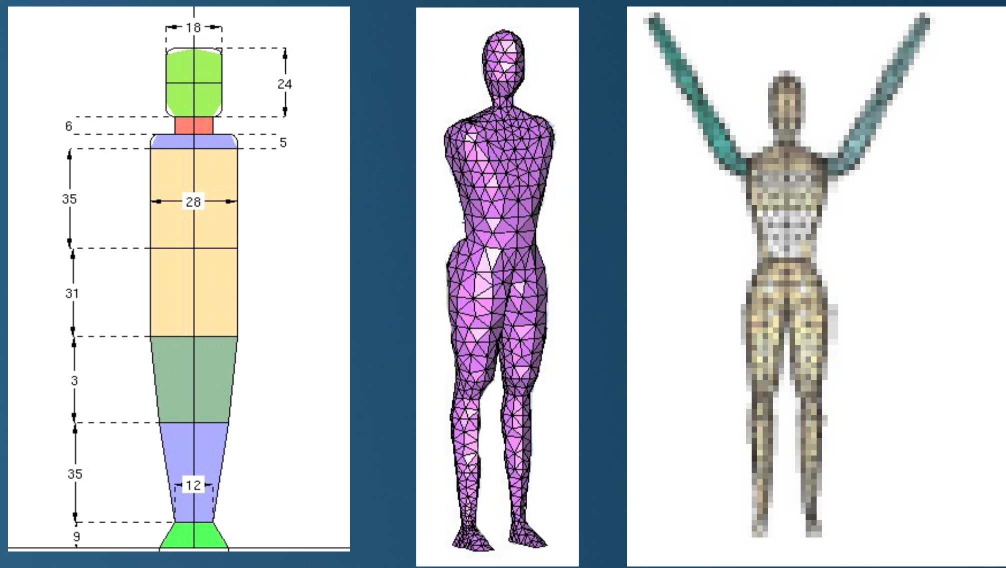

The air-body interface conditions

$$\vec{n} \times (\nabla\varphi_b - \nabla\varphi_a) = 0 \qquad \sigma_b \vec{n} \nabla \varphi_b = -j\omega\rho_s \qquad \varepsilon_0 \vec{n} \nabla \varphi_a = \rho_s$$

Department of Electronics
University of Split,
Split, Croatia

Human Exposure to Electromagnetic Fields

Numerical method: The Boundary Element Method

The beauty of BEM...

- BEM tends to avoid volume meshes for large-scale problems.
- BEM formulation is based on the fundamental solution of the leading operator for the governing equation thus being competitive with other well-established methods, such as FEM or FDM, in terms of accuracy and efficiency.

The problem consists of finding the solution of the Laplace equation in a non-homogenous media with prescribed boundary conditions

$$\nabla \cdot \left(\sigma \nabla \phi \right) = 0 \quad \text{on } \Omega$$

$$\phi = \overline{\phi} \quad \text{on } \Gamma_1$$

$$\frac{\partial \phi}{\partial x_j} n_j = \frac{\partial \overline{\phi}}{\partial n_j} \quad \text{on } \Gamma_2$$

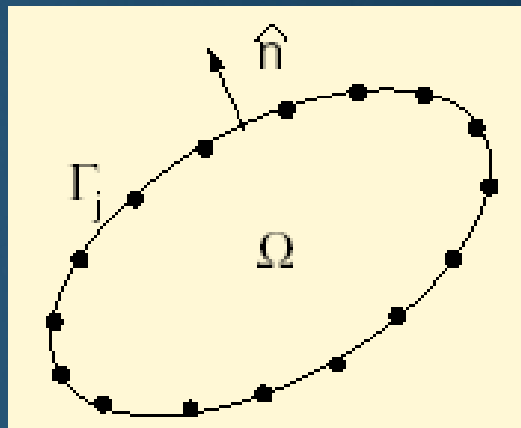

The integration domain is considered piecewise homogeneous, so it can be decomposed into an assembly of N homogeneous subdomains Ω_k ($k = 1, m$).

Department of Electronics
University of Split,
Split, Croatia

Human Exposure to Electromagnetic Fields

The Boundary Element Method

Green's theorem yields the following integral representation for a subdomain:

$$c(\xi)\phi(\xi) + \int_{\Gamma_k} \phi \frac{\partial \phi^*}{\partial n} d\Gamma = \int_{\Gamma_k} \frac{\partial \phi}{\partial n} \phi^* d\Gamma$$

where ϕ^* is the 3D fundamental solution of Laplace equation, $\partial \phi^* / \partial n$ is the derivative in normal direction to the boundary.

Discretization to N_k elements leads to an integral relation:

$$c_i \phi_i + \sum_{j=1}^{N_k} \int_{\Gamma_{k,j}} \phi \frac{\partial \phi^*}{\partial n} d\Gamma = \sum_{j=1}^{N_k} \int_{\Gamma_{k,j}} \frac{\partial \phi}{\partial n} \phi^* d\Gamma$$

Potential and its normal derivative can be written by means of the interpolation functions ψ_a

$$\phi(\xi) = \sum_{a=1}^{6} \psi_a(\xi)\phi_a$$

and

$$\frac{\partial \phi(\xi)}{\partial n} = \sum_{a=1}^{6} \psi_a(\xi)\phi_a$$

Department of Electronics
University of Split,
Split, Croatia

Human Exposure to Electromagnetic Fields

The Boundary Element Method

The system of equations for each subdomain can be written as:

$$\mathbf{H}\boldsymbol{\varphi} - \mathbf{G}\frac{\partial\boldsymbol{\varphi}}{\partial\mathbf{n}} = 0$$

where **H** and **G** are matrices defined by:

$$H = h_{ij}^{a} = \int_{\Gamma_{k,j}} \psi_a \left(\frac{\partial\phi^*}{\partial n}\right)_j d\Gamma \qquad G = g_{ij}^{a} = \int_{\Gamma_{k,j}} \psi_a \ \phi^* d\Gamma$$

The matching between two subdomains can be established through their shared nodes:

$$\phi_{j\ A}^{\alpha} = \phi_{j\ B}^{\alpha}$$

and

$$\left(-\tau_A \left.\frac{\partial\phi}{\partial n}\right|_j^{\alpha}\right)_A = \left(\tau_A \left.\frac{\partial\phi}{\partial n}\right|_j^{\alpha}\right)_B$$

UNIVERSITÉ Clermont Auvergne

Department of Electronics
University of Split,
Split, Croatia

Human Exposure to Electromagnetic Fields

Computational Examples: Exposure to power lines

The multidomain body of revolution model

The well-grounded body of 175cm height exposed to the10kV/m/60Hz power line E-field. The height of the power line is 10m above ground.

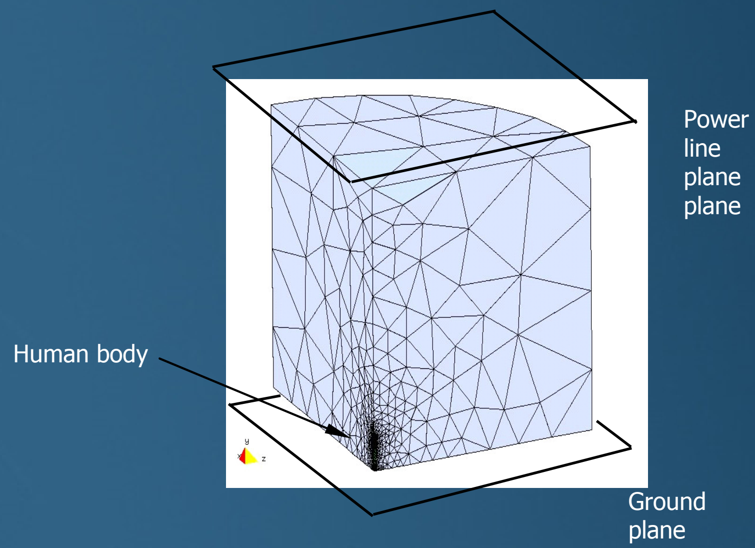

The boundary element mesh

UNIVERSITÉ Clermont Auvergne

Department of Electronics
University of Split,
Split, Croatia

Human Exposure to Electromagnetic Fields

Computational Examples (cont'd): Exposure to power lines

The current density values increase at narrow sections such as ankle and neck.

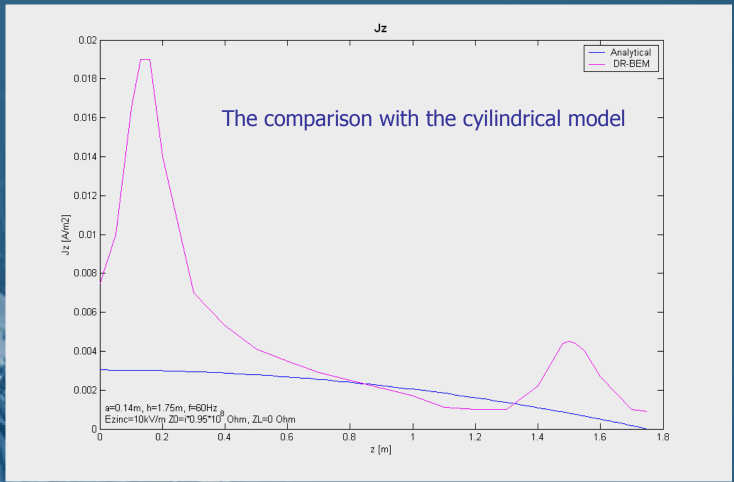

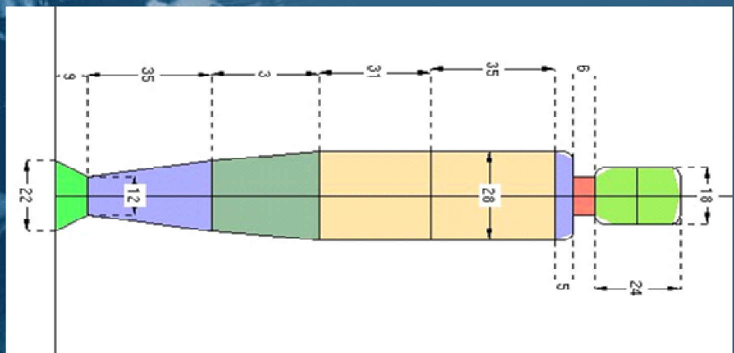

Comparison between the BEM, FEM and experimental results for the current density at various body portions, expressed in [mA/m²]

Part of the body	BEM	FEM	Experimental
Neck	4.52	4.62	4.66
Pelvis	2.32	2.27	2.25
Ankle	18.91	19.16	18.66

The calculated results via BEM agree well with FEM and experimental results.

*The main difference is in the area of ankles and neck. The peak values of **J** in those parts maintain the continuity of the axial current throughout the body.*

Exposure scenario	Current density $J [mA/m^2]$
ICNIRP guidelines for occupational exposure	10
ICNIRP guidelines for general public exposure	2
J_{zmax} (cylinder on earth)	3
J_{zmax} (body of revolution model)	19

Department of Electronics
University of Split,
Split, Croatia

Human Exposure to Electromagnetic Fields

Computational Examples (cont'd): Exposure to power lines

The realistic models of the human body

The electric field in the air begins to *sense* the presence of the grounded body at around 5m above ground level.

BEM with domain decomposition and triangular elements (40 000) is used.

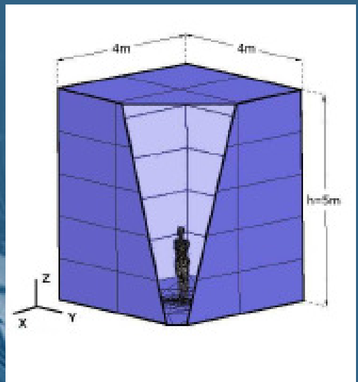

A plan view of the integration domain

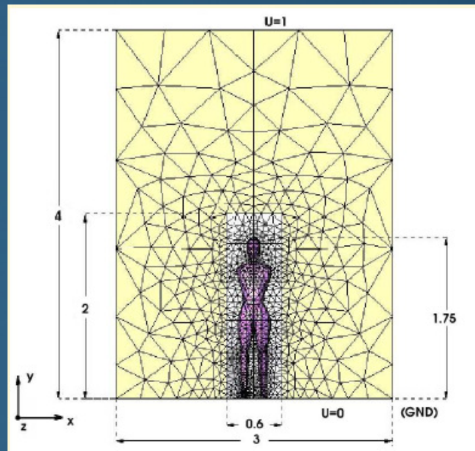

3D mesh: Linear Triangular Elements

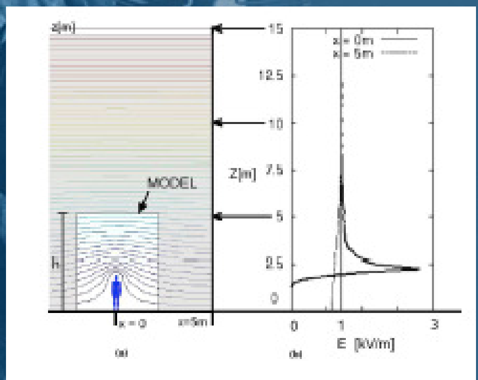

Electric field in the air near the body

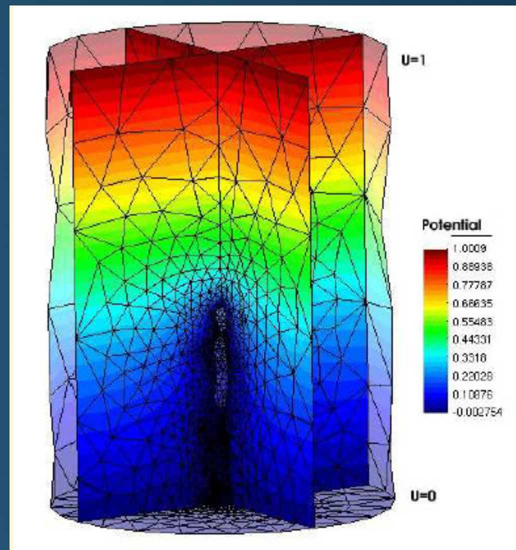

Scaled potential lines in air

Department of Electronics
University of Split,
Split, Croatia

Human Exposure to Electromagnetic Fields

Computational Examples (cont'd): Exposure to power lines

Front and side view of equipotential lines in air are presented.

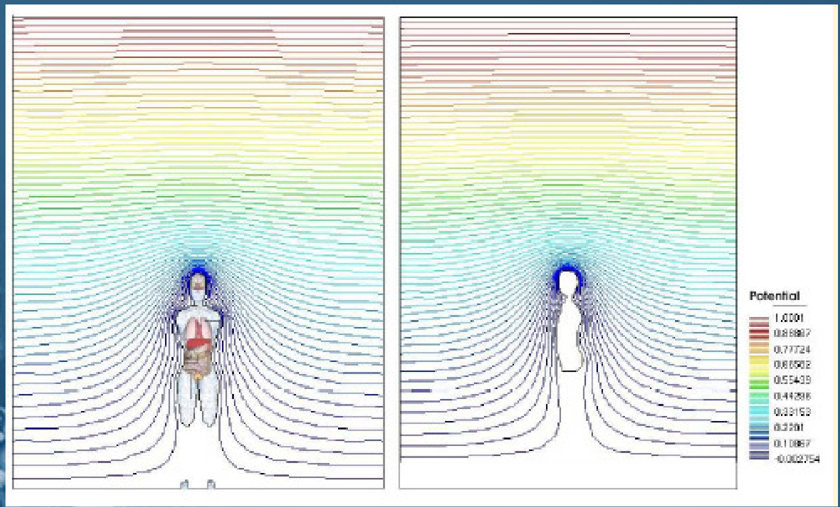

Scaled Equipotential lines in air

The presence of peaks in current density values corresponds to the position of the ankle and the neck.

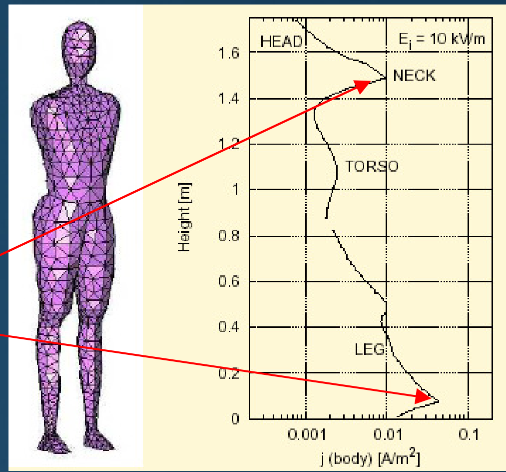

An oversimplified cylindrical representation of the body is unable to capture the current density peaks in the regions with narrow cross section.

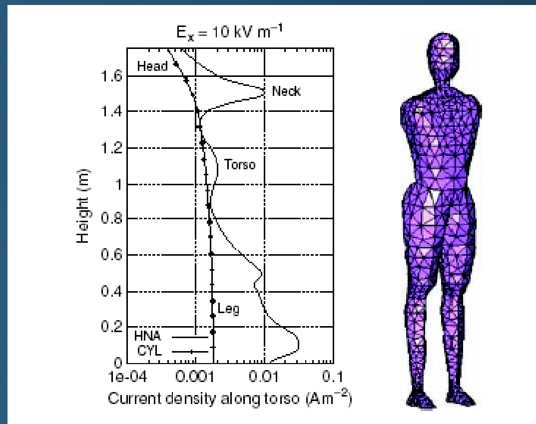

Figure 1 Axial current density induced in the cylindrical and anatomical body model exposed to ELF external electric field ($E = 10\,\mathrm{kV\,m^{-1}}$, $f = 60$ kHz).

Department of Electronics
University of Split,
Split, Croatia

Human Exposure to Electromagnetic Fields

Computational Examples (cont'd): Exposure to power lines

The mesh and scalar potential for the body model with arms up is presented.

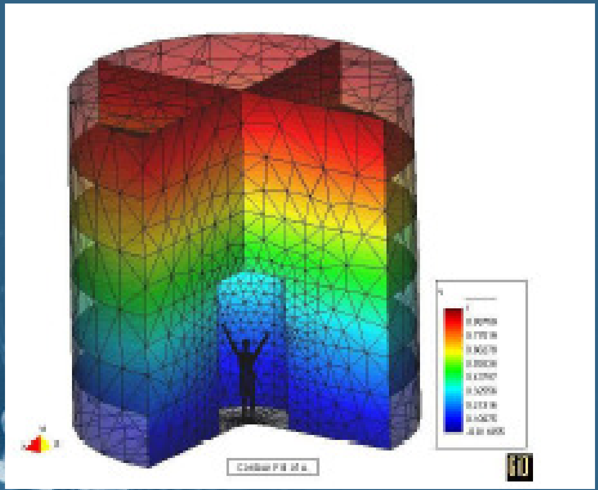

3D mesh: the realistic model of the body with arms up

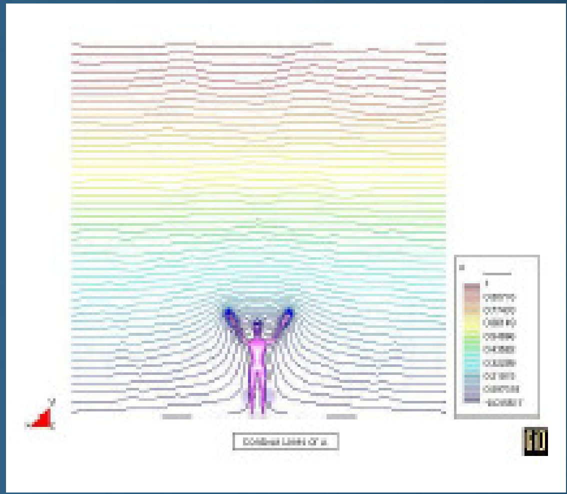

Scalar potential in the vicinity of the body

Front and lateral view of equipotential surfaces for the HAU model exposed to a reference incident field *Ez* = 0.25 *V/m.*

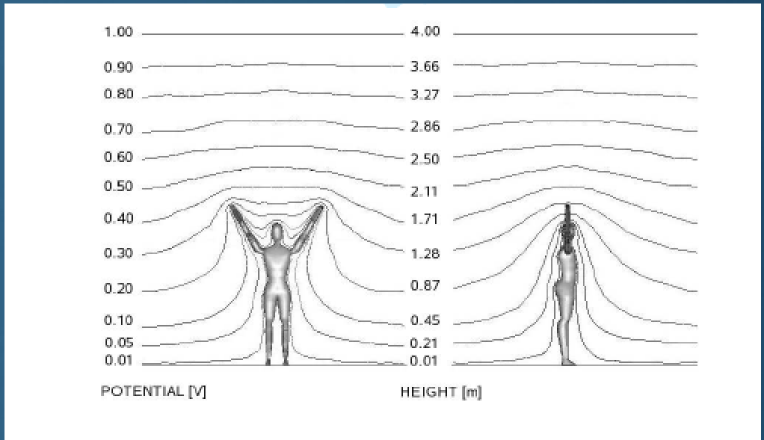

The numbers on the left indicate voltage, while the numbers on the right indicate height of the equipotentials taken at 2.5m away from the subject, i.e. when equipotential surface become parallel to the ground.

Department of Electronics
University of Split,
Split, Croatia

Human Exposure to Electromagnetic Fields

Computational Examples (cont'd):Exposure to power lines

Distribution of axial current density along the torso and head in function of the height for the HAU, HAO, HAD and HNA models. The observation line corresponds to the line connecting points A and B.

The bigger cross-sectional area acts as a natural protection to the heart, while the raised arms protect the neck.

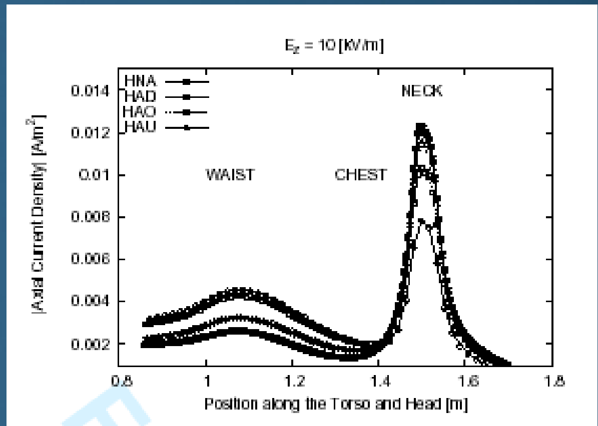

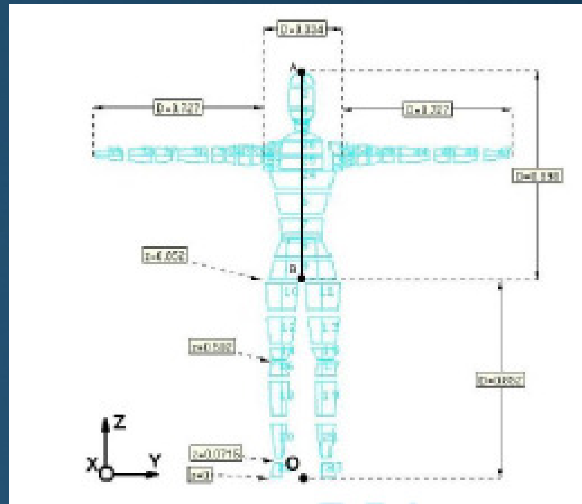

The observation line corresponds to the line connecting points A and B.

Absolute value for the axial current density along the arms in function of the HAU, HAO and HAD models.

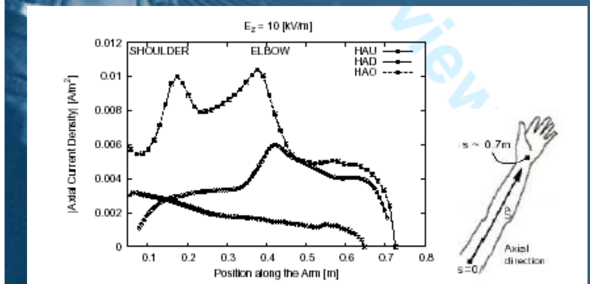

Maximal values of current density are reached by the HAO model, in accordance to the larger area exposed to the normal field.

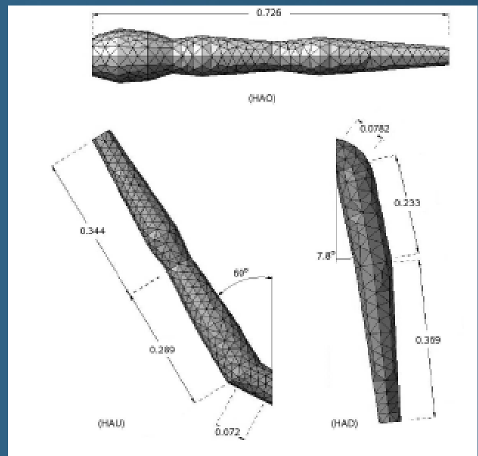

Geometry of the arms in HAU, HAO and HAD models.

Department of Electronics
University of Split,
Split, Croatia

Human Exposure to Electromagnetic Fields

Computational Examples (cont'd):Exposure to power lines

Axial current density along the legs for the HNA, HAU, HAO and HAD

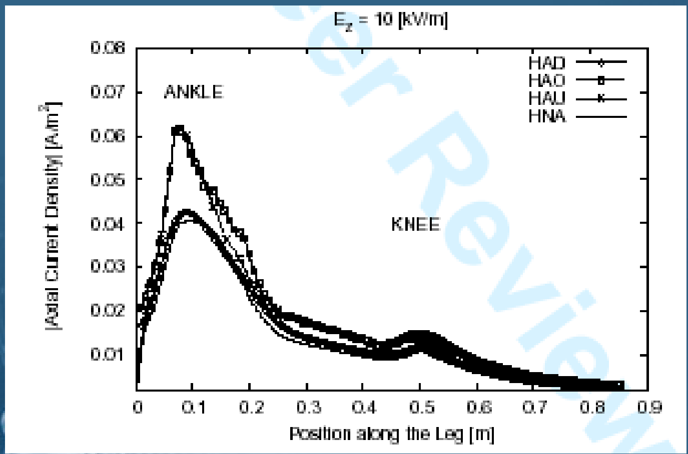

The maximum values the current density at the height of the ankle are obtained for the HAU and HAO models.

Induced current density for the various body models

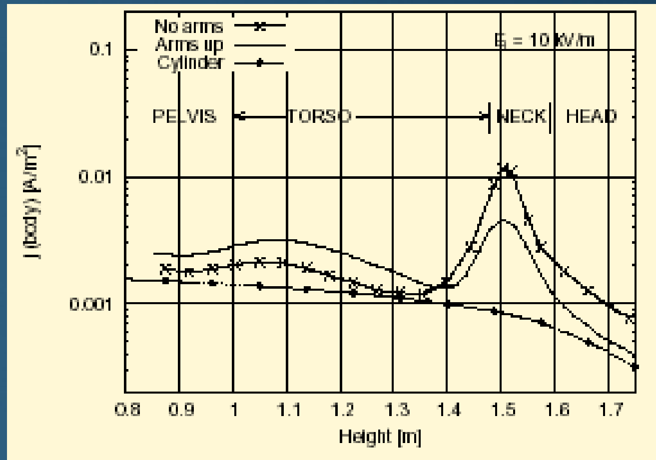

Comparison between the following body models is presented:

- No arms
- Arms up (60° from horizontal plane)
- Cylinder

Peak values of the J_z versus E

ICNIRP Safety Standards	J[mA/m²]
Occupational exposure	10
General public exposure	2

Exposure limits for J_z

E [kV/m]	J_z[mA/m²]
1	2
5	10
10	19

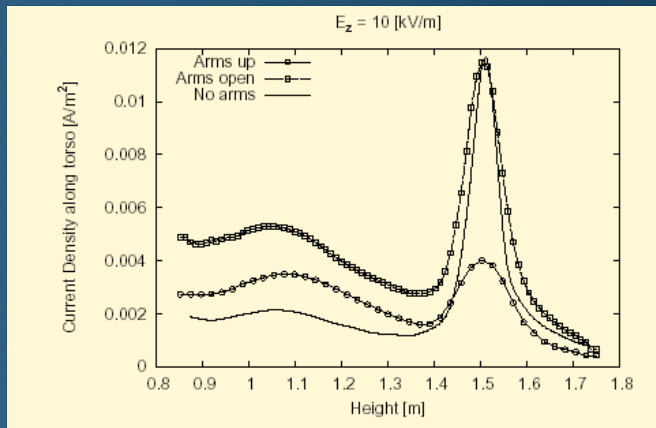

Comparison between the following body models is presented:

- No arms
- Arms up (60° from horizontal plane)
- Open arms

Peak values of the current density in the ankle for some typical values of electric field near ground under power lines are presented in the table.

UNIVERSITÉ Clermont Auvergne

Department of Electronics
University of Split,
Split, Croatia

Human Exposure to Electromagnetic Fields

Computational Examples (cont'd): Exposure to power lines

Variations of conductivity in the heterogeneous representation

Tissue conductivities in S/m at 60 Hz

Tissue	SETA	σ_t/σ_m	SETG	σ_t/σ_m	SETD
Embedding tissue	0.50	1.00	0.22	1.00	0.44
Heart	0.11	0.22	0.08	0.36	0.16
Brain	0.12	0.24	0.04	0.18	0.08
Eye	0.11	0.22	1.0	4.55	2.0
Liver	0.13	0.26	0.07	0.32	0.14
Intestine	0.16	0.32	1.15	5.27	2.30

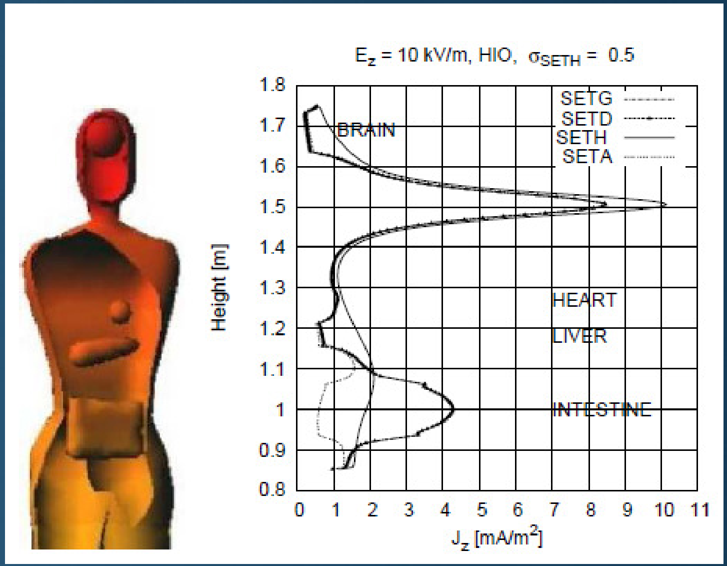

Axial current density along the centre of with different sets of conductivities

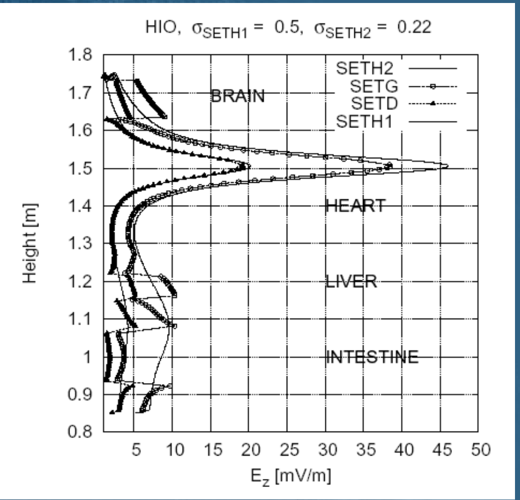

E- field along the centre of the torso and head for the HIO model for SETG and SETD conductivity scenarios

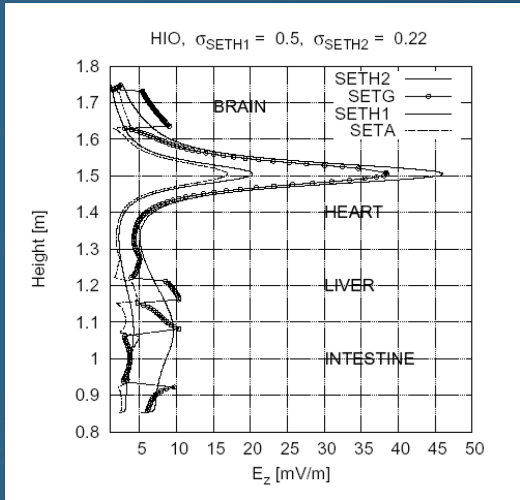

E- field along the centre of the torso and head for the HIO model for SETG and SETA conductivity scenarios

Note on numerical results

•Due to the variation in the conductivity there is a significant variation in the induced *E*-field while the variations of the current density are negligible.

Department of Electronics
University of Split,
Split, Croatia

Human Exposure to Electromagnetic Fields

Computational Examples (cont'd): Pregnant woman Exposure...

BEM model and exposure results (left).
Observation line along the spine of the foetus

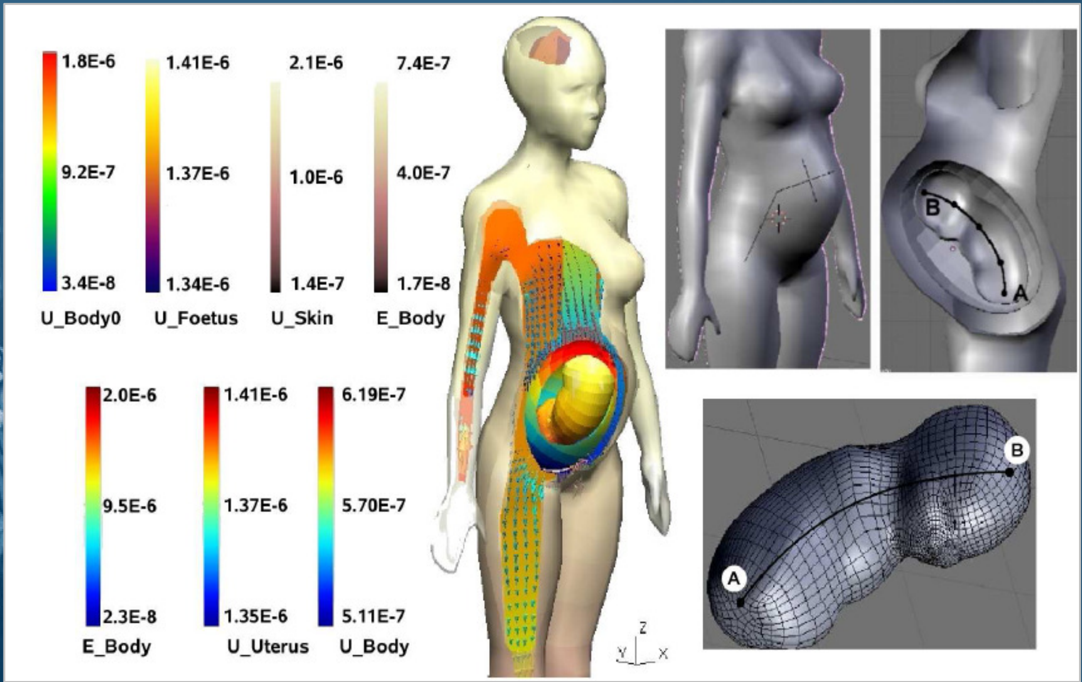

Conductivity Scenarios

Scenario	[S/m]	Week 8	Week 13	Week 26	Week 38
	σ_f	0.23	0.23	0.23	0.23
1	σ_{AF}	1.28	1.28	1.27	1.10
	σ_m	0.20	0.20	0.20	0.20
	σ_f	0.996	0.996	0.574	0.574
2	σ_{AF}	1.70	1.70	1.64	1.64
	σ_m	0.52	0.52	0.52	0.52
	σ_f	0.732	0.732	0.396	0.396
3	σ_{AF}	1.70	1.70	1.64	1.64
	σ_m	0.17	0.17	0.17	0.17

UNIVERSITÉ Clermont Auvergne

Department of Electronics
University of Split,
Split, Croatia

Human Exposure to Electromagnetic Fields

UNIVERSITÉ Clermont Auvergne

Computational Examples (cont'd): Pregnant woman Exposure...

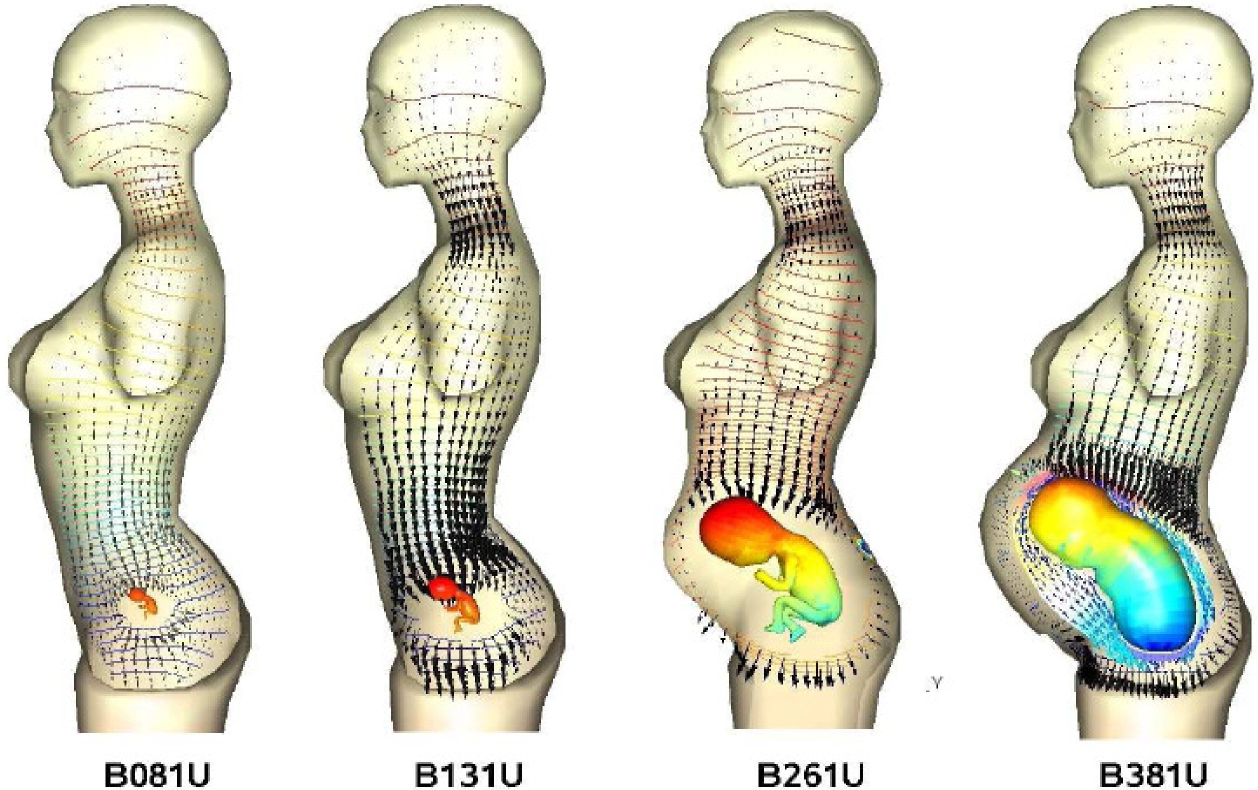

E- field and scalar potential Lateral view at 8,13, 26 and 38 gestational weeks

The uterus, due to its higher conductivity comparing to the maternal tissue, tends to concentrate the field lines.

Department of Electronics
University of Split,
Split, Croatia

Human Exposure to Electromagnetic Fields

Dosimetry: HF Exposures

- The key point in HF bioelectromagnetics is how much EM energy is absorbed by a biological body and where it is deposited.

- The basic dosimetric quantity for HF fields is the specific absorption rate (SAR) being defined as the rate of energy *W* absorbed by or dissipated in a unit mass of the body:

$$SAR = \frac{dP}{dm} = \frac{d}{dm}\frac{dW}{dt} = C\frac{dT}{dt}$$

expressed in watts per kilogram of tissue, [W/kg], where *C* is the specific heat capacity of tissue, *T* is the temperature and *t* denotes time.

- In tissue, *SAR* is proportional to the square of the internal electric field strength:

$$SAR = \frac{dP}{dm} = \frac{dP}{\rho dV} = \frac{\sigma}{\rho}|E|^2$$

where *E* is the root-mean-square value of the electric field, ρ is the tissue density and σ is the tissue conductivity.

- The localized SAR is directly related to the internal field and the main task of dosimetry involves the assessment of the electric field distribution inside the biological body.

Department of Electronics
University of Split,
Split, Croatia

Human Exposure to Electromagnetic Fields

Dosimetry: HF Exposures

Electromagnetic scattering problem – Solution method

Hybrid Element Method (HEM - BEM/FEM)

Advantages of HEM

- HEM combines the symmetric matrix generated by FEM with the accuracy provided by BIE formulations.
- Efficiently terminates the computational domain.
- Material properties can vary arbitrarily within the computational domain.
- Manipulating the Maxwell equations the time-harmonic EM fields can be expressed as follows:

$$\nabla\times\left(\frac{1}{\omega\mu}\nabla\times\vec{E}\right)+\left(j\sigma-\omega\varepsilon\right)\vec{E}=0$$

$$\nabla\times\left(\frac{1}{\sigma+j\omega\varepsilon}\nabla\times\vec{H}\right)+j\omega\mu\vec{H}=0$$

Department of Electronics
University of Split,
Split, Croatia

Human Exposure to Electromagnetic Fields

Dosimetry: HF Exposures

Boundary Integral Equations for EM fields

Applying the 2nd Green Theorem yields the integral representations of the *E* and *H* fields:

$$E_z(\vec{r}) = E_z^{inc}(\vec{r}) + \oiint_{S'} \left[E_z \frac{\partial G(\vec{r},\vec{r}')}{\partial n} - G(\vec{r},\vec{r}') \frac{\partial E_z}{\partial n} \right] dS'$$

$$H_z(\vec{r}) = H_z^{inc}(\vec{r}) + \oiint_{S'} \left[H_z \frac{\partial G(\vec{r},\vec{r}')}{\partial n} - G(\vec{r},\vec{r}') \frac{\partial H_z}{\partial n} \right] dS'$$

FEM formulation

Applying the Green theorems to FEM governing equations and featuring the weak formulation of the problem for 2D it follows:

$$\iint_{\Omega} \left[\frac{1}{\omega\mu} \nabla E_z \cdot \nabla W_i + \left(j\sigma - \omega\varepsilon \right) E_z W_i \right] d\Omega = \int_{\Gamma} \frac{1}{\omega\mu} W_i \frac{\partial E_z}{\partial n} d\Gamma$$

$$\iint_{\Omega} \left[\frac{1}{\sigma + j\omega\varepsilon} \nabla H_z \cdot \nabla W_i + j\omega\mu H_z W_i \right] d\Omega = \int_{\Gamma} \frac{1}{\sigma + j\omega\varepsilon} W_i \frac{\partial H_z}{\partial n} d\Gamma$$

Department of Electronics
University of Split,
Split, Croatia

Human Exposure to Electromagnetic Fields

Dosimetry: Thermal response

- The principal biological effect of HF exposure is heating of the tissue.

- Therefore, to quantify hazardous EM field levels thermal response of a human exposed to the HF radiation is also considered.

- The bio-transfer equation expresses the energy balance between conductive heat transfer in a volume control of tissue, heat loss due to perfusion effect, metabolism and energy absorption due to radiation.

- The stationary bio-heat transfer equation is given by:

$$\nabla(\lambda \nabla T) + W_b C_{pb}(T_a - T) + Q_m + Q_{EM} = 0$$

thermal conductivity

tissue temperature

the volumetric perfusion rate

the specific heat of blood

the arterial temperature

the power produced by metabolic process

the electromagnetic power deposition

UNIVERSITÉ Clermont Auvergne

Department of Electronics
University of Split,
Split, Croatia

Human Exposure to Electromagnetic Fields

Dosimetry: Thermal response

The electromagnetic power deposition Q_{EM} is a source term deduced from the electromagnetic modelling, and determined by relation:

$$Q_{EM} = \rho \cdot SAR$$

The inhomogeneous Helmholtz-type equation is given by:

$$\nabla(\lambda \nabla T) - W_b C_{pb} T = -(W_b C_{pb} T_a + Q_m + Q_{EM})$$

The boundary condition for the bio-heat transfer equation, imposed to the interface between skin and air, is given by:

$$q = H\left(T_s - T_a\right)$$

where q denotes the heat flux defined as:

$$q = -\lambda \frac{\partial T}{\partial n}$$

while H, T_s and T_a denote, respectively, the convection coefficient, the temperature of the skin, and the temperature of the air.

UNIVERSITÉ Clermont Auvergne

Department of Electronics
University of Split,
Split, Croatia

Human Exposure to Electromagnetic Fields

Dosimetry: Thermal response

The Bio-heat Transfer Equation: The solution by FEM

Applying the FEM solution the bio-heat transfer equation one obtains the following matrix equation:

$$[K]\{T\}=\{M\}+\{P\}$$

The matrix system elements are:

$$K_{ji}=\int_{\Omega_e}\nabla f_j(\lambda\nabla f_i)d\Omega_e+\int_{\Omega_e}W_b C_{pb} f_j f_i d\Omega_e$$

$$M_j=\int_{\Gamma_e}\lambda\frac{\partial T}{\partial n}f_j d\Omega_e$$

$$p_{ji}=\int_{\Omega_e}(W_b C_{pb} T_a+Q_m+Q_{EM})f_j d\Omega_e$$

Department of Electronics
University of Split,
Split, Croatia

Human Exposure to Electromagnetic Fields

Dosimetry: HF Exposures

Computational examples: HF exposures

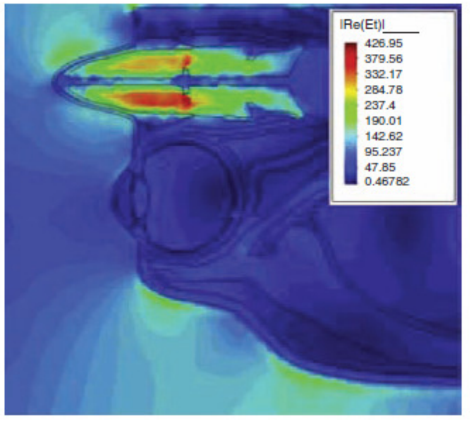

Figure 2 Electric field distribution in the upper left portion of the human head due to TM plane wave at frequency $f = 0.85$ GHz and power density $\bar{P}_d = 5.0\ \mathrm{mW\ cm^{-2}}$.

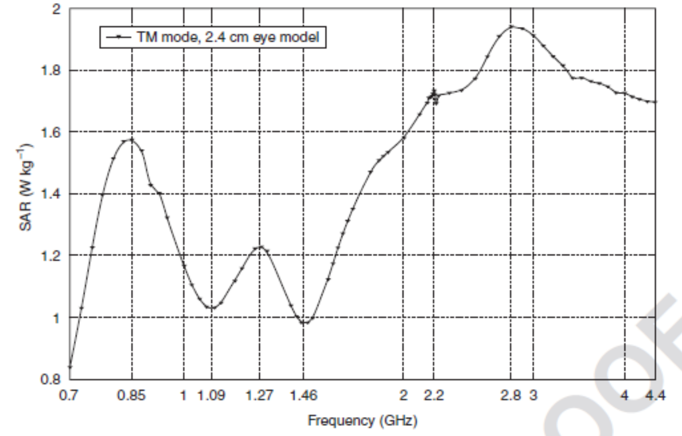

Figure 3 Logarithmic plot of whole eye averaged SAR for TM plane wave in the frequency range 0.7–4.4 GHz and power density $\bar{P}_d = 5\ \mathrm{mW\ cm^{-2}}$.

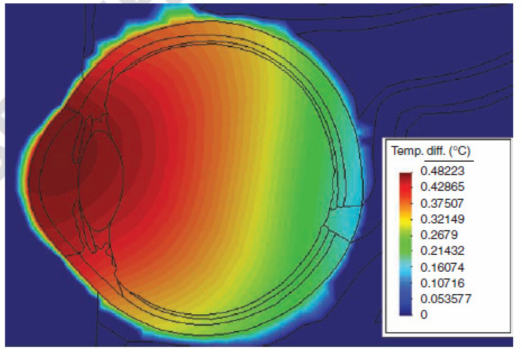

Figure 4 Temperature rise in the human eye due to a TM plane wave with frequency $f = 0.85$ GHz and power density $\bar{P}_d = 5\ \mathrm{mW\ cm^{-2}}$.

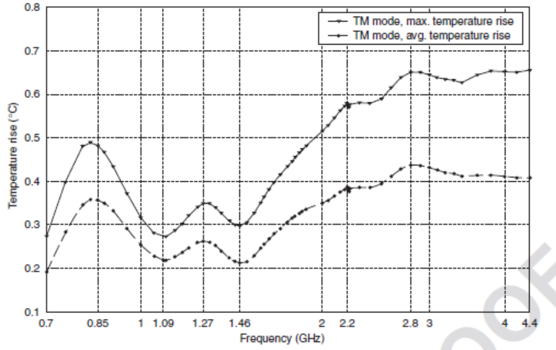

Figure 5 Logarithmic plot of average and maximum temperature rise in the human eyes due to TM plane wave in the frequency range 0.7–4.4 GHz and power density $\bar{P}_d = 5\ \mathrm{mW\ cm^{-2}}$.

Department of Electronics
University of Split,
Split, Croatia

Human Exposure to Electromagnetic Fields

Dosimetry: HF Exposures

Computational examples: HF exposures

- the results from hybrid BEM/FEM numerical computation of electric field induced by plane wave with power density of 10 W/m^2

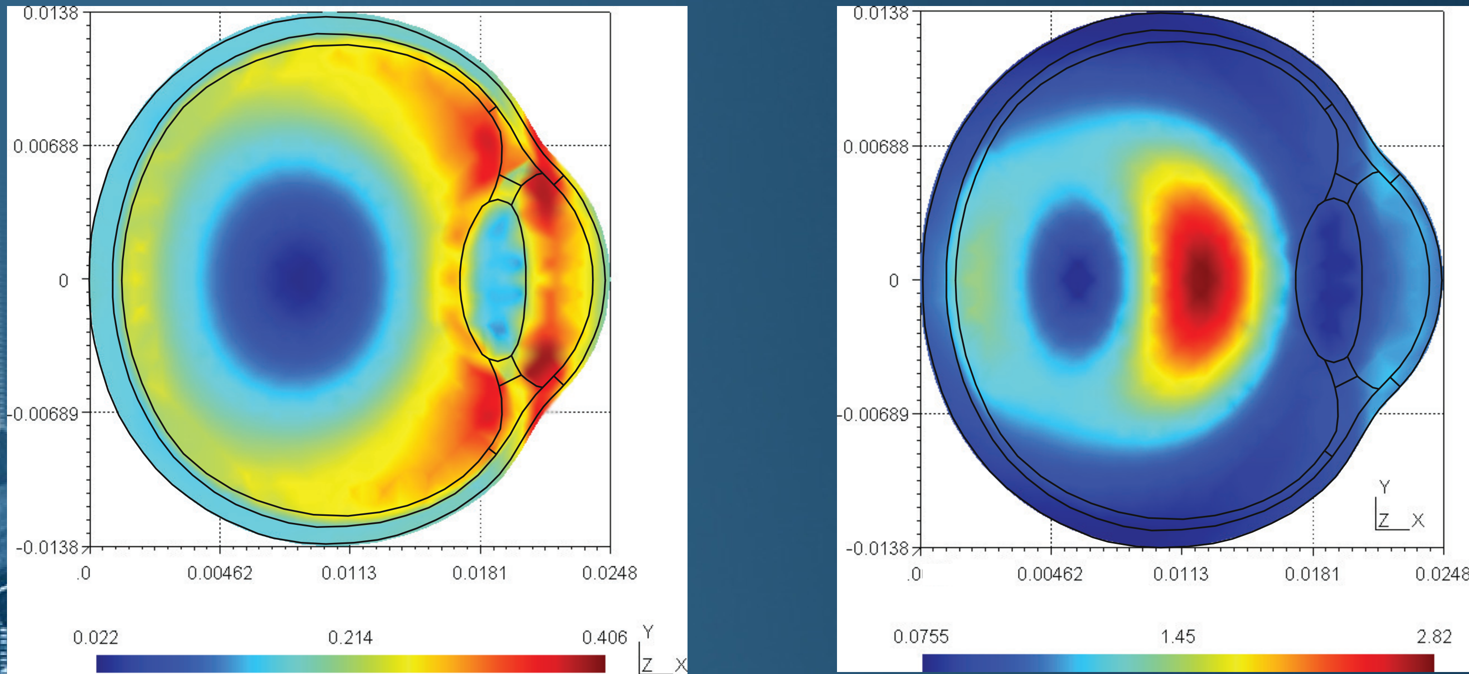

SAR in the eye due to EM wave with power density 10 W/m^2 at: (a) f=1 GHz (b) f=2 GHz.

Department of Electronics
University of Split,
Split, Croatia

Human Exposure to Electromagnetic Fields

Dosimetry: HF Exposures

Computational examples: HF exposures

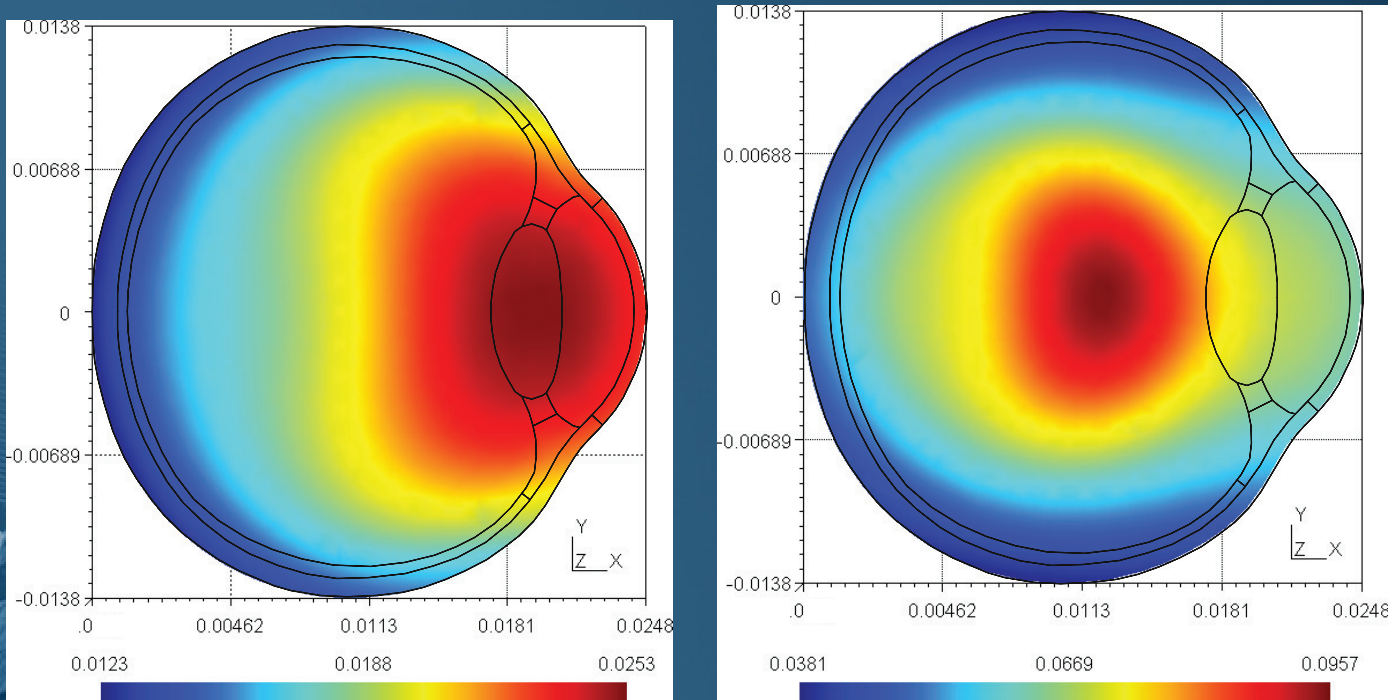

Temperature rise in the eye due to EM wave with power density 10 W/m^2 at (a) f=1 GHz (b) f=2 GHz.

Department of Electronics
University of Split,
Split, Croatia

Human Exposure to Electromagnetic Fields

Dosimetry: Human Exposure to Transient Radiation

Laser Source Modelling

- Laser energy $H(r, z, t)$, absorbed by the eye tissue at the n^{th} node with cylindrical coordinates (r,z), is given by a product:

$$H(r,z,t) = \alpha I(r,z,t) \qquad (5)$$

- where:
- α - is the wavelength dependent absorption coefficient of the specific tissue
- I - is the irradiance of the n^{th} node, given by:

$$I(r,z,t) = I_0 \exp\left(-\frac{2r^2}{w^2} - \alpha z\right) \exp\left(-\frac{8t^2}{\tau^2}\right) \qquad (6)$$

- where:
- I_0 - is the incident value of intensity
- w - is the beam waist
- τ - is the pulse duration

Heat transfer

- The mathematical model is based on the Pennes' bioheat transfer equation
- In Pennes' model, the rate of tissue temperature increase is given by the sum of the net heat conduction into the tissue, metabolic heat generation, and the heating (cooling) effects due to arterial blood flow:

$$\rho C \frac{\partial T}{\partial t} = \nabla(k \nabla T) + W_b C_{pb}(T_a - T) + Q_m + H \qquad (1)$$

- Bioheat equation is extended with the new term H representing heat generated inside the tissue due to laser radiation

- Bioheat equation is supplemented with natural boundary condition equations for cornea, sclera and domain inside the eye, respectively:

$$-k\frac{\partial T}{\partial n} = h_c(T - T_{amb}) + \sigma\epsilon(T^4 - T_{amb}^4) \in \Gamma_1 \qquad (2)$$

$$-k\frac{\partial T}{\partial n} = h_s(T - T_a) \in \Gamma_2 \qquad (3)$$

$$-k\frac{\partial T}{\partial n} = 0 \in \Gamma_3 \qquad (4)$$

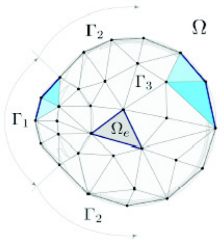

- where:
- k - specific tissue thermal conductivity
- h_c - heat transfer coefficient of cornea
- h_s - heat transfer coefficient of sclera
- σ - Stefan–Boltzmann constant
- ε - emissivity of the corneal surface
- T_{amb} - temperature of the ambient air anterior to the cornea
- T_a - arterial blood temperature taken to be 36.7°C

- Second term on the right handside of Eq. (2) is approximated by $\sigma\varepsilon T^3{}_F (T - T_{amb})$

Numerical Method

- The equation (1) is discretized in two spatial dimensions and solved using the weak formulation and the Galerkin–Bubnov procedure
- A total number of *21,595* triangular elements and *11,094* nodes were generated using the GID 7.2 mesh generator
- Solving part was done by algorithm written in MATLAB
- The equation is first solved for the steady-state case, i.e. when no external sources are present
- Latter, these results are used as initial conditions in the time domain analysis with included external source, i.e. laser radiation

$$\lambda^e [A]\{T^i\}^e + (W_b^e c_b^e + \frac{\rho^e c^e}{\Delta t})[B]\{T^i\}^e + \left\{ \begin{array}{rl} (h_c + \sigma\epsilon T_F^3)[C_1]\{T_b^i\}^e & \in \Gamma_1 \\ h_s [C_2]\{T_b^i\}^e & \in \Gamma_2 \end{array} \right\} =$$

$$= (W_b^e c_b^e T_a + Q_m^e + H^e)\{D\} + \left\{ \begin{array}{rl} (h_c T_{amb} + \sigma\epsilon T_F^3 T_{amb})\{F_b\} & \in \Gamma_1 \\ h_s T_a \{F_b\} & \in \Gamma_2 \end{array} \right\} + \frac{\rho^e c^e}{\Delta t}[B]\{T^{i-1}\}^e$$

- Finite element formulation of the equation including the boundary conditions.

Université Clermont Auvergne

Clermont-Ferrand, 03 April 2018

Department of Electronics
University of Split,
Split, Croatia

Human Exposure to Electromagnetic Fields

Dosimetry: Human Exposure to Transient Radiation

Results (2090 nm Ho:YAG laser)

- Maximum temperature of 69.424°C, is obtained on cornea-aqueous boundary, as shown on Fig. 6.

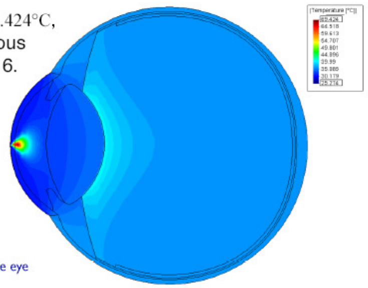

Figure 6: Temperature distribution in the eye

- Used in contactless thermal keratoplasty (cornea).

Results (193 nm ArF laser, 2nd setup)

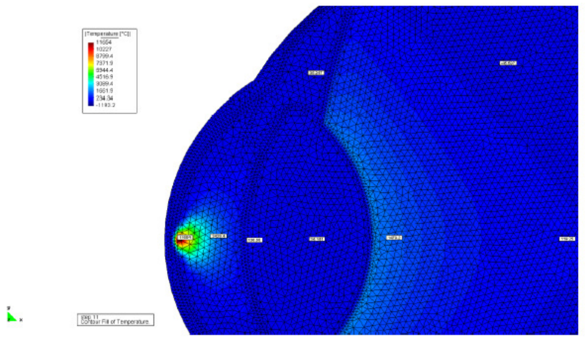

Figure 8: Detail of temperature distribution around anterior part of the eye, due to 15 ns pulse of 193 nm ArF excimer laser

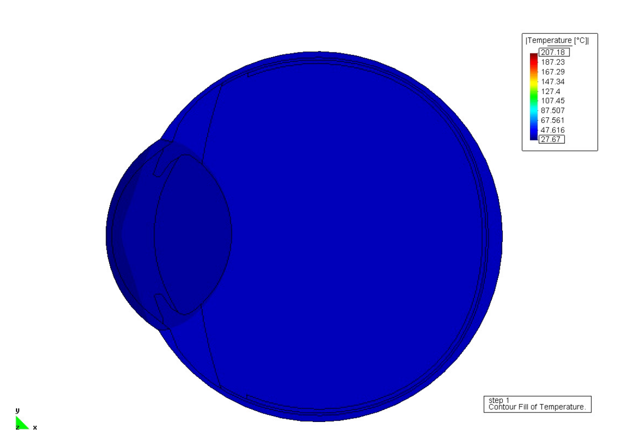

Results (1053 nm Nd:YLF laser)

- Versatile laser, alongside thermal effects, can evoke the plasma-induced ablation and photodisruption

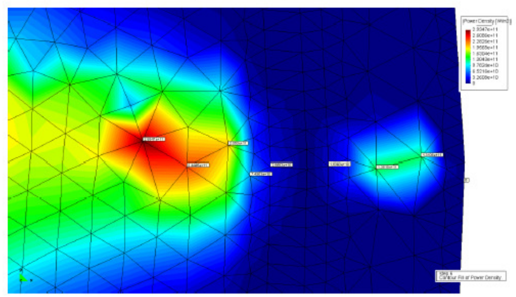

Figure 9: Detail of power density distribution around posterior part of the eye

Department of Electronics
University of Split,
Split, Croatia

Integral methods in HF dosimetry and biomedical applications: Ongoing work

Set of coupled surface integral equations (SIE) - solution via Method of Moments (MoM)

- Fig shows the *SAR* distribution in the brain at *f*=900MHz due to the vertically polarized incident plane wave (P = 5mW/cm^2).
- The brain electrical parameters are: ε r=46, σ =0.8S/m.
- The obtained numerical results for peak and average SAR:

*SAR*max=0.866W/kg,
*SAR*avg=0.158W/kg.

(9)

(13)

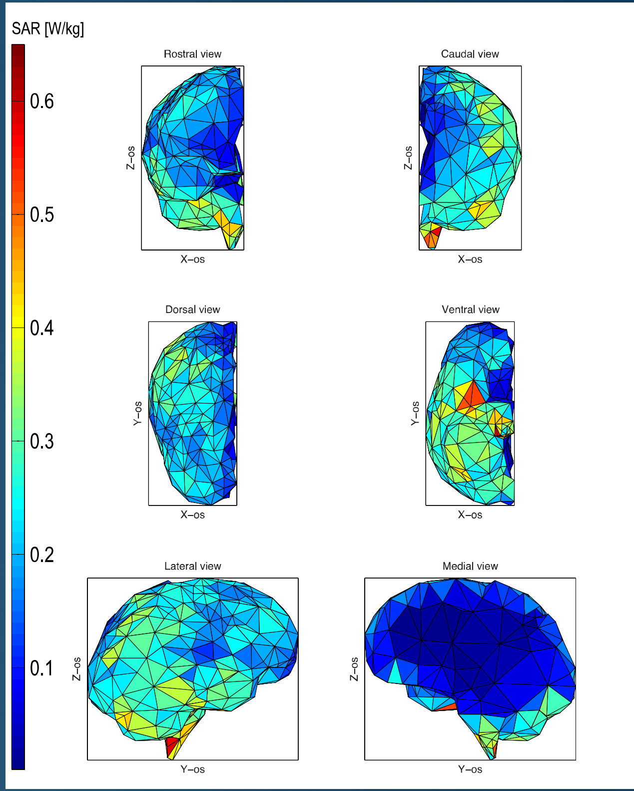

SAR distribution at f=900MHz

Department of Electronics
University of Split,
Split, Croatia

Human Exposure to Electromagnetic Fields

HF Dosimetry: Ongoing work

ONGOING WORK...

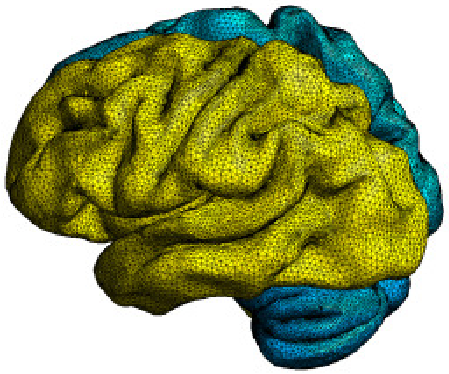

- More realistic brain geometry (sulci, gyri)

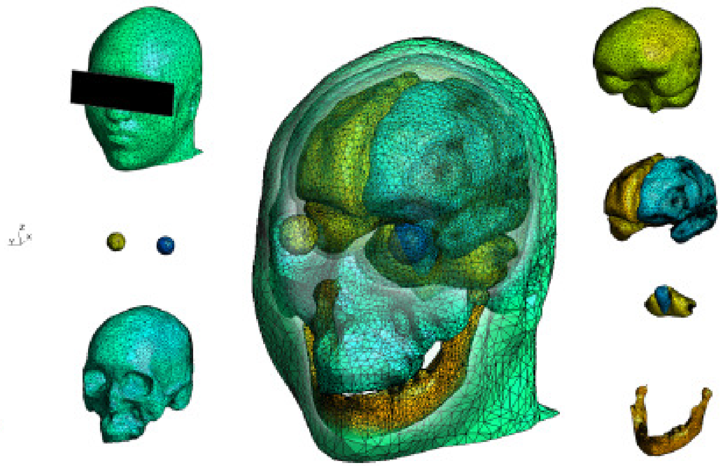

- Incorporation into more realistic simulation scenario (whole head), hybrid FEM/BEM formulation
- The model was constructed from magnetic resonance imaging (MRI) of a 24-year old male *[Laakso, Brain stimulation 8(5), pp. 906-813, 2015.]*
- Study on difference when using compound and extracted organ models (when to use single organ, when complete body) - work currently under way, eye example...

Human Exposure to EM Fields: Biomedical Applications - TMS

Department of Electronics
University of Split,
Split, Croatia

Various TMS coils, arbitrary position

	Circular	8-coil	Butterfly (10°)
Frequency	2.44 kHz	2.44 kHz	2.44 kHz
Radius	4.5 cm	3.5 cm	3.5 cm
Turns	14	15	15
Current (max)	2843 A (8kA)	2843 A (8kA)	2843 A (8kA)

Frequency dependent brain tissue params

Tissue parameters (avg. Brain) [C. Gabriel, Tech.Rep. AL/OE-TR-1996-0037]:
ϵ_r = 46940
σ = 0.08585 S/m

Development of geometrical brain model

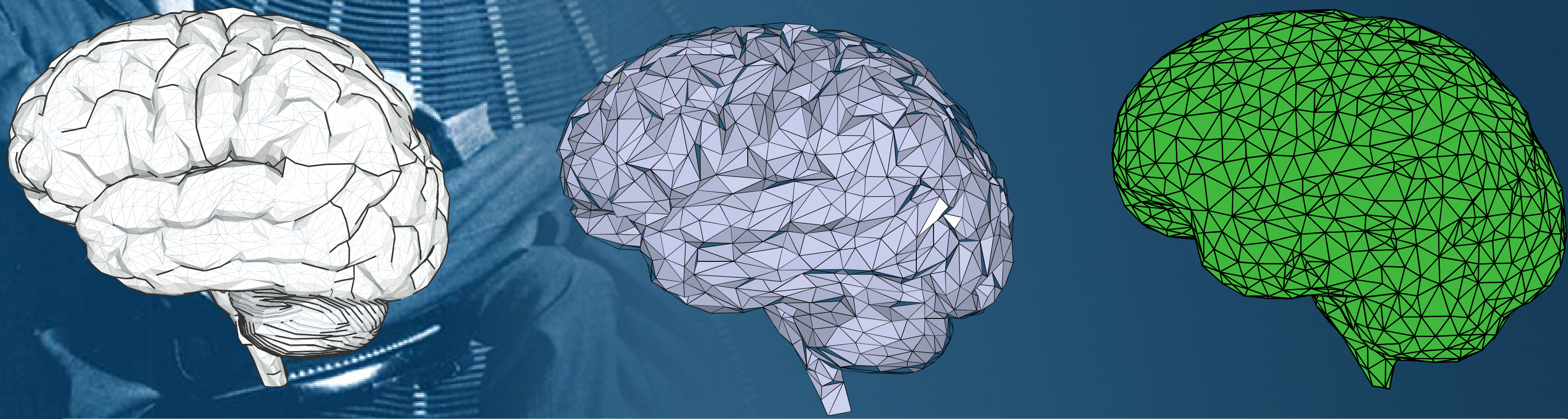

CAD model	Discretised (MeshLab)	MATLAB

Brain model dimensions (average human brain size [Blikov, Glezer 1968])

Length	167 mm
Width	140 mm
Height	93 mm

Department of Electronics
University of Split
Split, Croatia

On the Use of Boundary Element Method in Bioelectromagnetics

Transcranial Magnetic Stimulation (TMS)

FORMULATION: Equivalence theorem

- Equivalent electric and magnetic currents

$$\vec{J}_1 = \hat{n} \times \vec{H}_1 \qquad \vec{M}_1 = -\hat{n} \times \vec{E}_1$$

$$\vec{J}_2 = -\hat{n} \times \vec{H}_2 \qquad \vec{M}_2 = \hat{n} \times \vec{E}_2$$

- Relationship between scattered and incident fields

$$\left[-\vec{E}_1^{sca}(\vec{J},\vec{M})\right]_{tan} = \left[\vec{E}^{inc}\right]_{tan} \qquad \left[-\vec{E}_2^{sca}(\vec{J},\vec{M})\right]_{tan} = 0$$

$$\left[-\vec{H}_1^{sca}(\vec{J},\vec{M})\right]_{tan} = \left[\vec{H}^{inc}\right]_{tan} \qquad \left[-\vec{H}_2^{sca}(\vec{J},\vec{M})\right]_{tan} = 0$$

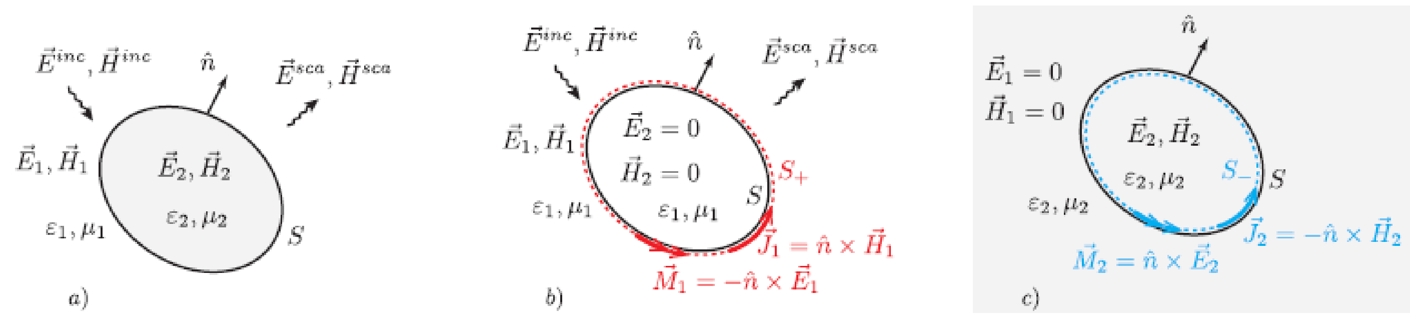

Fig. 1. Human brain as a lossy homogeneous dielectric (ε_2, μ_2) placed in the incident field ($\vec{E}^{inc}, \vec{H}^{inc}$) of a TMS coil. a) Original problem, b) Equivalent problem for region 1, c) Equivalent problem for region 2.

Department of Electronics
University of Split
Split, Croatia

On the Use of Boundary Element Method in Bioelectromagnetics

Transcranial Magnetic Stimulation (TMS)

FORMULATION: Equivalence theorem

- Scattered fields

$$\vec{E}_n^{sca}(\vec{J},\vec{M}) = -j\omega\vec{A}_n - \nabla\varphi_n - \frac{1}{\varepsilon_n}\nabla\times\vec{F}_n$$

$$\vec{H}_n^{sca}(\vec{J},\vec{M}) = -j\omega\vec{F}_n - \nabla\psi_n + \frac{1}{\mu_n}\nabla\times\vec{A}_n$$

- Green function

$$G_n(\vec{r},\vec{r}') = \frac{e^{-jk_nR}}{4\pi R};\, R = |\vec{r}-\vec{r}'|$$

- Scalar and vector potential

$$\vec{A}_n(\vec{r}) = \mu_n\int_S \vec{J}(\vec{r}')G_n(\vec{r},\vec{r}')\,\mathrm{d}S'$$

$$\vec{F}_n(\vec{r}) = \varepsilon_n\int_S \vec{M}(\vec{r}')G_n(\vec{r},\vec{r}')\,\mathrm{d}S'$$

$$\varphi_n(\vec{r}) = \frac{j}{\omega\varepsilon_n}\int_S \nabla'_S\cdot\vec{J}(\vec{r}')G_n(\vec{r},\vec{r}')\,\mathrm{d}S'$$

$$\psi_n(\vec{r}) = \frac{j}{\omega\mu_n}\int_S \nabla'_S\cdot\vec{M}(\vec{r}')G_n(\vec{r},\vec{r}')\,\mathrm{d}S'$$

- System of Electric Field Integral Equations (EFIEs)

$$\vec{E}_1^{inc} = j\omega\mu_1\int_S \vec{J}(\vec{r}')G_1(\vec{r},\vec{r}')\,\mathrm{d}S' + \\ + \frac{j}{\omega\varepsilon_1}\int_S \nabla'_S\cdot\vec{J}(\vec{r}')\nabla G_1(\vec{r},\vec{r}')\,\mathrm{d}S' + \int_S \vec{M}(\vec{r}')\times\nabla' G_1(\vec{r},\vec{r}')\,\mathrm{d}S'$$

$$0 = j\omega\mu_2\int_S \vec{J}(\vec{r}')G_2(\vec{r},\vec{r}')\,\mathrm{d}S' + \\ + \frac{j}{\omega\varepsilon_2}\int_S \nabla'_S\cdot\vec{J}(\vec{r}')\nabla G_2(\vec{r},\vec{r}')\,\mathrm{d}S' + \int_S \vec{M}(\vec{r}')\times\nabla' G_2(\vec{r},\vec{r}')\,\mathrm{d}S'$$

UNIVERSITÉ Clermont Auvergne

Department of Electronics
University of Split
Split, Croatia

On the Use of Boundary Element Method in Bioelectromagnetics

Transcranial Magnetic Stimulation (TMS)

NUMERICAL SOLUTION: Method of Moments (MoM)

- Approximate solution over the element

$$\vec{J}(\vec{r}) = \sum_{n=1}^{N} J_n \vec{f}_n(\vec{r})$$

$$\vec{M}(\vec{r}) = \sum_{n=1}^{N} M_n \vec{g}_n(\vec{r})$$

- Base functions

$$\vec{f}_n^{\pm}(\vec{r}) = \begin{cases} \dfrac{l_n}{2A_n^{\pm}} \vec{\rho}_n^{\pm} & , \vec{r} \in T_n^{\pm} \\ 0 & , \vec{r} \notin T_n^{\pm} \end{cases}$$

$$\vec{g}_n(\vec{r}) = \hat{n} \times \vec{f}_n(\vec{r})$$

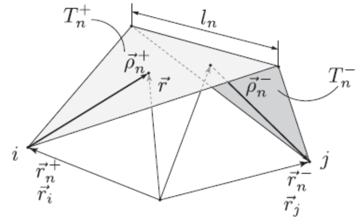

Slika 2.1: Prikaz bazne funkcije $\vec{f}_n(\vec{r})$ definirane na paru trokuta u R^3

$$\begin{bmatrix} \left[j\omega\mu_1 A_{mn,1} - \frac{j}{\omega\varepsilon_1} B_{mn,1} \right] & \left[C_{mn,1} + D_{mn,1} \right] \\ \left[j\omega\mu_2 A_{mn,2} - \frac{j}{\omega\varepsilon_2} B_{mn,2} \right] & \left[C_{mn,2} + D_{mn,2} \right] \end{bmatrix} \begin{bmatrix} J_n \\ M_n \end{bmatrix} = \begin{bmatrix} \left[V_m \right] \\ \left[0 \right] \end{bmatrix}$$

$$\begin{aligned} j\omega\mu_i \sum_{n=1}^{N} J_n \int_S \int_{S'} \vec{f}_m(\vec{r}) \cdot \vec{f}_n(\vec{r}\,') G_i(\vec{r}, \vec{r}\,') \, \mathrm{d}S' \, \mathrm{d}S + \\ + \frac{j}{\omega\varepsilon_i} \sum_{n=1}^{N} J_n \int_S \int_{S'} \vec{f}_m(\vec{r}) \cdot \nabla'_S \cdot \vec{f}_n(\vec{r}\,') \nabla G_i(\vec{r}, \vec{r}\,') \, \mathrm{d}S' \, \mathrm{d}S + \\ + \sum_{n=1}^{N} M_n \int_S \int_{S'} \vec{f}_m(\vec{r}) \cdot \left[\hat{n}' \times \vec{f}_n(\vec{r}\,') \right] \times \nabla' G_i(\vec{r}, \vec{r}\,') \, \mathrm{d}S' \, \mathrm{d}S = \\ = \begin{cases} \int \vec{f}_m(\vec{r}) \cdot \vec{E}^{inc} \, \mathrm{d}S & , i = 1 \\ 0 & , i = 2 \end{cases} \end{aligned}$$

Department of Electronics
University of Split,
Split, Croatia

On the Use of Boundary Element Method in Bioelectromagnetics

Transcranial Magnetic Stimulation (TMS)

NUMERICAL SOLUTION: Method of Moments (MoM)

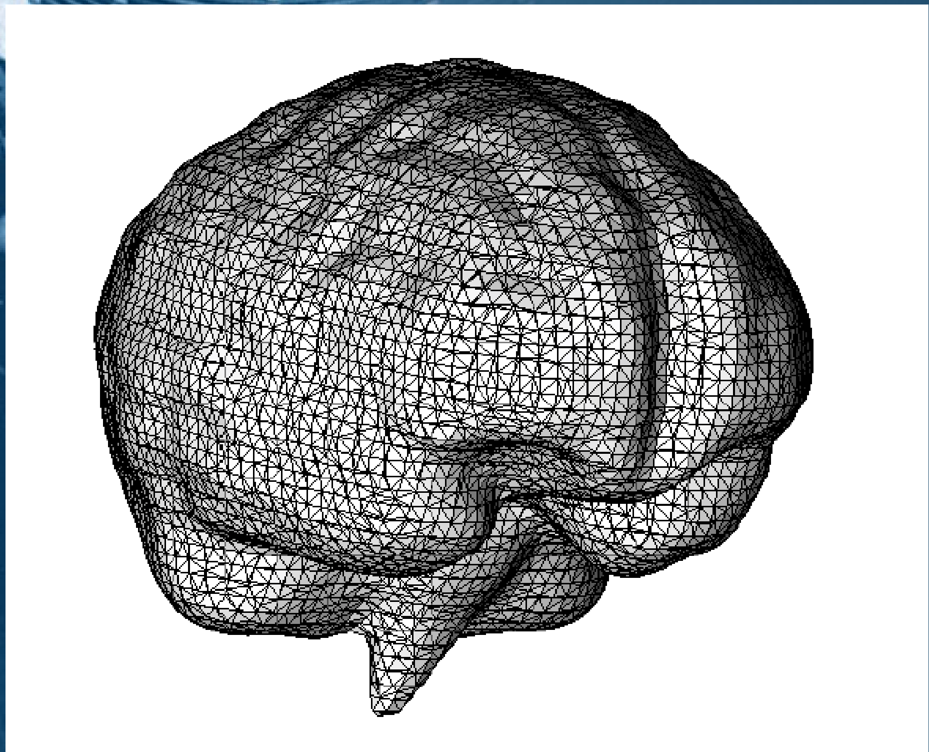

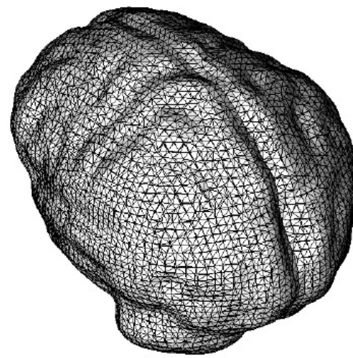

Brain model

Slika 4.2: Detaljni model mozga

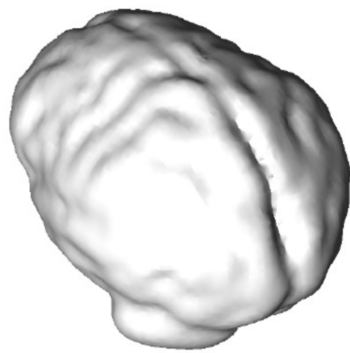

Brain model

Slika 4.3: Detaljni model mozga

Clermont-Ferrand, 03 April 2018

Human Exposure to EM Fields: Biomedical Applications - TMS

Department of Electronics
University of Split,
Split, Croatia

Electric field distribution in the model of a human brain (coil positioned 1 cm over primary motor cortex)

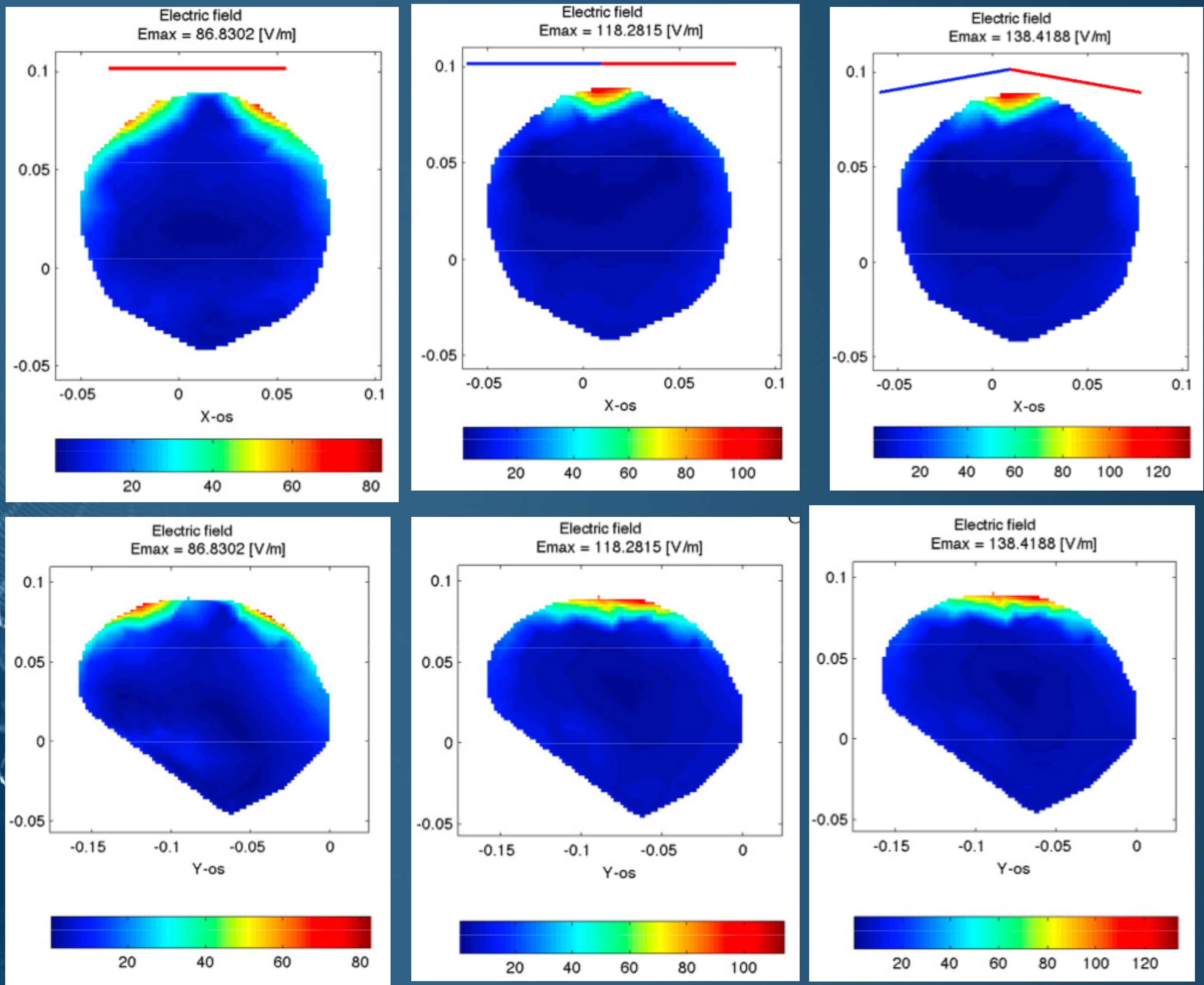

UNIVERSITÉ Clermont Auvergne

Human Exposure to EM Fields: Biomedical Applications - TMS

Department of Electronics
University of Split,
Split, Croatia

Induced electric field vector directed parallel to the surface of a brain

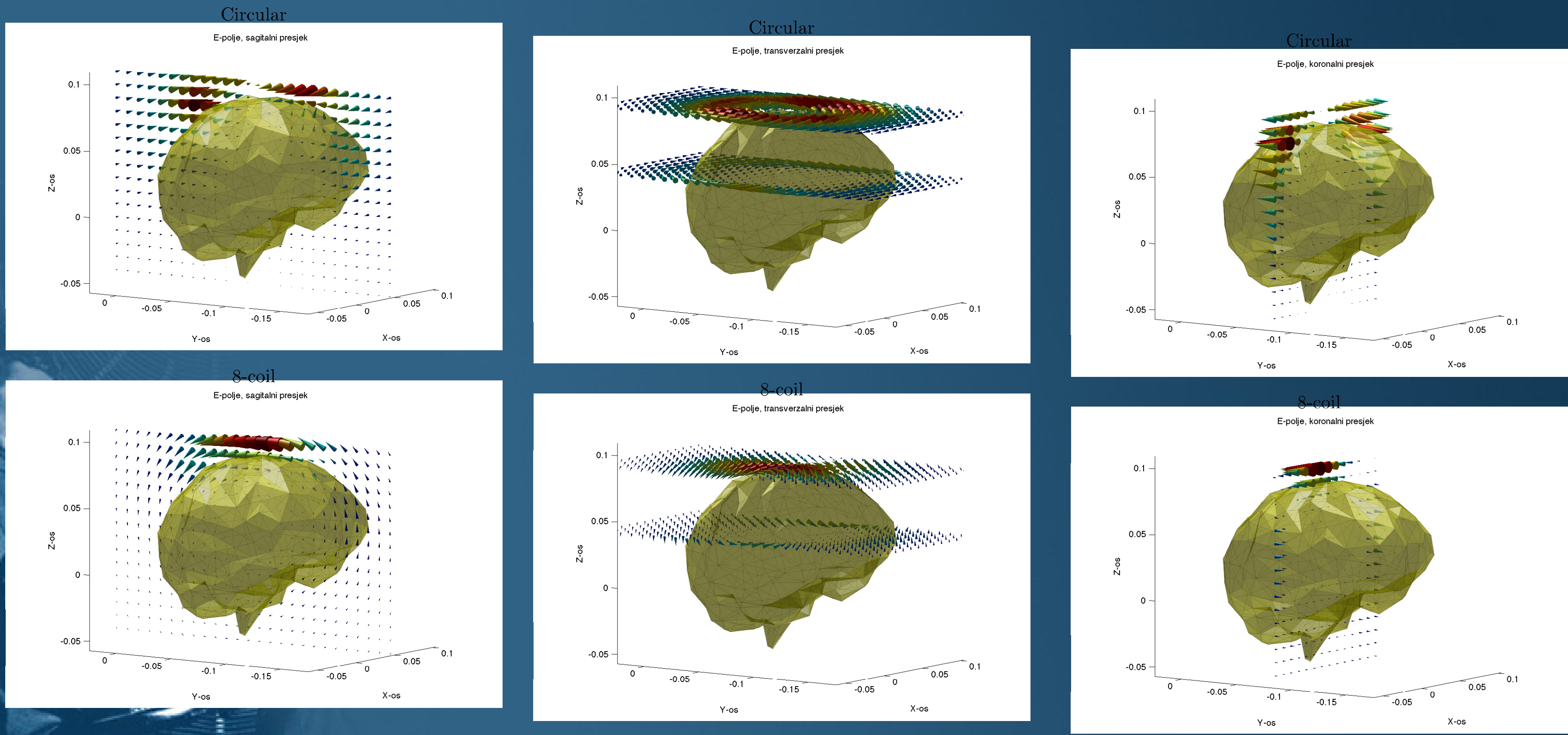

Sagittal	Transversal	Coronal

Clermont-Ferrand, 03 April 2018

Human Exposure to EM Fields: Biomedical Applications - TMS

Department of Electronics
University of Split,
Split, Croatia

An Efficient Model of Transcranial Magnetic Stimulation Based on Surface Integral Equation Formulation

Mario Cvetković, *Student Member, IEEE,* Dragan Poljak, *Senior Member, IEEE* and Jens Haueisen, *Member, IEEE*

TABLE II
COIL PARAMETERS

	Circular	8-coil	Butterfly
Frequency	2.44 kHz	2.44 kHz	2.44 kHz
Radius of turn	4.5 cm	3.5 cm	3.5 cm
No. of turns	14	15	15
Coil current	2843 A	2843 A	2843 A

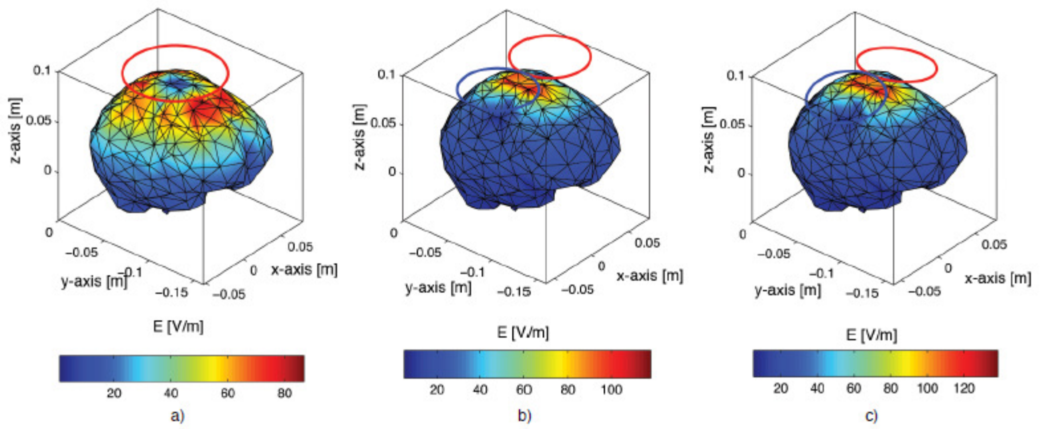

Fig. 4. Induced electric field on the brain surface due to: a) Circular coil, b) Figure-of-8 coil, and c) Butterfly coil. All coils are placed 1 cm over the primary motor cortex.

Induced E – field at the brain surface

Induced B – field at the brain surfaceJens

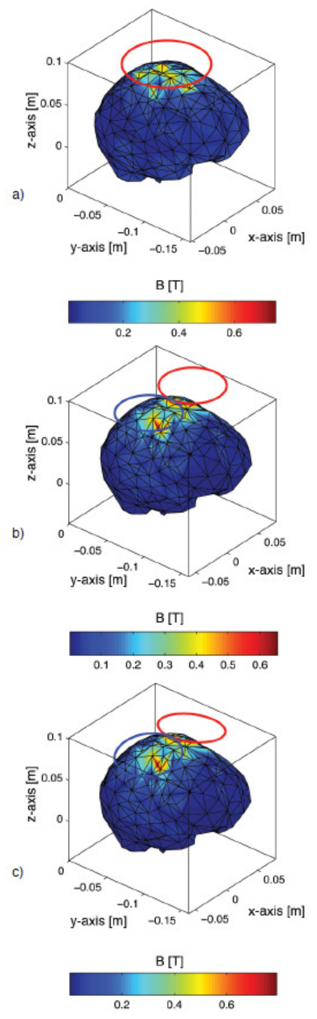

Fig. 6. Magnetic flux density on the brain surface due to: a) Circular coil, b) Figure-of-8 coil, and c) Butterfly coil. All coils are placed 1 cm over the primary motor cortex.

Department of Electronics
University of Split,
Split, Croatia

Human Exposure to EM Fields: Biomedical Applications - Modeling of nerve fiber excitation

- Fig shows the myelinated nerve fiber with an arbitrary number of Ranvier's nodes represented by a straight thin wire antenna.

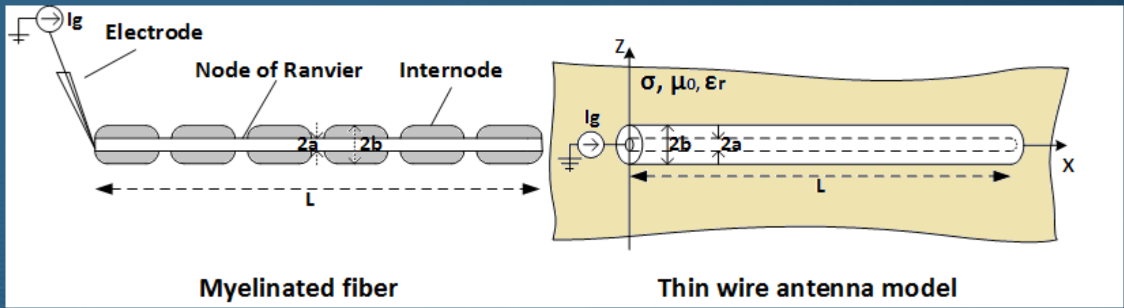

- Electrode nerve fiber stimulation is taken into account by the equivalent current source I_g located at the fiber beginning.

- The current source I_g represents the nerve fiber stimulation used in electro-acupuncture or *PENS*, which both make use of thin needles injected through the skin.

Department of Electronics
University of Split,
Split, Croatia

Human Exposure to EM Fields: Biomedical Applications - Modeling of nerve fiber excitation

Antenna Model

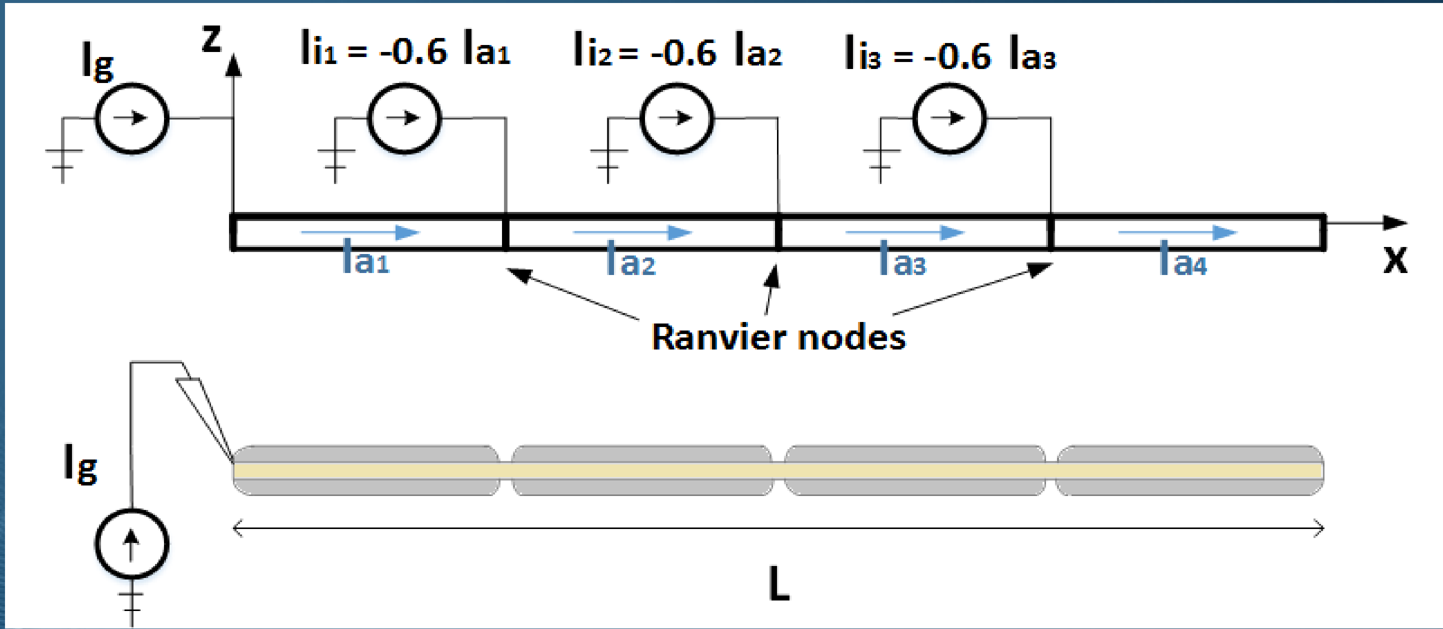

- Passive nerve fiber model
- $I_i = -0.6\ I_a$
- I_i – ionic current in non-activated Ranvier's node
- I_a - intracellular current flowing into the observed Ranvier's node

UNIVERSITÉ Clermont Auvergne

Department of Electronics
University of Split,
Split, Croatia

Mathematical Model

- *Intracellular current distribution* along a straight thin wire is governed by the FD Pocklington integro-differential equation:

$$-\frac{1}{j4\pi\omega\varepsilon_{eff}}\int_0^L\left(\frac{\partial^2}{\partial x^2}-\gamma^2\right)g(x,x')I_a(x')dx'=0$$

- g(x,x') - lossy medium Green's function: $g(x,x')=\frac{e^{-\gamma R}}{R}$
- γ - complex propagation constant: $\gamma=\sqrt{j\omega\mu\sigma-\omega^2\mu\varepsilon_0\varepsilon_r}$
- *R* - a distance from the source to the observation point: $R=\sqrt{(x-x')^2+a^2}$
- ε_{eff} - complex permittivity of a medium: $\varepsilon_{eff}=\varepsilon_0\varepsilon_r-j\frac{\sigma}{\omega}$

Department of Electronics
University of Split,
Split, Croatia

Mathematical Model

Boundary conditions at the nerve fiber ends:

$$I_a(0) = I_g,\ \ I_a(L) = 0$$

- The current generator I_g at the fiber beginning
- Sealed-end boundary condition at the fiber end

The properties of the lossy medium, nerve fiber membrane and myelin sheath are taken into account by means of the conductivity and relative permittivity which are obtained from the cable equation and TL equation:

$$\frac{\partial^2 V}{\partial x^2} - \gamma_m^2 V = 0,$$

$$\gamma_m = \sqrt{\frac{1 + j\omega\tau}{\lambda^2}}$$

$$\lambda = \sqrt{\frac{r_m a}{2\rho_a}}$$

$$\tau = r_m c_m$$

where V is the transmembrane voltage.

Department of Electronics
University of Split,
Split, Croatia

Mathematical Model

Combining previous equations yields:

$$\sigma = \frac{2\rho_a c_m}{\mu a} \qquad \varepsilon_r = \frac{2\rho_a}{a\omega^2 \mu \varepsilon_0 r_m}$$

- ***ρ a***: the resistivity of axoplasm
- ***r*m**: the myelin layer resistance for unit area
- ***c*m**: capacitance of the Ranvier's node membrane per unit area
- ***a***: the inner axon radius
- ***ω***: angular frequency

Department of Electronics
University of Split,
Split, Croatia

UNIVERSITÉ Clermont Auvergne

Numerical Solution

Homogeneous Pocklington integro-differential equation is numerically solved via **GB-IBEM**

Using the boundary element formalism, Pocklington equation is transformed into the set of linear equations:

$$\sum_{i=1}^{n}[Z]_{ji}^{e}\{\alpha\}_{i}^{e}=0,\quad j=1,2,\dots n$$

n - number of boundary elements

$[\boldsymbol{Z}]_{\boldsymbol{ji}}^{\boldsymbol{e}}$ - mutual impedance matrix representing the interaction of the observation boundary element *j* with the source boundary element *i*

$$[Z]_{ji}^{e}=-\frac{1}{j4\pi\omega\varepsilon_{eff}}\left[\int_{\Delta l_j}\int_{\Delta l_i}\{D\}_j\{D'\}_i^T g(x,x')-\gamma^2\int_{\Delta l_j}\int_{\Delta l_i}\{f\}_j\{f'\}_i^T g(x,x')dxdx'\right]$$

$\{\boldsymbol{\alpha}\}_{\boldsymbol{i}}^{\boldsymbol{e}}$ - solution vector

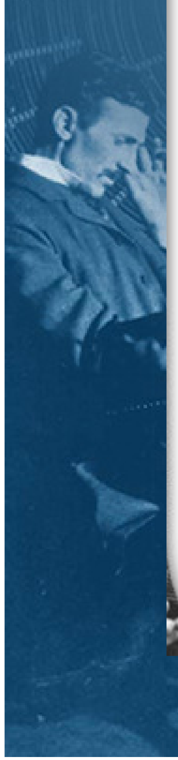

Department of Electronics
University of Split,
Split, Croatia

Parameters

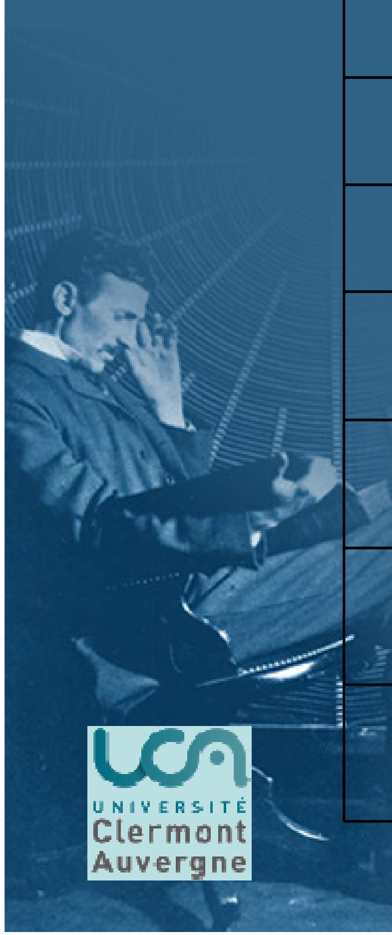

Parameter	Description	Value	Unit
b	Radius including the myelin sheath	10	µm
a	Inner axon radius	0.64·b	µm
$\mathbf{l_{int}}$	Internode length	100·2b	µm
L	Nerve fiber length	l_{int}·4, l_{int}·10	µm
ρ_a	Resistivity of the axoplasm	1.1	□m
$\mathbf{r_m}$	Myelin resistance for unit area	10	□m²
$\mathbf{c_m}$	Membrane capacitance per unit area	7.3	µF/m

Department of Electronics
University of Split,
Split, Croatia

Human Exposure to EM Fields:
Biomedical Applications - Modeling of nerve fiber excitation

Passive nerve fiber

- When modeling the passive nerve fiber, the ionic current in each Ranvier's node is to be taken into account.

Three Ranvier's Nodes Fiber

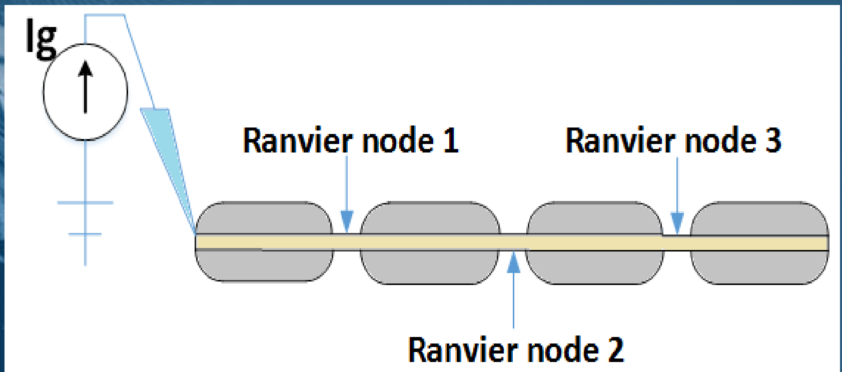

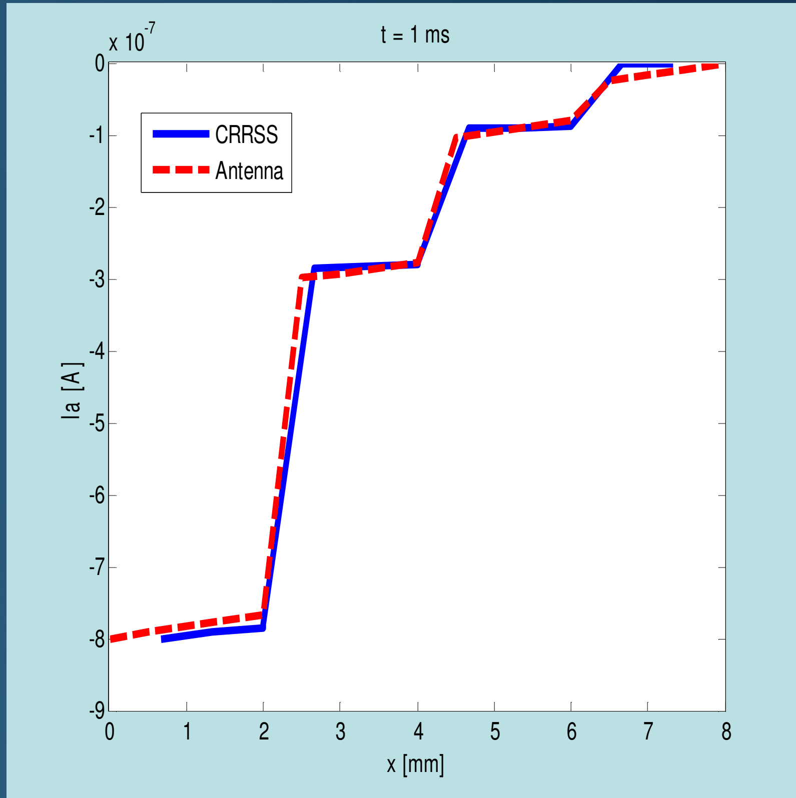

Intracellular current along the nerve fiber, *t* = 1 ms, *L* = 8 mm

Department of Electronics
University of Split,
Split, Croatia

Human Exposure to EM Fields: Biomedical Applications - Modeling of nerve fiber excitation

Passive nerve fiber

Nine Ranvier's nodes Fiber

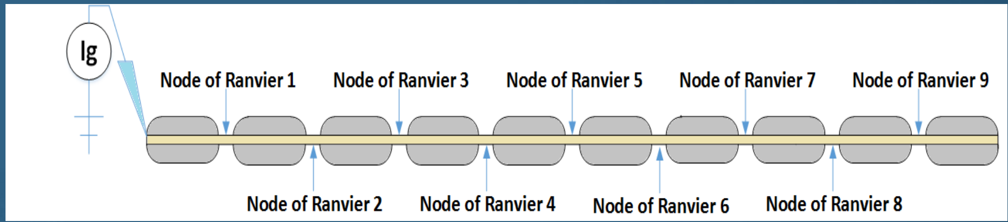

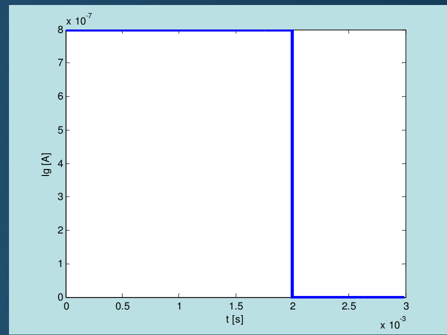

Rectangular subthreshold current pulse

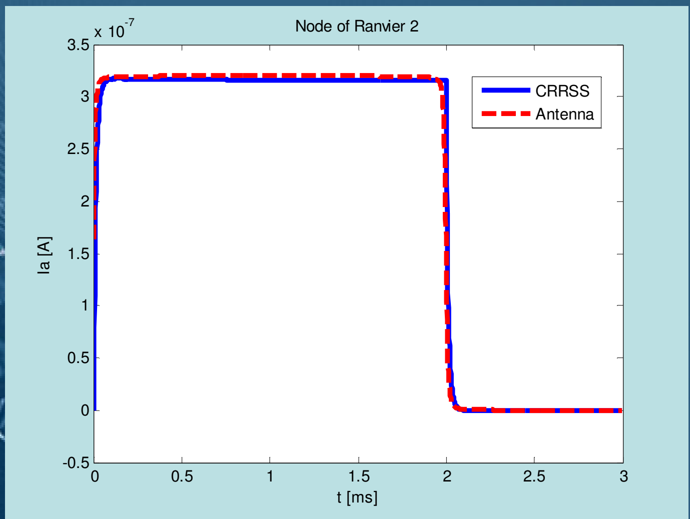

Intracellular current in the passive Ranvier's node 2, L = 2 cm

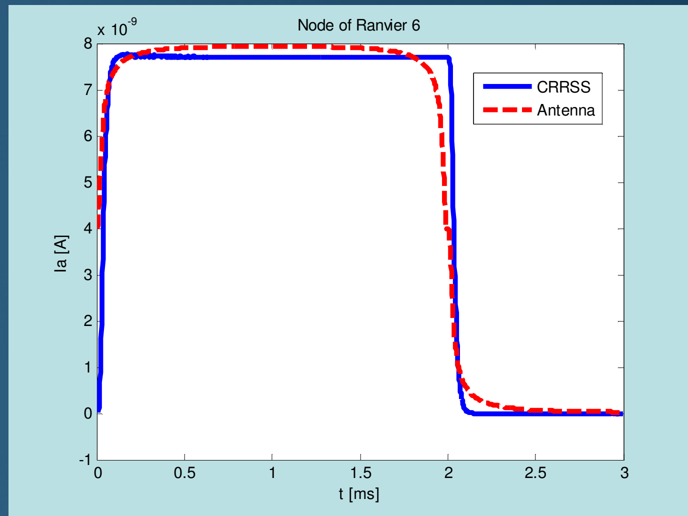

Intracellular current in the passive Ranvier's node 6, L = 2 cm

Department of Electronics
University of Split,
Split, Croatia

Active nerve fiber

- Fig shows the model of an active nerve fiber presented on a myelinated nerve fiber with 3 active Ranvier's nodes and 4 internodes.

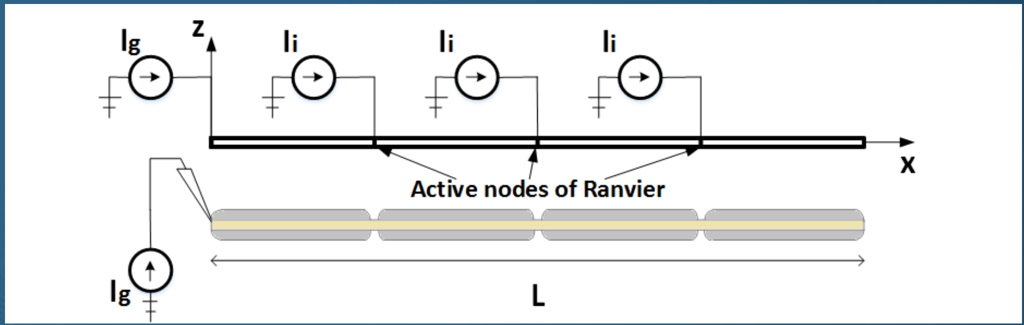

Active nerve fiber model

- Each node is represented by a wire junction of 2 thin wires representing an active Ranvier's node. Three additional current sources at the active Ranvier nodes represent an ionic current I_i of the activated node, determined by analyzing the *CRRSS* model and the analytical expression for the ion current.

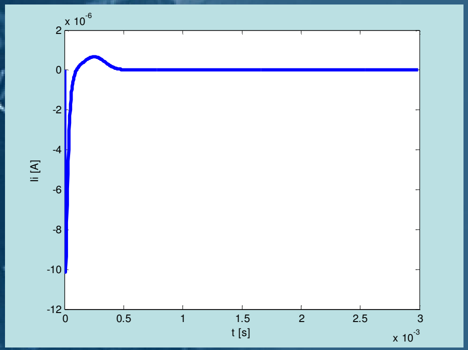

Ionic current of activated node of Ranvier

$$I_i(t) = Au(t)\left[e^{-Bt} - e^{-Dt}\right] - Eu(t-t_1)e^{-G(t-t_2)^2}$$

UNIVERSITÉ Clermont Auvergne

Department of Electronics
University of Split,
Split, Croatia

Active nerve fiber

- The Kirchhoff's law has to be satisfied at the junction:

$$I_i = 0.4 I_{i,j+1} + 0.6 I_{i,j+2}$$

where $I_{i,j+1}$ represents the ionic current value flowing out of the junction in one direction and $I_{i,j+2}$ is current flowing out of the junction in the opposite direction.

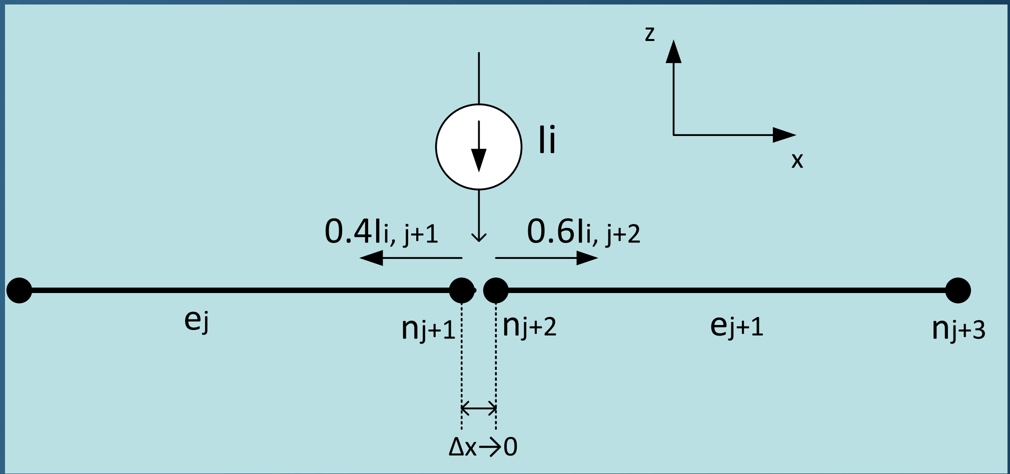

Two wire junction representation of the active nodeted node of Ranvier

Department of Electronics
University of Split,
Split, Croatia

UNIVERSITÉ Clermont Auvergne

Active nerve fiber

- The intracellular current for the active nerve fiber is also calculated with 9 Ranvier's nodes and 10 internodes.

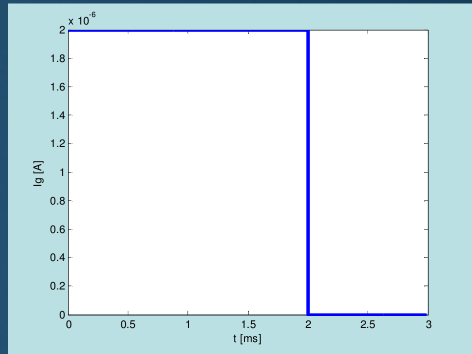

Rectangular superthreshold current pulse

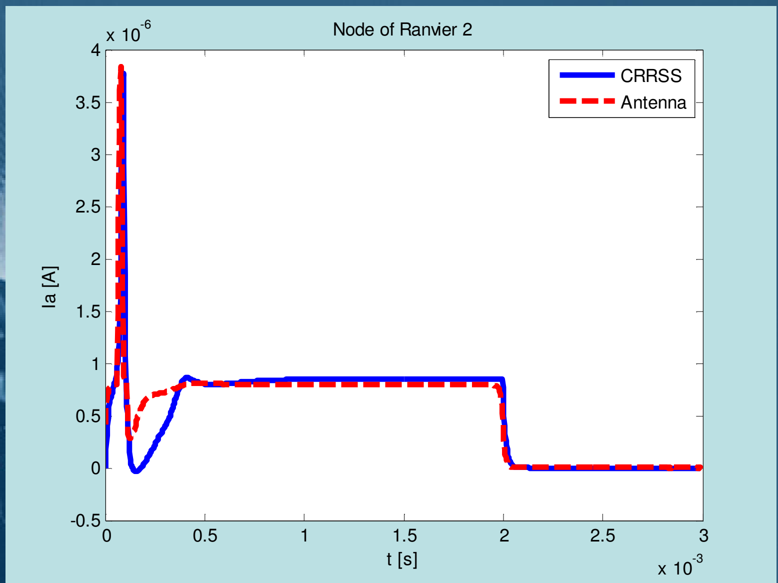

Intracellular current in the active Ranvier's node 2, *L* = 2 cm

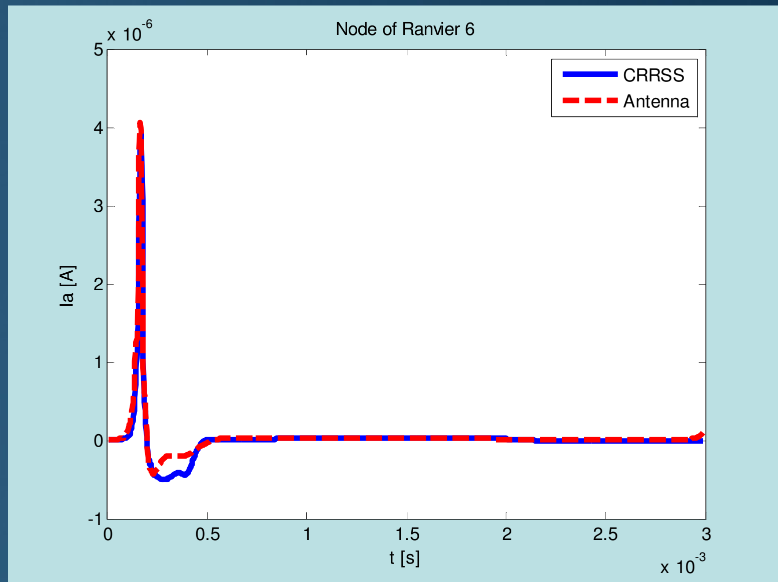

Intracellular current in the active Ranvier's node 6, *L* = 2 cm

Department of Electronics
University of Split,
Split, Croatia

Ongoing work

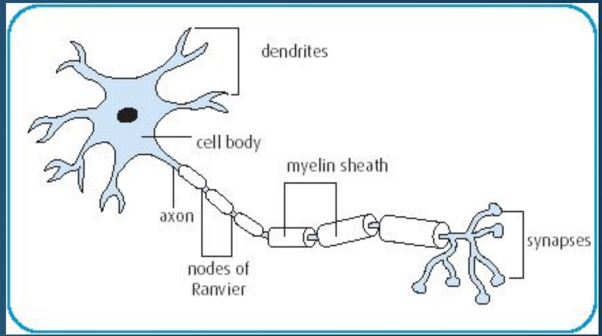

- The specific research activities (RA):

  - This enhanced nerve model finds the application not only in diagnostics and therapeutic purposes but also in gaining a fundamental knowledge regarding potential adverse effects on human health due to undesired exposure to EM fields.

  - Studies on electrical excitation of nerves, among other aspects involve;

- nerve excitation using stimulating electrodes,
- nerve conduction velocity tests,
- non-invasive stimulation of nerves via EM fields,
- external field coupling to nerves due to human exposure to EM radiation sources.

Department of Electronics
University of Split,
Split, Croatia

Human Exposure to Electromagnetic Fields

Concluding remarks

- The presence of electromagnetic fields in the environment and related possible health risk represent a controversial scientific, technical, and often public, issue.
- Theoretical models for electromagnetic and thermal dosimetry are required to interpret and confirm the experiment, develop an extrapolation process, and thereby establish safety guidelines and exposure limits for humans.
- Some examples of possibleb biomedical applications of EM fields are discussed (Transcranial magntic Stimulation – TMS, Nerve fiber excitation.)
- The use of sophisticated numerical methods is necessary to accurately predict the distribution of internal fields.

Department of Electronics
University of Split,
Split, Croatia

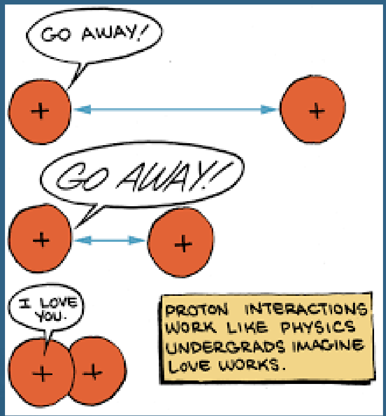

NUMERICAL MODELING OF PLASMA PYSICS PHENOMENA

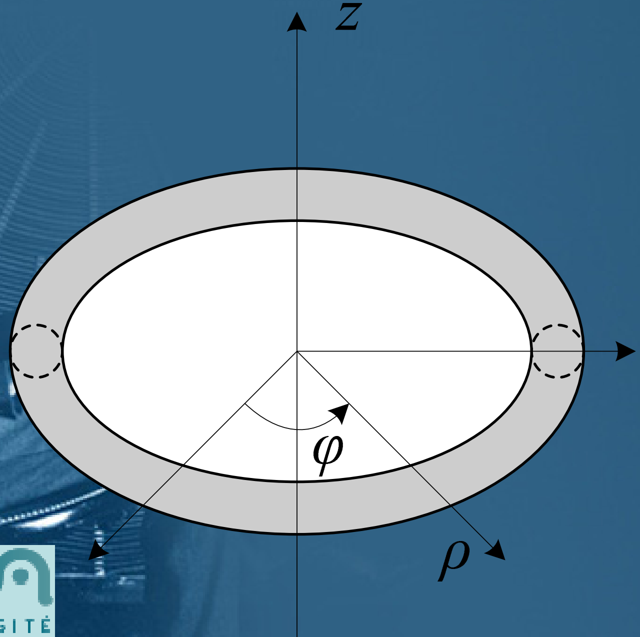

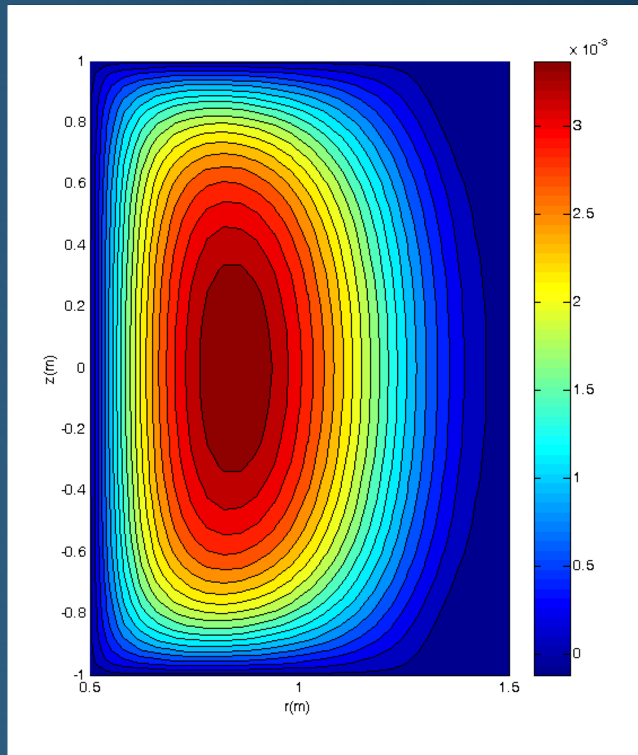

UNIVERSITÉ Clermont Auvergne

Clermont-Ferrand, 03 April 2018

CROATIAN RESEARCH UNIT

Department of Electronics
University of Split,
Split, Croatia

On the Numerical Modeling of Some Fusion Related Phenomena - applications of CEM methods in magnethohydrodynamics (MHD) phenomena analysis

- Some modification and extension of the GB-IBEM, FEM, BEM and various hybrid techniques are required for an efficient numerical treatment of specific fusion-related problems.
- In particular, MHD equilibrium in an axisymmetric plasma shape, as depicted in Fig.

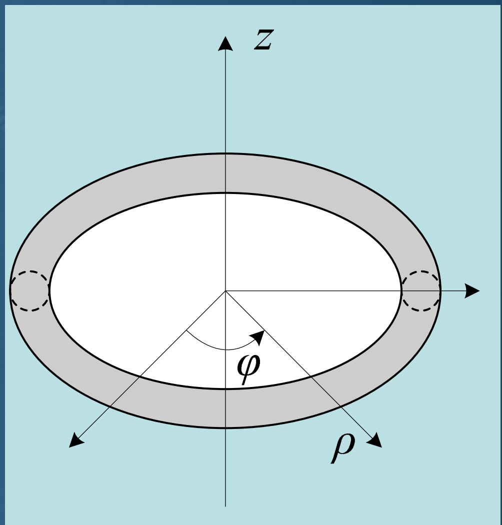

CROATIAN RESEARCH UNIT

Department of Electronics
University of Split,
Split, Croatia

Applications of CEM methods in MHD phenomena analysis

- The dynamics phenomana in tokamaks are governed by quasi-stationary Maxwell's equations:

$$\nabla \times \vec{E} = -\frac{\partial \vec{B}}{\partial t}$$ Faraday's law

$$\nabla \times \vec{B} = \mu_0 \vec{J}$$ Ampere's law

$$\nabla \cdot \vec{B} = 0$$ Gauss' law for magnetism

with the generalized Ohm's law $\vec{J} = \sigma(\vec{E} + \vec{v} \times \vec{B})$

and force balance equation $\vec{J} \times \vec{B} = \nabla p$

where p stands for the kinetic pressure.

CROATIAN RESEARCH UNIT

Department of Electronics
University of Split,
Split, Croatia

Applications of CEM methods in MHD phenomena analysis

In the plasma region, the plasma velocity is determined by the momentum balance

$$\frac{\partial \rho}{\partial t} + \nabla \cdot (\rho v) = 0$$

while mass density ρ conservation yields the continuity equation

$$\rho\left(\frac{\partial v}{\partial t} + v\nabla \cdot v\right) = \vec{J}x\vec{B} - \nabla \cdot \mathrm{p}$$

- On the basis of previous set of equations MHD problems is formulated in terms of the Grad Shafranov equation (GSE) which is in cylindrical coordinates (ρ , Φ, z) given by:

$$\left[\rho\frac{\partial}{\partial \rho}\left(\frac{1}{\rho}\frac{\partial}{\partial \rho}\right) + \frac{\partial^2}{\partial z^2}\right]\psi = \mu_0 \rho J_\phi$$

where ψ is the magnetic flux function, while J is the toroidal component of the plasma current.

CROATIAN RESEARCH UNIT

Department of Electronics
University of Split,
Split, Croatia

FEM solution of Grad-Shafranov equation

- The Grad-Shafranov equation could be written in a form:

$$-\left(\frac{\partial^2\Psi}{\partial r^2}+\frac{\partial^2\Psi}{\partial z^2}-\frac{1}{r}\frac{\partial\Psi}{\partial r}\right)=\mu_0 r J_\varphi$$

- Scalar product over the calculation domain yields:

$$-\int_\Omega\left(\frac{\partial^2\Psi}{\partial r^2}+\frac{\partial^2\Psi}{\partial z^2}-\frac{1}{r}\frac{\partial\Psi}{\partial r}\right)W_j d\Omega=\int_\Omega \mu_0 r J_\varphi W_j d\Omega$$

- Performing some mathematical manipulations leads to the weak formulation of GSE:

$$-\int_\Gamma\frac{\partial\Psi}{\partial n}W_j d\Gamma+\int_\Omega\left(\frac{\partial\Psi}{\partial r}\frac{\partial W_j}{\partial r}+\frac{\partial\Psi}{\partial z}\frac{\partial W_j}{\partial z}\right)d\Omega+\int_\Omega\frac{1}{r}\frac{\partial\Psi}{\partial r}W_j d\Omega=\int_\Omega \mu_0 r J_\varphi W_j d\Omega$$

CROATIAN RESEARCH UNIT
Department of Electronics
University of Split,
Split, Croatia

FEM solution of Grad-Shafranov equation

- Using the triangular finite elements and linear shape functions, solution over the element is given by:

$$\Psi^e(r,z)=\sum_{i=1}^{3}\Psi_i^e f_i(r,z);\quad W_j=f_j(r,z)$$

- By choosing the same shape and test functions (Galerkin-Bubnov scheme) the local matrix system on the element is given by:

$$\sum_{i=1}^{3}\left\{\int_{\Omega^e}\left(\frac{\partial f_i}{\partial r}\frac{\partial f_j}{\partial r}+\frac{\partial f_i}{\partial z}\frac{\partial f_j}{\partial z}\right)d\Omega+\int_{\Omega^e}\frac{1}{r}\frac{\partial f_i}{\partial r}f_j d\Omega\right\}=\int_{\Omega^e}\mu_0 rJ_\varphi f_j d\Omega;\ j=1,2,3$$

- The solution for the integrals on the left hand side is analytically obtained, while the integral on the right hand side should be, in general, calculated numerically.

- In this case the Gaussian three point quadrature rule for the integration over triangle has been used.

UNIVERSITÉ Clermont Auvergne

CROATIAN RESEARCH UNIT

Department of Electronics
University of Split,
Split, Croatia

FEM solution of Grad-Shafranov equation

- In this case each triangular element has been transformed to the unitary triangle:

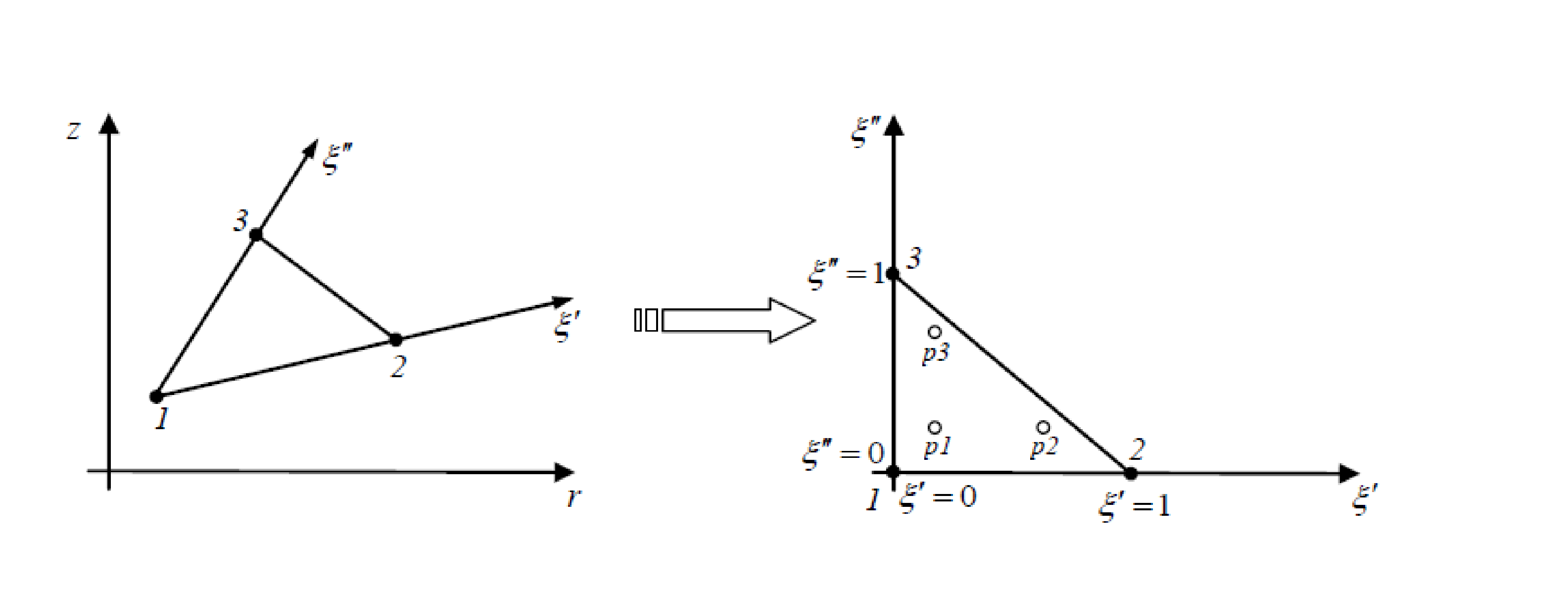

- Transformation is given by:

$$r = \sum_{i=1}^{3} r_i \phi_i(\xi', \xi''); \quad z = \sum_{i=1}^{3} z_i \phi_i(\xi', \xi'');$$

where

$$\phi_1(\xi', \xi'') = 1 - \xi' - \xi''$$
$$\phi_2(\xi', \xi'') = \xi'$$
$$\phi_3(\xi', \xi'') = \xi''$$

CROATIAN RESEARCH UNIT

Department of Electronics
University of Split,
Split, Croatia

FEM solution of Grad-Shafranov equation

- To evaluate integral over triangular element, the values of the integrating function in the predefined points p_1 to p_3 have to be calculated.

- Coordinates and corresponding weights are given in the table:

p	1	2	3
ξ'_p	1/6	2/3	1/6
ξ''_p	1/6	1/6	2/3
w_p	1/6	1/6	1/6

- Numerical integration is carried out using the expression:

$$I = J \cdot \sum_{p=1}^{3} w_p F(\xi'_p, \xi''_p)$$

where J is Jacobian:

$$J = \begin{vmatrix} \dfrac{\partial r}{\partial \xi'} & \dfrac{\partial z}{\partial \xi'} \\ \dfrac{\partial r}{\partial \xi''} & \dfrac{\partial z}{\partial \xi''} \end{vmatrix}$$

CROATIAN RESEARCH UNIT

Department of Electronics
University of Split,
Split, Croatia

Test example No 1 : Rectangular plasma

$\Psi(Wb)$ for rectangular plasma – FEM solution for $\mu_0 r J_\phi = 1$

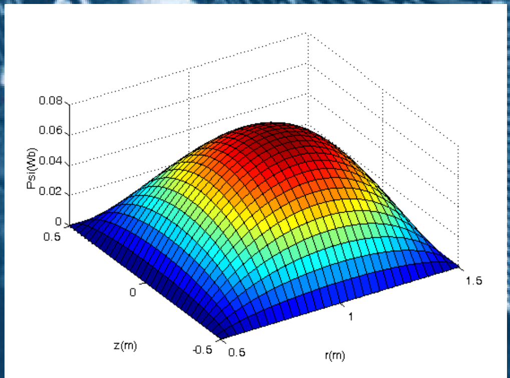

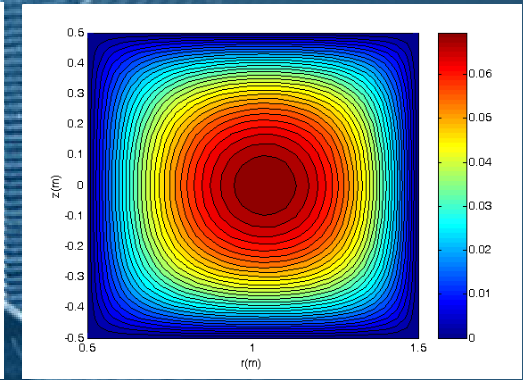

$\Psi(Wb)$ for rectangular plasma - FEM solution for: $\mu_0 r J_\phi = r^3 z^2$

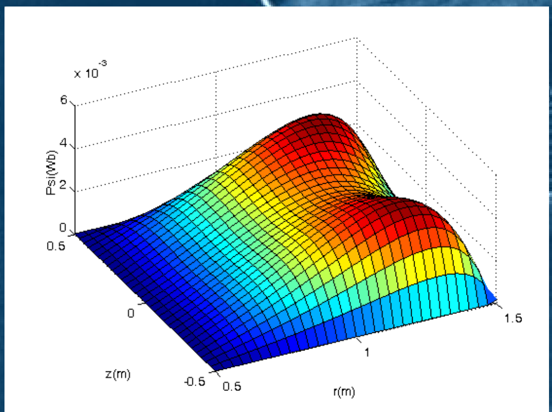

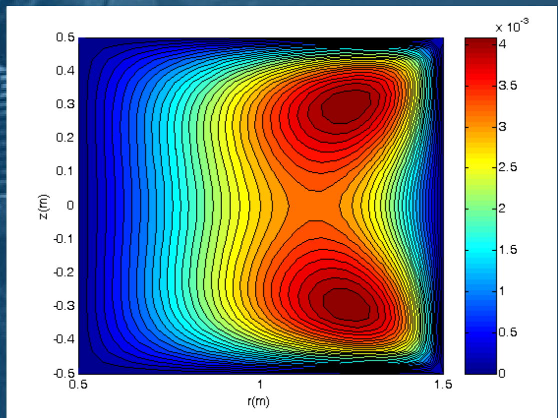

CROATIAN RESEARCH UNIT

Department of Electronics
University of Split,
Split, Croatia

MÄLARDALENS HÖGSKOLA ESKILSTUNA VÄSTERÅS

Test example No 1: Rectangular plasma

$\Psi(Wb)$ for rectangular plasma FEM solution for: $\mu_0 r J_\phi = r^2 z^3$

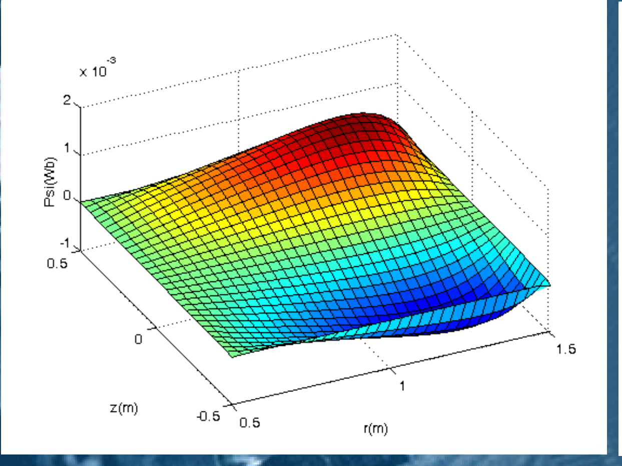

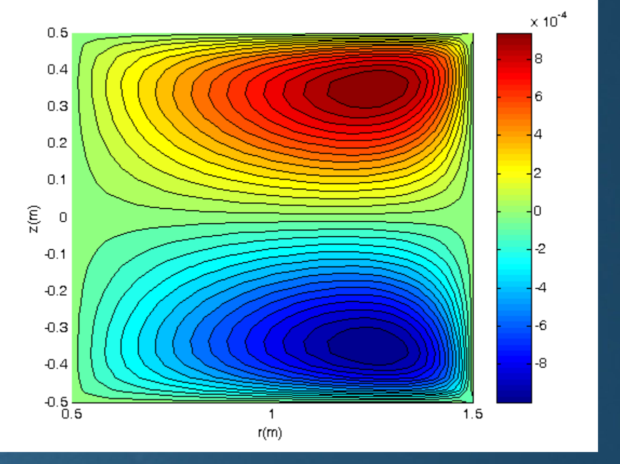

Test example No 2 : D- shaped plasma

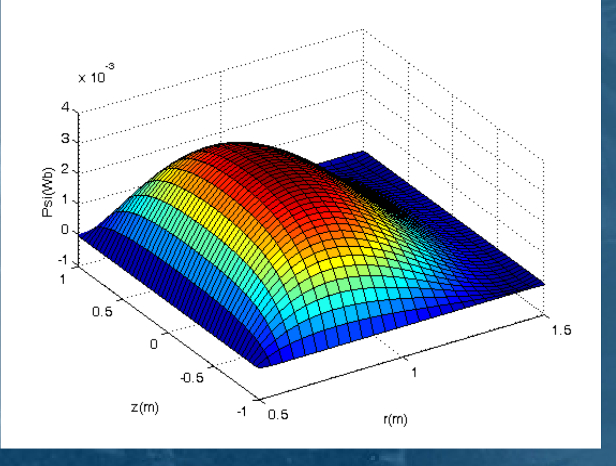

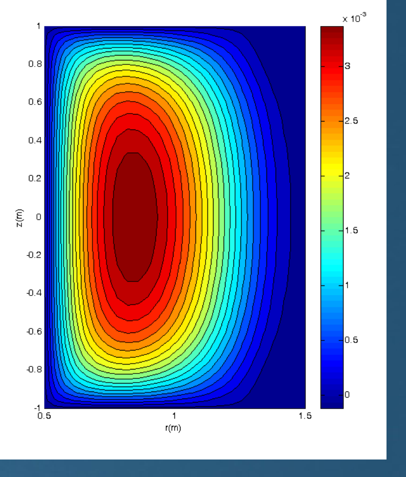

CROATIAN RESEARCH UNIT

Department of Electronics
University of Split,
Split, Croatia

Future work: Boundary element solution of Grad-Shafranov equation (GSE)

- Furthermore, the Green integral representation of GSE:

$$\left[\rho\frac{\partial}{\partial\rho}\left(\frac{1}{\rho}\frac{\partial}{\partial\rho}\right)+\frac{\partial^2}{\partial z^2}\right]\psi=\mu_0\rho J_\phi$$

can be written in the form:

$$c_i\psi_i=\int_\Gamma\left[\frac{\psi^*}{\rho}\frac{\partial\psi}{\partial n}-\frac{\psi}{\rho}\frac{\partial\psi^*}{\partial n}\right]d\Gamma-\int_\Omega\frac{\psi^*}{\rho^2}\left(\mu\rho J_\phi\right)d\Omega$$

where ψ^* stands for the fundamental solution.

Department of Electronics
University of Split,
Split, Croatia

On-going work in deterministic and stochastic modeling

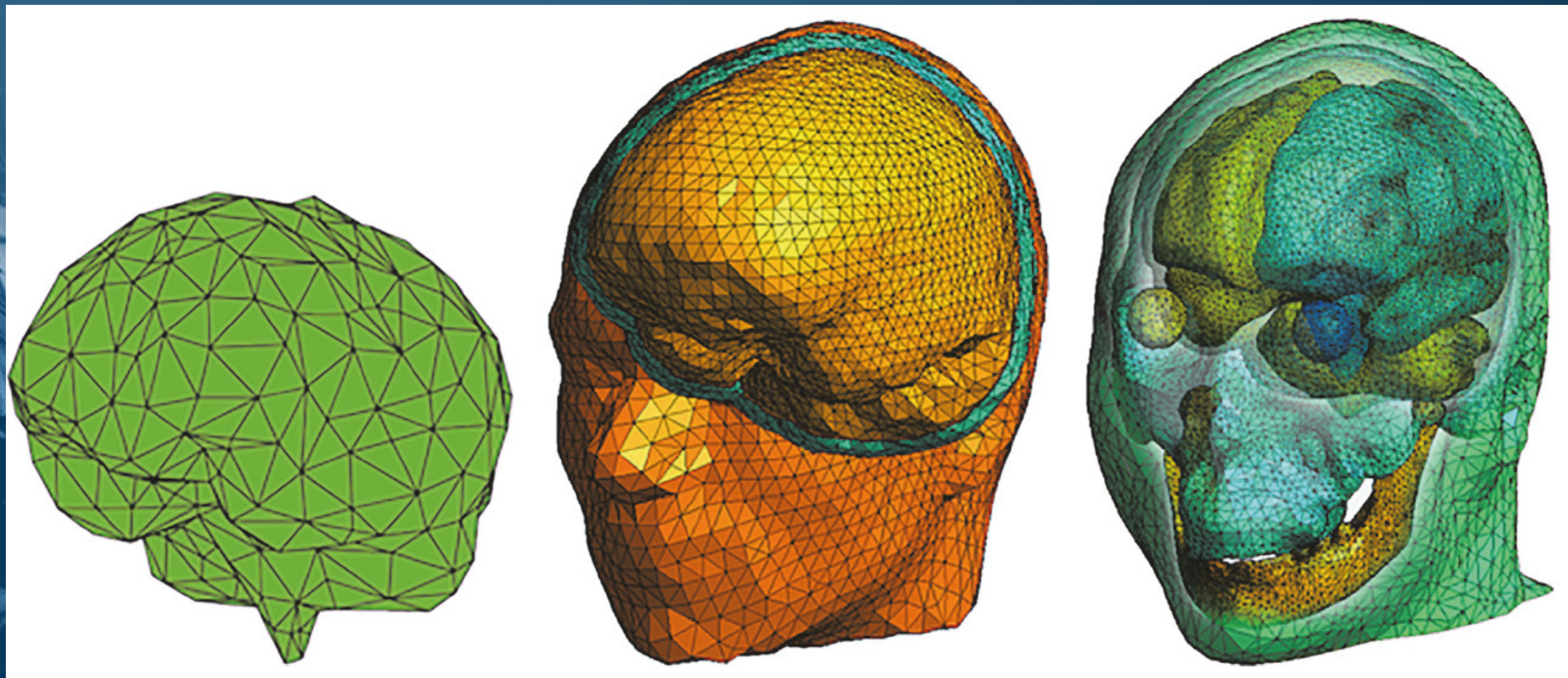

Clermont-Ferrand, 03 April 2018

CROATIAN RESEARCH UNIT

Department of Electronics
University of Split,
Split, Croatia

CIRCLE ELECTROMAGNETIC

Ongoing work: Finite element (FE) solution of Current Diffusion Equation (CDE)

- In static equilibrium, the governing equations of resistive MHD

$\nabla \cdot \vec{B} = 0$	Gauss' law for magnetism
$\nabla \times \vec{B} = \mu_0 \vec{J}$	Ampere's law
$\nabla \times \vec{E} = -\dfrac{\partial \vec{B}}{\partial t}$	Faraday's law
$\vec{J} \times \vec{B} = \nabla p$	Force balance equation
$\vec{J} = \sigma(\vec{E} + \vec{v} \times \vec{B})$	Generalized Ohm's law

UNIVERSITÉ Clermont Auvergne

CROATIAN RESEARCH UNIT

Department of Electronics
University of Split,
Split, Croatia

Ongoing work: FE solution of CDE

- Assumption of axisymmetric plasma, in cylindrical coords, hence (3D problem >> 2D)

$$\frac{\partial}{\partial \varphi} = 0$$

- Magnetic field B and current density *J* via *magnetic flux function* and *poloidal current function*

$$\psi = \psi(R, z)$$

$$f = f(R, z)$$

$$B_R = -\frac{1}{R}\frac{\partial \psi}{\partial z}$$

$$B_z = \frac{1}{R}\frac{\partial \psi}{\partial R}$$

$$f = \frac{R B_\varphi}{\mu_0}$$

$$J_R = -\frac{1}{\mu_0}\frac{\partial B_\varphi}{\partial z}$$

$$J_\varphi = \frac{1}{\mu_0}\left(\frac{\partial B_R}{\partial z} - \frac{\partial B_z}{\partial R}\right)$$

$$J_z = \frac{1}{\mu_0}\frac{1}{R}\frac{\partial}{\partial R}(R B_\varphi)$$

$$(R, \varphi, z)$$

UNIVERSITÉ Clermont Auvergne

CROATIAN RESEARCH UNIT

Department of Electronics
University of Split,
Split, Croatia

CIRCLE ELECTROMAGNETIC

Ongoing work: FE solution of CDE

- Evolution of poloidal magnetic flux, hence plasma current

$$\vec{J} = \vec{J}_o + \vec{J}_{ni} \qquad J_{ni} = J_{boot} + J_{nbi} + J_{lh} + J_{ic} + J_{ec} + J_{ext}$$

$$\vec{J} \cdot \vec{B} = \sigma \vec{E} \cdot \vec{B} + \vec{J}_{NI} \cdot \vec{B}$$

- Averaging on surface of constant radius, (2D problem >> 1D problem)

$$\rho = \sqrt{\frac{\Phi}{\pi B_{\varphi 0}}}$$

$$\left\langle \vec{J} \cdot \vec{B} \right\rangle = -\frac{f^2}{\mu_0 V'} \left\{ \frac{\partial}{\partial \rho} \left[\frac{V'}{f} \left\langle \frac{|\nabla \rho|^2}{R^2} \right\rangle \frac{\partial \psi}{\partial \rho} \right] \right\}$$

$$\left\langle \vec{E} \cdot \vec{B} \right\rangle = -f \left\langle \frac{1}{R^2} \right\rangle \frac{\partial \psi}{\partial t}$$

CROATIAN RESEARCH UNIT

Department of Electronics
University of Split,
Split, Croatia

Ongoing work: FE solution of CDE

- Current diffusion equation or magnetic flux diffusion equation

$$\frac{\partial \psi}{\partial t} = \frac{f}{\mu_0 \sigma \left\langle \frac{1}{R^2} \right\rangle V'} \left\{ \frac{\partial}{\partial \rho} \left(\frac{V'}{f} \left\langle \frac{|\nabla \rho|^2}{R^2} \right\rangle \frac{\partial \psi}{\partial \rho} \right) \right\} + \frac{1}{\sigma f \left\langle \frac{1}{R^2} \right\rangle} \left\langle \vec{J_{NI}} \cdot \vec{B} \right\rangle$$

- Initial and boundary conditions

- Parabolic type PDE

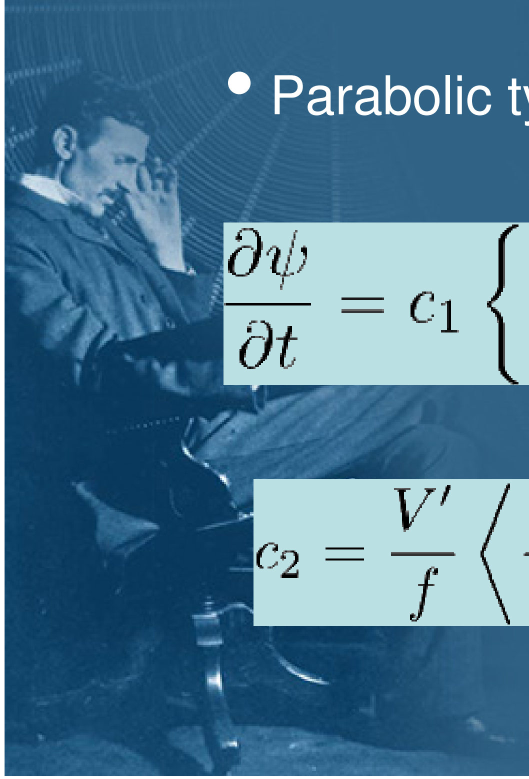

$$\frac{\partial \psi}{\partial t} = c_1 \left\{ \frac{\partial}{\partial \rho} \left(c_2 \frac{\partial \psi}{\partial \rho} \right) \right\} + c_3$$

$$c_1 = -\frac{f^2}{\mu_0 V'}$$

$$c_2 = \frac{V'}{f} \left\langle \frac{|\nabla \rho|^2}{R^2} \right\rangle$$

$$c_3 = \frac{1}{\sigma f \left\langle \frac{1}{R^2} \right\rangle} \left\langle \vec{J_{NI}} \cdot \vec{B} \right\rangle$$

$$V' = \frac{\partial V}{\partial \rho}$$

UNIVERSITÉ Clermont Auvergne

CROATIAN RESEARCH UNIT

Department of Electronics
University of Split,
Split, Croatia

Ongoing work: FE solution of CDE

- Weighted residual approach

$$\psi \approx \widetilde{\psi} = \sum_{i=1}^{n} \alpha_i N_i$$

- Solution domain (radial profile):

$$\Omega : \rho \in [0, \rho_b]$$

- Multiplying by W_j and integrating over domain, strong formulation

$$\int_\Omega \frac{1}{c_1} \frac{\partial \widetilde{\psi}^t}{\partial t} W_j \, d\rho = \int_\Omega \frac{\partial}{\partial \rho} \left(\lambda \frac{\partial \widetilde{\psi}}{\partial \rho} \right) W_j \, d\rho - \int_\Omega p W_j \, d\rho \, ; \, j = 1, 2, .., n$$

$$\lambda = c_2 \, ; p = -c_3/c_1$$

- Integrating by parts and rearranging, weak formulation of CDE

$$\lambda \frac{\partial \widetilde{\psi}}{\partial \rho} W_j \Bigg|_0^{\rho_b} - \int_\Omega \lambda \frac{\partial \widetilde{\psi}}{\partial \rho} \frac{\partial W_j}{\partial \rho} \, d\rho + \int_\Omega \frac{1}{c_1} \frac{\partial \widetilde{\psi}^t}{\partial t} W_j \, d\rho = \int_\Omega p W_j \, d\rho$$

- Time derivative discretized by the finite differences scheme.

Department of Electronics
University of Split,
Split, Croatia

Ongoing work: FE solution of CDE

Some numerical results:

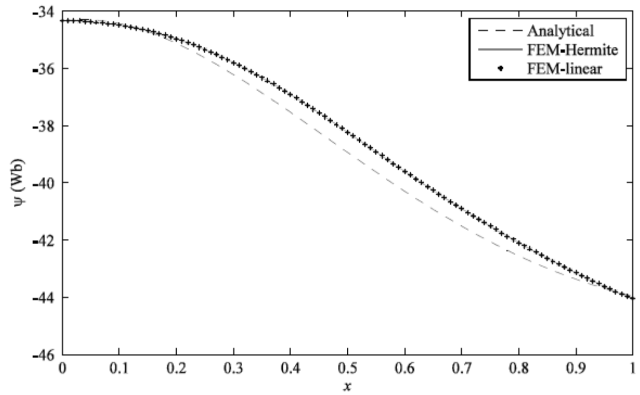

Fig. 3. Poloidal magnetic flux for t=905 s.

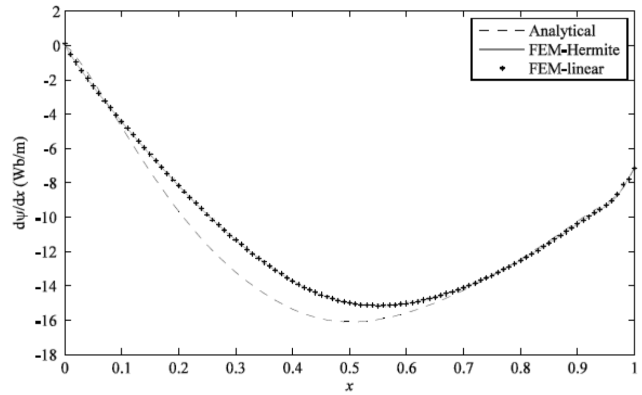

Fig. 6. First derivative of the poloidal magnetic flux for t=1095 s.

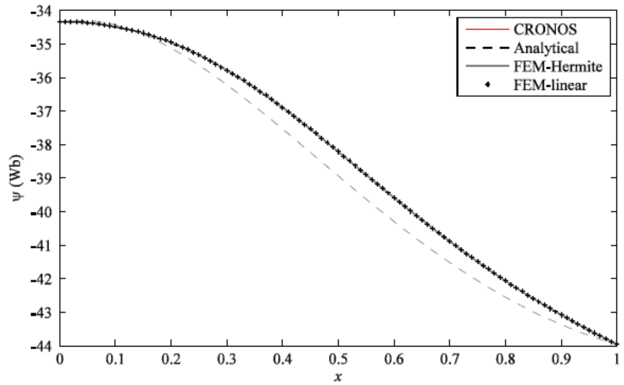

Fig. 8. Poloidal magnetic flux for t=905 s with non-inductive current sources.

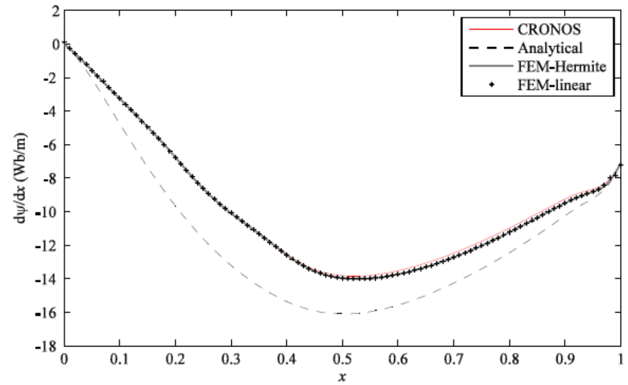

Fig. 11. First derivative of the poloidal magnetic flux for t=1095 s with non-inductive current sources.

Department of Electronics
University of Split,
Split, Croatia

Ongoing work: FE solution of transport equations

WP-CD: Croatian team activities

EUROfusion

The main activity – implementation of the **FORTRAN** solver for tokamak transport equations based on the **Finite Element Method (FEM).**

There are 6 1D transport equations:

- current diffusion
- ion density
- electron density
- ion temperatures
- electron energy transport
- rotation transport

UNIVERSITÉ Clermont Auvergne

Department of Electronics
University of Split,
Split, Croatia

Ongoing work: FE solution of transport equations

WP-CD: Croatian team activities

EUROfusion

CURRENT DIFFUSION

$$\sigma_{||}\left(\frac{\partial\Psi}{\partial t}\Big|_{\rho} - \frac{\rho\dot{B}_0}{2B_0}\frac{\partial\Psi}{\partial\rho}\right) = \frac{F^2}{\mu_0 B_0 \rho}\frac{\partial}{\partial\rho}\left[\frac{V'}{4\pi^2}\left\langle\frac{\nabla\rho^2}{R}\right\rangle\frac{1}{F}\frac{\partial\Psi}{\partial\rho}\right] - \frac{V'}{2\pi\rho}\left(j_{ni,exp} + j_{ni,imp}\cdot\Psi\right)$$

ION DENSITY

$$\left(\frac{\partial}{\partial t}\Big|_{\rho} - \frac{\dot{B}_0}{2B_0}\cdot\frac{\partial}{\partial\rho}\rho\right)(V'n_i) + \frac{\partial}{\partial\rho}\Gamma_i = V'\left(S_{i,exp} - S_{i,imp}\cdot n_i\right)$$

ELECTRON DENSITY

$$\left(\frac{\partial}{\partial t}\Big|_{\rho} - \frac{\dot{B}_0}{2B_0}\cdot\frac{\partial}{\partial\rho}\rho\right)(V'n_e) + \frac{\partial}{\partial\rho}\Gamma_e = V'\left(S_{e,exp} - S_{e,imp}\cdot n_e\right)$$

ION TEMPERATURES

$$\frac{3}{2}\left(\frac{\partial}{\partial t} - \frac{\dot{B}_0}{2B_0}\cdot\frac{\partial}{\partial\rho}\rho\right)\left(n_i T_i V'^{\frac{5}{3}}\right) + V'^{\frac{2}{3}}\frac{\partial}{\partial\rho}(q_i + T_i\gamma_i) = V'^{\frac{5}{3}}\left[Q_{i,exp} - Q_{i,imp}\cdot T_i + Q_{ei} + Q_{zi} + Q_{\gamma i}\right]$$

ELECTRON ENERGY TRANSPORT

$$\frac{3}{2}\left(\frac{\partial}{\partial t} - \frac{\dot{B}_0}{2B_0}\cdot\frac{\partial}{\partial\rho}\rho\right)\left(n_e T_e V'^{\frac{5}{3}}\right) + V'^{\frac{2}{3}}\frac{\partial}{\partial\rho}(q_e + T_e\gamma_e) = V'^{\frac{5}{3}}\left[Q_{e,exp} - Q_{e,imp}\cdot T_e + Q_{ie} - Q_{\gamma i}\right]$$

ROTATION TRANSPORT

$$\left(\frac{\partial}{\partial t}\Big|_{\rho} - \frac{\dot{B}_0}{2B_0}\cdot\frac{\partial}{\partial\rho}\rho\right)\left(V'\langle R\rangle m_i n_i u_{i,\varphi}\right) + \frac{\partial}{\partial\rho}\Phi_i = V'\left(U_{i,\varphi,exp} - U_{i,\varphi,imp}\cdot u_{i,\varphi} + U_{zi,\varphi}\right)$$

UNIVERSITÉ Clermont Auvergne

Department of Electronics
University of Split,
Split, Croatia

Ongoing work: FE solution of transport equations

WP-CD: Croatian team activities

EUROfusion

$$\sigma_{\|}\left(\left.\frac{\partial\Psi}{\partial t}\right|_{\rho}-\frac{\rho\dot{B}_0}{2B_0}\frac{\partial\Psi}{\partial\rho}\right)=\frac{F^2}{\mu_0 B_0\rho}\frac{\partial}{\partial\rho}\left[\frac{V'}{4\pi^2}\left\langle\frac{\nabla\rho^2}{R}\right\rangle\frac{1}{F}\frac{\partial\Psi}{\partial\rho}\right]-\frac{V'}{2\pi\rho}\left(j_{ni,exp}+j_{ni,imp}\cdot\Psi\right)$$

$$\left(\left.\frac{\partial}{\partial t}\right|_{\rho}-\frac{\dot{B}_0}{2B_0}\cdot\frac{\partial}{\partial\rho}\rho\right)\left(V'\langle R\rangle m_i n_i u_{i,\varphi}\right)+\frac{\partial}{\partial\rho}\Phi_i=V'\left(U_{i,\varphi,exp}-U_{i,\varphi,imp}\cdot u_{i,\varphi}+U_{zi,\varphi}\right)$$

$$\frac{3}{2}\left(\frac{\partial}{\partial t}-\frac{\dot{B}_0}{2B_0}\cdot\frac{\partial}{\partial\rho}\rho\right)\left(n_i T_i V'^{\frac{5}{3}}\right)+V'^{\frac{2}{3}}\frac{\partial}{\partial\rho}\left(q_i+T_i\gamma_i\right)=V'^{\frac{5}{3}}\left[Q_{i,exp}-Q_{i,imp}\cdot T_i+Q_{ei}+Q_{zi}+Q_{\gamma i}\right]$$

$$\left(\left.\frac{\partial}{\partial t}\right|_{\rho}-\frac{\dot{B}_0}{2B_0}\cdot\frac{\partial}{\partial\rho}\rho\right)\left(V'n_e\right)+\frac{\partial}{\partial\rho}\Gamma_e=V'\left(S_{e,exp}-S_{e,imp}\cdot n_e\right)$$

$$\frac{3}{2}\left(\frac{\partial}{\partial t}-\frac{\dot{B}_0}{2B_0}\cdot\frac{\partial}{\partial\rho}\rho\right)\left(n_e T_e V'^{\frac{5}{3}}\right)+V'^{\frac{2}{3}}\frac{\partial}{\partial\rho}\left(q_e+T_e\gamma_e\right)=V'^{\frac{5}{3}}\left[Q_{e,exp}-Q_{e,imp}\cdot T_e+Q_{ie}-Q_{\gamma i}\right]$$

$$\left(\left.\frac{\partial}{\partial t}\right|_{\rho}-\frac{\dot{B}_0}{2B_0}\cdot\frac{\partial}{\partial\rho}\rho\right)\left(V'n_i\right)+\frac{\partial}{\partial\rho}\Gamma_i=V'\left(S_{i,exp}-S_{i,imp}\cdot n_i\right)$$

1D core transport equations are given in generalized form:

$$\frac{a(x)\cdot Y(x,t)-b(x)\cdot Y(x,t-1)}{h}+\frac{1}{c(x)}\frac{\partial}{\partial x}\left(-d(x)\frac{\partial Y(x,t)}{\partial x}+e(x)\cdot Y(x,t)\right)=f(x)-g(x)\cdot Y(x,t)$$

with generalized form of boundary condition:

$$v(x_{bnd})\cdot\left.\frac{\partial Y(x,t)}{\partial x}\right|_{bnd}+u(x_{bnd})Y(x_{bnd},t)=w(x_{bnd})$$

h ... time step

a(x), b(x), c(x), d(x), e(x), f(x) and g(x) ... transport coefficients computed separately for each equation

Y(x,t) and Y(x,t-1) are the value of interest at the current and the previous time step, respectively

Université Clermont Auvergne

Department of Electronics
University of Split,
Split, Croatia

Ongoing work: FE solution of transport equations

WP-CD: Croatian team activities

EUROfusion

Numerical solution: Finite element method

The solution on a segment is expressed in terms of a polynomial expansion over a set of basis functions:

$$Y(x,t) = \sum_i Y_i N_i(x)$$

Base and test functions are chosen to be the same (**Galerkin Bubnov's scheme**).

$$N_i(x) = W_j(x) \text{ for } i=j$$

Linear shape functions:

$$N_1^e(x) = \frac{x_2^e - x}{x_2^e - x_1^e} \qquad N_2^e(x) = \frac{x - x_1^e}{x_2^e - x_1^e}$$

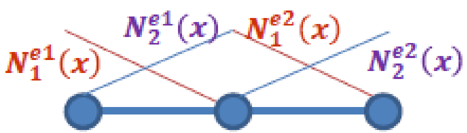

UNIVERSITÉ Clermont Auvergne

Department of Electronics
University of Split,
Split, Croatia

Ongoing work: FE solution of transport equations

WP-CD: Croatian team activities

EUROfusion

Applying the Galerkin Bubnov discretization procedure he global matrices are obtained in the following form:

$$\boldsymbol{LHS} \cdot \boldsymbol{Y}^{n+1} = \boldsymbol{RHS}$$

$$\boldsymbol{LHS} = \int_0^1 \left[c(x)\cdot a(x) + c(x)\cdot g(x)\cdot h + \frac{de(x)}{dx}\cdot h \right]\cdot N_i(x)N_j(x)dx + \int_0^1 h\cdot e(x)D_i(x)N_j(x)dx + \int_0^1 h\cdot d(x)D_i(x)D_j(x)dx$$

$$D_i(x) = \frac{\partial N_i(x)}{\partial x}$$

$$\boldsymbol{RHS} = Y^n \cdot \int_0^1 c(x)b(x)N_i(x)N_j(x)dx + \int_0^1 h\cdot c(x)f(x)N_j(x)dx + h\cdot \boldsymbol{BOUNDARY}$$

$$\boldsymbol{BOUNDARY} = d(x)\cdot N_j(x)\cdot \left.\frac{\partial Y}{\partial x}\right|_0^1$$

UNIVERSITÉ Clermont Auvergne

Department of Electronics
University of Split,
Split, Croatia

Ongoing work: FE solution of transport equations

WP-CD: Croatian team activities

EUROfusion

Numerical solution: Finite Element Method (FEM)

According to weighted residual approach the generalized form of transport equation:

$$c(x)\cdot a(x)\cdot \boldsymbol{Y(x,t)} - c(x)\cdot b(x)\cdot \boldsymbol{Y(x,t-1)} - h\cdot\frac{\partial d(x)}{\partial x}\cdot\frac{\partial \boldsymbol{Y(x,t)}}{\partial x} - h\cdot d(x)\frac{\partial^2 \boldsymbol{Y(x,t)}}{\partial x^2} + h\cdot\frac{\partial e(x)}{\partial x}\boldsymbol{Y(x,t)} + h\cdot e(x)\cdot\frac{\partial \boldsymbol{Y(x,t)}}{\partial x} = h\cdot c(x)\cdot f(x) - h\cdot c(x)\cdot g(x)\cdot \boldsymbol{Y(x,t)}$$

is multiplied by the set of test functions and integrated over domain:

$$\int_0^1 c(x)\cdot a(x)\cdot \boldsymbol{Y(x,t)}\cdot \boldsymbol{W_j(x)} - \int_0^1 c(x)\cdot b(x)\cdot \boldsymbol{Y(x,t-1)}\cdot \boldsymbol{W_j(x)} - \int_0^1 h\cdot\frac{\partial d(x)}{\partial x}\cdot\frac{\partial \boldsymbol{Y(x,t)}}{\partial x}\cdot \boldsymbol{W_j(x)}$$
$$- \int_0^1 h\cdot d(x)\frac{\partial^2 \boldsymbol{Y(x,t)}}{\partial x^2}\cdot \boldsymbol{W_j(x)} + \int_0^1 h\cdot\frac{\partial e(x)}{\partial x}\boldsymbol{Y(x,t)}\cdot \boldsymbol{W_j(x)} + \int_0^1 h\cdot e(x)\cdot\frac{\partial \boldsymbol{Y(x,t)}}{\partial x}\cdot \boldsymbol{W_j(x)}$$
$$= \int_0^1 h\cdot c(x)\cdot f(x)\cdot \boldsymbol{W_j(x)} - \int_0^1 h\cdot c(x)\cdot g(x)\cdot \boldsymbol{Y(x,t)}\cdot \boldsymbol{W_j(x)}$$

UNIVERSITÉ Clermont Auvergne

Department of Electronics
University of Split,
Split, Croatia

Ongoing work: FE solution of transport equations

EUROfusion

Output profiles from 1D core transport equation obtained by using FEM solver:

Input data:

equilibrium code: EMEQ
number of radial points: 50
time step: 1e-3 s
number of time points: 10

Initial profiles are from mdsplus database.

UNIVERSITÉ Clermont Auvergne

Department of Electronics
University of Split,
Split, Croatia

Ongoing work: FE solution of transport equations

WP-CD: Croatian team activities

EUROfusion

Output profiles from 1D core transport equation obtained by using FEM solver:

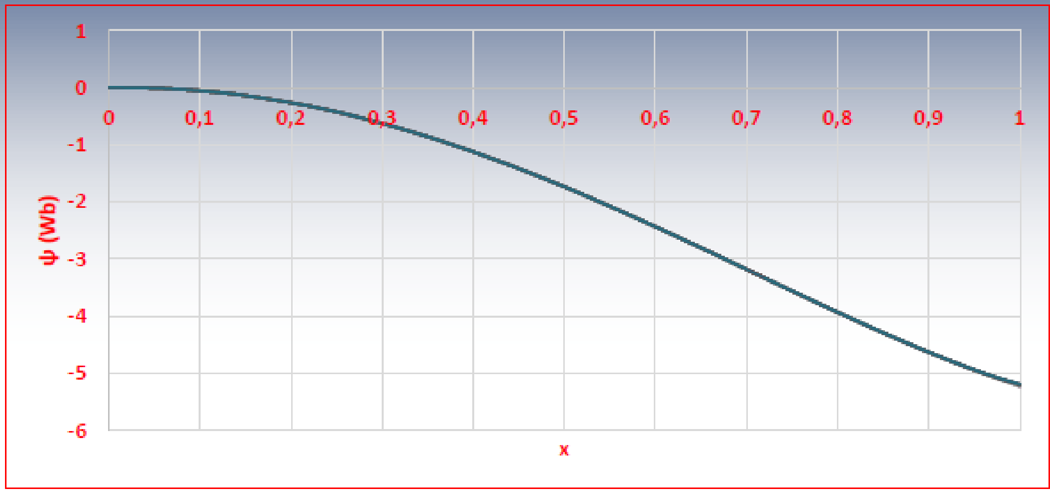

- current diffusion

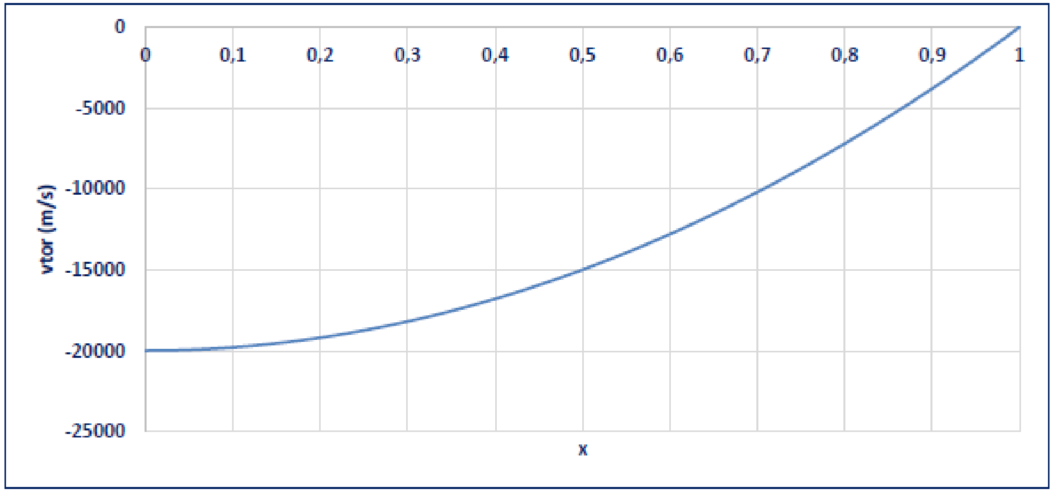

- rotation transport

UNIVERSITÉ Clermont Auvergne

Department of Electronics
University of Split,
Split, Croatia

Ongoing work: FE solution of transport equations

WP-CD: Croatian team activities

EUROfusion

Output profiles from 1D core transport equation obtained by using FEM solver:

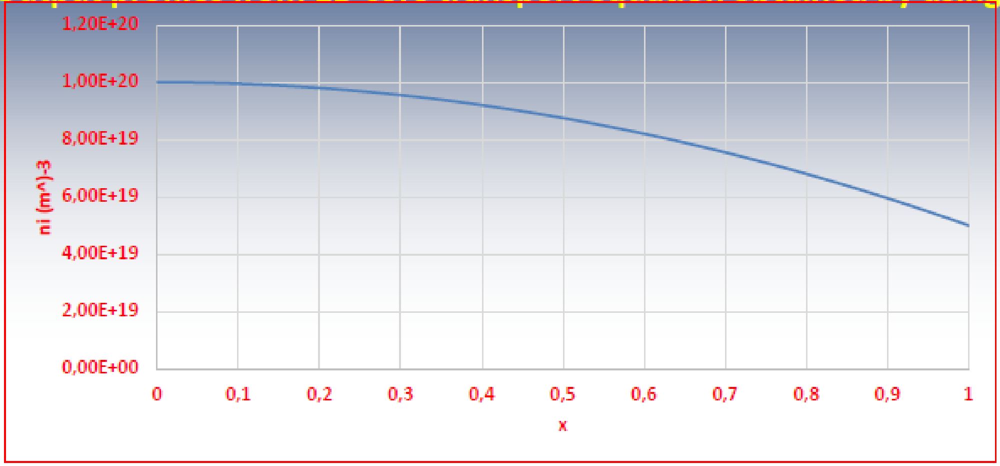

- ion density

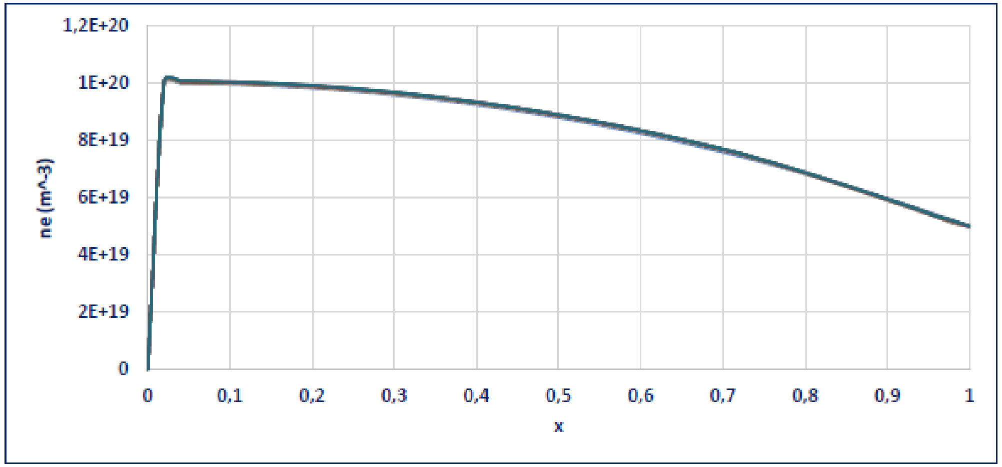

- electron density

UNIVERSITÉ Clermont Auvergne

Department of Electronics
University of Split,
Split, Croatia

Ongoing work: FE solution of transport equations

WP-CD: Croatian team activities

EUROfusion

Output profiles from 1D core transport equation obtained by using FEM solver:

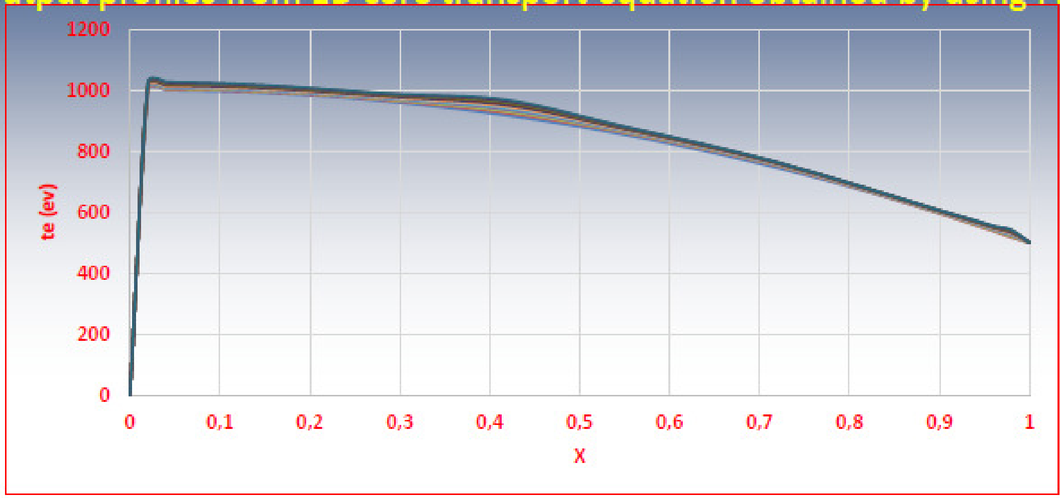

- ion temperatures

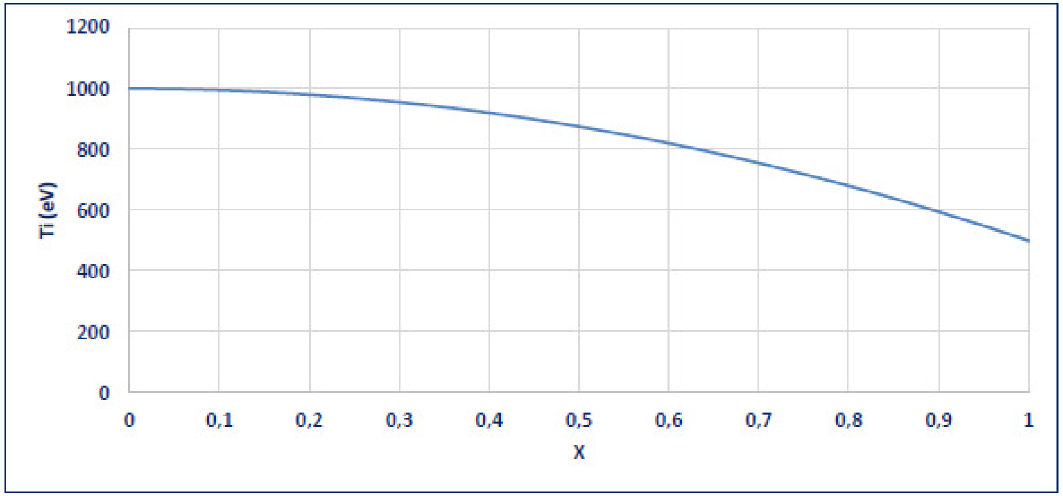

- electron energy transport

Department of Electronics
University of Split,
Split, Croatia

Ongoing work: FD and TD analyzes of the transient field generated by GPR dipole antenna

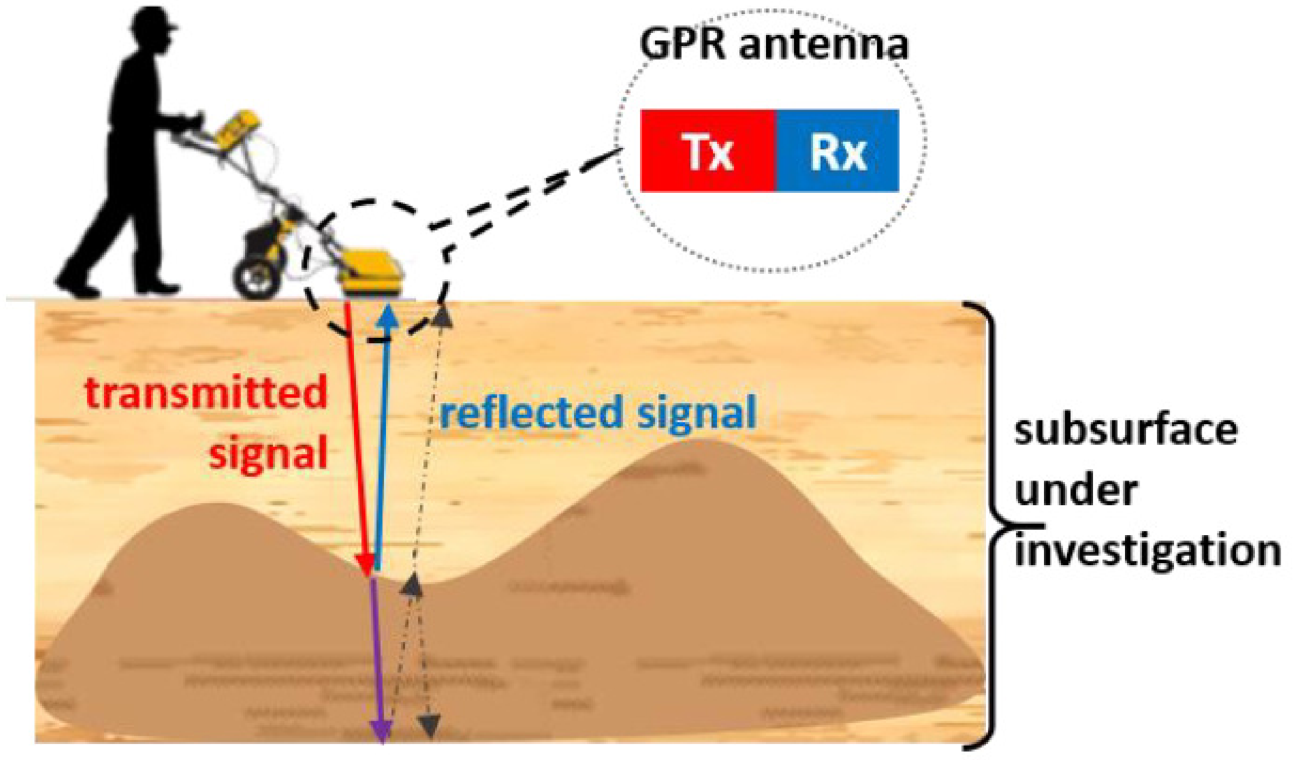

Fig. 1. Principles of GPR use

Department of Electronics
University of Split,
Split, Croatia

Ongoing work: FD and TD analyzes of the transient field generated by GPR dipole antenna

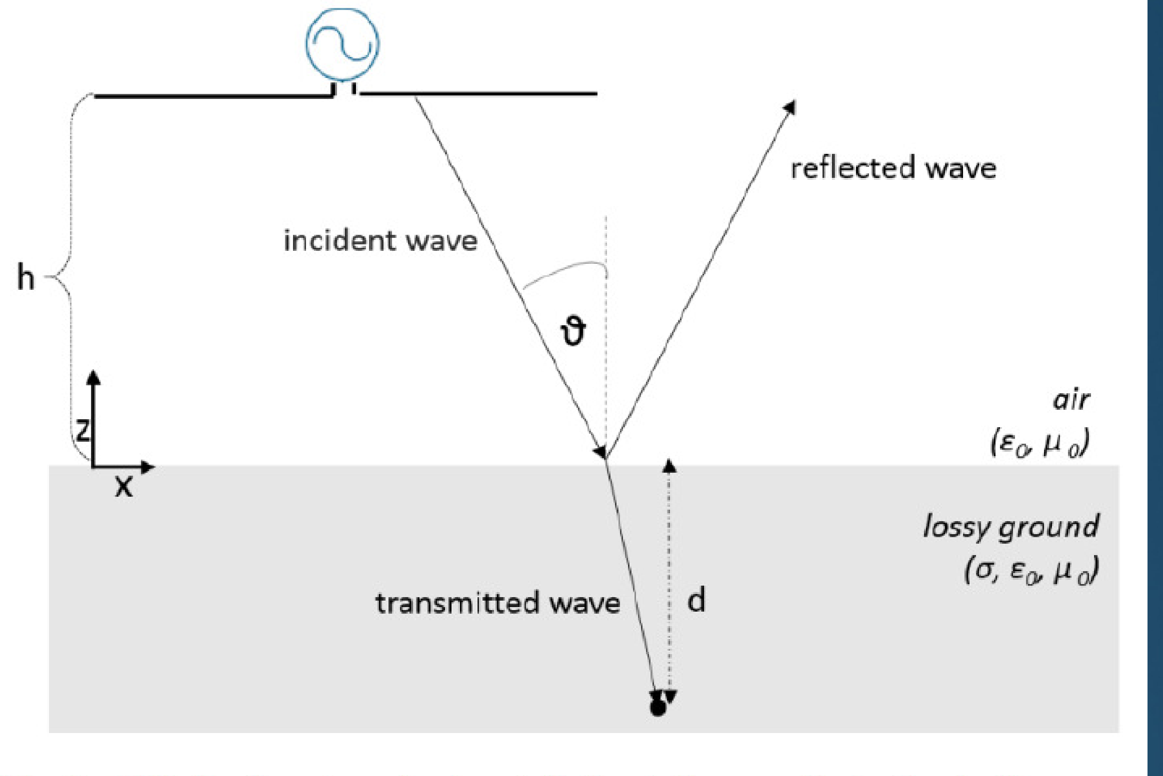

Fig. 2. GPR dipole antenna horizontally located over a dissipative half-space

Clermont-Ferrand, 03 April 2018

UNIVERSITÉ Clermont Auvergne

Department of Electronics
University of Split,
Split, Croatia

Ongoing work: FD formulation

- Reflected/transmitted field formulas:

$$E_x = \frac{1}{j4\pi\omega\varepsilon_{eff}}\left[-\int_{-L/2}^{L/2}\frac{\partial I(x')}{\partial x'}\frac{\partial g(x,y,z,x')}{\partial x}dx' - \gamma^2\int_{-L/2}^{L/2} \mathrm{I}(\mathrm{x}')\mathrm{g}(\mathrm{x},\mathrm{x}')\mathrm{dx}'\right]$$

$$E_y = \frac{1}{j4\pi\omega\varepsilon_{eff}}\int_{-L/2}^{L/2}\frac{\partial I(x')}{\partial x'}\frac{\partial g(x,y,z,x')}{\partial y}dx'$$

$$E_z = \frac{1}{j4\pi\omega\varepsilon_{eff}}\int_{-L/2}^{L/2}\frac{\partial I(x')}{\partial x'}\frac{\partial g(x,y,z,x')}{\partial z}dx'$$

$$g(x,x') = \frac{e^{-jk_0R_0}}{R_0} - R_{TM}\frac{e^{-jk_iR_i}}{R_i}$$

$$g(x,y,z,x') = T\cdot\frac{e^{-\gamma R_0}}{R_0}$$

$$R_{TM} = \frac{n\cos\vartheta - \sqrt{n-(\sin\vartheta)^2}}{n\cos\vartheta + \sqrt{n-(\sin\vartheta)^2}}$$

$$T = \Gamma_{TM} = \frac{2\sqrt{n}\cos\vartheta}{n\cos\vartheta + \sqrt{n-(\sin\vartheta)^2}}$$

$$\Gamma_{refl}^{MIT} = \frac{n-1}{n+1}$$

$$\Gamma_{trans}^{MIT} = \frac{2n}{n+1}$$

UNIVERSITÉ Clermont Auvergne

Department of Electronics
University of Split,
Split, Croatia

Ongoing work: TD formulation

- Reflected/transmitted field formulas:

$$E_x(r,t)=\frac{\mu_0}{4\pi}\left(\int_0^L \frac{\partial}{\partial t}\frac{I(x',t')}{R_1}dx'-\int_{-\infty}^{t}\Gamma_{ref}(\tau)\int_0^L \frac{\partial}{\partial t}\frac{I(x',t-\frac{R_1^*}{c}-\tau)}{R_1^*}dx'd\tau\right)$$

$$\Gamma_{ref}^{MIT}(t)=\frac{\tau_1}{\tau_2}\delta(t)+\frac{1}{\tau_2}\left(1-\frac{\tau_1}{\tau_2}\right)$$

$$\tau_1=\frac{\varepsilon_0(\varepsilon_r-1)}{\sigma}$$

$$\tau_2=\frac{\varepsilon_0(\varepsilon_r+1)}{\sigma}$$

$$E_x^{tr}(r,t)=\frac{\mu_0}{4\pi}\int_{-\infty}^{t}\int_0^L \Gamma_{tr}^{MIT}(\tau)\frac{\partial I(x',t-R''/v-\tau)}{\partial t}\frac{e^{-\frac{1}{\tau_g}\frac{R''}{v}}}{R''}dx'd\tau$$

$$\Gamma_{tr}(t)=\frac{\tau_3}{\tau_2}\delta(t)+\frac{1}{\tau_2}\left(2-\frac{\tau_3}{\tau_2}\right)e^{-\frac{t}{\tau_2}}$$

$$R_1^*=\sqrt{(x-x')^2+(2h+z)^2}$$

$$R''=\sqrt{(x-x')^2+(z+h)^2}$$

$$\tau_2=\frac{\varepsilon_r+1}{\sigma}\varepsilon_0,\ \tau_3=\frac{2\varepsilon}{\sigma}$$

UNIVERSITÉ Clermont Auvergne

Department of Electronics
University of Split,
Split, Croatia

Ongoing work: Numerical results

A The field above the lossy ground

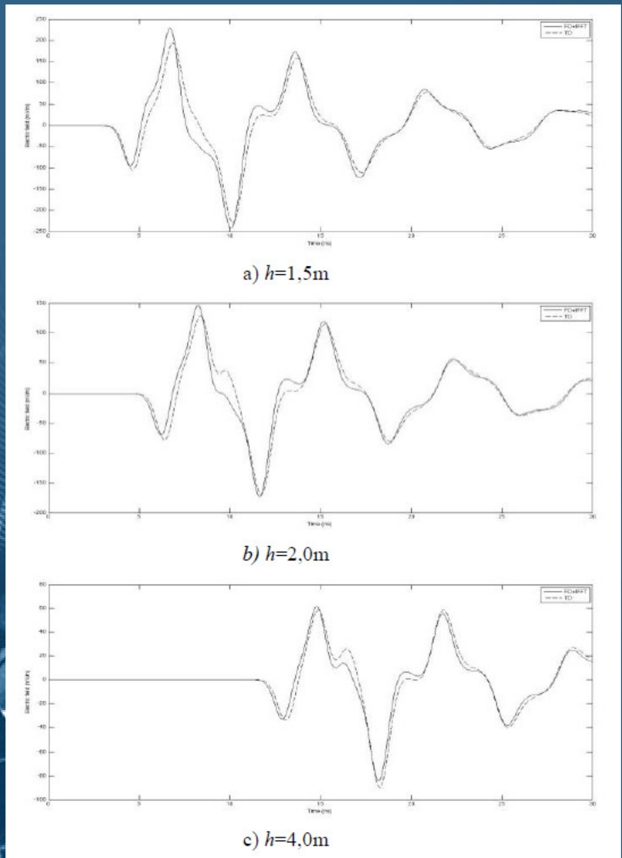

Fig. 3. Radiated field above a lossy half-space (ε_r=10, σ=1mS/m)

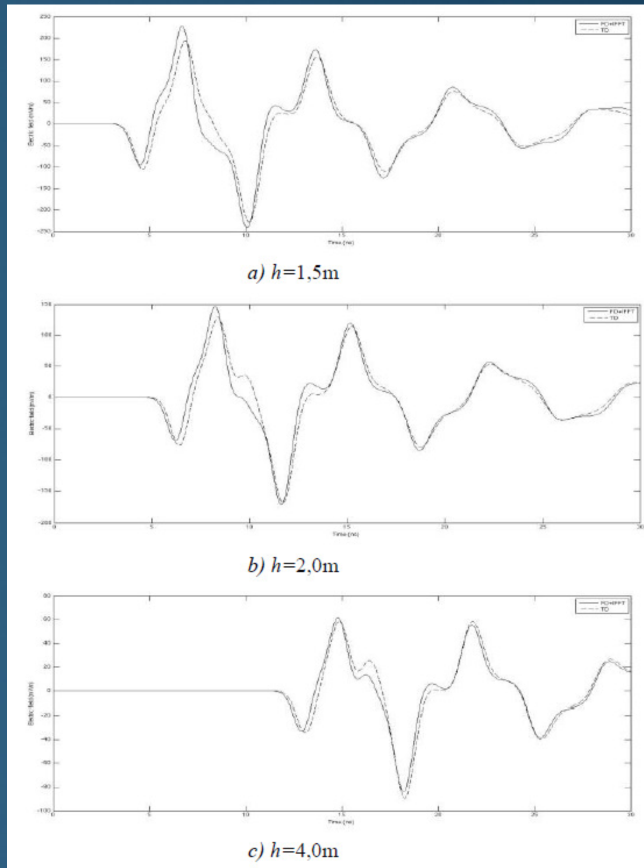

Fig. 4. Radiated field above a lossy half-space (ε_r=10, σ=10mS/m)

Department of Electronics
University of Split,
Split, Croatia

Ongoing work: Numerical results

B The field propagating into the lossy ground

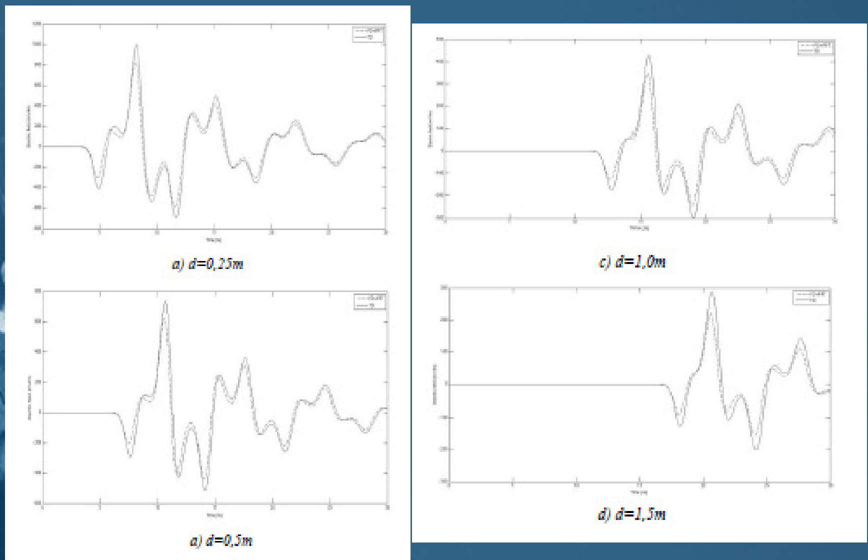

Fig. 5.Transmitted field into soil ($\varepsilon_r=10$, $\sigma=1mS/m$)

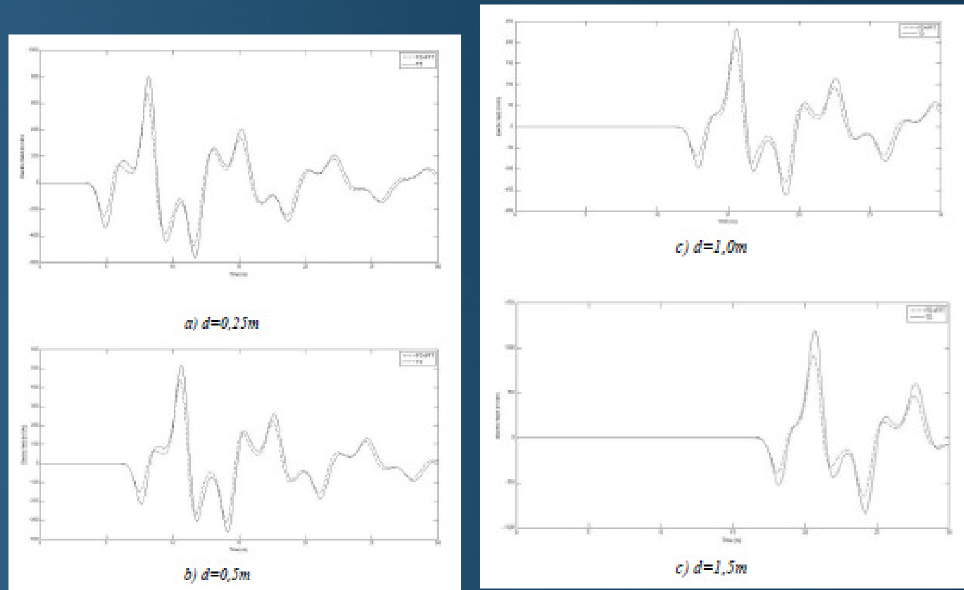

Fig. 6. Transmitted field into soil ($\varepsilon_r=10$, $\sigma=10mS/m$)

UNIVERSITÉ Clermont Auvergne

CROATIAN RESEARCH UNIT

Department of Electronics
University of Split,
Split, Croatia

Ongoing work : Determinsitic modeling

ICES
IEEE
International Committee on Electromagnetic Safety

WG2: Numerical Artifacts

On-going WG 2 Activities

Table 1: Smoothed geometry parameters

Geometry	Points	Triangles	Tetrahedra
sphere_199_244_809	199	244	809
sphere_406_494_1690	406	494	1690
sphere_803_734_3815	803	734	3815
sphere_1081_976_5194	1081	976	5194
brain_250	232	360	814
brain_500	483	696	1871
brain_800	885	1224	3542
brain_1200	1405	1870	5771

Table 2: TMS coil parameters

	Circular	Figure-8	Inclined
Radius [cm]	4.5	3.5	3.5
Turns [-]	14	15	15
Current [kA]	2.843	2.843	2.843

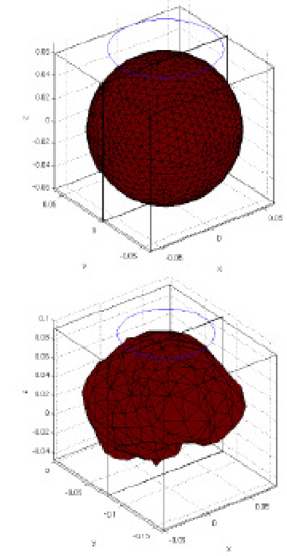

Fig. 1. Homogeneous sphere model and realistic brain geometry

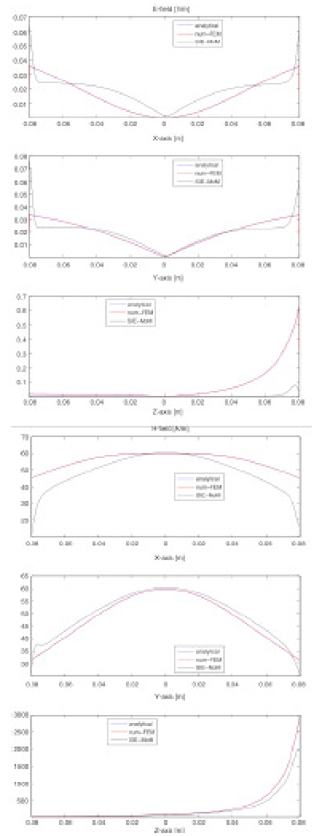

IEEE/ICES TC95 - Subcommittee 6: EMF Dosimetry Modeling
January 2017, Plantation, FL, USA

10

UNIVERSITÉ Clermont Auvergne

Department of Electronics
University of Split,
Split, Croatia

Ongoing work : Determinsitic modeling

ICES

IEEE

International Committee on Electromagnetic Safety

WG2: Numerical Artifacts

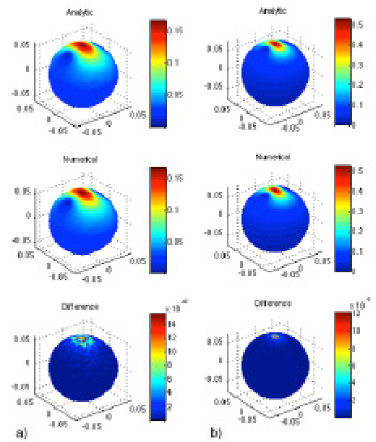

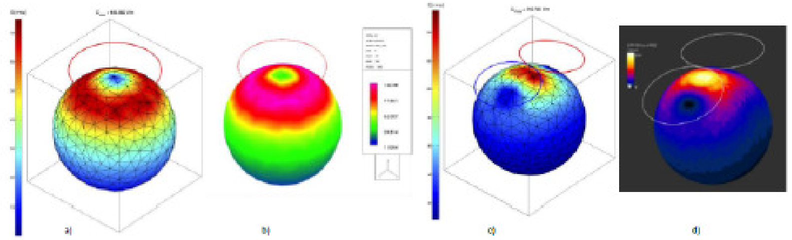

Fig. 8. Maps of the induced electric field over the sphere surface, due to circular coil a)-b) and butterfly coil c)-d). Results obtained by a) and c) SIE/MoM for smoothed surface comprising of 976 triangles, b) approximate EM solution using BEM (E as unknowns, B imposed by the source), and d) FEM using grid resolution of 0.5 mm.

Table 4 Comparison of maximum induced electric field (V/m) obtained using different numerical models for the case of cirular coil and spherical geometry

Surface, conforming				Voxels, nonconforming		Surface, conforming	
Triangles	BEM complete	BEM approximate	Voxels	FEM/BEM complete	FEM/BEM approximate	Triangles	SIE
244	83,394	88,093	**854 (10mm)**	69,300	55,217	**244**	98,8401
494	90,013	89,598	**1718 (8mm)**	70,050	70,102	**494**	105,5986
734	90,546	91,691	**4105 (6mm)**	92,204	92,199	**734**	105,6624
976	92,022	92,357	**5347 (5.5mm)**	84,786	84,778	**976**	108,2849

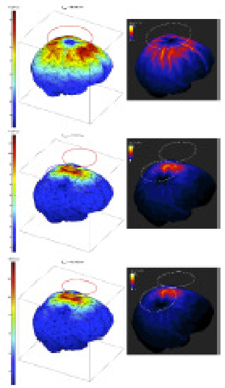

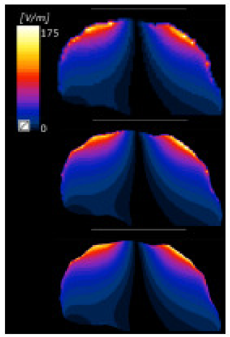

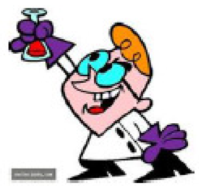

IEEE/ICES TC95 - Subcommittee 6: EMF Dosimetry Modeling
January 2017, Plantation, FL, USA

11

Department of Electronics
University of Split,
Split, Croatia

Ongoing work : Determinsitic modeling

- Non-homogeneous head model

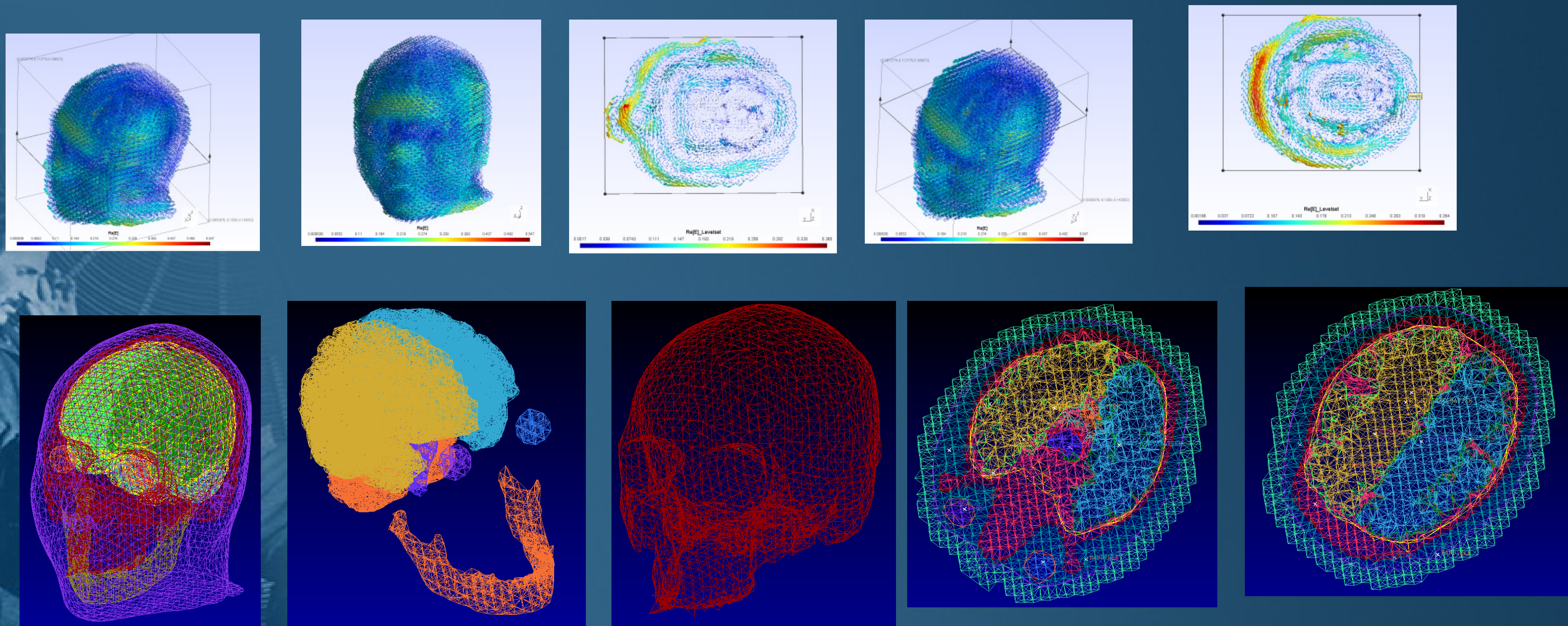

UNIVERSITÉ Clermont Auvergne

Department of Electronics
University of Split,
Split, Croatia

Ongoing work : Determinsitic modeling

- Non-homogeneous head model

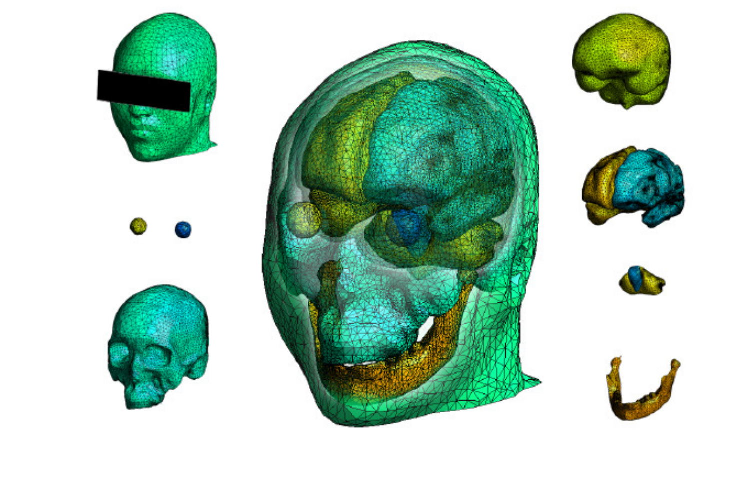

Figure 2: Model of the human head with insets showing different subdomains (tissues).

Table 1: Tissue dielectric parameters according to the 4-Cole-Cole Model described in [14]

	900 MHz		1800 MHz	
Tissue	σ (S/m)	ε (-)	σ (S/m)	ε (-)
Brainstem	0.591	38.886	0.915	37.011
Cerebellum	1.263	49.444	1.709	46.114
Eye (vitreous)	1.636	68.902	2.032	68.573
Head skin	0.867	41.405	1.185	38.872
Skull and mandible	0.339	20.788	0.588	19.343
Grey matter	0.942	52.725	1.391	50.079
Muscle tissue	0.943	55.032	1.341	53.549

Department of Electronics
University of Split,
Split, Croatia

Ongoing work : Determinsitic modeling

- Non-homogeneous head model

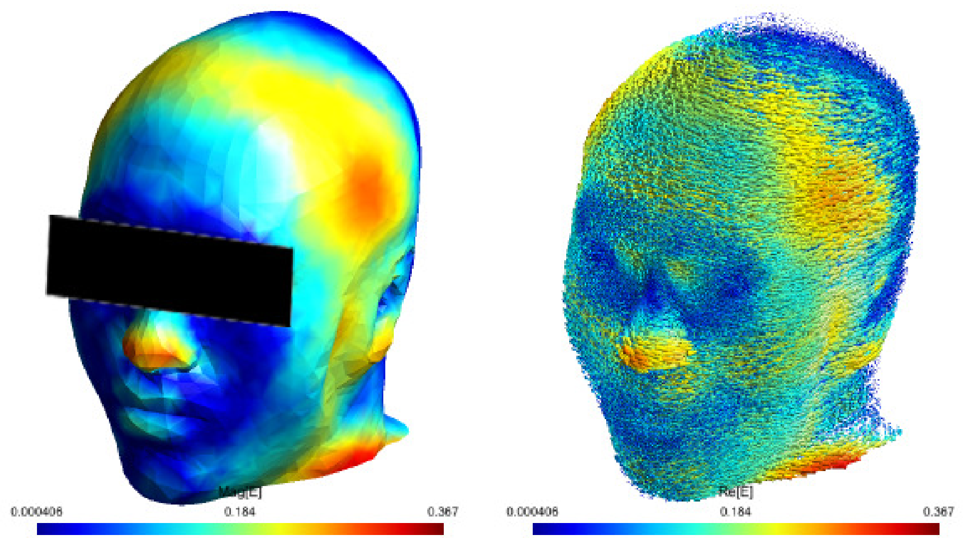

Figure 3: Electric field induced on the surface of the human head model due to 900 MHz horizontally polarized plane wave a). Direction of the electric field b).

Université Clermont Auvergne

Department of Electronics
University of Split,
Split, Croatia

Ongoing work : Determinsitic modeling

- Non-homogeneous head model

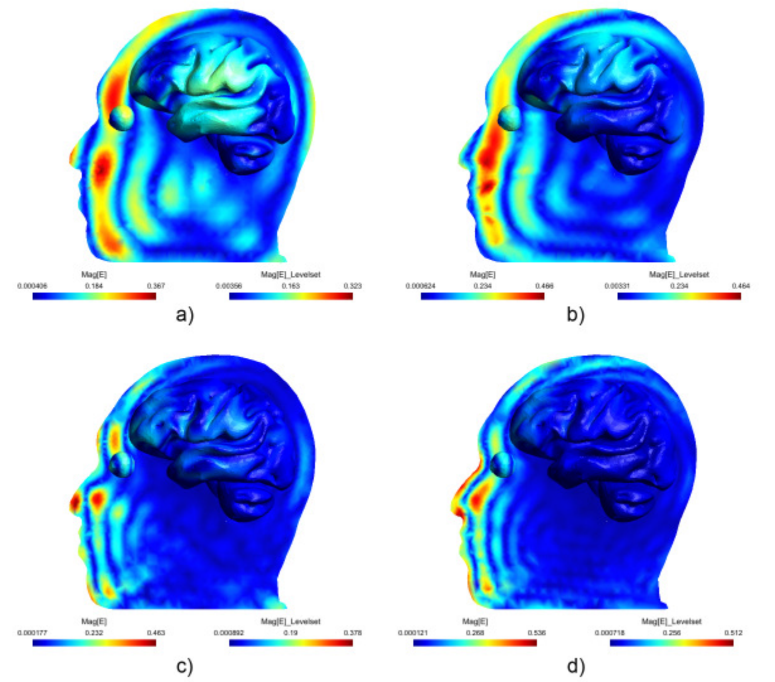

Figure 4: Induced electric field in the sagittal cross-section of the head due to: a) 900 MHz HP, b) 900 MHz VP, c) 1800 MHz HP, d) 1800 MHz VP.

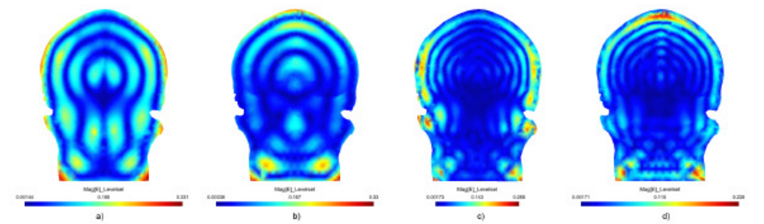

Figure 5: Induced electric field in the coronal cross-section of the head due to: a) 900 MHz HP, b) 900 MHz VP, c) 1800 MHz HP, d) 1800 MHz VP.

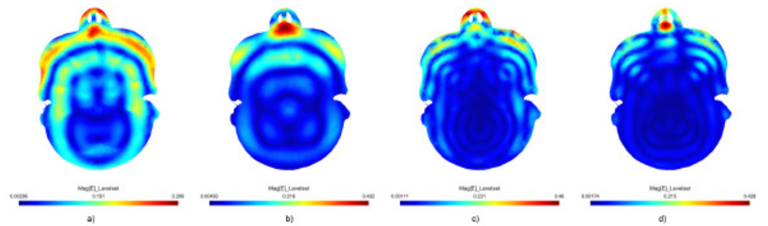

Figure 6: Induced electric field in the transverse cross-section of the head due to: a) 900 MHz HP, b) 900 MHz VP, c) 1800 MHz HP, d) 1800 MHz VP.

Department of Electronics
University of Split,
Split, Croatia

Ongoing work : Determinsitic modeling

- Non-homogeneous head model

Hindawi
Mathematical Problems in Engineering
Volume 2017, Article ID 7932604, 12 pages
https://doi.org/10.1155/2017/7932604

Research Article

A Study on the Use of Compound and Extracted Models in the High Frequency Electromagnetic Exposure Assessment

Mario Cvetković,[1] Hrvoje Dodig,[2] and Dragan Poljak[1]

[1] *Faculty of Electrical Engineering, Mechanical Engineering and Naval Architecture, University of Split, R. Boškovića 32, 21000 Split, Croatia*
[2] *Faculty of Maritime Studies, University of Split, R. Boškovića 37, 21000 Split, Croatia*

Table 1: Tissue parameters used in eye and head models.

Tissue	900 MHz		1800 MHz		ρ (g/m^3)
	σ (S/m)	ε (-)	σ (S/m)	ε (-)	
Brainstem	0.622	38.577	0.915	37.011	1043
Cerebellum	1.308	48.858	1.709	46.114	1039
Head skin	0.899	40.936	1.185	38.872	1050
Liquor	1.667	68.875	2.032	68.573	1035
Skull	0.364	20.584	0.588	19.343	1900
Mandible	0.364	20.584	0.588	19.343	1900
Grey matter	0.985	52.282	1.391	50.079	1039
Anterior chamber	1.667	68.875	2.032	68.573	1003
Choroid	0.729	44.561	1.066	43.343	1000
Ciliary body	0.978	54.811	1.341	53.549	1040
Cornea	1.438	54.835	1.858	52.768	1076
Iris	0.978	54.811	1.341	53.549	1040
Ligaments	0.760	45.634	1.201	44.252	1000
Ora serrata	0.882	45.711	1.232	43.850	1000
Posterior chamber	1.667	68.875	2.032	68.573	1000
Retina	1.206	55.017	1.602	53.568	1039
Sclera	1.206	55.017	1.602	53.568	1076
Vitreous body	1.667	68.875	2.032	68.573	1009
Lens-I	0.824	46.399	1.147	45.353	1100
Lens-II	0.824	47.011	1.147	45.925	1100
Lens-III	0.824	47.694	1.147	46.221	1100
Lens-IV	0.824	48.383	1.147	46.883	1100
Lens-V	0.824	49.076	1.147	47.554	1100

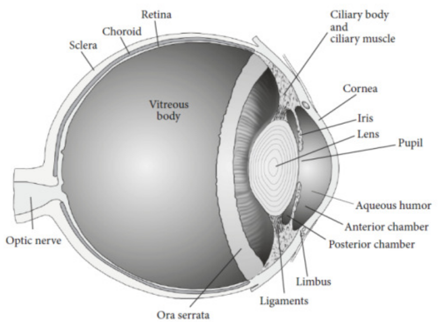

Figure 1: Sagittal cross-section of the human eye depicting various tissues.

Clermont-Ferrand, 03 April 2018

Université Clermont Auvergne

Department of Electronics
University of Split,
Split, Croatia

Ongoing work : Determinsitic modeling

- Non-homogeneous head model

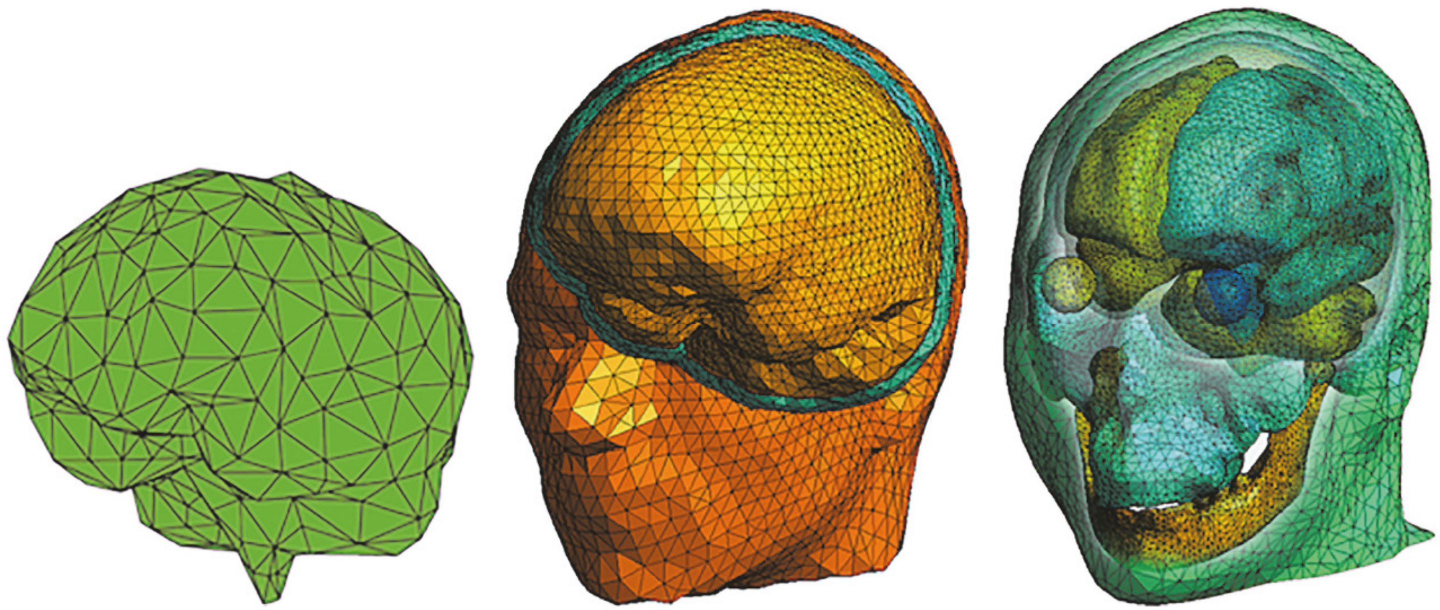

(a) (b) (c)

FIGURE 3: Models for the brain comparison: (a) homogeneous brain model, (b) three-compartment head model, and (c) compound model. Overlay on two latter models is showing various head tissues surrounding the brain.

UNIVERSITÉ Clermont Auvergne

Department of Electronics
University of Split,
Split, Croatia

Ongoing work : Determinsitic modeling

- Non-homogeneous head model

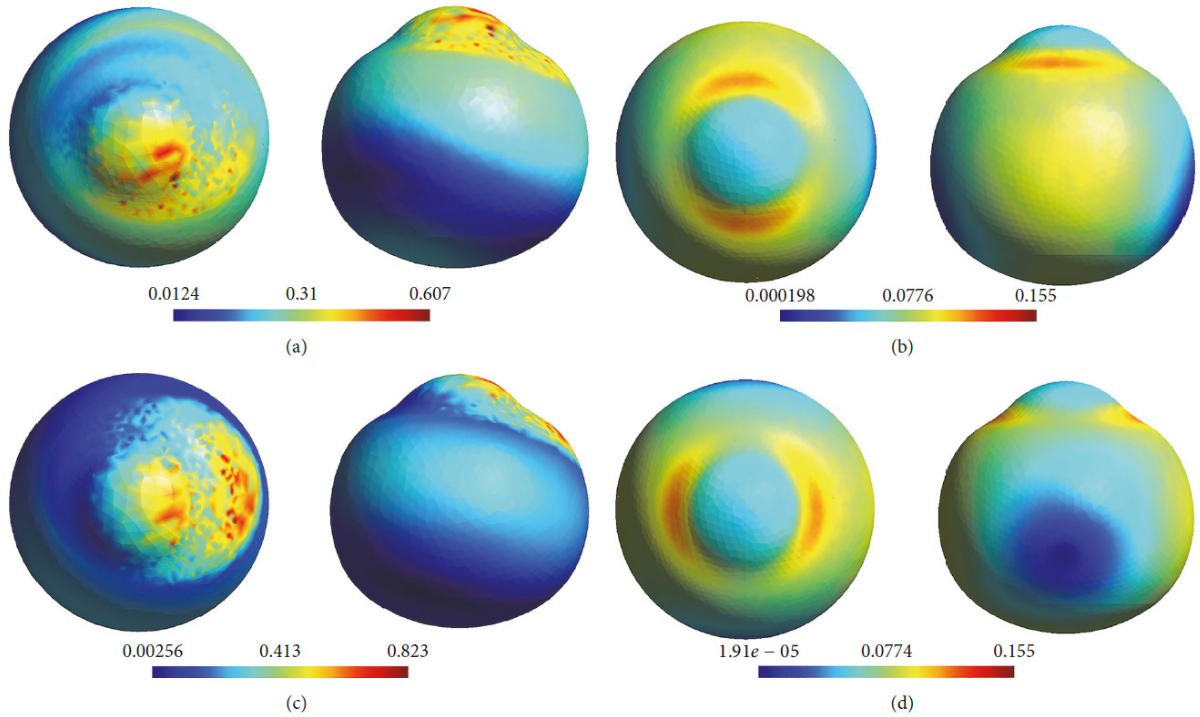

FIGURE 4: Induced electric field due to 1 GHz EM wave on the surface of the eye (anterior and top view). (a, c) Compound eye model: (a) horizontal polarization and (c) vertical polarization. (b, d) Extracted eye model: (b) horizontal polarization and (d) vertical polarization.

Department of Electronics
University of Split,
Split, Croatia

Ongoing work : Determinsitic modeling

- Non-homogeneous head model

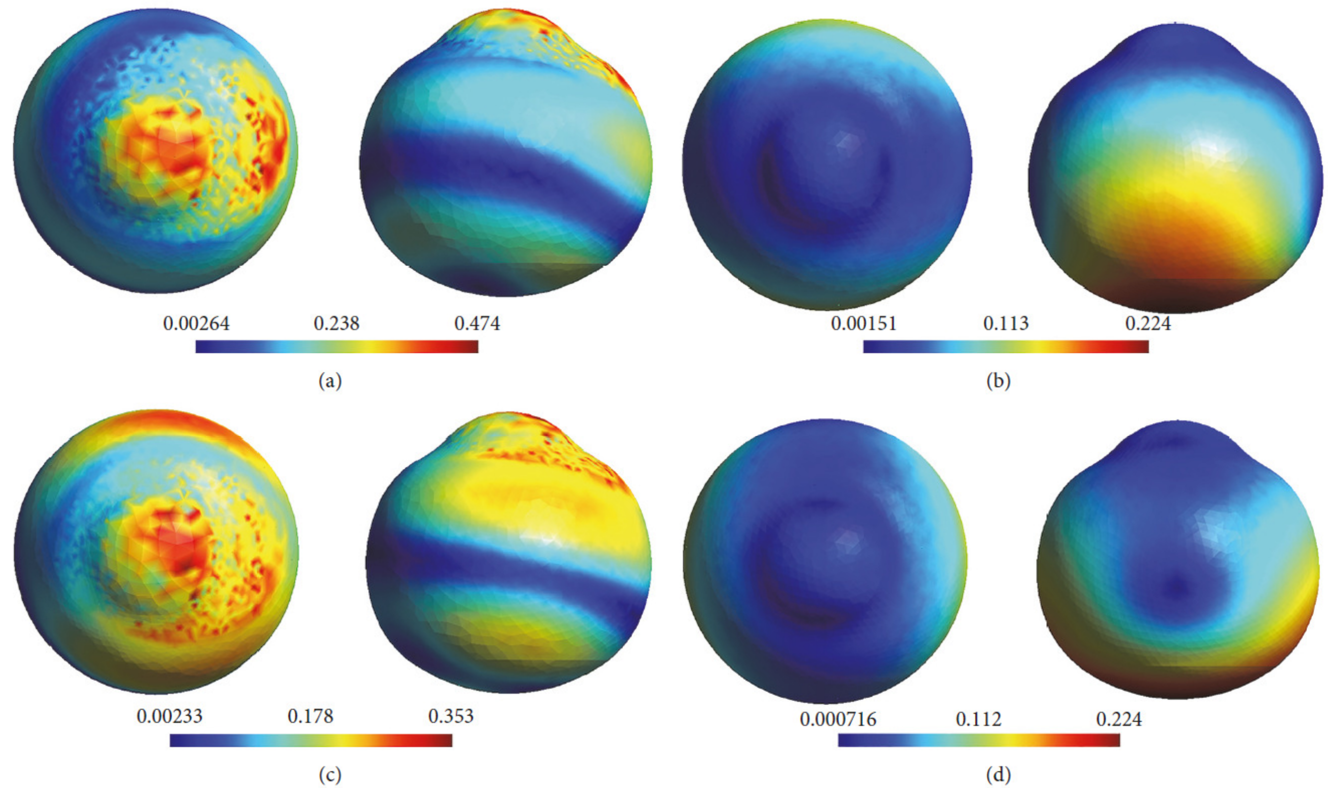

FIGURE 5: Induced electric field due to 1800 MHz EM wave on the surface of the eye (anterior and top view). (a, c) Compound eye model: (a) horizontal polarization and (c) vertical polarization. (b, d) Extracted eye model: (b) horizontal polarization and (d) vertical polarization.

UNIVERSITÉ Clermont Auvergne

Department of Electronics
University of Split,
Split, Croatia

Ongoing work : Determinsitic modeling

- Non-homogeneous head model

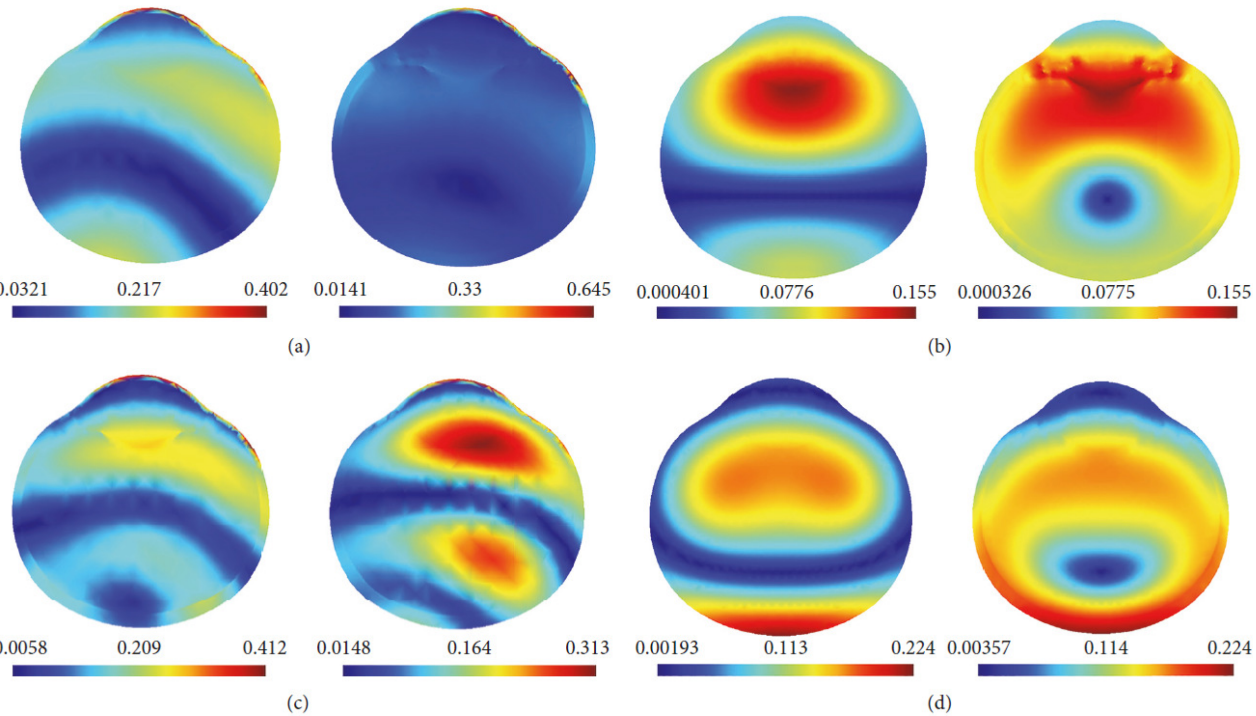

FIGURE 6: Induced electric field in the transverse cross-section of the compound eye model (a, c) and the extracted eye model (b, d). Incident EM wave of (a) and (b) 1 GHz horizontal (left) and vertical (right) polarization and (c) and (d) 1800 MHz horizontal (left) and vertical (right) polarization.

Department of Electronics
University of Split,
Split, Croatia

Ongoing work : Determinsitic modeling

- Non-homogeneous head model

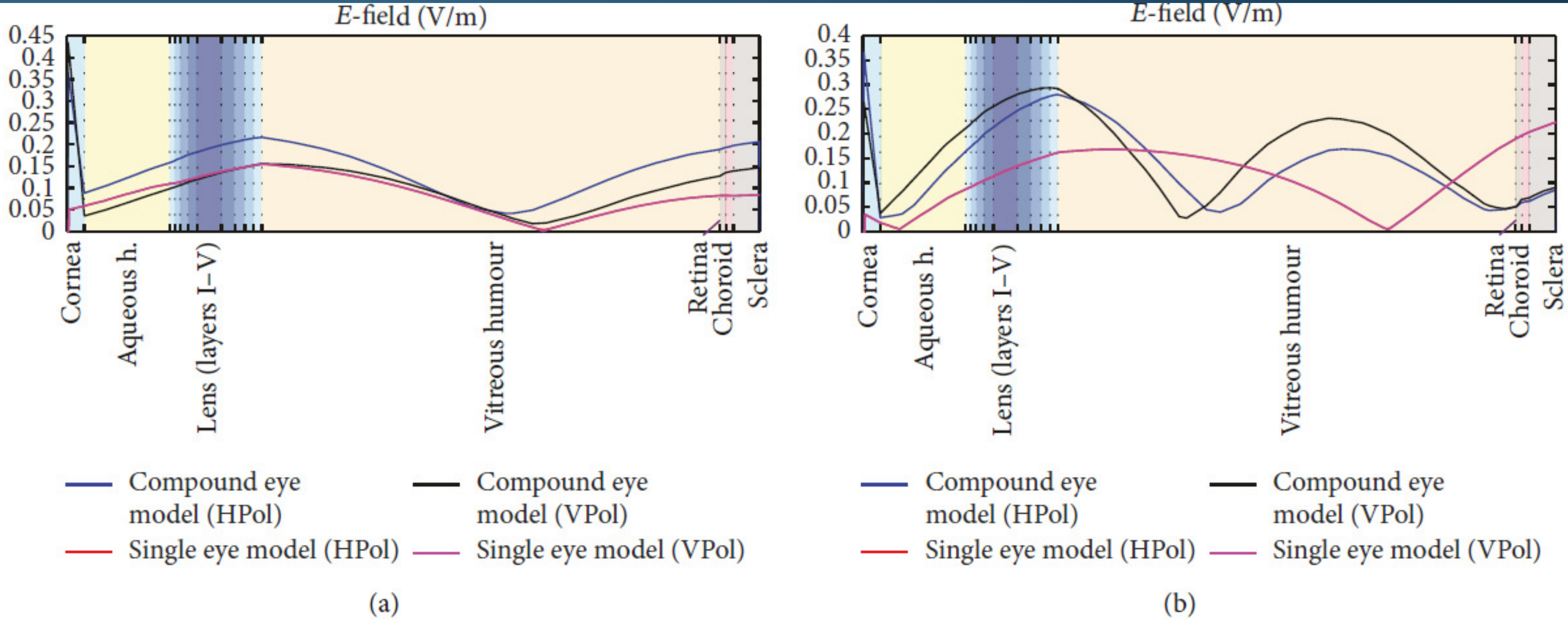

FIGURE 7: Comparison of the induced electric field along the pupillary axis of the compound and the extracted eye models, respectively, (a) 1 GHz, both polarizations; (b) 1800 MHz, both polarizations.

Université Clermont Auvergne

Department of Electronics
University of Split,
Split, Croatia

UNIVERSITÉ Clermont Auvergne

Ongoing work : Determinsitic modeling

- Non-homogeneous head model

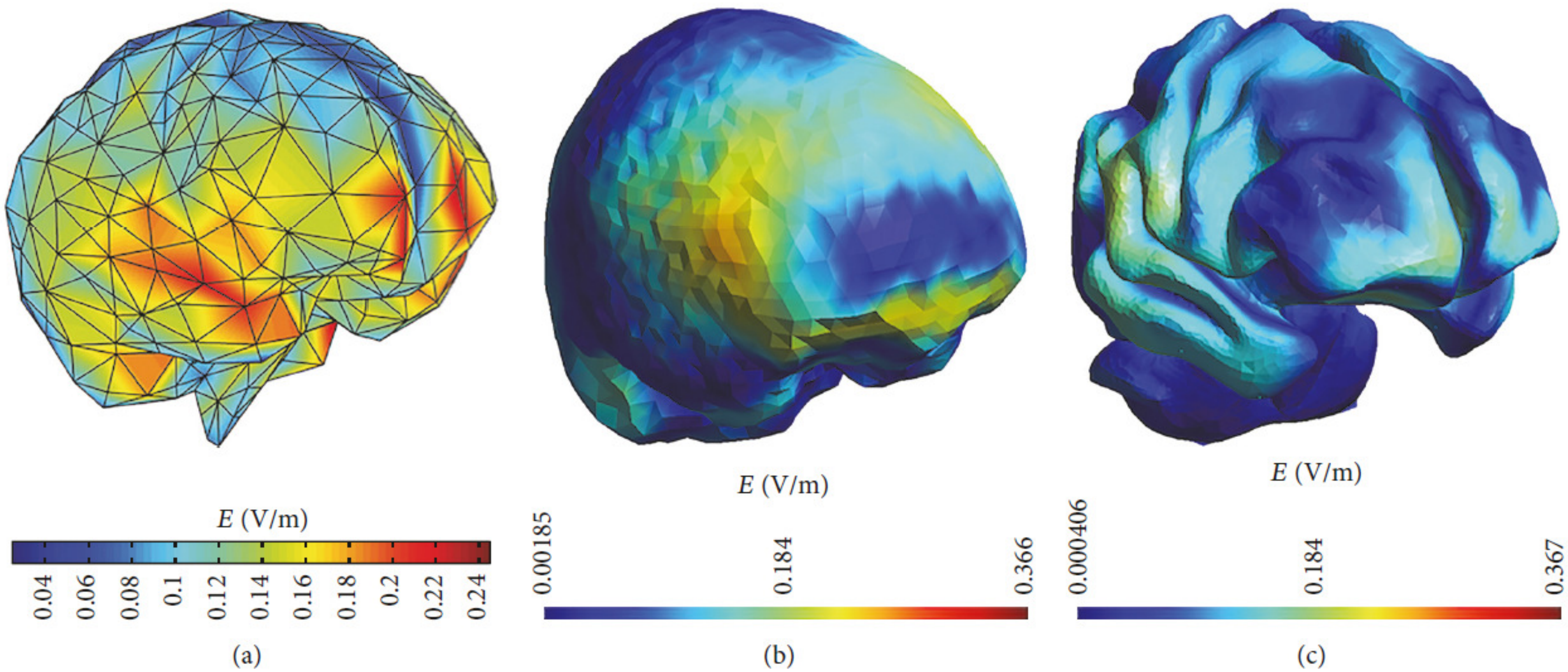

FIGURE 8: Induced electric field on the surface of the brain due to 900 MHz horizontally polarized EM wave: (a) homogeneous model, (b) three-compartment model, and (c) compound model.

Department of Electronics
University of Split,
Split, Croatia

Ongoing work : Determinsitic modeling

- Non-homogeneous head model

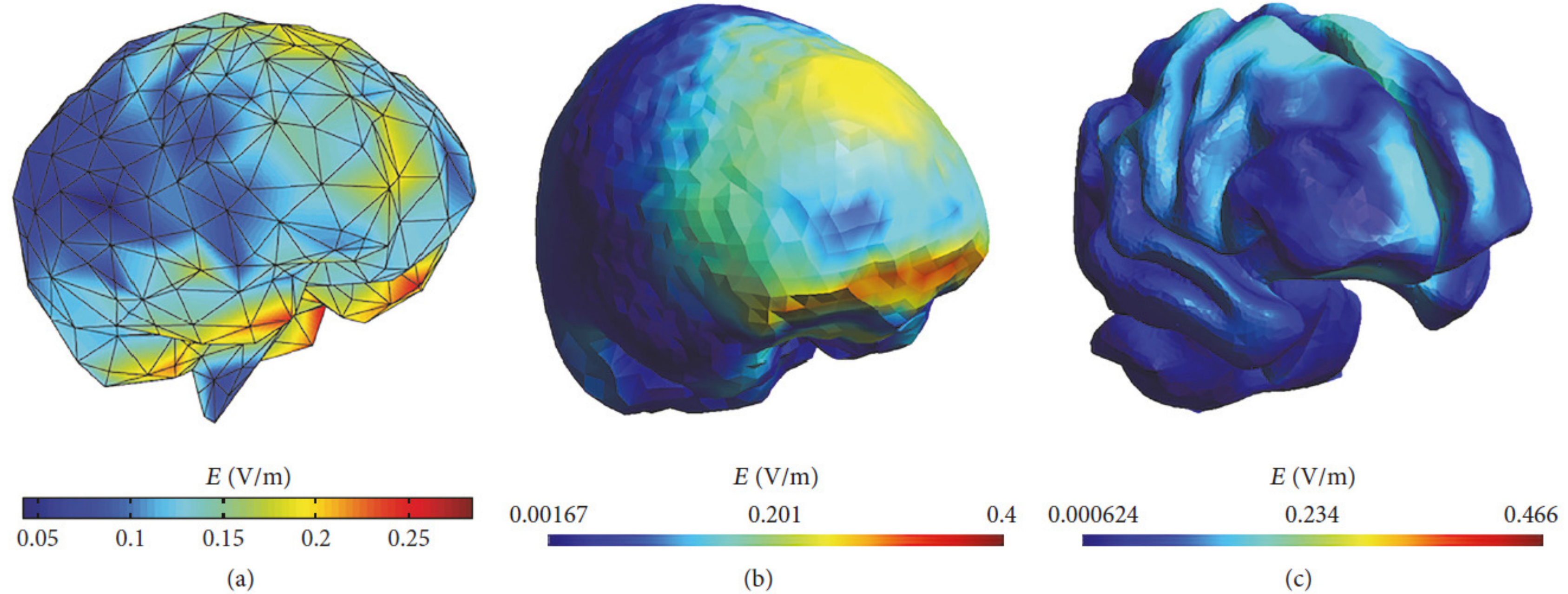

FIGURE 9: Induced electric field on the surface of the brain due to 900 MHz vertically polarized EM wave: (a) homogeneous model, (b) three-compartment model, and (c) compound model.

Department of Electronics
University of Split,
Split, Croatia

Ongoing work : Determinsitic modeling

- Non-homogeneous head model

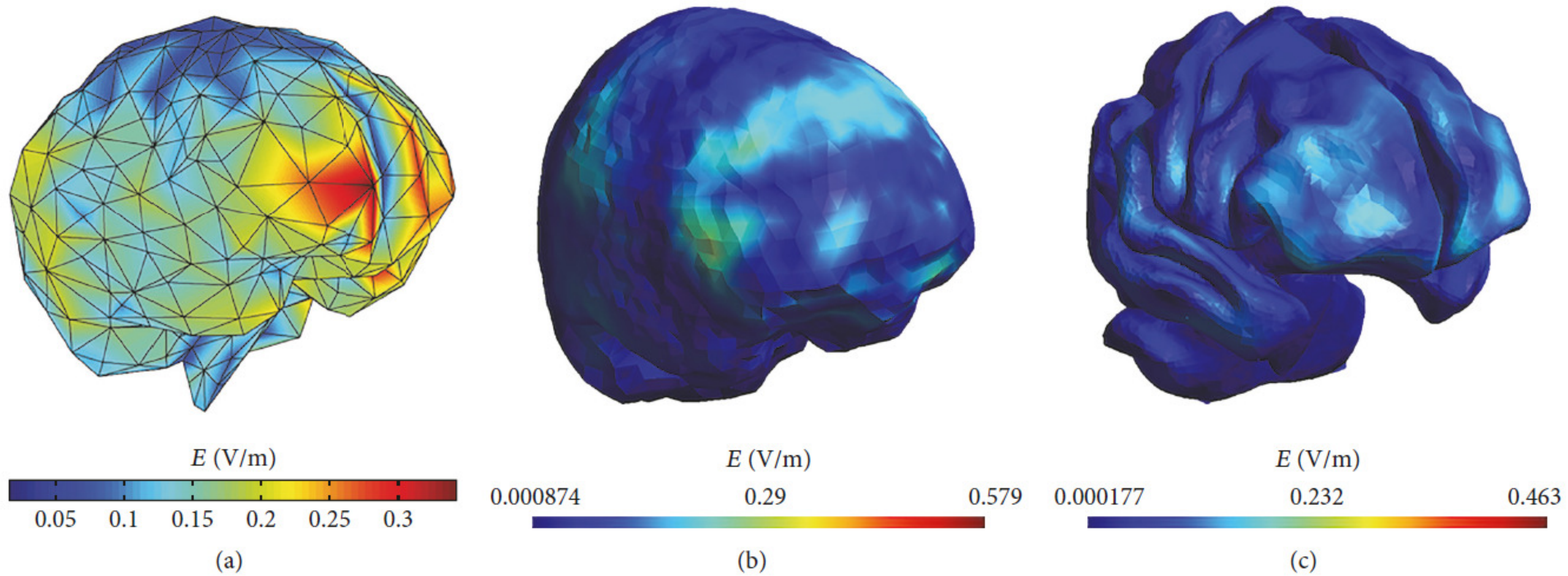

FIGURE 10: Induced electric field on the surface of the brain due to 1800 MHz horizontally polarized EM wave: (a) homogeneous model, (b) three-compartment model, and (c) compound model.

Department of Electronics
University of Split,
Split, Croatia

Ongoing work : Determinsitic modeling

- Non-homogeneous head model

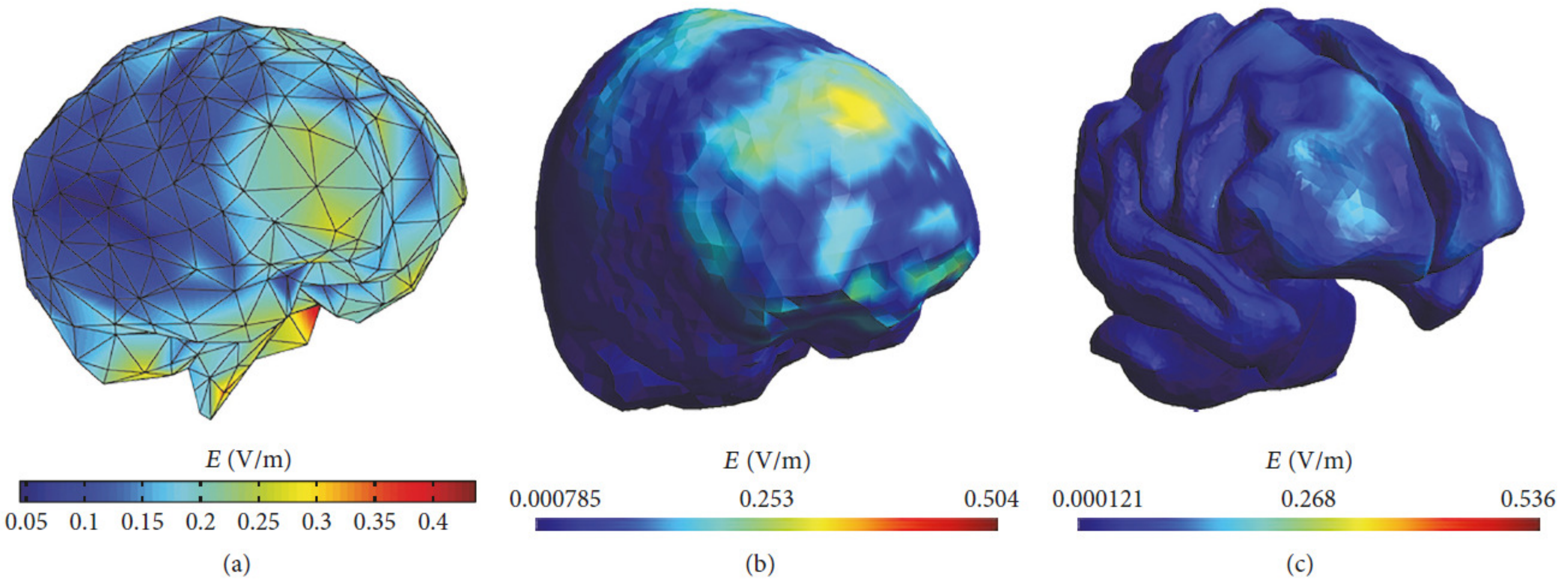

FIGURE 11: Induced electric field on the surface of the brain due to 900 MHz vertically polarized EM wave: (a) homogeneous model, (b) three-compartment model, and (c) compound model.

Department of Electronics
University of Split,
Split, Croatia

Ongoing work : Determinsitic modeling

- Non-homogeneous head model

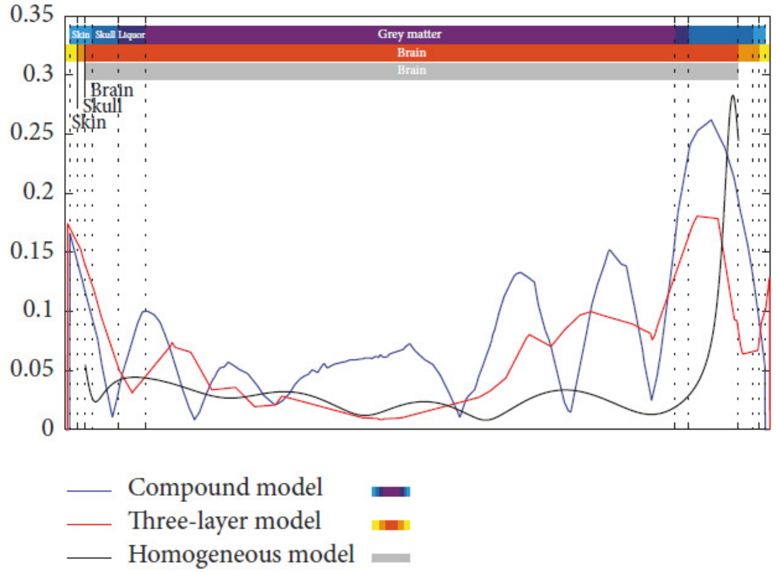

FIGURE 12: Comparison of the induced electric field along the sagittal axis of the homogeneous, the three-compartment, and the compound models, respectively, due to 900 MHz EM wave, horizontal polarization, and incident on the anterior side.

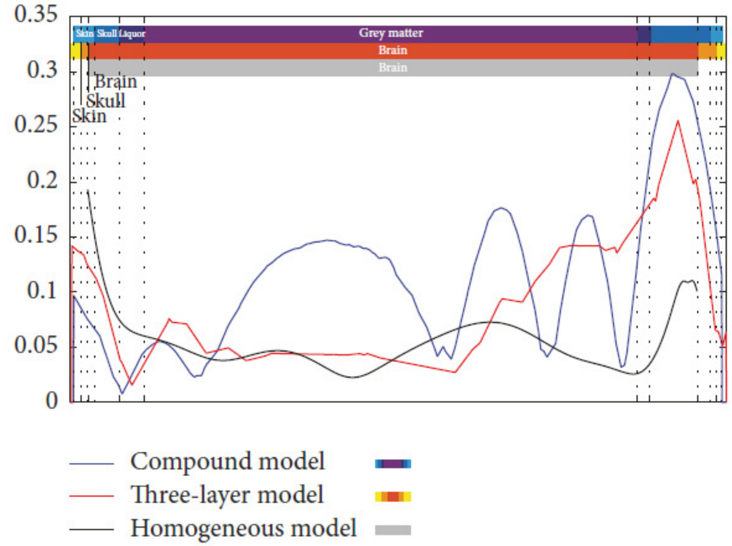

FIGURE 13: Comparison of the induced electric field along the sagittal axis of the homogeneous, the three-compartment, and the compound models, respectively, due to 900 MHz EM wave, vertical polarization, and incident on the anterior side.

Department of Electronics
University of Split,
Split, Croatia

Ongoing work : Determinsitic modeling

- Non-homogeneous head model

Mathematical Problems in Engineering

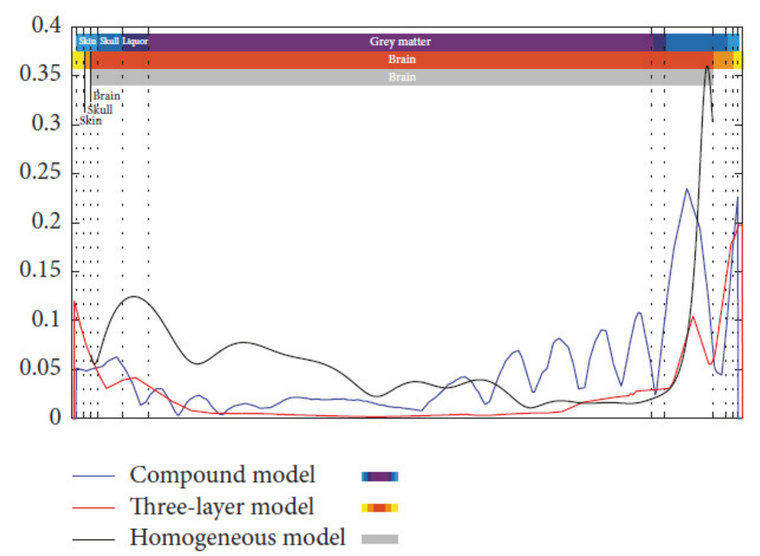

FIGURE 14: Comparison of the induced electric field along the sagittal axis of the homogeneous, the three-compartment, and the compound models, respectively, due to 1800 MHz EM wave, horizontal polarization, and incident on the anterior side.

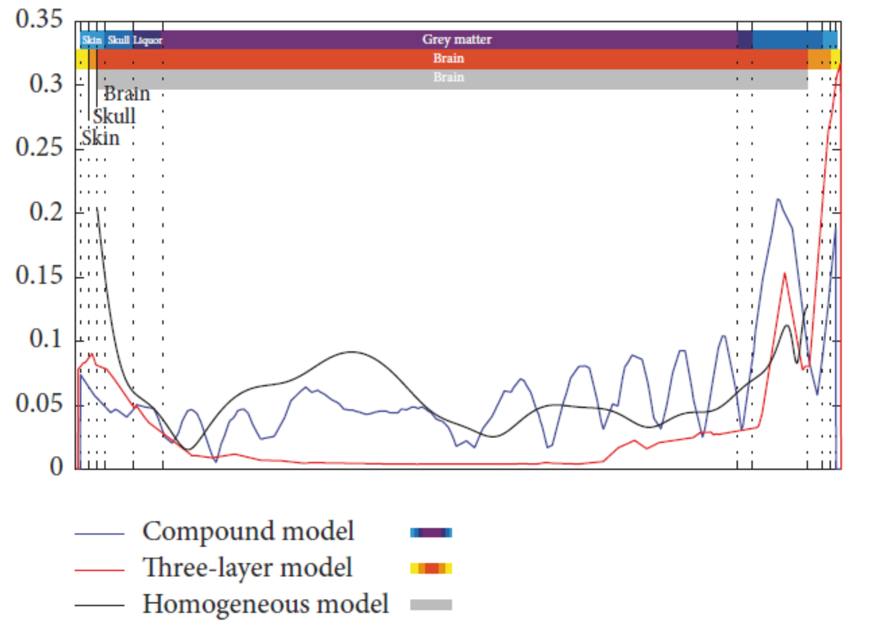

FIGURE 15: Comparison of the induced electric field along the sagittal axis of the homogeneous, the three-compartment, and the compound models, respectively, due to 1800 MHz EM wave, vertical polarization, and incident on the anterior side.

UNIVERSITÉ Clermont Auvergne

Department of Electronics
University of Split,
Split, Croatia

Ongoing work : stochastic electromagnetics

Possible future work of Croatian team for fusion...?

EUROfusion

UNCERTAINTY QUANTIFICATION (UQ)

- Generally, there is a need for uncertainty quantification:
- Sources of uncertainty (environmental facts, unknown or partially known input data, geometry variations and variations in material properties)
- Monte Carlo simulation allows the assessment of a large number of virtual systems relying on various scenarios of the input parameters.

- Advantages:
  - universal method, i.e. it does not depend on the model type
  - statistically well defined: convergence, confidence intervals, ...
  - non intrusive, i.e. it is based on repeated runs of the model
  - convenient for distributed computing (clusters of PCs)
- Drawbacks:
  - Scattering of output is investigated point-by-point.
  - The convergence rate is low.

Department of Electronics
University of Split,
Split, Croatia

Ongoing work : stochastic electromagnetics

- We have used an efficient stochastic collocation (SC) formalism to accurately account for uncertainties and to assess confidence intervals in the set of obtained numerical results.

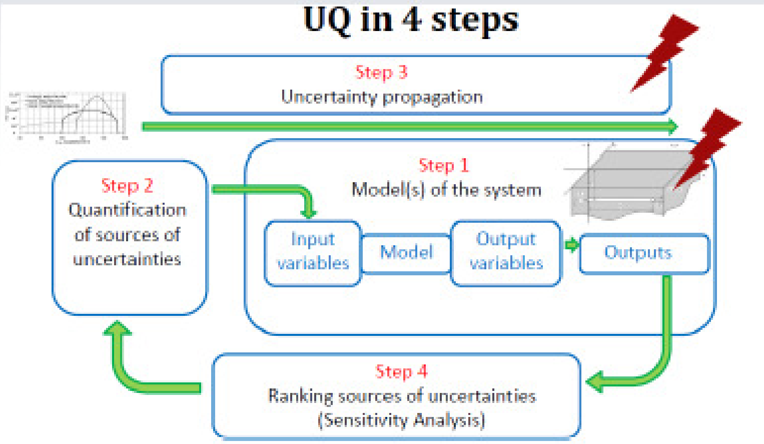

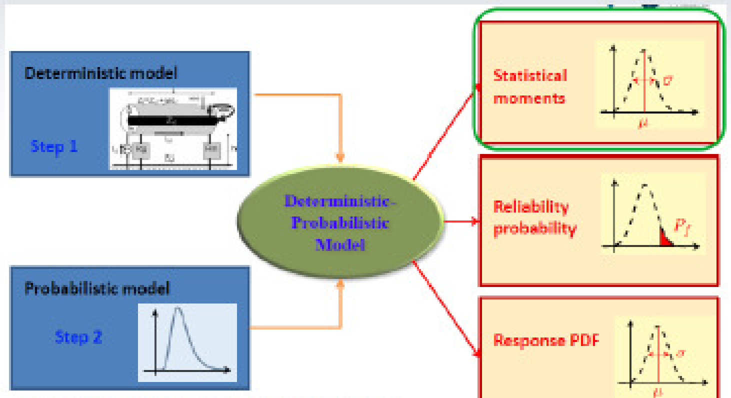

Sudret, Uncertainty propagation and sensitivity analysis in mechanical models, HDR, 2007

- So far, we have applied the method in the areas such as:
  - Ground Penetrating Radar (GPR)
  - Electromagnetic-thermal dosimetry
  - Biomedical applications of EM fields
  - Buried lines
  - Grounding systems
  - Instrumental landing systems for air traffic control applications

Department of Electronics
University of Split,
Split, Croatia

Ongoing work : stochastic electromagnetics

- **Heuristic**
  - Instead of considering the random output Y = M(X) through samples, Y is represented by a series expansion

$$Y = \sum_{j=0}^{+\infty} y_j Z_j$$

where:

Sudret, PCE Theory, Numerical Methods & Applications Parts I & II, MNMUQ, 2014

- $\{Z_j\}_{j=0}^{+\infty}$ is a numerable set of random variables that forms a basis of a suitable space $\mathcal{H} \supset Y$
- $\{y_j\}_{j=0}^{+\infty}$ is the set of coordinates of Y in this basis

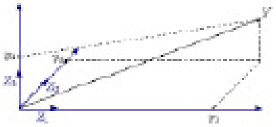

- **Actually**
  - Truncated series expansion
  - EMC illustration: Y = current I

Random N-vector: $\mathbf{X} = (X_1, X_2, \ldots, X_N)$

Polynomial basis: $\Phi^{\nu}(\mathbf{X})$ function of $\mathbf{X}$

$$\boxed{[I]_{\nu}(\mathbf{X}) \approx \sum_{\nu_1=0}^{n_1} \cdots \sum_{\nu_N=0}^{n_N} \eta_{\nu}^{\nu_1 \cdots \nu_N} \Phi^{\nu}(\mathbf{X})}$$

Expansion coefficient: $\eta_{\nu}^{\nu_1 \cdots \nu_N}$

Basic idea: close to PCE (spectral method) → choice of polynomial basis

Finding a polynomial approximation of the function of a real variable

$$f(x) = \frac{1}{1+x^2}$$

Lagrange polynomials

$$f(x) \approx \sum_{i=0}^{n} f_i L_i(x)$$

$\{L_i(x)\}_{0 \le i \le n}$ nth order polynomial basis

$$L_i(x) = \prod_{\substack{j=0 \\ j \ne i}}^{n} \frac{x - x_j}{x_i - x_j}$$

We can demonstrate:

$$\boxed{f_i = f(x_i)}$$

Finding a polynomial approximation of the function of a random variable:

$$f(X) = \frac{1}{1+X^2}$$

Lagrange polynomials

$$f(X) \approx \sum_{i=0}^{n} f_i L_i(X)$$

$\Downarrow$

Stochastic collocation method

Problem:

$$p(x) = \frac{1}{\sqrt{2\pi}} e^{-\frac{x^2}{2}} \qquad \boxed{Y = f(X)}$$

Bonnet et al., *Numerical simulation of a Reverberation Chamber with a stochastic collocation method, 2009*

$$E(Z^0;t) = \sum_{i=0}^{n} E_i(Z^0) L_i(t) \qquad L_i(t_j) = \delta_{ij} \qquad E_i(Z^0) = E(Z^0;t_i) \qquad \int_D pdf(u) f(u) du = \sum_{i=0}^{n} \omega_i f(t_i)$$

Mean value derivation

$$\langle E(Z^0;t)\rangle = \int_D E(Z^0;u) pdf(u) du \qquad \langle E(Z^0;t)\rangle = \sum_{i=0}^{n} E_i(Z^0) \int_D L_i(u) pdf(u) du = \sum_{i=0}^{n} \omega_i E_i(Z^0)$$

Variance derivation

$$\sigma^2 = \int_D \left[E(Z^0;u) - \langle E(Z^0;t)\rangle\right]^2 pdf(u) du \qquad \sigma^2 = \int_D \left[\sum_{i=0}^{n} E_i(Z^0) L_i(u) - \sum_{i=0}^{n} \omega_i E_i(Z^0)\right]^2 pdf(u) du$$

$$\sigma^2 = \int_D E^2(Z^0,u) pdf(u) du - 2\int_D E(Z^0,u)\langle E(Z^0,t)\rangle pdf(u) du + \langle E(Z^0,t)\rangle^2 \int_D pdf(u) du$$

$$\sigma^2 = \int_D E^2(Z^0,u) pdf(u) du - 2\langle E(Z^0,t)\rangle \int_D E(Z^0,u) pdf(u) du + \langle E(Z^0,t)\rangle^2$$

$$\sigma^2 = \int_D E^2(Z^0,u) pdf(u) du - \langle E(Z^0,t)\rangle^2 = \langle E^2(Z^0,t)\rangle - \langle E(Z^0,t)\rangle^2$$

$$\sigma^2 = \sum_{i=0}^{n} \omega_i E_i^2(Z^0) - \left(\sum_{i=0}^{n} \omega_i E_i(Z^0)\right)^2 \qquad \sigma^2 = \langle E^2(Z^0,t)\rangle - \langle E(Z^0,t)\rangle^2$$

- Random parameter: $Z \equiv \tilde{u} = Z^0 + \tilde{u}^0$
  Z^0 central value, $\tilde{u}^0$ Random Variable (RV) arbitrarily given
- Uniform, normal, exponential … laws ($\tilde{u}$)
- Stat. moments from output I computed from "$n+1$ well chosen" weighted (ω_i) points I_i [3]

Mean $\langle I \rangle = \sum_{i=0}^{n} \omega_i I_i$	Variance $\sigma_I^2 = \sum_{i=0}^{n} \omega_i I_i^2 - \langle I \rangle^2$

Extension to multi-RV

Statistical moment	Computation
1st	$\mathrm{mean}(I) = \sum_{i=0}^{n_1} \sum_{j=0}^{n_2} \omega_i^x \omega_j^y I_{ij}$
2nd	$\mathrm{variance}(I) = \sum_{i=0}^{n_1} \sum_{j=0}^{n_2} \omega_i^x \omega_j^y I_{ij}^2 - [\mathrm{mean}(I)]^2$
3rd	$\mathrm{skewness}(I) = \sum_{i=0}^{n_1} \sum_{j=0}^{n_2} \frac{[\omega_i^x \omega_j^y I_{ij} - \mathrm{mean}(I)]^3}{[\mathrm{variance}(I)]^{\frac{3}{2}}}$
4th	$\mathrm{kurtosis}(I) = \sum_{i=0}^{n_1} \sum_{j=0}^{n_2} \frac{[\omega_i^x \omega_j^y I_{ij} - \mathrm{mean}(I)]^4}{[\mathrm{variance}(I)]^2}$

Modeling « Uncertainties »

Validation

SC = smart MC

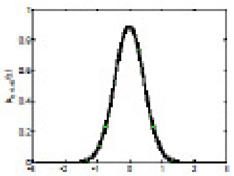

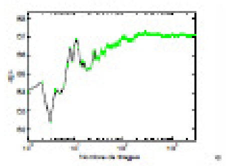

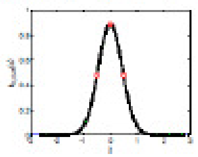

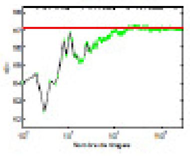

UNIVERSITÉ Clermont Auvergne

Department of Electronics
University of Split,
Split, Croatia

Ongoing work : stochastic electromagnetics

Application of the Stochastic Collocation to:

- GPR antennas
- HF dosimetry: the brain and eye exposures
- Grounding electrodes
- Buried wire scatterers

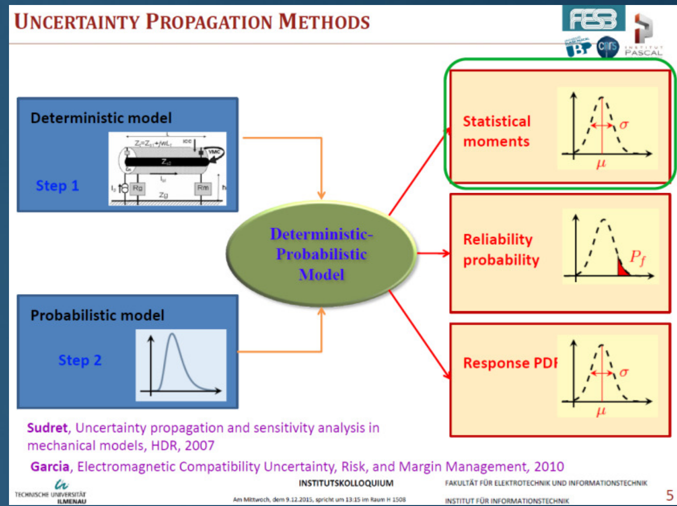

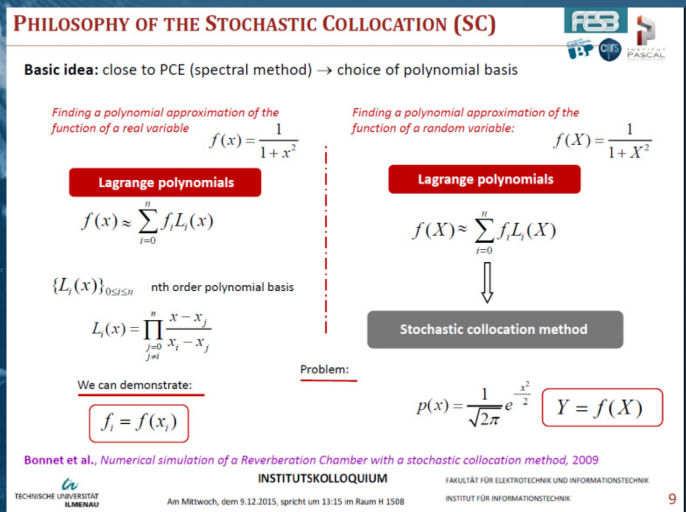

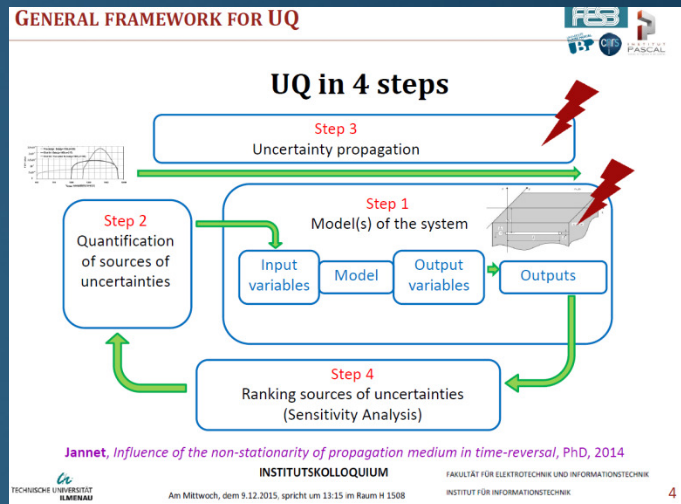

CROATIAN RESEARCH UNIT

Department of Electronics
University of Split,
Split, Croatia

Ongoing work : stochastic electromagnetics

The Stochastic Collocation: Principle (1)

$$E(Z^0;t)=\sum_{i=0}^{n}E_i(Z^0)L_i(t) \qquad L_i(t_j)=\delta_{ij} \qquad E_i(Z^0)=E(Z^0;t_i) \qquad \int_D pdf(u)f(u)du=\sum_{i=0}^{n}\omega_i f(t_i)$$

Mean value derivation

$$\langle E(Z^0;t)\rangle=\int_D E(Z^0;u)\,pdf(u)du \qquad \langle E(Z^0;t)\rangle=\sum_{i=0}^{n}E_i(Z^0)\int_D L_i(u)\,pdf(u)du=\sum_{i=0}^{n}\omega_i E_i(Z^0)$$

Variance derivation

$$\sigma^2=\int_D\left[E(Z^0;u)-\langle E(Z^0;t)\rangle\right]^2 pdf(u)du \qquad \sigma^2=\int_D\left[\sum_{i=0}^{n}E_i(Z^0)L_i(u)-\sum_{i=0}^{n}\omega_i E_i(Z^0)\right]^2 pdf(u)du$$

$$\sigma^2=\int_D E^2(Z^0,u)pdf(u)du-2\int_D E(Z^0,u)\langle E(Z^0,t)\rangle pdf(u)du+\langle E(Z^0,t)\rangle^2\int_D pdf(u)du$$

$$\sigma^2=\int_D E^2(Z^0,u)pdf(u)du-2\langle E(Z^0,t)\rangle\int_D E(Z^0,u)pdf(u)du+\langle E(Z^0,t)\rangle^2$$

$$\sigma^2=\int_D E^2(Z^0,u)pdf(u)du-\langle E(Z^0,t)\rangle^2=\langle E^2(Z^0,t)\rangle-\langle E(Z^0,t)\rangle^2$$

$$\sigma^2=\sum_{i=0}^{n}\omega_i E_i^2(Z^0)-\left(\sum_{i=0}^{n}\omega_i E_i(Z^0)\right)^2 \qquad \sigma^2=\langle E^2(Z^0,t)\rangle-\langle E(Z^0,t)\rangle^2$$

TECHNISCHE UNIVERSITÄT ILMENAU

INSTITUTSKOLLOQUIUM

Am Mittwoch, dem 9.12.2015, spricht um 13:15 im Raum H 1508

FAKULTÄT FÜR ELEKTROTECHNIK UND INFORMATIONSTECHNIK

INSTITUT FÜR INFORMATIONSTECHNIK

11

UNIVERSITÉ Clermont Auvergne

CROATIAN RESEARCH UNIT

Department of Electronics
University of Split,
Split, Croatia

Ongoing work : stochastic electromagnetics

- GPR antenna

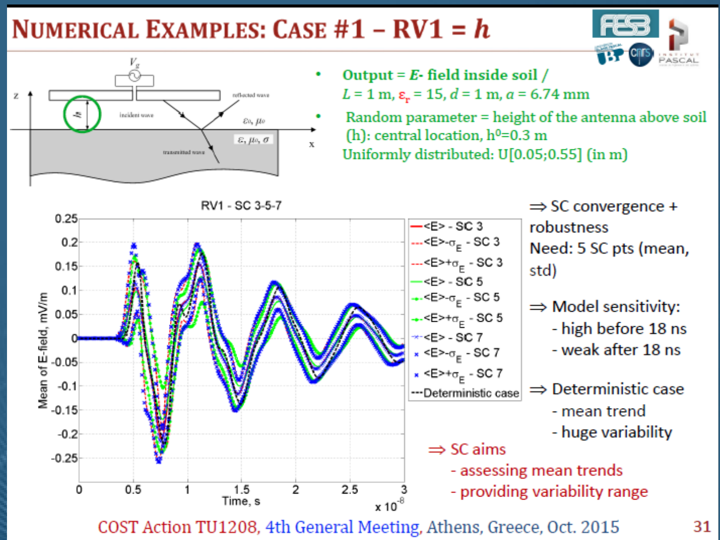

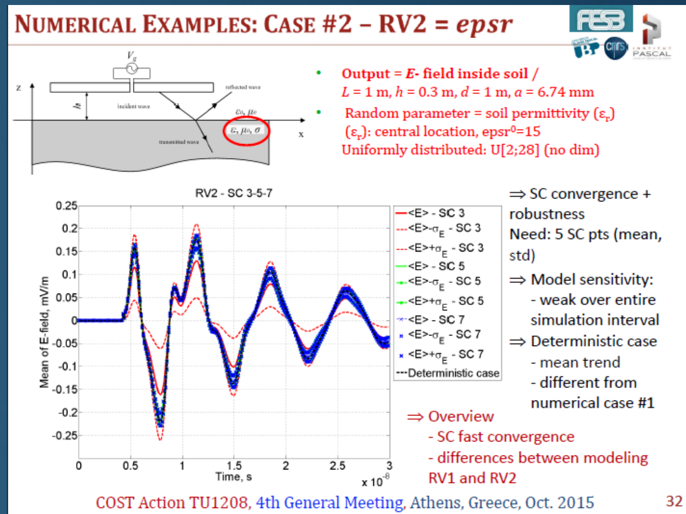

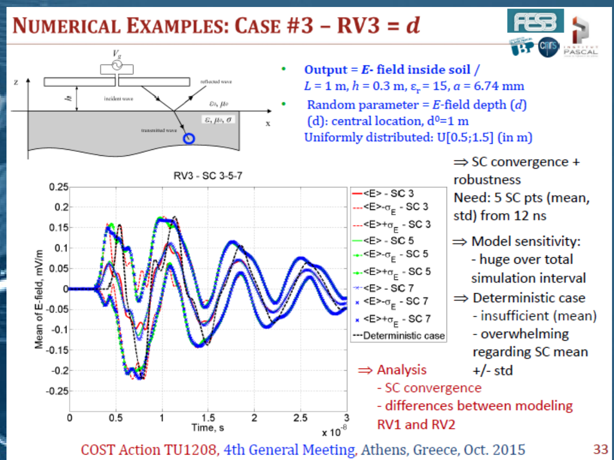

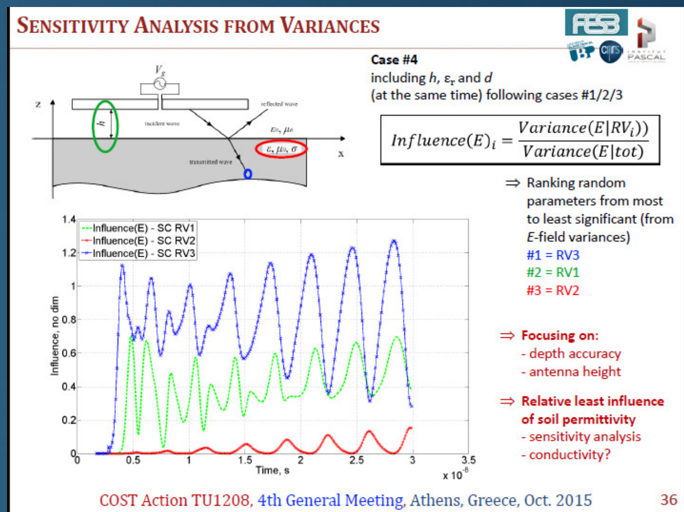

CROATIAN RESEARCH UNIT

Department of Electronics
University of Split,
Split, Croatia

Ongoing work : stochastic electromagnetics

- Grounding electrode

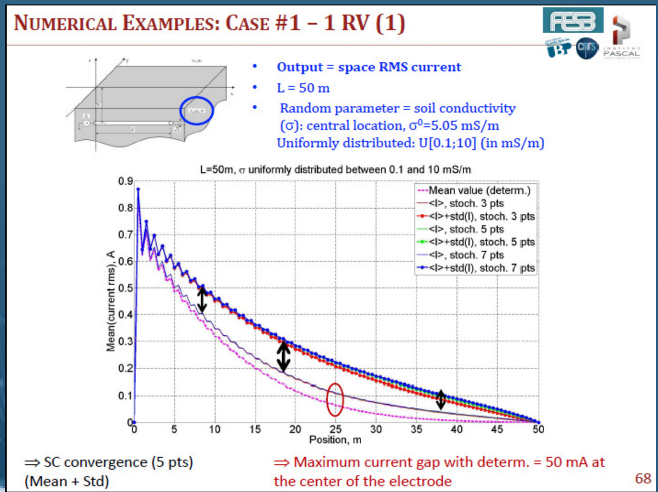

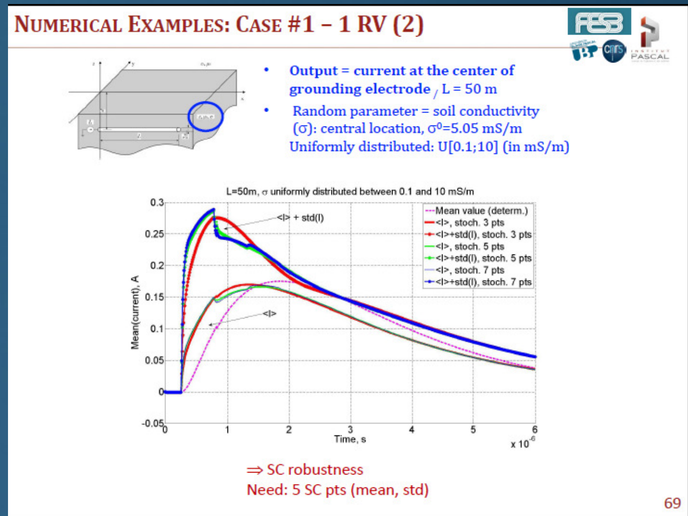

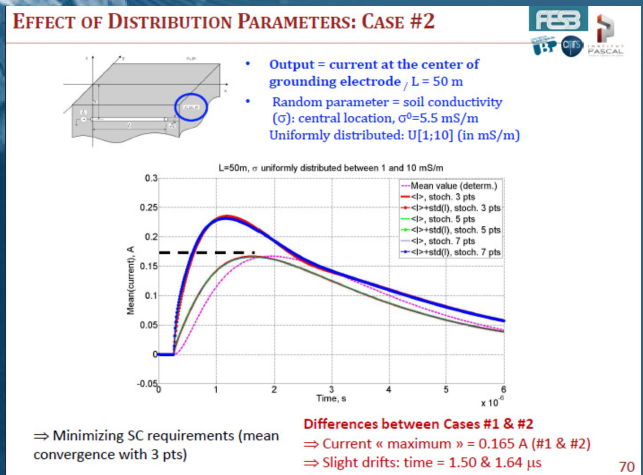

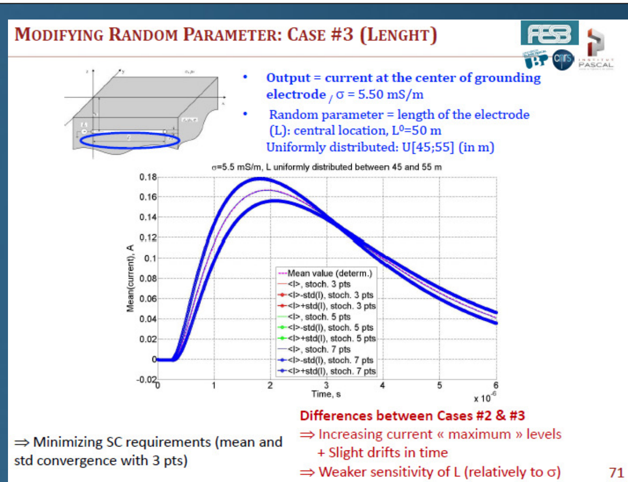

UNIVERSITÉ Clermont Auvergne

CROATIAN RESEARCH UNIT

Department of Electronics
University of Split,
Split, Croatia

Ongoing work : stochastic electromagnetics

- Buried line

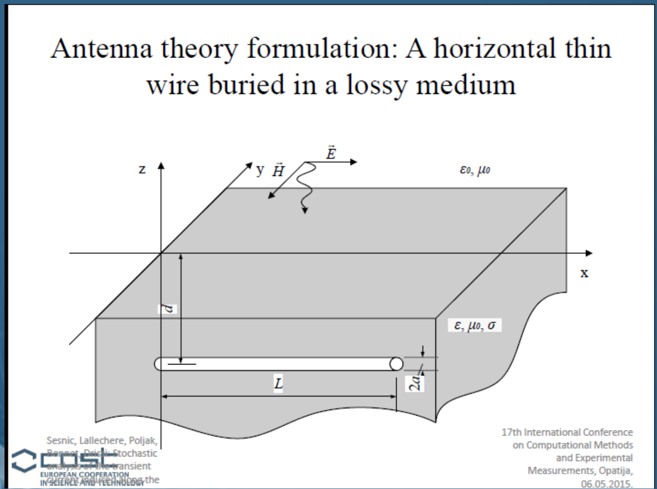

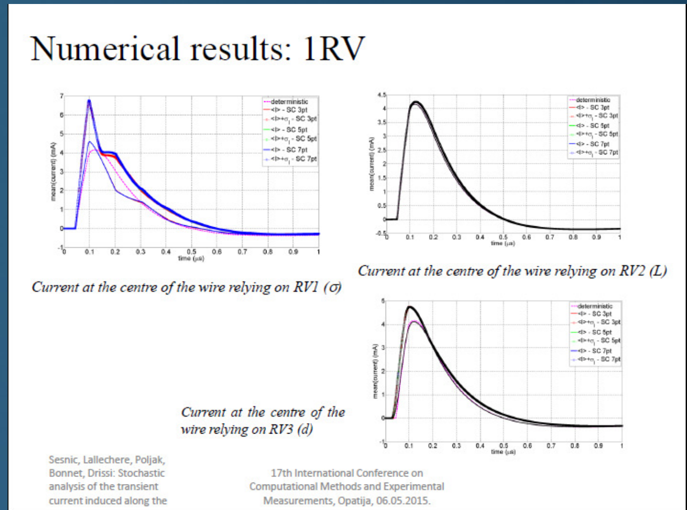

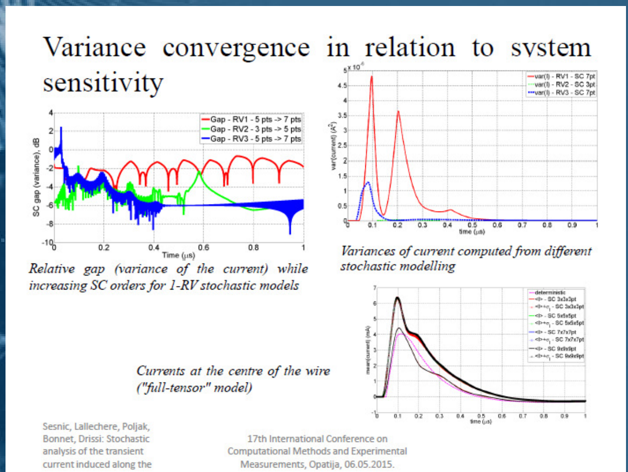

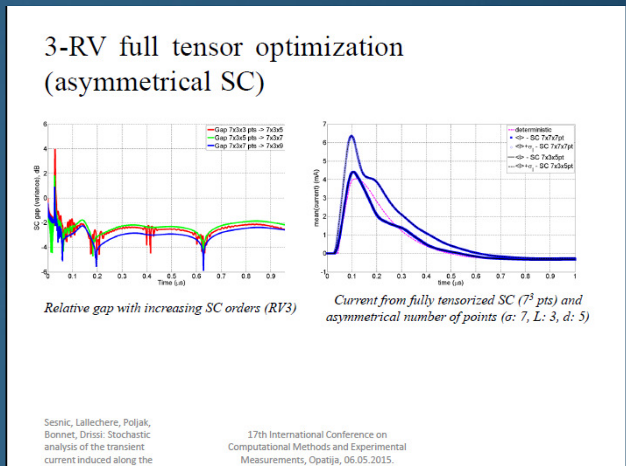

CROATIAN RESEARCH UNIT

Department of Electronics
University of Split,
Split, Croatia

Ongoing work : stochastic electromagnetics

- Human eye

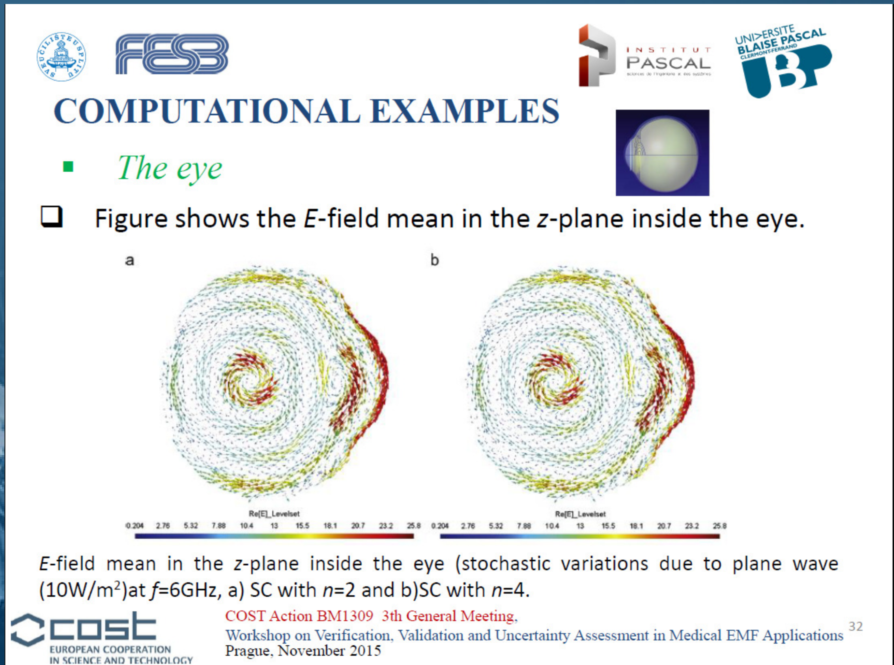

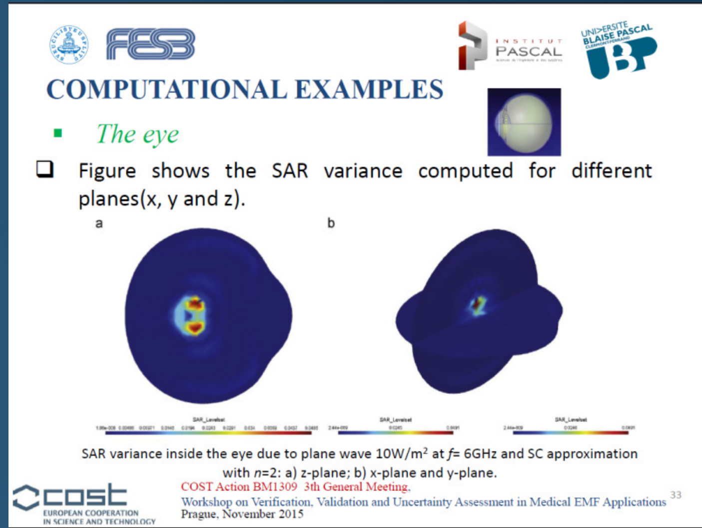

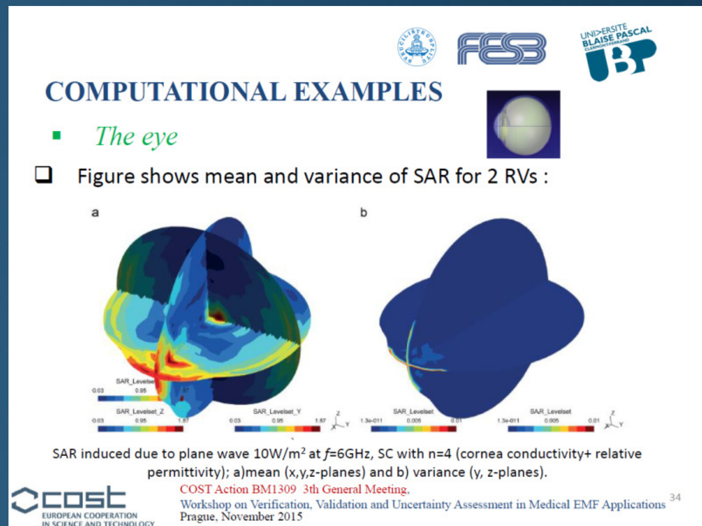

UNIVERSITÉ Clermont Auvergne

CROATIAN RESEARCH UNIT

UNIVERSITÉ Clermont Auvergne

Department of Electronics
University of Split,
Split, Croatia

Ongoing work : stochastic electromagnetics

- Human brain

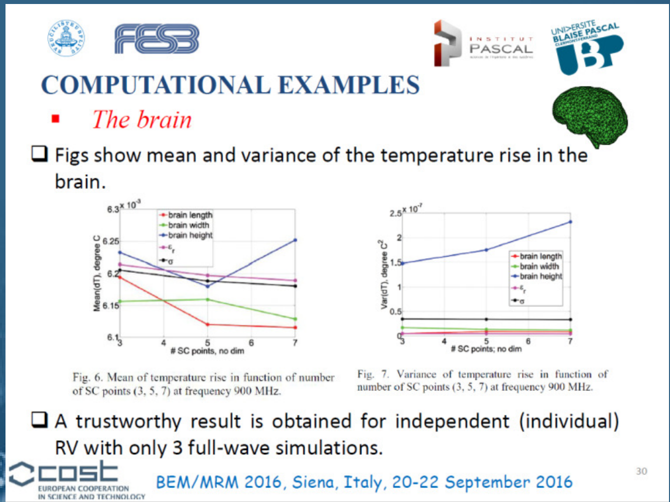

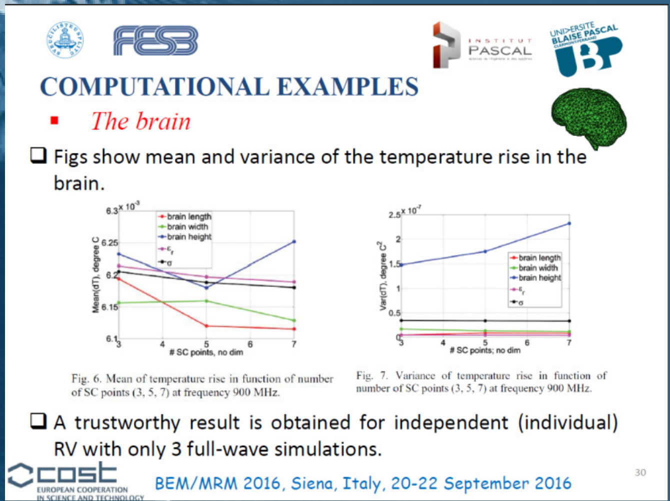

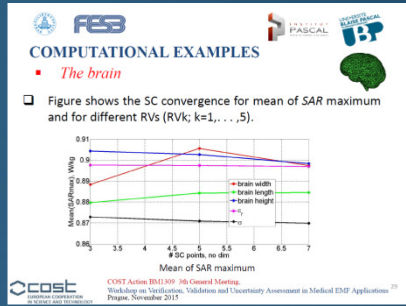

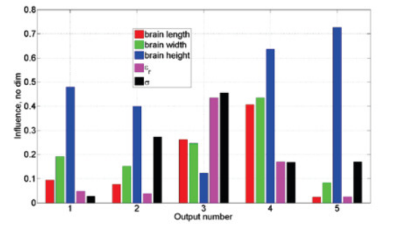

Fig. 8. Influence criterion I_i^j in function of outputs (1: E-field, 2: maximum SAR, 3: mean SAR, 4:max temperature, 5: temperature rise) and RV (brain's length, brain's width, brain's height, relative permittivity (ε_r) brain, conductivity (σ) brain) for vertical polarization.

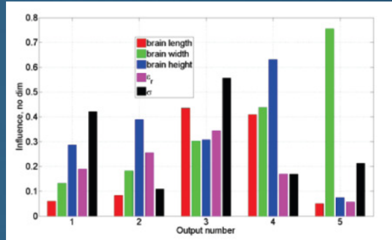

Fig. 9. Influence criterion I_i^j in function of outputs (1: E-field, 2: maximum SAR, 3: mean SAR, 4:max temperature, 5: temperature rise) and RV (brain's length, brain's width, brain's height, relative permittivity (ε_r) brain, conductivity (σ) brain) for horizontal polarization.

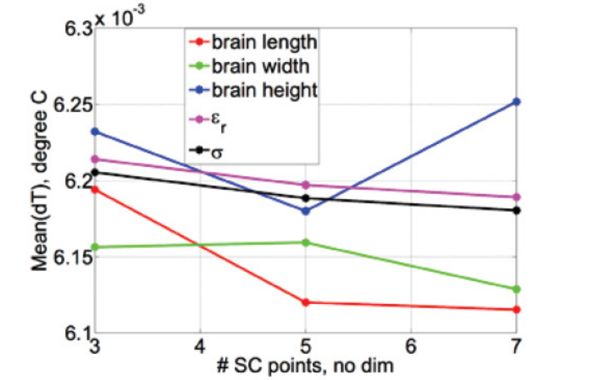

Fig. 6. Mean of temperature rise in function of number of SC points (3, 5, 7) at frequency 900 MHz.

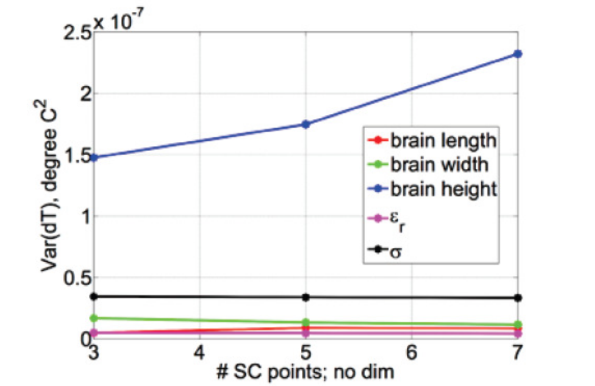

Fig. 7. Variance of temperature rise in function of number of SC points (3, 5, 7) at frequency 900 MHz.

Department of Electronics
University of Split,
Split, Croatia

Ongoing work : stochastic electromagnetics

BioEM 2016 (Annual Joint Meeting of the Bioelectromagnetics Society -BEMS)and the European BioElectromagnetics Association – EBEA), 5-10 June 2016, Ghent, Belgium

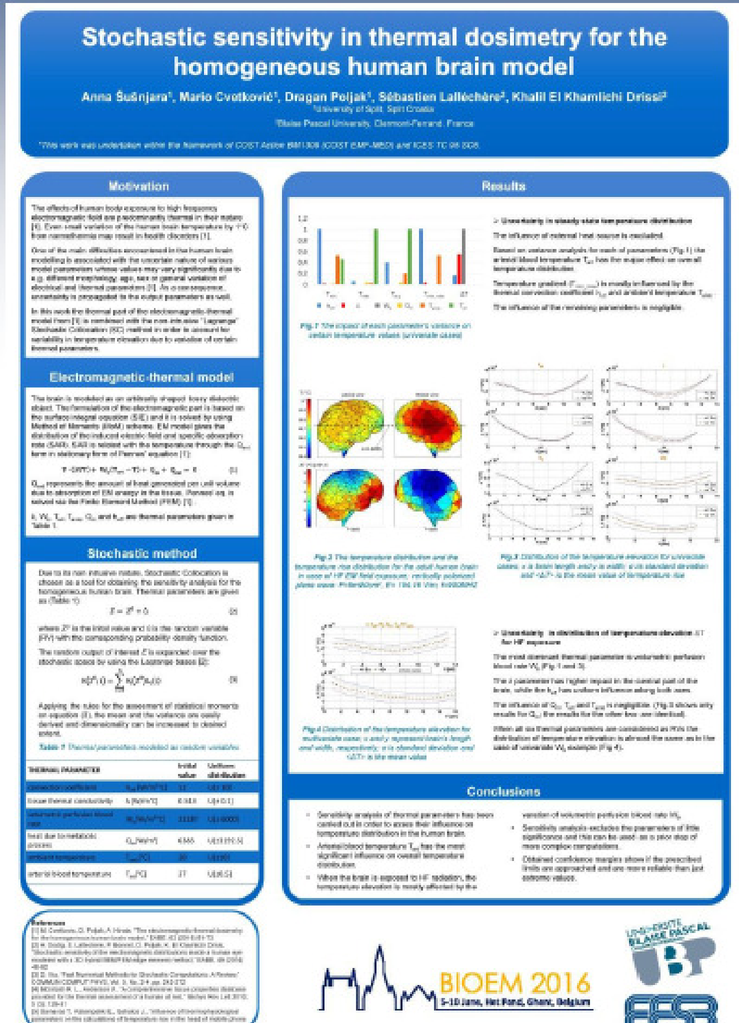

Department of Electronics
University of Split,
Split, Croatia

Ongoing work : stochastic electromagnetics

UMEMA 2017 (Uncertainty Modeling for Engineering Applications) , 23-24 November 2017, Turin, Italy

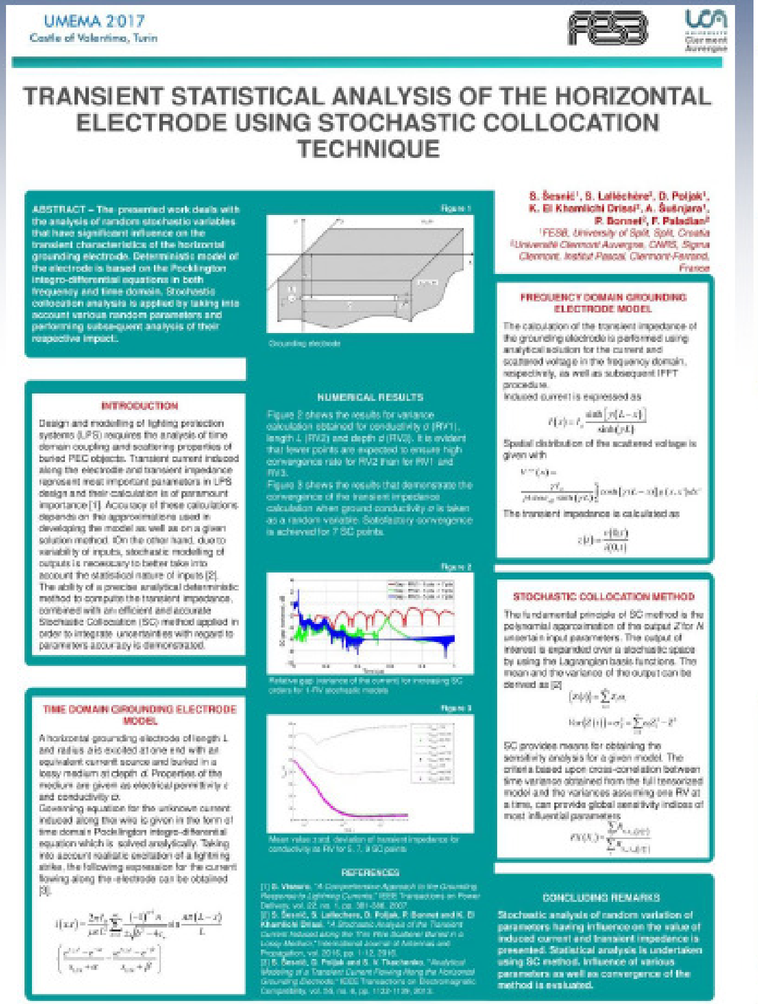

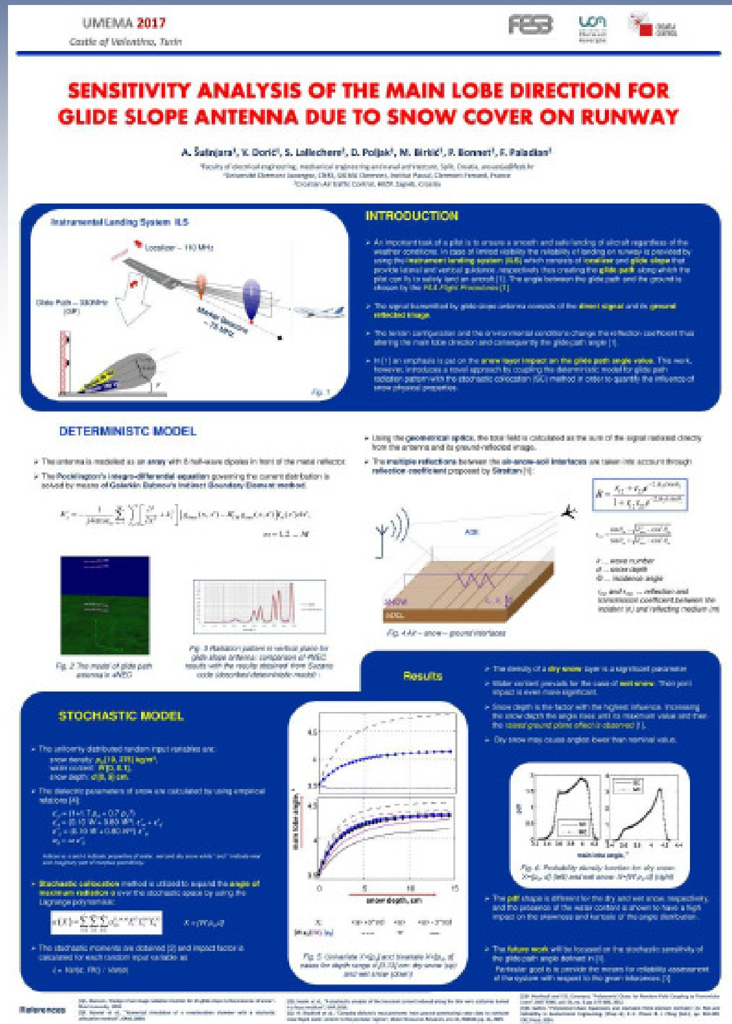

Department of Electronics
University of Split,
Split, Croatia

Ongoing work : stochastic electromagnetics

UMEMA 2017 (Uncertainty Modeling for Engineering Applications) , 23-24 November 2017, Turin, Italy

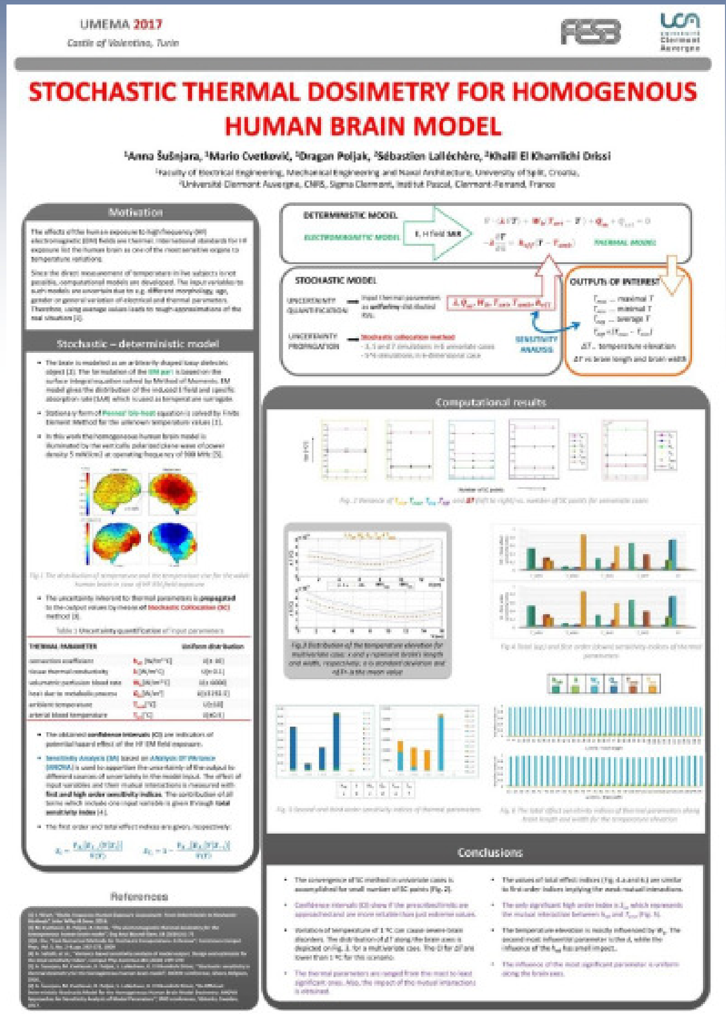

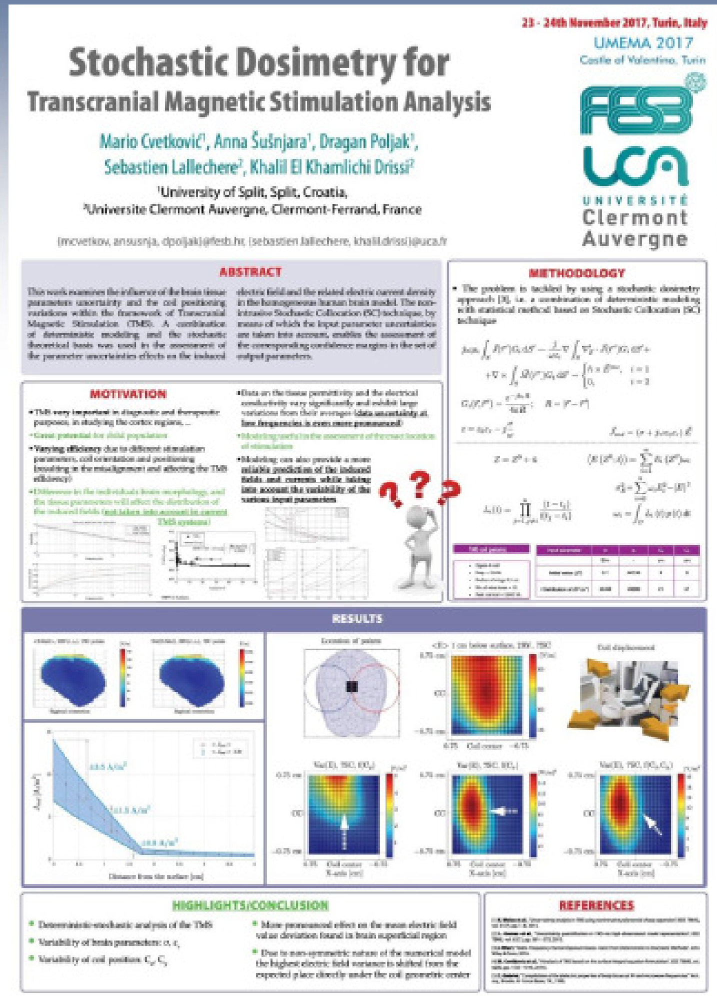

Department of Electronics
University of Split,
Split, Croatia

Concluding remarks

- The presentation deals with computational models applied in CEM, EMC, BIOEM and MHD.
- A crash-course on the theory of thin wire antennas and related numerical methods for solving some FD and TD integral equations, together with some engineering applications, is given.
- Furthermore, AT and TL models are used to analyze overhead wires, buried lines, PLC configurations, lightning channel and grounding systems.
- Human exposure to non-ionizing EM fields, LF and HF exposures are studied. Some biomedical applications of EM fields, related to TMS, PENS and TENS are also covered.
- The last part of the presentation is devoted to some MHD topics pertaining to the modeling of fusion phenomena.
- Finally, some stochastic analysis methods applied to various area of CEM pertaining to on-going research activities are outlined.

Department of Electronics
University of Split,
Split, Croatia

There is scarcely a subject that cannot be mathematically treated and the effect calculated beforehand, or the results determined beforehand from the available theoretical and practical data.

Nikola Tesla

"After solving the towns equation, the stranger rode off, into the setting sun."

Université Clermont Auvergne

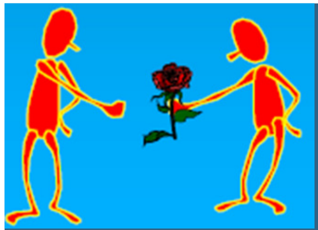

Department of Electronics
University of Split,
Split, Croatia

We made models in science, but we also made them in everyday life.
STEPHEN HAWKING

Thank you for your attention

Clermont-Ferrand, 03 April 2018